

YEREVAN STATE UNIVERSITY

MINISTRY OF EDUCATION AND SCIENCE, REPUBLIC OF ARMENIA

Badalian Samvel Michael

Carrier Interaction in Quantum Nanosystems

Speciality: **A.04.10** – Semiconductor and dielectric physics

A dissertation submitted to the 049 Specialized Council of
Yerevan State University for the scientific degree of
Doctor of Physical and Mathematical Sciences

Yerevan – 1997

The work is done at Yerevan State University

Official opponents

Dr. phys. math. sc. A A Kirakosyan

Dr. phys. math. sc. H R Minasyan

Dr. phys. math. sc. A Ya Shik

Leading institution Institute for Radiophysics and Electronics,
the National Academy of Sciences of Armenia

The public defense will take place on December 27, 1997 at 13:00 at the session of YSU Specialized Council 049 (1 A Manoogian St., Yerevan, Armenia, 375049).

The dissertation is available at YSU library.

The abstract of the dissertation is sent out on October 27, 1997.

Secretary of the Specialized Council 049,
cand. phys. math. sc.

V P Qalantaryan

©Copyright 1997
by
Badalian Samvel Michael

Contents

1	General	13
1.1	Introduction	13
1.2	Scientific novelty and practical value of the dissertation	16
1.3	Main goals and tasks of the dissertation	22
1.4	Basic theses of the dissertation submitted to the defense	24
1.5	Approbation of the work	27
1.6	Structure and volume of the dissertation	29
2	Electron-optical phonon bound states	30
2.1	Introduction	30
2.2	The 2D magneto-polaron spectrum	37
2.2.1	”Threshold” behavior of the polaron spectrum	37
2.2.2	Integral equation for the electron-phonon scattering amplitude and bound states	38
2.3	Cyclotron-phonon resonance	44
2.3.1	Absorption coefficient and bound states	45
2.4	Binding energies and oscillator strengths	49
2.4.1	The averaged form factors	49
2.4.2	Strong magnetic fields	51
2.4.3	Weak magnetic fields	53
2.5	Discussion of results	56
2.5.1	Numerical estimates	56
2.5.2	Conclusion	59

3	Electron-phonon relaxation. Interface effect	62
3.1	Introduction	62
3.2	Interface effect on the electron-phonon interaction	65
3.3	Scattering in a Fermi 2DEG near interfaces separating elastic semi-spaces	67
3.4	Scattering probability in a Fermi gas	72
3.5	Energy and momentum relaxation of a test electron	78
3.6	Relaxation of electron temperature	83
3.7	Discussion of results	85
4	Phonon emission by Landau states	89
4.1	Introduction	89
4.2	Electron transition probability between Landau levels: Free surface effect on electron-acoustic phonon interaction	96
4.3	Ballistic acoustic phonon emission by Landau states	101
4.3.1	Acoustic energy flux density	102
4.3.2	Suppression of surface acoustic phonon emission	106
4.3.3	Interference and conversion effects	108
4.3.4	Angular distribution of the emitted phonon field	110
4.4	Optical phonon emission: One phonon processes	113
4.4.1	Polar optical phonon scattering	115
4.4.2	Surface optical phonon scattering	119
4.5	Phonon emission: Two-phonon processes	120
4.5.1	Low magnetic fields	121
4.5.2	High magnetic fields	123
4.6	Summary	125
5	Edge state scattering	127
5.1	Introduction	127
5.2	Inter-edge-state relaxation	134
5.2.1	Impurity scattering	134
5.2.2	Acoustic phonon scattering	137
5.2.3	Impurity-assisted phonon scattering	139
5.2.4	Discussion	142

5.3	Phonon Emission by Quantum Edge States	146
5.3.1	Acoustic energy flux: Deformation Potential	146
5.3.2	Low and High Temperature Regimes	148
5.3.3	Acoustic Phonon Emission: Piezoelectric Potential	151
5.3.4	Angular distribution of emitted acoustic phonons	152
5.4	LO-phonon assisted edge state relaxation	154
5.4.1	Inter edge state transition probability	154
5.4.2	Kinematics of PO phonon emission	158
5.4.3	Energy relaxation of a test electron	160
6	Theory of Auger-upconversion	164
6.1	Introduction	164
6.2	Auger scattering between Landau levels	167
6.3	Electron-acoustic phonon scattering between Landau levels	171
6.4	Analysis of the rate equations.	175
7	Magneto-transport in a non-planar 2DEG	182
7.1	Introduction	182
7.2	Theoretical model	188
7.3	Results and Discussion	193
8	Summary	199
	Acknowledgements	203
	Appendix	203
	A	204
	B	205
	Bibliography	208
	List of publications underlying the dissertation	237
	Biographical Sketch	240

List of Figures

2.1	Energy levels $\varepsilon_{nl} = \varepsilon_n + (l + 1/2)\hbar\omega_B$ in the 2DEG exposed to the quantizing magnetic field normal to the electron sheet. ε_n is the energy of subband n	36
2.2	Simplest diagrams for the electron-phonon scattering amplitude Σ with dangerous intersections in one electron and one phonon lines.	38
2.3	Integral equation for the scattering amplitude Σ of an electron by a phonon.	39
2.4	Irreducible electron-phonon scattering amplitude \square	42
2.5	Photon polarization operator $\Pi^\pm(\nu)$	46
2.6	Sum of diagrams for the photon polarization operator $-iP^\pm(\nu)$	47
2.7	Cyclotron phonon resonance spectrum. The dashed line shows the absorption spectrum when no bound states are taken into account. The bold line is the skirt.	57
3.1	In usual method for calculating the transition probability an infinite crystal is replace by finite box of length L	64
3.2	The Fermi 2DEG located near the interface separating elastic semi-spaces.	73
3.3	The energy-loss power \bar{Q} of the Fermi 2DEG located near the free crystal surface. The dashed line corresponds to the case of the infinitely distant, $(\bar{z} \rightarrow \infty)$, boundary.	87

4.1	Schematic representation of phonon emission from the 2DEG with account of the phonon reflection. A_L and A_{LL} are the amplitudes of LA phonons emitted, respectively, directly into the bulk of crystal and to the crystal surface side then reflected from it. A_{LT} is the amplitude of TA phonons converted from the emitted LA phonons at the reflection from the crystal surface.	90
4.2	Schematic view of the ballistic acoustic phonon emission.	92
4.3	Transition probability $W_{1 \rightarrow 0}$ between Landau levels $l_1 = 1$ and $l_2 = 0$ versus magnetic field B for the distance $\bar{z} = 100$ nm and $\bar{z} = \infty$ from the 2DEG to the free surface.	101
4.4	Transition probability $W_{1 \rightarrow 0}$ between Landau levels $l_1 = 1$ and $l_2 = 0$ versus distance from the 2DEG to the free surface for the magnetic field $B = 0.5$ T. The transition probability is also shown when no phonon reflection is taken into account.	102
4.5	Angular distribution of the phonon emission intensity at $\bar{z} = 105$ nm when the Landau level broadening is not taken into account. Inset shows dependence of the ratio $\mathcal{W}^L/\mathcal{W}^{3D}$ on the emission angle.	111
4.6	Angular distribution of the phonon emission intensity at $\bar{z} = 109$ nm when the Landau level broadening is not taken into account. Inset shows the interference oscillations.	112
4.7	Angular distribution of the phonon emission intensity at $\bar{z} = 105$ nm when the Landau level broadening is taken into account. . . .	113
4.8	Angular distribution of the phonon emission intensity at $\bar{z} = 109$ nm when the Landau level broadening is taken into account. . . .	114
4.9	The Landau level broadening contribution to the PO phonon emission rate versus on the inter-level-spacing $\Delta l \omega_B$ for the electron transitions between $l = 3$ and $l' = 0$ levels in the vicinity of the PO phonon energy ω_{PO}	117
4.10	The PO phonon dispersion contribution to the PO phonon emission rate as a function on the inter-level-spacing $\Delta l \omega_B$ for the electron transitions between $l = 3$ and $l' = 0$ levels.	119

4.11	The PO+DA phonon emission rate versus on the inter-Landau-level separation $\Delta l \omega_B$ for the electron transitions between $l = 3$ and $l' = 0$ levels in the energy range $(3\omega_B - \omega_{PO}) \ll \omega_B, \omega_{PO}$. . .	123
5.1	A schematic diagram of the edge state energy spectrum. (a) Transitions $0 \rightarrow 1$ and $1 \rightarrow 0$ due to acoustic phonon emission are shown. At low temperatures, states close to the $0k_1$ are important. (b) If the Fermi level is close to the bulk Landau level, the transitions $0 \rightarrow 1$ involving states above the threshold k_c are only possible. At high temperatures, states disposed at the separations of T_e above and below ε_F are important.	128
5.2	Emission intensity distribution (piezoelectric interaction) in phonon momenta at low temperatures $T_e \ll \hbar\omega_{th} \equiv sq_{th} \equiv s\delta k_{10}$ and for the non-smooth confining potential.	153
5.3	Emission intensity distribution (deformation interaction) in phonon momenta at high temperatures $T_e \gg \hbar\omega_{th} \equiv sq_{th} \equiv s\delta k_{10}$ and for the non-smooth confining potential.	154
5.4	Emission intensity distribution (piezoelectric interaction) in phonon momenta at high temperatures $T_e \gg \hbar\omega_{th} \equiv sq_{th} \equiv s\delta k_{10}$ and for the non-smooth confining potential.	155
5.5	Hybrid edge state spectrum in the parabolic lateral confinement. All possible transitions due to polar optical phonon emission are shown.	156
5.6	The PO phonon emission rate versus the electron initial energy for the $l = 1 \Rightarrow l = 0$ transition and for different values of the magnetic field.	161
5.7	The PO phonon emission rate versus the electron initial energy for the $l = 2 \Rightarrow l = 0$ transition and for different values of the magnetic field.	162
6.1	Magnetic field dependence of the probabilities for the transitions between Landau levels $L'_0 \rightarrow L_1(\{I\})$ and $L_2 \rightarrow L'_0(\{II\})$ caused by acoustic phonon emission.	165

- 6.2 (a) Intensity of the luminescence detected at $\hbar\omega_{det}$ as a function of the exciting energy (left) and luminescence spectra at different excitation energies $\hbar\omega_{exc}$ (right). Two-dimensional and bulk structures are observed when the excitation energy corresponds to the peak of the two-dimensional density of states (solid line), and mainly bulk-related luminescence is visible when exciting in the gap between the two-dimensional levels (dashed line). (b) The Landau level fan chart of the optically active transitions observed in luminescence (crosses) and luminescence-excitation (open circles) spectra. The size of the symbol reflects the transition intensity. The L'_{01} absorption line involves the light-hole level. The Fermi-level position is shown with the dashed line. 178
- 6.3 (a) Solid circles: variation of the peak intensity (I'_0) of the above-laser emission as a function off the magnetic-field-dependent filling factor ν or the separation Δ between the excitation- and the emission-peak energies. The peak intensity of the L_0 -related luminescence (I_0) is shown with open circles. Solid lines are guides for the eye. (b) Power dependence (in relative units) of the I'_0 and I_0 when exciting into the L_1 level. Solid lines represent quadratic (for I'_0) and linear (for I_0) variations. 179
- 6.4 Probability of the Auger process W_{Auger} from the level L_1 into the levels L_0 and L_2 . Dashed line shows the overlap integral $\Phi(a_B/z_0)$. 180
- 6.5 Magnetic field dependence of the luminescence intensities I_0 and I'_0 for recombination from the Landau levels L_0 and L'_0 , respectively. 181
- 7.1 Applying a uniform magnetic field produces a spatially non-homogeneous field component normal to the 2DEG. Different magnetic superstructures can be obtained, depending on the θ angle between the magnetic field and the substrate normal, magnetic barriers ($\theta = 90^\circ$), magnetic wells ($\theta = 0^\circ$), and novel situations when the normal component of the field changes its sign on the magnetic interface. 185

7.2	A magnetic barrier is created in a non-planar 2DEG exposed to the uniform magnetic field. Dimensions and voltage probe locations correspond to the experimental situation. Boundary conditions are given in terms of angle which makes the electric field with respect to the sides and ends of the 2DEG. The current flows between voltage probes 1 and 8.	190
7.3	Conformal mapping $w(z)$ of the rectangular domain of the 2DEG onto the domain of a parallelogram form where boundary conditions are satisfied by a uniform electric field (the upper picture). Conformal mapping $\xi(z)$ of the rectangular domain of the 2DEG onto the upper half plane of the $\text{Im}\xi > 0$ such that the perimeter of the rectangle goes into the real axis (the lower picture).	192
7.4	Spatial distribution of the argument (in units of π) of \vec{E} for the facet situated between the points 498.5 and 501.5 μm . $L = 1000 \mu\text{m}$, $2w = 40 \mu\text{m}$, $B = 1 \text{ T}$	194
7.5	Spatial distribution of the absolute value of \vec{E} for the facet situated between the points 498.5 and 501.5 μm . $L = 1000 \mu\text{m}$, $2w = 40 \mu\text{m}$, $B = 1 \text{ T}$	195
7.6	The electric field profile at the edge of the 2DEG for different values of the magnetic field.	196
7.7	Magneto-resistance across the facet corresponding to for $L(3-4) = 255 \mu\text{m}$, $L(5-6) = 220 \mu\text{m}$, and $L(2-3) = 200 \mu\text{m}$	197
7.8	Magneto-resistance in the planar regions corresponding to for $L(3-4) = 255 \mu\text{m}$, $L(5-6) = 220 \mu\text{m}$, and $L(2-3) = 200 \mu\text{m}$	198

List of Tables

2.1	Binding energies and oscillator strengths in the strong magnetic fields. Recall that $W_{2D} = \alpha \hbar \omega_0$ denotes the characteristic binding energy scale for the 2DEG. The bound state index $r = 2, 3, 4, \dots$	53
2.2	Binding energies and oscillator strengths in the weak magnetic fields for the PO phonon assisted bound states in quantum wells. .	54
2.3	Binding energies and oscillator strengths in the weak magnetic fields for the SO phonon assisted bound states at the heterofaces.	55
2.4	Binding energies and oscillator strengths in the weak magnetic fields for the PO phonon assisted bound states in quantum wells. In these formulas d , B and W should be taken in nm, T, and meV, respectively.	59
A.1	Some physical and material parameters used in the dissertation. .	204

Chapter 1

General

1.1 Introduction

For decades, the microelectronics is the key-technology whose device structures are widely adopted for industry production being in great market demand. Giant efforts and resources are directed to the growth of the microelectronics in such industry developed countries as Japan, Germany and the USA. Alone in Germany, expenditures in the field of the microelectronics account for more than a third of the annual turnover (*circa* 600 milliard DM) with 3 million workers involved in this sphere [1]. Nowadays, development of submicron electronic structures is being pursued in many countries because these structures give promise of new material systems with enhanced optical, transport and thermalization properties that could make an impact in a variety of technologies, including semiconductor lasers and modulators, detectors, and optical filters.

Recent rapid advances in semiconductor technology of ultrafine lithography and modern etching technique have enable the fabrication of a large diversity of ultra-narrow synthetic structures with perfect atomic interfaces separating different materials including silicon, III-V and II-IV semiconductors and others ([2], for a review see [3, 4, 5]). In these material systems, both composition and doping can be controlled on a scale of the order of the de Broglie wavelength of carriers. Such a class of artificial semiconductor nanostructures (contacts of metal-insulator-semiconductor types, heterojunctions, superlattices, *etc.*) with dimensions in the range of 1–100 nm has opened up a new dimension in solid state

and semiconductor physics in the regime when the quantum size effect appears. This new freedom in engineering the electronic states and their properties offer a feasibility to study physics laws in real low dimensional systems and an exciting potential for electronic applications as well for investigations of new tantalizing phenomena principal for fundamental physics.

During the last decade, the semiconductor nanoscale systems with carrier confinement in one (quantum wells [QW]), two (quantum wires [QWr]), and all three dimensions (quantum dots [QD]) have been studied intensively in theory and experiment [6, 7, 8] to characterize, understand conceptually, and exploit quantum effects in technologically important semiconductor device structures. Already, a set of novel results such as the weak and Anderson localization [9], the effect of very high electron mobility in modulation doped heterojunctions [10, 11] has been discovered in 2D nanosystems. Quantum effects in 2D nanosystems have been exploited to provide enhanced semiconductor lasers, a new class of infrared detectors, and resonant tunneling diodes. The high electron mobility transistors on GaAs heterostructures are used in a source-drain channel to construct high frequency amplifiers with the limiting frequency above than 100 GHz [12].

However, investigations of nanosystems with a two dimensional electron gas (2DEG) is frequently connected with the use of high magnetic fields. For example, high mobility samples with the 2DEG of nanoscale dimensions exposed to the normal high magnetic field exhibit quantized resistance (the integer quantum Hall effect [QHE], [13], for a review see [14]) and exotic charge correlation (the fractional QHE, [15, 16], for a review see [17]). Understanding the integer and the fractional QHE has intrigued and challenged researchers for more than 10 years now, both for the wide range of new phenomena discovered [18, 19, 20, 21, 22] and for the potential for high precision metrology based on the QHE [23, 24].

Another key feature of the 2DEG in the QHE geometry is the existence of quantum edge states localized in the vicinity of the sample boundary. The quantization of the Hall resistance into the h/e^2 portions can be explained easily under assumption that the edge states are not influenced by scattering and the transport is adiabatic (see reviews on the edge states and QHE [21, 25, 26] and references cited therein).

QWrS and QDs give promise to provide even greater enhancement in optical

and relaxation properties of semiconductor device structures because the wave functions are further compressed by lateral confinement and the quantum effects can be used to concentrate the optical oscillator strengths at the active transitions [27, 28, 29]. In this limit these structures behave as manmade artificial *quasiatoms* [30]. Furthermore, these structures under different new environments exhibit discrete charging effects and give promise of devices operating in the limit of single electron transport.

Carrier scattering is a fundamental process that always exist in crystals. Characterizing and understanding carrier scattering processes in the quantum nanosystems are critical both for unraveling the basic phenomena of quantum effects in nanophysics and for controlling carrier dynamics in the nanoscale device structures, such as relaxation rates for carrier thermalization, equilibration and Auger scattering rates for carrier distribution, and diffusion rates for carrier transport. Carrier scattering is strategic for identifying the lateral confinement effects and for developing enhanced, useful device structures. For example, blueshifts in QWr photoluminescence are typically attributed to lateral confinement. Recently, blueshifts observed in QWr magneto-photoluminescence have been attributed to suppression of carrier transport and incomplete relaxation in QWr's [31] rather than to lateral confinement induced level shifts. Small deep-dry-etched QDs often exhibit poor luminescence efficiency. It has been suggested that this poor luminescence has an intrinsic origin, resulting from a suppression of phonon scattering in small QDs that leads to a "phonon bottleneck" for electron relaxation [32, 33]. If this intrinsic mechanism for suppressing luminescence dominates extrinsic effects due to processing, then the possibilities for using the effectively 0D nanosystems (QDs, QWr's and 2D nanostructures in normal quantizing magnetic fields) in any application that relies on carrier relaxation, such as injection lasers, would be severely limited. Thus it is critical that the character of carrier scattering, relaxation and transport in effectively 0D nanostructures be established thoroughly to separate transport from confinement effects and better control and relieve the suppression of transport. Multiphonon processes [34] provide additional evidence for this phonon bottleneck in these 0D systems [35]. It has been suggested that multiphonon processes [36] and Auger scattering [37] can break this "bottleneck". in deep-etched QDs. Thus a careful analysis of all of these

scattering mechanisms for low dimensional nanostructures is imperative. Clearly, recent theoretical progress, and the many experiments in this hot topic will lead to a number of novel questions.

In this work I present theoretical investigations of carrier scattering in quantum nanosystems carried out during the last ten years by coworkers and me. Carrier interaction with phonons, photons, impurities, and electrons in semiconductor nanoscale systems with carrier confinement in one and two dimensions in zero and quantizing magnetic fields has been addressed. Most importantly, our calculations allow to better understand phonon signature in optical, thermalization, and transport experiments that can be used to identify and characterize the basic phenomena of quantum confinement in these quantum nanostructures.

1.2 Scientific novelty and practical value of the dissertation

We have investigated peculiarities of the polaron (elementary excitations in the electron+phonon system) spectrum near the longitudinal optical phonon emission threshold. In spite of weak electron-phonon coupling, we have obtained that in the 2DEG in the QHE geometry, new complex quasiparticles, electron-phonon bound states, appear in magneto-polaron spectrum. They constitute an infinite set which is coagulated to the threshold both above and below it [38, 39]. In contrast to the virtual phonons taking part in the formation of the usual Frölich polaron, phonons in the bound states are almost real. The characteristic scale of the binding energies is essentially greater than the corresponding scale in massive samples.

The existence of the electron-phonon bound states results to the fine structure of the cyclotron-phonon resonance [40]. According to the perturbation theory, photon absorption was to be expected at the phonon emission threshold. In reality, the perturbation theory becomes inapplicable in the immediate vicinity of the threshold. The true spectrum is obtained from the solution of an integral equation for the electron-phonon scattering amplitude. Absorption entirely

governed by the bound states with the total angular momentum ± 1 . The absorption spectrum consists of two groups of peaks which are approximately of the same amplitude and are located approximately asymmetrically relative to the "threshold".

Our calculations explain the dynamics of carrier relaxation in the 1D and 2D quantum nanosystems both in zero and quantizing magnetic fields. Understanding and controlling this dynamics is critical because rapid carrier relaxation is crucial for many of the technological applications proposed for semiconductor nanoscale quantum devices. We have investigated thoroughly the main relaxation characteristics of 1D and 2D electron systems due to acoustic phonon (deformation DA and piezoelectric PA) and polar optical PO phonon scattering.

Special attention has been paid to the presence of various interfaces separating different materials in 2D nanostructures. These interfaces influence the acoustic phonon normal modes and can affect essentially electron-phonon interaction. We have proposed a new method for calculating the probability of electron scattering from the deformation potential of acoustic phonons [41]. Such a probability summed over all phonon modes of the layered elastic medium can be expressed in terms of the elasticity theory Green function which contains all information about structure geometry.

Exploiting this method, the energy and momentum relaxation times of a test electron as well as the relaxation rate of electron temperature for the whole Fermi 2DEG located in the vicinity of an interface between elastic semi-spaces have been calculated [42, 43]. Analysis of limiting cases for an interface between solid and liquid semi-spaces, for a free and rigid surfaces has shown that there are situations when the phonon reflection from various interfaces alters the energy (or electron temperature) dependence of the relaxation times and leads to a strong reduction of the relaxation rates.

To illustrate the interface effect in quantizing magnetic fields, electron relaxation between discrete Landau levels in 2DEG located near free crystal surface has been studied [44, 45]. The interface effect is obtained to be highest in the magnetic field since the 2DEG interacts with almost monochromatic cyclotron phonons in this case. The electron transition probability has an oscillating behavior of the magnetic field and of the distance from the 2DEG to the interface.

Scattering from the deformation potential of acoustic phonons has been only considered since in quantizing magnetic fields, scattering from piezoelectric potential is strongly suppressed [46].

Optical phonons determine the character of electron relaxation at high temperatures and in various experiments with an optical excitation or Auger processes. In the 2DEG subjected to strong magnetic fields with rather thin electron layers and subjected to rather strong magnetic fields, a large separation between Landau levels cannot be covered by an acoustical LA phonon [45] so the multiphonon 2LA [47] or an optical phonon assisted [48] processes become more efficient. Longitudinal optical phonon assisted inter Landau level transitions via one-phonon emission mechanism requires a precise resonance. Away from the resonance, efficiency of this process falls steeply. Non-resonant optical phonon emission in the effectively 0D systems should be accompanied by acoustic phonon emission via the two-phonon emission mechanism. We have calculated polar optical PO phonon assisted electron relaxation as a function of the inter Landau level spacing in the 2DEG in the QHE geometry [48]. The interface optical SO phonon relaxation has been found to be at least by an order weaker than relaxation via polar optical PO phonon emission. To obtain a finite relaxation rate associated with one-phonon emission, the allowance for the Landau level broadening and for the PO phonon dispersion has been made. Immediately below the phonon energy, $\hbar\omega_{PO}$, the PO phonon dispersion contribution gives rise to a sharp peak with the peak value approximately 0.17 fs^{-1} . The Landau level broadening contribution has a rather broad peak with relatively lower peak value. Below $\hbar\omega_{PO}$ within an energy range of the order of $\hbar\sqrt{\omega_B/\tau}$, the one-phonon relaxation rate exceeds 1 ps^{-1} (τ is the relaxation time deduced from the mobility. In GaAs/AlGaAs with mobility $\mu = 25 \text{ V}^{-1} \text{ s}^{-1} \text{ m}^2$ this range makes up 0.7 meV).

Two-phonon emission is a controlling relaxation mechanism above $\hbar\omega_{PO}$ [48]. For energies $\Delta\hbar\omega_B$ immediately above $\hbar\omega_{PO}$, PO+DA phonon relaxation has a sharp onset. The relaxation rate increases as a fifth power in the magnetic field achieving to the peak value exceeding 1 ps^{-1} at energy separations of the order of $\hbar s/a_B$ (s is the sound velocity, a_B is the magnetic length. In GaAs at $B = 7 \text{ T}$ we have $\hbar s/a_B \approx 0.4 \text{ meV}$). At higher magnetic fields in the energy range $sa_B^{-1} \lesssim \Delta\hbar\omega_B - \omega_{PO} \lesssim sd^{-1}$ (in GaAs with $d = 3 \text{ nm}$ we have $\hbar s/d \approx 1.2 \text{ meV}$), the

two-phonon peak decreases linearly in the magnetic field. Above $\hbar\omega_{PO}$ within the wide energy range (in GaAs this range makes up approximately 5 meV), the magnetic field dependence of the relaxation rate is rather weak and the subnanosecond relaxation between Landau levels can be achieved via the two-phonon emission mechanism. Our analysis has demonstrated that in some experimental situations the PO+DA-phonon emission mechanism is more efficient than relaxation in two consecutive emission acts: PO phonon emission (even under the sharp resonance) with subsequent emission of either LA- or 2LA-phonons.

As distinct from the conventional relaxation experiments where the relaxation rates are measured directly, in the ballistic phonon emission experiments, the intensity and the angular distribution of the phonon signal are detected on the sample reverse face which provide a worthy source of information on electronic properties. Such experiments are especially valuable in systems of reduced dimensionality since carriers are confined to small nanoscale regions while other quasiparticles such as phonons can be not localized and more reachable for study.

In the dissertation I present calculations of ballistic acoustic phonon emission at electron transitions between fully discrete Landau levels in a 2DEG with account of the phonon reflection from a GaAs/AlGaAs type interface [49, 50]. In accordance with the experimental results, we have obtained that the angular distribution of emitted phonons has a distinctly expressed peak for small angles. Account for the interface effect affects essentially the intensity and the composition of the detected phonon field. Upon their *reflection* and *conversion* at the crystal surface, longitudinal acoustic LA phonons propagate backwards in the forms of LA and transverse acoustic TA phonons. The reflected LA phonons interfere with the initial LA phonons emitted by the 2DEG in the same direction. Therefore, we have obtained that under the deformation electron-phonon interaction, the detector records on the sample reverse face both the *interference* field of the LA phonons and, which is most intriguing for experiment, the *conversion* field of the TA phonons [49]. Our calculations of emission spectrum for surface acoustic phonons show that an exponential suppression of the emission of surface acoustic phonons occurs in a wide range of the magnetic field variation [50]. So, the cooling of the heated 2DEG is only at the expense of bulk LA and TA phonons.

Investigation of edge state scattering is one of key stages of the dissertation [51, 52, 53, 54]. The single particle energy spectrum in a 2DEG exposed to a homogeneous magnetic field normal to the electron plane is separated into the edge states and the bulk Landau states. The edge states correspond to the classical skipping orbits and are confined near sample edges. Edge states exist also in QWrs. If the wire width L is much greater than the magnetic length a_B , $L \gg a_B$, then the edge states both in 2DEGs and QWrs can be treated in the same way as a 1D electron system. The edge states play an important role both in conventional transport measurement experiments and in ballistic phonon emission and absorption experiments. In the latter case, equally with the bulk Landau states, the quantum edge states also give a contribution to emission and absorption of ballistic phonons. We have calculated ballistic acoustic (both for deformation DA and piezoelectric PA interactions) [54] and polar optical phonon emission by the quantum edge states. An analytic expression for the ballistic acoustic energy flux emitted by the quantum edge states has been derived. Detailed analysis of the phonon emission intensity distribution has been made in low and high temperature regimes and for different positions of the Fermi level. At the same time as phonon emission by the bulk Landau states is concentrated within a narrow cone around the magnetic field, at the inter edge state transitions and at low temperatures, the emitted phonon field is predominantly concentrated within a narrow cone around the direction of edge state propagation, while at high temperatures – around the magnetic field normal to the electron plane. At low temperatures the emission intensity decreases exponentially with decreasing filling of Fermi level. In contrast to the case of bulk Landau states where piezoelectric interaction is always suppressed with respect to the deformation interaction, in the edge state case, the relative contributions of piezoelectric and deformation interactions depend on the magnetic field and temperature.

We have studied an optical phonon assisted edge state relaxation for a test electron in QWrs with a rectangular cross section exposed to the normal magnetic field. The intrasubband scattering rates as a function of the initial electron energy for different values of the magnetic field has been calculated. By considering different limiting cases of the ratio of the cyclotron frequency to the strength of the lateral confinement, results for edge state relaxation both in 2DEGs and

QWrs as well as for the magnetic field free case can be obtained.

We have calculated the inter edge state scattering length for an arbitrary confining potential [51, 52]. Phonon (deformation acoustic DA and piezoelectric PA interactions) and impurity scatterings are discussed and analytical expressions for scattering lengths are derived. As follows from energy and momentum conservation, only phonons with frequencies above some threshold can participate in the transitions between edge states. As a result, phonon scattering is exponentially suppressed at low temperatures. According to our evaluations, the observed temperature dependence of the scattering length cannot be attributed to phonon scattering.

Auger scattering in semiconductors is well known from investigations of non-radiative recombination. Free electrons and holes are a prerequisite for this process: the energy obtained in the recombination of an electron-hole pair is taken to excite another electron. The latter electron may loose its excess energy by electron-lattice relaxation; thus the recombination energy is converted into heat. In quantum nanosystems, Auger processes become possible between different subbands. The reduction of Auger scattering rate in effectively 0D nanosystems due to the discreteness of the electronic states has been used as an argument to propose quantum dots lasers.

In recent magneto-luminescence experiments by Potemski *et al.* [55, 56] on one-side modulation doped GaAs/AlGaAs quantum wells, an up-conversion has been observed and interpreted as being due to an Auger process. The luminescence spectrum under interband excitation at low temperatures and for low excitation powers shows two peaks: besides the luminescence due to recombination of an electron from lowest Landau level with a hole in a valence band, a second peak is observed above the exciting laser energy and is related to recombination of an Auger up-converted electron with a hole. We have developed a theory of Auger up-conversion in quantum wells in quantizing magnetic fields to explain these experimental results [57, 46]. We have calculated the characteristic times of electron-electron scattering processes between Landau levels of the lowest electric subband and of electron-acoustic phonon scattering between Landau levels of the two lowest electric subbands as well as the lifetime of a test hole both with respect to the Auger process and phonon emission. By analyzing rate equations

for these processes as well as for the pumping by interband excitation and the recombination of electrons with photo-induced holes, we have found the Auger process time. As well the magnetic field and the excitation power dependencies of the two luminescence peaks have been obtained which are consistent with the experimental findings. Thus, an understanding of the Auger up-conversion observed in the magneto-luminescence in quantum wells is provided.

Recently a research group from the Toshiba Cambridge Research Center Ltd. and Cavendish Laboratory have proposed a new technique to produce non-homogeneous magnetic fields [58, 59, 60, 61, 62]. A remotely doped GaAs/Al_xGa_{1-x}As heterojunction is grown over wafer previously patterned with series of facet. The use of *in situ* cleaning technique enables to regrow uniform high quality 2DEGs which is no longer planar but follows the contour of the original wafer. Application of a homogeneous magnetic field to this structure results a spatially varying field component normal to the 2DEG. Thus, this technique offers possibilities to investigate the effect of varying *the topography* of an electron gas in addition to varying the *dimensionality*. This new technology will open up a new dimension in nanophysics.

We have investigated theoretically the magneto-transport of the non-planar 2DEG [63, 64, 65, 66, 67]. As an example the electric field distribution of the 2DEG with a magnetic field barrier is calculated. The system satisfies the Poisson equation in which linear charges develop at the magnetic/non-magnetic field interface. The magneto-resistance across the facet as well as in the planar regions of the 2DEG have been calculated which explain the main features of the magnetic field dependencies observed experimentally by M L Leadbeater *et al* [59, 60].

1.3 Main goals and tasks of the dissertation

1. Investigation of threshold peculiarities of the polaron spectrum in the 2DEG in a quantizing magnetic field normal to the electron sheet. Demonstration of the existence of the spectrum new branches which describe the bound states of an electron and an optical phonon.

2. Study of photon absorption on these electron-phonon bound states. Establishment of the fine structure of the cyclotron-phonon resonance in quantum wells and heterostructures. Consideration both bulk and surface optical phonons in formation of the bound states.
3. Development of a new method for calculating the probability of electron scattering from the deformation potential of acoustic phonons. Use of this method to treat the phonon reflection from a crystal surface and interfaces separating different materials.
4. Exploiting the proposed method to calculate the electron energy and momentum relaxation times for a test electron as well as the relaxation rate of electron temperature for the whole Fermi 2DEG taking into account the phonon reflection from the interface between semi-infinite elastic media.
5. Calculation of the transition probability between fully quantized Landau levels and taking into account the crystal free surface effect on interaction of the 2DEG with acoustic phonons.
6. Study of ballistic acoustic phonon emission in quantizing magnetic fields normal to the 2DEG plane when reflection of these phonons from a GaAs/AlGaAs type interface is taken into account.
7. Investigation of longitudinal polar PO optical phonon assisted electron relaxation in the 2DEG in the QHE geometry. Consideration of inter Landau level relaxation via one phonon (for bulk PO and interface SO phonons) and two PO+DA phonon (for deformation acoustic DA and PO phonons) emission processes.
8. Calculation of the scattering length for inter edge states transitions in quantizing magnetic fields due to acoustic phonons (DA and PA interactions) and short- and long-range impurities, assuming that the shape of the confining potential is arbitrary.
9. Study of emission of ballistic acoustic phonons (due to deformation and piezoelectric interactions) by quantum edge states in quantizing magnetic

fields. Detailed analysis of the emission intensity and the angular distribution in low and high temperature regimes. Consideration of different positions of the Fermi level.

10. Calculation of the optical phonon assisted edge state relaxation rates in quantum wires exposed to quantizing magnetic fields. Derivation of the PO phonon emission rate dependence on the electron initial energy and magnetic field.
11. Construction of a theory of the Auger up-conversion observed in recent magneto-luminescence experiment. Calculation of the relaxation rates of the carrier-carrier (between discrete Landau levels of the lowest electric subband) and the carrier-phonon (between discrete Landau levels of the two lowest electric subbands) scattering processes in quantum wells exposed to the normal quantizing magnetic field.
12. Investigation of the magneto-transport of a non-planar 2DEG. Calculation of the electric field distribution in the presence of a magnetic tunnel barrier of μm width. Derivation of the magnetic field dependence of the magneto-resistance both across the facet and in the planar regions of the 2DEG.

1.4 Basic theses of the dissertation submitted to the defense

1. Despite to the weak electron-phonon coupling, an infinite set of bound states of an electron with an optical phonon exists both above and below the threshold of optical phonon emission in the magneto-polaron spectrum in the 2DEG.
2. The spectrum of the cyclotron-phonon resonance has a fine structure which is governed entirely by the electron-phonon bound states. Therefore, electromagnetic absorption is concentrated not at the threshold but below and above it at the separations of the binding energies. The absorption spectrum consists of two groups of peaks which constitute an "asymmetric doublet".

3. It is easy to account for the phonon reflection from various interfaces separating different materials using the proposed method for calculating the probability of electron scattering from the deformation potential of acoustic phonons.
4. There are situations when the presence of an interface, near which the Fermi 2DEG is located, leads to a strong reduction of the energy and the momentum relaxation and alters the dependence of the relaxation rates on the electron energy (or on electron temperature).
5. The interface effect in the 2DEG is strongest in quantizing magnetic fields normal to the plane of electrons and for the free crystal surface. Surface effect becomes weaker with a distance z_0 between the 2DEG and the crystal surface for two reasons: because of the spread of momenta and the spread of frequencies of emitted phonons. Even in high-quality heterostructures, the Landau level broadening is essential.
6. The transition probability between two Landau levels via deformation acoustic phonons is an oscillating function both of the magnetic field B and of the distance z_0 . The magnetic field oscillations are on top of a smooth background of the transition probability which has a subnanosecond peak for intermediate values of B (in GaAs, for fields of the order of 1 T) and decreases as a fourth power of B for large B . For vanishing fields, selection rules force the transition probability to fall to zero.
7. In quantizing magnetic fields, inter Landau level electron transitions in the 2DEG via piezoelectric acoustic phonon interaction suppressed with respect to the deformation interaction mechanism.
8. Acoustic energy flux of ballistic cyclotron phonons emitted from the 2DEG in a normal quantizing magnetic field is concentrated in a narrow cone around the magnetic field. The interface affects essentially both the intensity and composition of the emitted phonon field so on the sample reverse face, the detector records an *interference* field of longitudinal LA phonons and a *conversion* field of transverse TA phonons.

9. Exponential suppression of emission of cyclotron surface acoustic SA phonons occurs in a wide range of the magnetic field variation, $\hbar\omega_B \gg 2mc_R^2$ (ω_B is the cyclotron frequency, m_e is the electron mass and c_R is the velocity of surface waves). So cooling of the heated 2DEG is only at the expense of emission of bulk LA and TA phonons.
10. An allowance for the polar optical PO phonon dispersion and the Landau level broadening yield a finite relaxation rate associated with one-phonon emission. Immediately below the PO phonon energy, $\hbar\omega_{LO}$, the PO phonon dispersion contribution give rise to a very sharp peak with peak value approximately 0.17 fs^{-1} . The Landau level broadening contribution has a rather broad peak with relatively lower peak value. Within an energy range of the order of $\hbar\sqrt{\omega_B/\tau}$ (τ is a relaxation time deduced from the mobility.), the one-phonon relaxation rate exceeds 1 ps^{-1} . Relaxation via surface SO phonon emission mechanism at least by an order is weaker than via bulk phonons.
11. The two-phonon emission is a controlling relaxation mechanism above $\hbar\omega_{PO}$. For energies $\Delta\hbar\omega_B$ immediately above $\hbar\omega_{PO}$, PO+DA phonon relaxation rate increases as a fifth power in the magnetic field B . At energy separations of the order of sa_B^{-1} (s is the sound velocity, a_B is the magnetic length), PO+DA phonon emission provides a mechanism of subpicosecond relaxation. At higher B , the two-phonon relaxation peak decreases linearly in B and within a wide energy range of the order of $\hbar\omega_B$, subnanosecond relaxation can be achieved.
12. Inter edge state relaxation due to acoustic phonon scattering is strongly suppressed at low temperatures in comparison with short- and long-range impurity scattering since only phonons with frequencies above some threshold can cause transitions.
13. At low temperatures emission of ballistic acoustic phonons (due to deformation and piezoelectric interactions) at inter edge state transitions is predominantly concentrated within a narrow cone around the direction of edge state propagation while at high temperatures – around the magnetic field

normal to the electron plane. The emission intensity decreases with decreasing filling of the Fermi level. This diminution is exponential at low temperatures.

14. In contrast to the bulk Landau state, relative contributions of piezoelectric and deformation interactions depend on the magnetic field, electron temperature, and on the shape of the confining potential. At low temperatures and for the non-smooth confining potential, DA interaction suppressed with respect to PA while for the smooth potential as well as for both cases at high temperatures, DA and PA interactions give roughly the same contribution to the emitted phonon field.
15. Polar optical phonon emission provides a picosecond edge state relaxation for a test electron in quantum wires. The scattering rate as functions of the electron initial energy has a peak for magnetic fields not far from the resonance field while for lower fields, the scattering rate shows a monotonous increase in energy.
16. Our theory of the Auger up-conversion in a 2DEG in a normal quantizing magnetic field provides an understanding of the up-conversion observed in magneto-luminescence of one-side modulation doped GaAs/AlGaAs quantum wells [55], in particular, its dependence on the excitation power and the magnetic field.
17. According to our theory of the magneto-transport in a non-planar 2DEG, the system satisfies the Poisson equation in which a line charges develop at the magnetic/non-magnetic field interface. The magneto-resistance calculated across the facet and in planar regions of the 2DEG explains the main features of the magnetic field dependencies observed in the experiment [59, 60].

1.5 Approbation of the work

The results of the investigation presented in the dissertation have been reported and discussed at the following conferences, schools, and seminars:

- 1996 Seminar, Institute for Theoretical Physics, University of Regensburg, Germany
- 1996 12th International Conference "on the Application of High Magnetic Fields", Würzburg, Germany
- 1996 9th International Conference on "Superlattices, Microstructures, and Microdevices, July, 14-19 1996, Liège, Belgium.
- 1996 Research Workshop on Condensed Matter Physics, ICTP, Italy
- 1996 Seminar, Department of Condensed Matter Theory, University of Antwerp, Belgium
- 1995 Research Workshop on Condensed Matter Physics, ICTP, Italy
- 1993 Winter school, University of Wroclaw, Poland
- 1992 NATO ASI, Ultrashort Processes in, Lucca, Italy
- 1992 Seminar, Institute for Theoretical Physics, University of Regensburg, Germany
- 1993 13th General Conference of Condensed Matter Division, European Physical Society, Regensburg, Germany
- 1989 14th All-Union Conference on "Theory of Semiconductors", Donetsk, The Ukraine
- 1988 Seminar, Institute of Physical Investigations, Ashtarak, Armenia
- 1988 Seminar, Landau Institute for Theoretical Physics, Institute of Solid State Physics, and Institute of Microelectronics Technology and High Purity Materials, Chernogolovka, Moscow district, Russia
- 1987 All-Union Conference on "Non-classical crystals", Sevan, Armenia

1.6 Structure and volume of the dissertation

The dissertation is presented on 227 pages including 41 figures and 5 tables. It consists of 7 Chapters, the Summary, 3 Appendixes, and the Bibliography of 327 names.

Chapter 2

Electron-optical phonon bound states

2.1 Introduction

Over a long period of time polarons, elementary excitations in the electron+phonon system, have been extensively studied both theoretically and experimentally in polar semiconductors and ionic crystals [68, 69, 70]. Recent rapid developments in the semiconductor nanotechnology have made it possible to create nanosystems of reduced dimensionality and have caused growing interest in polaron effects in such nanosystems, particularly in the 2DEG exposed to a normal quantizing external magnetic field. In such systems, due to the combined effect of the spatial confinement and Landau quantization, the electron energy becomes quantized into a series of completely discrete Landau levels with an infinite degeneracy. Interaction of such electrons with polar optical phonons leads to a formation of 2D magneto-polarons. Properties of the 2D magneto-polarons strongly depend on energy ranges considered in the exact spectrum and on a density of states on a Landau level. As far as in the 2DEG the density of states on the bottom of Landau band is stronger than in massive samples, it changes from square-root singularity to the delta-function, then the polaron binding energies and cyclotron resonance peaks should be greater and clearer for the 2DEG than in bulk samples. One can expect also qualitatively new effects in the 2D magneto-polaron spectrum.

Studies of the magneto-polaron problem in massive samples (see reviews [71, 72]) have shown that despite to the weak electron-optical phonon coupling, α , branches of the magneto-polaron spectrum can be classified into three groups according to the single-phonon states in the magneto-polaron, *i.e.* according to the effective number, N , of phonons contributing to the magneto-polaron. The first group includes states with $N \sim \alpha$. The exact spectrum of these branches differs from priming one only by a simple shift of the bottom of Landau band and by a polaron renormalization of the electron effective mass. Both these effects are of the order of α . The second and third groups are hybrid and bound states of electrons and phonons. For these states we have $N \approx 1/2$ and $N \approx 1$, respectively. Peculiarities of the polaron spectrum near the threshold of an optical phonon emission are responsible for existence of these two groups. These threshold non-analyticities of the spectrum are not connected with particular models but have an universal character [73]. For instance, the non-analyticity of the phonon spectrum near the disintegration threshold of an optical phonon into two acoustic phonons leads to the formation of the hybrid and bound states of the optical and acoustic phonons [74, 38]. Notice that for the formation of the hybrid states, a resonance situation is necessary.

The problem of calculation of the electron and optical phonon hybrid state spectrum (the spectrum of the resonance magneto-polaron) has been arisen in connection with experiments of the inter-band magneto-absorption and of the cyclotron resonance [75, 76], in which a splitting of the absorption peak near the resonance $\omega_B = \omega_0$ has been observed (ω_B and ω_0 are the cyclotron and the longitudinal optical LO phonon frequencies, respectively). The first theoretical studies of the resonance magneto-polaron spectrum have been based on the single-phonon model, in which only no-phonon and one-phonon states have been taking into account. It has been shown [77, 78, 79] that if no interaction is taken into account, two terms of the electron+phonon system (the first is the electron in the Landau level $l + 1$, the second is the electron in the level l and one LO phonon) are intersected at the resonance. Switching on the electron-phonon interaction takes off the degeneracy and leads to the splitting of the absorption peak which is of the order of $\alpha^{3/2}\hbar\omega_0$. The above peak, as distinct from the peak below, is

smearred by the electron-phonon interaction. At present the resonant magneto-polaron effect is well studied in massive samples [80, 81] and is an unique tool to study the electron-phonon interaction.

In the last years in view of its importance, the resonant magneto-polaron in the 2D nanosystems has attracted considerable attention. Theoretical investigations of the problem show [82, 83, 84, 85] that electron-phonon interaction in the 2D systems is stronger than in the massive samples. There are two reasons to account for such situation. The first is, *ut sup*, the singularity of the density of states on a Landau level is stronger for 2D electrons than that of in the bulk samples. The second is that the presence of interfaces separating different materials in layered nanostructures violates the translation invariance in the growing direction. Hence, in acts of electron-phonon interaction, phonon modes with any value of the momentum component in that dimension can take part. Such reinforcement of electron-phonon interaction leads to the 2D magneto-phonon resonance with the characteristic binding energy scale $\alpha^{1/2}\hbar\omega_0$ which is for $\alpha \ll 1$ essentially greater than the analogous scale $\alpha^{3/2}\hbar\omega_0$ in the massive samples. Moreover, the branches of the spectrum are rigorously stationary both above and below the phonon emission threshold so that two infinitely narrow peaks correspond them in the absorption spectrum.

Recently the 2D resonance magneto-polaron effect has been observed in the cyclotron resonance experiments in electron inversion layers on InSb [86], accumulation layers on HgCdTe [87], and in II-IV CdTe/CdMgTe quantum wells [88], as well as in GaAs/AlGaAs heterostructures and quantum wells [89, 90, 91, 92]. Analysis of experimental results [93] shows that the 2D resonance magneto-polaron effect is approximately by 3 – 6 times stronger than that of for massive samples which is in good agreement with the theoretical calculations [82, 84].

The characteristic feature of the resonance magneto-polaron is that the number of hybrid states in the exact spectrum do not exceed the number of states in the priming spectrum of the electron+phonon system. However, further theoretical developments in the problem of the magneto-polaron have shown that the exact spectrum near the LO phonon emission threshold can be considerably richer [94]. When the magnetic field decreases or increases, the resonance condition ceases to be fulfilled and, one would think that the hybrid states should be

transformed into the usual magneto-polaron states. As a matter of fact it does not take place. In the exact spectrum of the 3D magneto-polaron in the energy range of the order of $W_{3D} = \alpha^2 \hbar \omega_0$ below the threshold $\varepsilon_n = E_n + \hbar \omega_0$ there appear new branches of the electron+phonon system (E_n is the electron priming energy, n is the Landau index.). These terms are impossible to obtain in the framework of the single-phonon model which is equivalent to account for only the simplest diagram of the electron mass operator expanded in a power series in the electron-phonon interaction coupling constant. Moreover, the analysis of the perturbation theory shows [95] that despite to the small coupling constant, the sum of the perturbation theory series diverges in the energy range $|\varepsilon - \varepsilon_n| \lesssim W_{3D}$ and it nowise is connected with the resonance $\omega_B = \omega_0$. To find the exact spectrum in this energy range, it is necessary to sum infinite number of diagrams for the mass operator, or that is the same, to solve an integral equation for the electron-phonon vertex [96]. When this procedure has been explicitly completed by Y B Levinson [94], it has become clear that in the exact spectrum of the electron+phonon system there exists an infinite sequence of the electron and phonon bound states with the LO phonon emission threshold as a limit below. The maximum distance between two neighboring terms is of the order of W_{3D} for $\omega_B \sim \omega_0$ even if it depends on the magnetic field. The bound states ought to realize as a local lattice perturbation arisen at the center of the cyclotron orbit.

It was natural to expect that the bound states will become apparent in the cyclotron phonon resonance spectrum. The cyclotron phonon resonance has been predicted theoretically by F G Bass and Y B Levinson [97] (see also reviews [98, 99]). It is observed in semiconductors as a result of optical transitions of an electron from one Landau level to another accompanied by the emission or absorption of an optical LO phonon. Actuality of the cyclotron phonon resonance has been verified experimentally in the electromagnetic absorption [100]. The cyclotron phonon resonance phenomenon would be combination of two processes, of the cyclotron resonance observed at the frequency of electromagnetic radiation ν divisible by ω_B and of the Gurevich-Firsov magneto-phonon resonance [101, 102], coming at the magnetic fields for which LO phonon frequency ω_0 is divisible to ω_B . According to the simplest ideas based on perturbation theory [97, 103], the cyclotron phonon resonance absorption peak corresponding to the LO phonon

emission should be observed for photons of energies $\hbar\nu = E_n - E_{n'} + \hbar\omega_{LO}$. A more rigorous analysis [104] has shown that the cyclotron phonon resonance peak should have a fine structure due to appearance of the bound states of an electron and a newly created LO phonon. In bulk samples, the binding energies W and oscillatory strengths f of these states are very small: in magnetic fields such that $\omega_B \sim \omega_0$ we have $W \sim W_{3D}$ and $f \sim \alpha^2$. In the case of n -type InSb this gives $W \approx 0.01$ meV in a field $B = 3.5$ T. This makes hard for the experimental resolution of the bound states in the cyclotron phonon resonance peaks. The revealing of the bound states in massive samples is conjugated by additional difficulties for following reasons. In the simplest case, *e.g.*, the bound states could be detected in the light absorption at the photon energy $\hbar\nu = \hbar\omega_0 - W$ (the electron transitions absent; $n = n' = 0$) [105]. However, in this case bound states lie below the threshold and their observation is hindered by the strong lattice reflection in the energy range between the longitudinal and transverse optical phonon energies. The absorption spectrum seemed more convenient to study when $n \neq 0$ at the photon energy $\hbar\nu = \hbar\omega_B + \hbar\omega_0 - W$. This energy range of the spectrum, however, lays upon continuum of the electron+phonon states so that there cannot exist rigorously stationary bound states.

Taking into account the situation described above for the magneto-polaron problem, particularly, the transformations in the resonant magneto-polaron effect at the dimensional reduction from 3D to 2D, one can expect that the environmental factors for the electron-phonon bound state creation and their experimental observation in the 2DEG should be more favorably inclined.

Subject of this chapter is the bound states of the electron and LO phonon in the 2D nanostructures exposed to the quantizing magnetic field normal to the electron sheet. It will be shown that in the vicinity of the LO phonon emission "threshold" ε_n , the spectrum of the magneto-polaron is determined by an infinite sequence of the bound states coagulated to the "threshold" having it as a limit both above and below from it [39]. (In the 2DEG there is no continuum in the spectrum of the electron+phonon system, and therefore in this case, the "threshold" has no strict sense. To stress this fact, the inverted commas are used.) These bound states are always rigorously stationary and are manifested in the cyclotron phonon resonance spectrum as two groups of narrow peaks located

above and below the "threshold" on the distance of the order of $W_{2D} = \alpha \hbar \omega_0$ [40].

Existence of the bound states is determined by the competition of the kinetic energy of electrons and optical phonons, and their interaction energy. Therefore, the character of coupling and the energetic scale of the spectrum strongly depend on the localization extend of electrons and phonons. In 2D nanostructures besides the electron localization effect, there are certain special features associated with the optical phonon localization. Two situations are discussed below: electrons in an isolated quantum well located deep inside a sample and electrons at a heterojunction between two semiconductors. Low-momentum LO phonons do not usually penetrate from one material to another and, therefore, electrons in a quantum well or at a heterojunction interact solely with LO phonons in the semiconductor where they are located. Further these bulk-like polar LO phonons we denote as PO phonons. In addition to the bulk-like PO phonons, there exist also surface SO phonons with an electric field concentrated on both sides near an interface separating different materials. Recently polaron effect with such SO phonons in quantum wells and heterojunctions have been considered theoretically in several papers [106, 107, 108, 109, 110, 111, 40, 112, 113, 114]. It is obtained that the SO phonon contribution to the energy and effective mass is essential. In the recent magneto-phonon resonance experiment [115], the observed states have been interpreted as resonance 2D magneto-polarons with SO phonons [116]. Therefore, one can expect that SO phonons will also play an important role in the formation of the electron-phonon bound states. In the case of a heterojunction the SO phonons do not exhibit dispersion and, therefore, they behave in the same way as LO phonons. On the other hand, the SO phonons in a quantum well have a strong linear dispersion which smears out the threshold singularity. Such SO phonons are ignored in this work.

The energy levels of the considered system are shown on Fig. 2.1. The energy is reckoned from the lower electron level, whose height above the bottom is $\hbar\omega_d + \hbar\omega_B/2$, $\hbar\omega_d$ is the energy scale in the growing direction. The dashed line shows the "threshold" $\varepsilon_n = E_n + \hbar\omega_0$ referred to the Landau level n , near which the bound states of interest to us are located.

Following assumptions have been done in calculations of the bound state

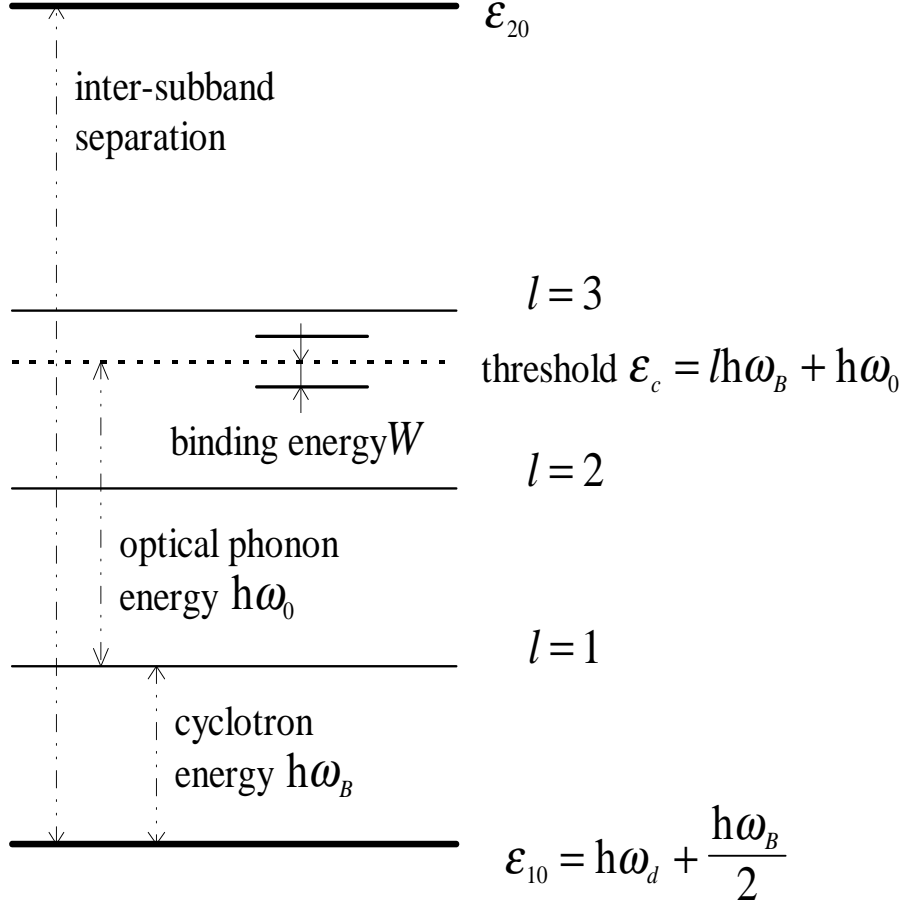


Figure 2.1: Energy levels $\epsilon_{nl} = \epsilon_n + (l + 1/2)\hbar\omega_B$ in the 2DEG exposed to the quantizing magnetic field normal to the electron sheet. ϵ_n is the energy of subband n .

spectrum:

- i) only the polar electron-phonon interaction is considered and the priming electron-phonon coupling constant is assumed to be small, $\alpha \ll 1$,
- ii) optical phonons have no dispersion, $\omega(\mathbf{q}) = \omega_0$,
- iii) crystal temperature is low enough, $T \ll \hbar\omega_0$ so that the phonon absorption processes, proportional to $\exp(-\hbar\omega_0/T)$, can be neglected (The units are used such that the Boltzmann constant $k_B = 1$.),

- iv) concentration of electrons is small so that their influence on phonons as well as interaction between them can be neglected,
- v) interaction of electrons with impurities and acoustic phonons is absent,
- vi) electrons are confined in a potential well with infinitely high walls, the well is also narrow enough so that spatial quantization energy scale is the largest parameter of the problem, *i.e.* the intersubband separation $\Delta\varepsilon_d \sim \hbar\omega_d \gg \hbar\omega_B, \hbar\omega_0$.

The present chapter is organized as follows. In the next section the threshold behavior of the magneto-polaron spectrum is analyzed and the integral equation for the electron-phonon scattering amplitude is derived from which we obtain the bound state spectrum. In Sec. 2.3 the absorption coefficient on these bound state is studied. The allowance for the presence of bulk and surface optical phonons is made. The actual calculations of the bound state binding energies and oscillator strengths are carried out in Sec. 2.4. Our conclusions and numerical estimates are presented in Sec. 2.5.

2.2 The 2D magneto-polaron spectrum

2.2.1 "Threshold" behavior of the polaron spectrum

The spectrum of two-particle elementary excitations in the electron-phonon system is determined by the poles of scattering amplitude Σ in the total energy parameter ε . Because the number of phonons is not conserved, the spectrum obtained from the poles of Σ and of the single-particle Green function are the same. The calculation of Σ by means of the perturbation theory cannot be acceptable since in the energy range of interest to us, $\varepsilon \approx \varepsilon_n$, the series of the perturbation theory stops to converge. In terms of the diagram technique, the diagrams with one phonon and one electron intersections are responsible for this divergence. Such diagram correspond to the processes in which phonons are almost real [117]. Some diagrams for the amplitude Σ with such dangerous intersections are shown in Fig. 2.2. It is seen that the number of the dangerous intersections increases in the diagram order. Direct calculations of these diagrams show that

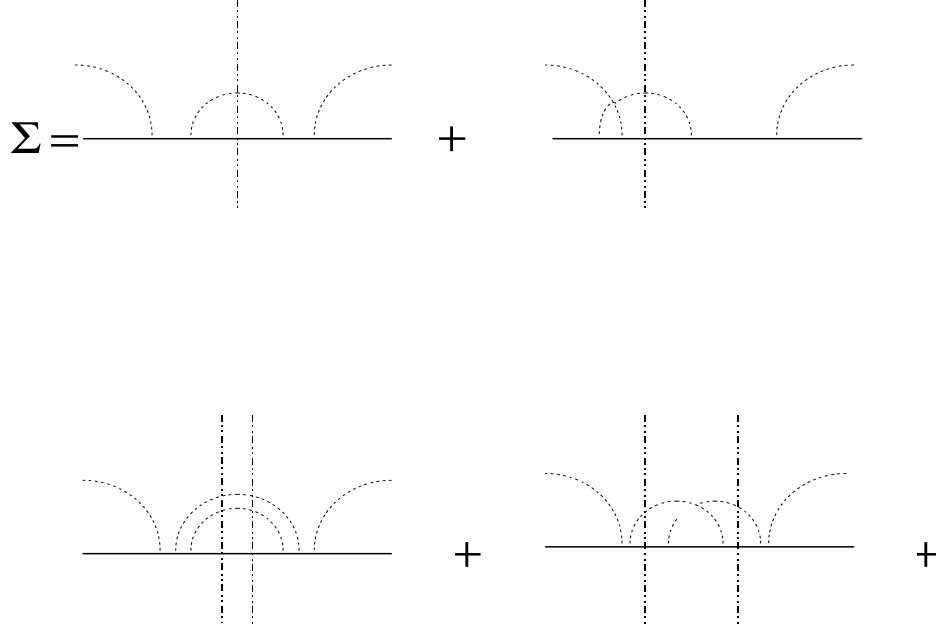


Figure 2.2: Simplest diagrams for the electron-phonon scattering amplitude Σ with dangerous intersections in one electron and one phonon lines.

the perturbation theory is inapplicable in the energy range $|\varepsilon - \varepsilon_n| \sim \alpha \hbar \omega_0$ where both diagrams with and without intersecting phonon lines (Fig. 2.2) become essential. Contributions of all diagrams with dangerous intersections tend to infinity when $\varepsilon \rightarrow \varepsilon_n$ and the growing velocity is proportional to the number of dangerous intersections in the diagram. Thus, to find the exact spectrum of the system in the region $|\varepsilon - \varepsilon_n| \sim \alpha \hbar \omega_0$, the whole series of the perturbation theory should be summed. This leads to an integral equation for the electron-phonon scattering amplitude Σ drawn on Fig. 2.3.

2.2.2 Integral equation for the electron-phonon scattering amplitude and bound states

This equation is written in the gauge invariant diagram technique [118], therefore only Landau index s is used for the electrons (solid lines) while the gauge non-invariant quantum number m of the spatial quantization is absent. The exact electron Green function, G is diagonal in s [118, 119, 120] but G is not diagonal

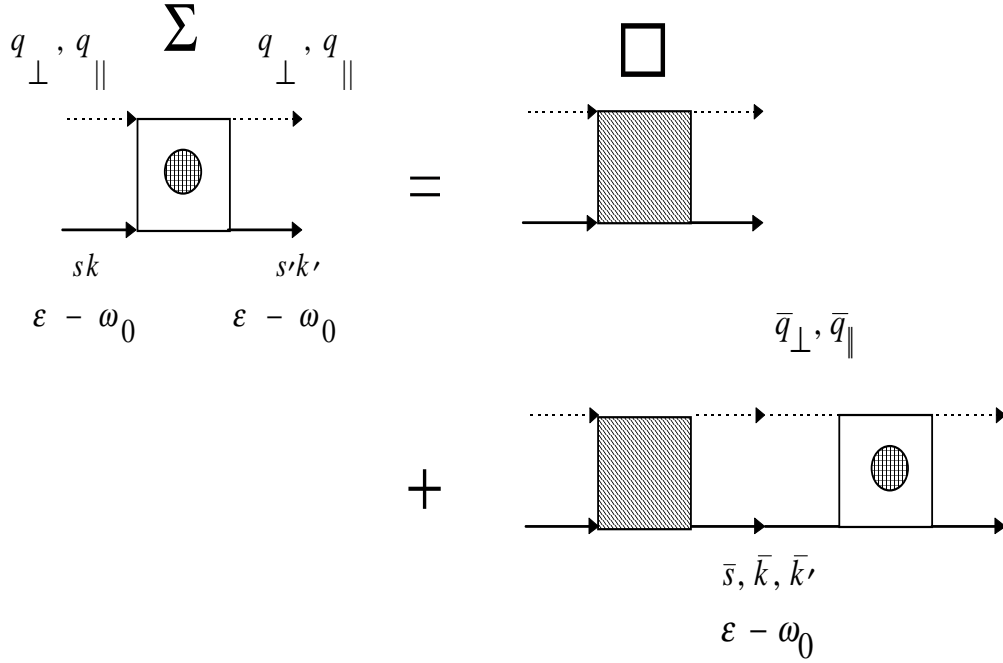


Figure 2.3: Integral equation for the scattering amplitude Σ of an electron by a phonon.

in m because lack of the translation invariance in the growth z -direction. The assumption $\Delta E_d \gg \hbar\omega_B, \hbar\omega_0$ permits, however, to neglect the off-diagonal elements of $G_{mm'}$ which simplifies essentially the integral equation for Σ . As far as the bound states are sought in the energy range near the "threshold" then the energetic parameter of the Green function is $\varepsilon_n - \hbar\omega_0$ in the dangerous intersection in the second term of the right-hand side of the equation in Fig. 2.3. It lies far from the "threshold" where the perturbation theory is valid. Therefore, the function G can be taken without allowance for the interaction with the phonons, and only the term $\bar{m} = 1$ is to be retained in the summation over \bar{m} . All the foregoing allows us to put everywhere $m = 1$ (and omit this index hereafter) so that

$$G_s(\varepsilon) = (\varepsilon - s\hbar\omega_B + i0)^{-1}. \quad (2.1)$$

By force of the assumption of the electron concentration smallness, all electron Green functions are retarded. For this reason as well as because system temperature is low, the renormalization of the phonon Green functions can be also neglected. Then the following expression corresponds to the phonon propagator D (the dashed lines)

$$D(\omega, \mathbf{q}) = \hbar^{-1} B(\mathbf{q}) \left[(\omega - \omega_0 + i0)^{-1} - (\omega + \omega_0 - i0)^{-1} \right]. \quad (2.2)$$

where $B(\mathbf{q})$ is the modulus squared of the electron-phonon matrix element. The longitudinal, q_{\parallel} and the transverse, q_{\perp} phonon momenta are shown separately in Fig. 2.3. It is convenient previously to carry out integration over the phonon energetic parameter ω , using the formula

$$\int \frac{d\omega}{2\pi} i D(\omega, \mathbf{q}) F(\omega) = B(\mathbf{q}) F(\omega_0 - i0) \quad (2.3)$$

where $F(\omega)$ is an analytical function for $\text{Im } \omega < 0$. Now it is clear that all ω ought to replace to ω_0 in all G so that only the integration over the phonon momenta q_{\parallel} and q_{\perp} as well the factor $B(\mathbf{q})$ correspond to all internal phonon lines. For the more important polar electron-phonon interaction we obtain

$$B(\mathbf{q}) = B_0 \Phi(\mathbf{q}_{\perp}, q_{\parallel}), \quad B_0 = \pi \alpha v_0^2, \quad v_0 = \frac{\hbar p_0}{m_c}, \quad \hbar p_0 = \sqrt{2m_c \hbar \omega_0}, \quad (2.4)$$

where m_c is the electron effective mass. The factor B_0 and the form factor $\Phi(\mathbf{q}_{\perp}, q_{\parallel})$ depend on the nature of the PO phonon localization. For the bulk polar optical PO phonon α is the usual Frölich coupling constant [121]

$$\alpha_{PO} = \frac{e^2}{\bar{\kappa}_{PO} v_{PO}}, \quad \bar{\kappa}_{PO}^{-1} = \kappa_{\infty}^{-1} - \kappa_0^{-1}, \quad \kappa_{\infty} = \frac{\omega_{TO}^2}{\omega_{PO}^2} \kappa_0, \quad (2.5)$$

where ω_{PO} and ω_{TO} are frequencies of the longitudinal and transverse optical phonons, κ_{∞} and κ_0 are the high and low frequency dielectric permittivities. In this case the form factor $\Phi(\mathbf{q}_{\perp}, q_{\parallel})$ is given by

$$\Phi(\mathbf{q}_{\perp}, q_{\parallel}) = \frac{p_{PO}}{q_{\perp}^2 + q_{\parallel}^2} \left| \int_0^d dz |\psi(z)|^2 \varphi_{q_{\parallel}}(z) \right|^2 \quad (2.6)$$

where ψ and φ are the wave functions of the electron and PO phonon for motion along z -direction.

For the surface SO phonons, the electron-phonon interaction coupling constant α_{SO} in a single heterostructure is defined on the analogy of the Frölich constant

$$\alpha_{SO} = \frac{e^2}{\bar{\kappa}_{SO} v_{SO}} \quad (2.7)$$

where $\bar{\kappa}_{SO}$ has the form [106, 40, 112]

$$\bar{\kappa}_{SO} = \frac{\omega_{SO}^2}{2} \sum_{\nu=1}^2 \kappa_{\infty\nu} \frac{\omega_{PO\nu}^2 - \omega_{TO\nu}^2}{(\omega_{SO}^2 - \omega_{TO\nu}^2)^2} \quad (2.8)$$

Here index $\nu = 1, 2$ denotes the different media in contact at the heteroface. The frequency of the interface SO phonon is the root of the following equation [122, 123]

$$\sum_{\nu=1}^2 \epsilon_{\nu}(\omega) = 0, \quad \epsilon_{\nu}(\omega) = \kappa_{\infty\nu} \frac{\omega^2 - \omega_{LO\nu}^2}{\omega^2 - \omega_{TO\nu}^2} \quad (2.9)$$

where ϵ_{ν} is the dielectric function of the medium ν . In this case, the form factor $\Phi(\mathbf{q}_{\perp})$ is given by

$$\Phi(\mathbf{q}_{\perp}) = \frac{p_{SO}}{2q_{\perp}} \left| \int_0^d dz |\psi(z)|^2 \exp(-q_{\perp} z) \right|^2 \quad (2.10)$$

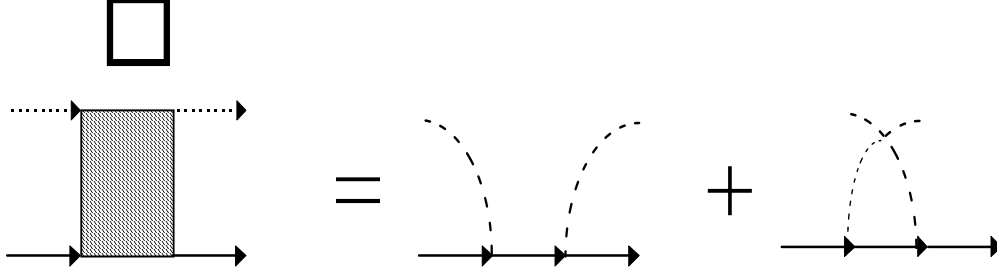
In formulas (2.5)-(2.10), v_{PO} , v_{SO} and p_{PO} , p_{SO} are defined in the same way as v_0 and p_0 in the formula (2.4). Below α and ω_0 will denote either α_{PO} and ω_{PO} or α_{SO} and ω_{SO} .

In Fig. 2.3 the shaded box shows the amplitude \square which has no dangerous intersections with one electron and one phonon lines, *i.e.* \square is regular at $\varepsilon \rightarrow \varepsilon_n$, and therefore, can be calculated using the expansion in coupling constant α . The irreducible amplitude \square can have an intersection in one electron line, therefore in the lowest order in α , the equation shown in Fig. 2.4 takes place. The point corresponds to a gauge invariant part of the electron-phonon interaction vertex:

$$\Lambda_{ss'}(\mathbf{q}_{\perp}) = e^{-i\phi(s-s')} Q_{ss'}(t), \quad t = \frac{1}{2} a_B^2 q_{\perp}^2, \quad a_B = \sqrt{\frac{\hbar c}{eB}}, \quad (2.11)$$

$$Q_{ss'}(t) = \sqrt{\frac{s!}{s'!}} t^{\frac{s-s'}{2}} e^{-\frac{t}{2}} L_s^{s-s'}(t) = (-1)^{s-s'} Q_{s's}(t) \quad (2.12)$$

where $L_s^{s-s'}(t)$ are the associated Laguerre polynomials and ϕ is the polar angle of the vector \mathbf{q}_{\perp} .

Figure 2.4: Irreducible electron-phonon scattering amplitude \square .

Since we are interested in the spectrum region near the "threshold" referred to the Landau level n then it is possible to avoid of the summation over the Landau quantum number \bar{s} in the dangerous intersection in the second term of the right-hand side of the equation for Σ . In this energy region $\varepsilon \approx \varepsilon_n$, only the non-analytical contributions from G are essential in the sum over quantum numbers of the internal electron lines. Thus in the equation for Σ only the term $\bar{s} = n$ should be retained in the sum over \bar{s} . For the same reason, in the equation for Σ in all electron external lines, we ought to put $s = s' = n$. Notice that in the gauge invariant diagram technique it is possible to choose for Σ and \square "four-tails" such a definition that these quantities will depend only on the difference $\phi - \phi'$ of the polar angles of the vectors \mathbf{q}_\perp and \mathbf{q}'_\perp . Therefore, expanding Σ and \square into the Fourier series, the angle variables l in the equation for Σ can be separated. Then the Fourier components

$$\Sigma_n^l(\varepsilon; t, t'; q_\parallel, q'_\parallel) = \int_0^{2\pi} \frac{d\phi}{2\pi} e^{-il(\phi - \phi')} \Sigma_n^l(\varepsilon; \mathbf{q}_\perp, \mathbf{q}'_\perp; q_\parallel, q'_\parallel) \exp\left\{\frac{ia_B^2}{2}[\mathbf{q}_\perp \mathbf{q}'_\perp]\right\} \quad (2.13)$$

with $l = 0, \pm 1, \pm 2, \dots$ will satisfy the independent equations

$$\Sigma_n^l(\varepsilon; t, t'; q_\parallel, q'_\parallel) = \square_n^l(t, t') + \tilde{M}_n(\varepsilon) \sum_{\bar{q}_\parallel} \int_0^\infty d\bar{t} \square_n^l(t\bar{t}) \Phi(t, \bar{q}_\parallel) \Sigma_n^l(\varepsilon; \bar{t}, t'; \bar{q}_\parallel, q_\parallel) \quad (2.14)$$

where \square_n^l are the Fourier components the of the kernel \square_n defined by analogy with Σ_n^l . The appearance of the phase factor $\exp\{\frac{ia_B^2}{2}[\mathbf{q}_\perp \mathbf{q}'_\perp]\}$ in Eq. (2.13) is connected with use of the gauge invariant diagram technique and is the result of the integration over gauge non-invariant quantum number k in usual diagram technique. The square brackets in this factor mean the longitudinal (along

the magnetic field \mathbf{B}) component of the vector product. The quantity $\tilde{M}(\varepsilon)$ in Eq. (2.14) is proportional to the priming electron-phonon interaction coupling constant α and the density of states on the Landau level

$$\tilde{M}_n(\varepsilon) = -\frac{\alpha\omega_B\omega_0}{\varepsilon - \varepsilon_n + i0}, \quad (2.15)$$

consequently, it determines the effective electron-phonon interaction in the region near the "threshold".

It is seen that the integral equation (2.14) is in two variables, t and q_{\parallel} . Moreover, the electron-phonon interaction vertex part Φ , arising from the integration over z coordinate of the electron-phonon interaction nodule and depending only on the phonon momenta, enters in the equation in non-explicit form. (Recall that based on the assumption $\Delta E_d \gg \omega_B, \omega_0$, we put $m = 1$ in all lines.) This vertex part with an external phonon line, however, enter as a factor into the amplitudes Σ and \square (the summation over m is absent in one electron line of the vertex in order to catch on the vertex with internal lines). Therefore, the integral equation (2.14) for the amplitude Σ_n^l can be simplified by symmetrizing it and averaging over q_{\parallel} . We introduce for this purpose the averaged form factors

$$\hat{\Phi}(t) = \sum_{q_{\parallel}} \Phi(\mathbf{q}_{\perp}, q_{\parallel}). \quad (2.16)$$

and new amplitudes

$$\hat{\Sigma}_n^l(\varepsilon; t, t') = [\hat{\Phi}(t)\hat{\Phi}(t')]^{-1/2} \sum_{q_{\parallel}, q'_{\parallel}} \Phi(t, q_{\parallel})\Phi(t', q'_{\parallel})\Sigma_n^l(\varepsilon; t, t'; q_{\parallel}, q'_{\parallel}), \quad (2.17)$$

$$\hat{\square}_n^l(t, t') = [\hat{\Phi}(t)\hat{\Phi}(t')]^{1/2}\square_n^l(t, t') \quad (2.18)$$

Transforming to the dimensionless quantities

$$R_n^l(\varepsilon; t, t') = -\omega_0\hat{\Sigma}_n^l(\varepsilon; t, t'), \quad K_n^l(t, t') = -\omega_0\hat{\square}_n^l(t, t'), \quad \lambda_l(\varepsilon) = -\omega_0^{-1}\tilde{M}_l(\varepsilon) \quad (2.19)$$

we obtain the final integral equation

$$R_l^l(\varepsilon; t, t') = K_l^l(t, t') + \lambda_l(\varepsilon) \int_0^\infty d\bar{t} K_l^l(t, \bar{t}) R_l^l(\varepsilon; \bar{t}, t'). \quad (2.20)$$

Thus, R is the Fredholm resolvent of the kernel K , which we now write out in explicit form

$$\begin{aligned} K_n^l(t, t') &= [\hat{\Phi}(t)\hat{\Phi}(t')]^{1/2} \sum_{s=0}^{\infty} Q_{ns}(t)Q_{ns}(t') \\ &\times \left[\frac{\sigma}{\sigma + s - n} J_{l+s-2n}(2\sqrt{tt'}) - \frac{\sigma}{\sigma - s + n} \delta_{ls} \right]. \end{aligned} \quad (2.21)$$

Here the J_l is the Bessel function, $\sigma = \omega_{LO}/\omega_B$, and the two terms in the square brackets are connected with the two terms in Fig. 2.4.

Now it is clear that the scattering amplitude Σ has a pole in ε if λ_l coincides with an eigenvalue of the kernel K_l^l . In other words, the equation for the energies of the bound states of the electron and optical phonon is

$$\lambda_l(\varepsilon) = \lambda_{n,r}^l, \quad r = 1, 2, 3, \dots \quad (2.22)$$

where the subscript r numbers different eigenvalues $\lambda_{n,r}^l$ of the kernel K_n^l . It follows from Eq. 2.22 that the energies of the bound states are

$$\varepsilon_{n,r}^l = \varepsilon_n - \frac{\alpha\omega_B}{\lambda_{n,r}^l} \equiv \varepsilon_n - W_{n,r}^l \quad (2.23)$$

where $W_{n,r}^l$ are binding energies of the bound state referred to the Landau level n . It is seen that for any $n = 1, 2, 3, \dots$, all bound states are rigorously stationary. The bound states are identified by the total angular momentum l of the rotation around \mathbf{B} . It takes both non-negative and negative integer values. For the wealth of the spectrum for a given n and l , participation in the formation of bound states of phonons with any momentum is liable. In the case of a 3D samples, the bound states appeared only below the threshold, for in this case a continuum of two-particle electron+phonon states is located above the threshold. There is no such continuum for the 2D electron systems so that bound states are present both below the "threshold" ($W > 0$) and above it ($W < 0$). This means that the energies of the bound states are determined, according to Eq. 2.23, by eigenvalues $\lambda_{n,r}^l$ of both signs.

2.3 Cyclotron-phonon resonance

In this section, the effect of the electron and optical phonon bound states on the spectrum of the cyclotron phonon resonance in the 2DEG is studied. The cyclotron phonon resonance is observed in semiconductors as a result of optical transitions of an electron from one Landau level to another accompanied by the emission and absorption of an optic phonon. According to the simplest ideas based on the perturbation theory [97, 103], the absorption peaks corresponding

to the emission of the optical phonons should be observed for photons of frequencies $\nu_n = n\omega_B + \omega_0$. The more rigorous analysis [104] shows, however, the cyclotron phonon resonance peaks should have fine structure due to appearance of the bound states of an electron and a newly created optical phonon. Thus, the bound states in the 2DEG should be developed in the absorption spectrum at energies

$$\hbar\nu = \hbar\nu_n - W_{nr}^l, \quad \nu_n = n\omega_B + \omega_0. \quad (2.24)$$

On absorbing a photon of this frequency, the electron is transferred from the initial $s = 0$ Landau level to the $s = n$ level and simultaneously creates the optical phonon which is bound to the electron in the final state.

In calculating the absorption coefficient it is assumed that the temperature and density of the carrier are low enough so that $T \ll W$ and the Fermi energy $\varepsilon_F \ll W$. Therefore before the light absorption, all electrons are in the level $s = 0$. The capacitance of one Landau level allowing for two spin orientations in a magnetic field $B = 5$ T amounts $N_0 = 2.4 \cdot 10^{15} \text{ m}^{-2}$. We assume also that electron transitions occur between the Landau levels corresponding to the lower transverse quantization level, $k = 1$, and the higher transverse quantization levels, $k > 1$ are located so far away that they can be ignored. The thickness of the 2DEG sheet, for which spatial quantization effects become apparent, is so small that the spatial dispersion of the light can be neglected.

2.3.1 Absorption coefficient and bound states

The absorption coefficient can be defined from Maxwell equations as a light energy fraction w at the frequency ν absorbed in the 2DEG in the \mathbf{z} -direction. It is convenient to express the electron current density in Maxwell equations in terms of the photon polarization operator Π . Then using the calculation methods in [124], the fraction w sought for can be represented in the form

$$w^\pm(\nu) = -\frac{4\pi c}{\nu\sqrt{\kappa(\nu)}} \text{Im}\Pi^\pm(\nu), \quad (2.25)$$

$$\Pi^\pm(\nu) = \int dz_1 dz_2 \Pi^\pm(\nu; z_1, z_2) |\psi(z_1)|^2 |\psi(z_2)|^2. \quad (2.26)$$

Here $\Pi^\pm(\nu; z_1, z_2)$ is the photon polarization operator in the coordinate representation. It is assumed that the incident light is along \mathbf{z} -direction and has circular

polarization. The plus and minus signs pertain here to right-hand and left-hand polarization of the light, and $\kappa(\nu)$ is the dielectric permeability of the well walls at the frequency ν . In the diagram technique, the sum of two diagrams in Fig. 2.5 corresponds to the polarization operator $\Pi^\pm(\nu)$. The diagrams consist of electron

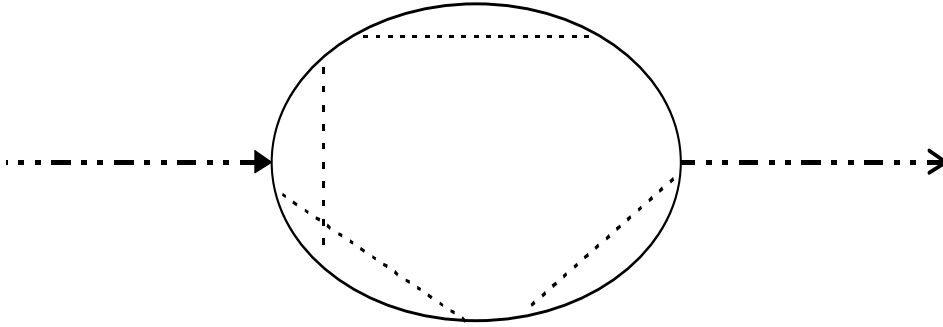


Figure 2.5: Photon polarization operator $\Pi^\pm(\nu)$.

loops with all possible phonon lines and, it is convenient, to consider that all the electron and phonon lines are "bold", *i.e.* the exact electron and phonon Green functions correspond them. Wave lines on this figure are referred to the photon lines. Each electron Green function, in general, is the sum of the retarded and advanced Green functions, $G = G^R + G^A$. However, G^A is finite only for a small range of electronic states, the volume of which is proportional to the electron concentration. If put $G = G^R$ in all lines and to carry out integration over the electron energetic parameter ε , then one can be convinced that $\Pi = 0$ as far as the expression to be integrated is analytical in upper half plane $\text{Im}\varepsilon > 0$. In order to obtain an expression for Π in the lowest order in the electron concentration it is necessary in each diagram to replace G by G^A in one electron line and to replace G by G^R in all remaining lines. The line G^A picked up in this way is referred to the initial electron state in the lowest energy level E_0 and so far as the perturbation theory is valid in this energy range then the free Green function

for G^A can be taken,

$$G_s^A(\varepsilon) = \frac{2\pi a_B^2 N}{\varepsilon - s\hbar\omega_B - i0} \delta_{s0}. \quad (2.27)$$

Here N is the carrier density for 1cm^2 area of the 2DEG plane. Now taking the integral over parameters of the function Eq. (2.27), Π can be represented in the form

$$\Pi^\pm(\nu) = NP^\pm(\nu), \quad (2.28)$$

where the quantity $-iP^\pm(\nu)$ is determined by the sum of diagrams shown in Fig. 2.6. In this figure shaded parts are represented by the compact diagrams

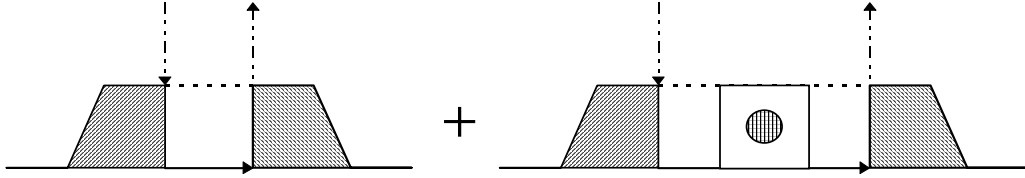


Figure 2.6: Sum of diagrams for the photon polarization operator $-iP^\pm(\nu)$.

without dangerous intersections in one electron and one phonon lines referred to the Landau level n . As far as we are interested in the frequency range $\nu \approx \nu_n$, it is clear that the main contribution to $-iP^\pm(\nu)$ comes from diagrams with dangerous intersections. Therefore in the sum in Fig. 2.6, the diagrams without dangerous intersections giving a smoothly varying contribution in $-iP^\pm(\nu)$ and coinciding with the free electron contribution in the absorption are not depicted.

Now making use of the gradient invariant diagram technique, the contributions of diagrams in Fig. 2.6 can be calculated explicitly. In terms of the scattering amplitude Σ^l with $l = \pm 1$, it gives

$$\Pi^\pm(\nu) = \frac{N}{2} \frac{e^2}{mc^2} \frac{\omega_B \omega_{LO}}{[\omega_0 + (n \mp 1)\omega_B]^2} \left\{ \lambda(\nu) \bar{\Phi}_n + \lambda(\nu)^2 \bar{R}_n^\pm(\nu) \right\}, \quad (2.29)$$

$$\bar{R}_n^\pm(\nu) = \frac{1}{n!} \int_0^\infty dt dt' e^{-(t+t')/2} (tt')^{(n+1)/2} [\hat{\Phi}(t) \hat{\Phi}(t')]^{1/2} R_n^{\pm 1}(\nu; t, t'). \quad (2.30)$$

$$\bar{\Phi}_n = \frac{1}{n!} \int_0^\infty dt e^{-t} t^{n+1} e^{-t} \hat{\Phi}(t). \quad (2.31)$$

Notice that two terms in the figure brackets in Eq. (2.29) are connected with the two terms of Fig. 2.6. Expanding the resolvent R as a sum over the poles, we bring $\bar{R}_n^\pm(\nu)$ to the form

$$\bar{R}_n^\pm(\nu) = - \sum_{r=0}^{\infty} \frac{|d_{nr}^\pm|^2}{\lambda(\nu) - \lambda_{nr}^{\pm 1} + i0}, \quad (2.32)$$

$$d_{nr}^\pm = \frac{1}{\sqrt{n!}} \int_0^\infty dt e^{-t/2} t^{(n+1)/2} \hat{\Phi}(t)^{1/2} \chi_{nr}^{\pm 1}(t), \quad (2.33)$$

where $\chi_{nr}^{\pm 1}(t)$ are the eigenfunctions of the kernel $K_n^{\pm 1}(t, t')$. Now for the absorbed fraction of the radiation energy w , we obtain ultimately

$$w^\pm(\nu) = 2\pi N \frac{e^2}{mc^2} \frac{c}{\sqrt{\kappa(\nu)}} \frac{\omega_B \omega_{LO}}{[\omega_0 + (n \mp 1)\omega_B]^2} \frac{1}{\nu_n} \text{Im} \mathcal{F}_n^\pm(\nu), \quad (2.34)$$

where

$$\mathcal{F}_n^\pm(\nu) = -\lambda(\nu) \sum_{r=0}^{\infty} \frac{\lambda_{nr}^{\pm 1} |d_{nr}^\pm|^2}{\lambda(\nu) - \lambda_{nr}^{\pm 1} + i0}. \quad (2.35)$$

Here we use the completeness of eigenfunctions $\chi_{nr}^{\pm 1}(t)$ and unify both terms in the figure brackets in Eq. (2.29). From Eq. (2.35) we see that for $\nu < \nu_n$, only terms of the sum contribute to $\text{Im} \mathcal{F}$ for which $\lambda_{nr}^{\pm 1} > 0$, and on the contrary, for $\nu > \nu_n$, only the terms, for which $\lambda_{nr}^{\pm 1} < 0$. It is easy to be convinced that $\text{Im} \mathcal{F} = 0$ for $\nu = \nu_n$. Taking the imaginary part of \mathcal{F} and using up the delta-function in ν variable, we obtain the following final formula for the absorption coefficient

$$w^\pm(\nu) = 2\pi N \frac{e^2}{mc^2} \frac{c}{\sqrt{\kappa(\nu_n)}} \sum_{r=0}^{\infty} f_{nr}^\pm \pi \delta(\nu - \nu_n + W_{nr}^{\pm 1}). \quad (2.36)$$

The oscillator strength for the transition to the bound state nr with $l = \pm 1$ is here

$$f_{nr}^\pm = \alpha \frac{\omega_0}{\omega_0 + n\omega_B} \frac{\omega_B \omega_{LO}}{[\omega_0 + (n \mp 1)\omega_B]^2} |d_{nr}^\pm|^2. \quad (2.37)$$

Recall that in Eq. (2.36), $W_{nr}^{\pm 1}$ denote the binding energies of the bound states with $l = \pm 1$, located near the "threshold" $\nu = \nu_n$. So far as for the initial state $l = 0$ then it is seen that the same selection rules as for free electrons are remained for the total momentum l . At the absorption of right-hand polarized light, the bound states with $l = +1$ are manifested while for left-hand polarized light, the

bound states with $l = -1$ are actual. Namely on this ground, one can consider $l < 0$ as a generalization of the Landau quantum number.

Using the identity

$$\sum_{r=0}^{\infty} |d_{nr}^{\pm}|^2 = \bar{\Phi}_n, \quad (2.38)$$

one can find for the total oscillatory strength

$$f_n^{\pm} \equiv \sum_{r=0}^{\infty} f_{nr}^{\pm} = \alpha \frac{\omega_0}{\omega_0 + n\omega_B} \frac{\omega_B \omega_{LO}}{[\omega_0 + (n \mp 1)\omega_B]^2} \bar{\Phi}_n. \quad (2.39)$$

It is seen that at $n = 1$ in the strong magnetic fields, $\omega_B \gg \omega_0$, there is an asymmetry in the absorption with respect to the left- and right-hand polarizations.

Notice that the first term in the figure brackets in Eq. 2.29 corresponds to a perturbation-theory calculation of the absorption and yields a delta-like absorption peak at the "threshold" for $\nu = \nu_n$. Actually, there is no such peak in absorption. It is canceled out when the second term is taken into account so that absorption is concentrated on the bound states below and above the "threshold" $\nu = \nu_n$. In the 3D case, this corresponds to the transformation of the threshold singularity $(\nu - \nu_n)^{-1/2}$, which becomes infinite at the threshold, into the singularity $(\nu - \nu_n)^{1/2}$, which goes to zero [105].

2.4 Binding energies and oscillator strengths

The investigation of the kernel (2.21) cannot be done in general case. Therefore in this section, the actual calculation of the binding energies and of the oscillator strengths are carried out by considering separately the limiting cases of strong and weak magnetic fields, *i.e.* $\omega_B \gg \omega_0$ and $\omega_B \ll \omega_0$.

2.4.1 The averaged form factors

We find first the averaged form factors $\bar{\Phi}$ and $\hat{\Phi}(t)$ for the bulk PO phonons inside quantum wells and in heterostructures as well as for the surface SO phonons created in single heterostructures near interfaces separating different materials. These form factors, just as the electron-phonon interaction coupling constants α , depend on the interaction mechanism and on the nature of the phonon localization. According to the experimental situation, we consider that in the quantum

wells, electrons are confined in the infinitely high quantum well (par example, in the *AlAs/GaAs/AlAs* type quantum wells, the height of the well walls is circa 1500 meV at the same time as the energy of the lowest level of the spatial quantization is around 50 meV). Hence the electron wave functions and energies for an electrons moving along $\mathbf{z} \parallel \mathbf{B}$ -direction are

$$\psi_k(z) = \sqrt{\frac{2}{d}} \sin \frac{\pi k}{d} z, \quad k = 1, 2, 3, \dots, \quad \varepsilon_k = k^2 \hbar \omega_d, \quad \hbar \omega_d = \frac{\pi^2 \hbar^2}{2m_c d^2} \quad (2.40)$$

where d is the width of the well. The bulk-like PO phonons in the quantum wells are confined between well facings [122, 123] and, therefore, their wave functions for the moving along \mathbf{z} are

$$\varphi_{q_{\parallel}}(z) = \sqrt{\frac{2}{d}} \sin q_{\parallel} z, \quad q_{\parallel} = \frac{\pi}{d} j, \quad j = 1, 2, 3, \dots \quad (2.41)$$

In the case of the heterostructure, we use the variation electron wave function for the lowest level of the spatial quantization suggested in [125, 126],

$$\psi(z) = \left(\frac{b^3}{2}\right)^{1/2} z \exp\left(-\frac{bz}{2}\right) \quad (2.42)$$

where the parameter b is determined from the minimum of the total electron energy. The average distance \bar{z} of electrons from the heteroface is $\bar{z} = 3/b$.

In this case, the bulk PO phonon motion along \mathbf{z} is confined from one side by the heteroface (PO phonons do not penetrate from one material of the heterostructures to another.). Therefore, wave functions are given by

$$\varphi_{q_{\parallel}}(z) = \sqrt{\frac{2}{L}} \sin q_{\parallel} z, \quad q_{\parallel} = \frac{\pi}{L} j, \quad j = 1, 2, 3, \dots, \quad (2.43)$$

where L is the normalizing length in that semiconductor where the 2DEG is located.

Now using the condition that the well be narrow, which is equivalent to $d \ll a_B, p_0$, we find the averaged form factors (2.16) and (2.31):

for the PO phonons in the quantum wells

$$\begin{aligned} \hat{\Phi}(t) &= \left(\frac{2}{\pi}\right)^3 \sum_{n=1}^{\infty} \frac{1}{n^2} \left| \int_0^{\pi} d\zeta \sin^2 \zeta \sin n\zeta \right|^2 \delta^{1/2} = \left(\frac{\pi}{12} + \frac{5}{8\pi}\right) \delta^{1/2} \approx 0.46 \delta^{1/2} \\ \bar{\Phi}_n &= (1+n) \hat{\Phi}(t), \quad \delta = \frac{\omega_{PO}}{\omega_d} = (p_{PO} d / \pi)^2, \end{aligned} \quad (2.45)$$

for the PO phonons in the heterostructures

$$\hat{\Phi}(t) = \frac{11\pi}{16}\delta^{1/2} \approx 2,16\delta^{1/2}, \quad \bar{\Phi}_n = (1+n)\hat{\Phi}(t), \quad \delta = (p_{PO}\bar{z}/\pi)^2. \quad (2.46)$$

For the surface SO phonons created at the single heterofaces one can obtain

$$\hat{\Phi}(t) = \frac{1}{2} \left(\frac{\sigma}{t} \right)^{1/2}, \quad \bar{\Phi}_n = \frac{(2n+1)!!}{2^{n+2}n!} \sqrt{\pi\sigma}, \quad \sigma = \frac{\omega_{SO}}{\omega_B}. \quad (2.47)$$

Notice that form factors $\hat{\Phi}(t)$ and $\bar{\Phi}_n$ which enter in the kernel (2.21) and in the polarization operator (2.29), respectively, do not depend on the width of the 2DEG in the case of the SO phonons (so long as $d \ll a_B, p_{SO}^{-1}$) while in the case of the bulk PO phonons, the width d enters in the form factors only as a factor. For the latter reason, the binding energies and oscillator strengths of the PO phonon assisted bound states in the quantum wells and heterostructures differ only by numerical factors appeared in the form factors $\hat{\Phi}(t)$ in Esq. (2.44) and (2.46). For brevity, therefore, below we adduce only results for PO phonons in quantum wells, bearing in mind that the binding energies and oscillator strengths for PO phonons in heterostructures can be obtained from W and f in the quantum wells by multiplying them with a numerical factor 4.7.

2.4.2 Strong magnetic fields

In the following we will consider the bound states for $l = \pm 1$, since only these branches of the bound states contribute to the light absorption.

In the strong fields we have $\sigma \equiv \omega_0/\omega_B \ll 1$, and therefore, only the term $s = 0$ is to be retained in the sum for the kernel (2.21), so that

$$K_n^{\pm 1}(t, t') = \pm [\hat{\Phi}(t)\hat{\Phi}(t')]^{1/2} Q_{nn}(t) Q_{nn}(t') \left[J_{\pm 1-n}(2\sqrt{tt'}) - \delta_{\pm 1n} \right]. \quad (2.48)$$

For the PO phonons at $n = 0$, one is managed to find the solution of this kernel using the invariance of the Laguerre polynomials with respect to the Bessel transformation. The kernel (2.48) differs only by a factor from the kernel investigated in Ref. [127]. Therefore, borrowing the eigenvalues and eigenfunctions from this reference, we get the binding energies and oscillator strengths in this case

$$W_r^{\pm} = \pm (-1)^r \left(\frac{\pi}{12} + \frac{5}{8\pi} \right) \rho^{2(r+1)} \delta^{1/2} \sigma^{-1} \alpha \omega_{LO}, \quad (2.49)$$

$$f_r^{\pm} = 5(r+1) \left(\frac{\pi}{12} + \frac{5}{8\pi} \right) \rho^{4(r+1)} \delta^{1/2} \alpha, \quad (2.50)$$

where $\rho = (\sqrt{5} - 1)/2 = 0.618\dots$ coincides with the golden ratio, $r = 1, 2, 3, \dots$. We see from here that the spectra and oscillator strengths of the branches $l = 1$ and $l = -1$ are obtained from each other by mirror reflection about the threshold. This is true also for the case of the SO phonons at $n = 0$. Comparison of the formulas (2.49) and (2.50) with corresponding formulas from [127, 105] shows that the binding energies and oscillator strengths fall slowly in the series than in the three dimensional case. As before, however, the first line contains the main part of the total absorption and is mostly removed from the "threshold". For the case of the SO phonons as well as for the PO phonons at $n \neq 0$, one is not succeeded to find the exact solution of the kernel $K_n^{\pm 1}$. Nonetheless, one can see from Eq. (2.48) that in this case, all the physical parameters, particularly d and B , enter in the kernel $K_n^{\pm 1}$ only in the form of multipliers (via the from factors). This means that the eigenvalues $\lambda_{nr}^{\pm 1}$ are proportional to these factors and the eigenfunctions $\chi_{nr}^{\pm 1}$ do not depend on them. As a result, the dependencies of the binding energies and the oscillator strengths on d and B are easily determined. Applying the methods related with the Sylvester determinants [128], one can show that eigenvalues of the kernel 2.48 of either sign exist, and their number in both signs is infinite. The increasing velocity of the eigenvalues is determined by the analytical features of the kernel [129]; as far as the later are the same both for the case of the PO phonons at $n = 0$ and for the case of the PO phonons at $n \neq 0$ as well as for the case of the SO phonons, then one can anticipate that the eigenfunctions of the kernel (2.48) will increase exponentially. This means that the formulas (2.49) and (2.50), obtained in the particular case, correctly illustrate the dependencies of the binding energies and the oscillator strengths on the series number r . Formulas for the binding energies and the oscillator strengths of the most removed bound states are collected in the Table 2.1. Thus, in the strong magnetic fields for any $l = \pm 1$ both for PO and SO phonons, there exist two sequences of bound states concentrated to the "threshold" both from above and below it.

Table 2.1: Binding energies and oscillator strengths in the strong magnetic fields. Recall that $W_{2D} = \alpha \hbar \omega_0$ denotes the characteristic binding energy scale for the 2DEG. The bound state index $r = 2, 3, 4, \dots$

Phonon mode	Binding energies	Oscillator strengths
PO	$W_{0r}^{\pm} = \mp(-1)^r \rho^{2r} \delta^{\frac{1}{2}} \sigma^{-1} W_{2D}^{PO}$ $ W_{nr}^{\pm} \sim \delta^{\frac{1}{2}} \sigma^{-1} W_{2D}^{PO}, n \geq 1$	$f_{0r}^{\pm} = r \rho^{4r} \delta^{\frac{1}{2}} \alpha_{PO}$ $f_{1r}^{+} \sim \delta^{\frac{1}{2}} \sigma^{-1} \alpha_{PO}, f_{1r}^{-} \sim \delta^{\frac{1}{2}} \sigma \alpha_{PO}$ $f_{nr}^{\pm} \sim \delta \sigma \alpha_{PO}, n \geq 2$
SO	$ W_{nr}^{\pm} \sim \sigma^{-\frac{1}{2}} W_{2D}^{SO}$	$f_{0r}^{\pm} \sim \sigma^{\frac{1}{2}} \alpha_{SO}$ $f_{1r}^{+} \sim \sigma^{-\frac{1}{2}} \alpha_{SO}, f_{1r}^{-} \sim \sigma^{\frac{3}{2}} \alpha_{SO}$ $f_{nr}^{\pm} \sim \sigma^{\frac{3}{2}} \alpha_{SO}, n \geq 2$

2.4.3 Weak magnetic fields

In weak fields ($\sigma \equiv \omega_0/\omega_B \gg 1$), the kernel (2.21) can be approximated by a sequence of degenerate kernels [127, 105], *i.e.* terms of the sum in (2.21) can be expanded in powers of σ^{-1} so that this (2.21) can be represented by

$$K_n^{\pm}(t, t') = \sum_{i,j=0}^{\infty} \left(K_n^{\pm} \right)_{ij} (g_n(t))_i (g_n(t'))_j \quad (2.51)$$

where

$$(g_n(t))_i = t^{\frac{1+n+2i}{2}} e^{-\frac{t}{2}} \sqrt{\hat{\Phi}(t)}. \quad (2.52)$$

The coefficients $(K_n^{\pm})_{ij}$ are constructed in such a way that if we retain a finite number of terms in the expansion in terms of σ^{-1} , an infinite matrix reduces to a finite one while the integral equation—to a finite system of linear equations. Solving the obtained finite system of linear equations one can find the eigenvalues $\lambda_{nr}^{\pm 1}$ and the integral (2.30) from the resolvent $R_n^{\pm 1}$. For example, in the principal

order retaining the terms of the order of σ^{-1} and dropping the terms of the higher order of $\sigma^{-2}, \sigma^{-3}, \dots$ we find for:

$$n = 0 \quad \left\| K_0^+ \right\| = \left\| \begin{pmatrix} \sigma^{-1} & 0 \\ 0 & \sigma^{-1} \end{pmatrix} \right\|, \quad \left\| K_0^- \right\| = \left\| -\sigma^{-1} \right\|, \quad (2.53)$$

for $n = 1$

$$\left\| K_1^+ \right\| = \left\| \begin{pmatrix} -3\sigma^{-1} & \sigma^{-1} \\ \sigma^{-1} & -\frac{1}{2}\sigma^{-1} \end{pmatrix} \right\|, \quad \left\| K_1^- \right\| = \left\| -\sigma^{-1} \right\|. \quad (2.54)$$

In this lowest order in B we get three bound states above the "threshold": two with $l = +1$ and one with $l = -1$. Expressions obtained for the binding energies and oscillator strengths at $n = 0$ and $n = 1$ are collected in Table 2.2 and 2.3, respectively for the bound states with assistance of the PO phonons in the quantum wells and heterostructures and of the SO phonons created at the single heterofaces. It is seen from Tables 2.2 and 2.3 that the state with $l = -1$ is

Table 2.2: Binding energies and oscillator strengths in the weak magnetic fields for the PO phonon assisted bound states in quantum wells.

n	Binding energies	Oscillator strengths
n=0	$W_{01,3}^+ = (2 \pm \sqrt{3}) \left(\frac{\pi}{12} + \frac{5}{8\pi} \right) \delta^{\frac{1}{2}} \sigma^{-2} W_{2D}^{PO}$ $W_{02}^- = - \left(\frac{\pi}{12} + \frac{5}{8\pi} \right) \delta^{\frac{1}{2}} \sigma^{-2} W_{2D}^{PO}$	$f_{01,3}^+ = \frac{\sqrt{3} \pm 1}{2\sqrt{3}} \left(\frac{\pi}{12} + \frac{5}{8\pi} \right) \delta^{\frac{1}{2}} \sigma^{-2} \alpha_{PO}$ $f_{02}^- = \left(\frac{\pi}{12} + \frac{5}{8\pi} \right) \delta^{\frac{1}{2}} \sigma^{-2} \alpha_{PO}$
n=1	$W_{11,3}^+ = -(3 \pm \sqrt{3}) \left(\frac{\pi}{12} + \frac{5}{8\pi} \right) \delta^{\frac{1}{2}} \sigma^{-2} W_{2D}^{PO}$ $W_{12}^- = -2 \left(\frac{\pi}{12} + \frac{5}{8\pi} \right) \delta^{\frac{1}{2}} \sigma^{-2} W_{2D}^{PO}$	$f_{11,3}^+ = \left(\frac{\pi}{12} + \frac{5}{8\pi} \right) \delta^{\frac{1}{2}} \sigma^{-2} \alpha_{PO}$ $f_{12}^- = 2 \left(\frac{\pi}{12} + \frac{5}{8\pi} \right) \delta^{\frac{1}{2}} \sigma^{-2} \alpha_{PO}$

located between the two states with $l = +1$ and the oscillator strength of the state with $l = -1$ is the sum of the oscillator strengths of the two states with $l = +1$. If retain also terms of the orders of σ^{-2} , the order of the matrixes $(K_n^\pm)_{ij}$

Table 2.3: Binding energies and oscillator strengths in the weak magnetic fields for the SO phonon assisted bound states at the heterofaces.

n	Binding energies	Oscillator strengths
n=0	$W_{01,3}^+ = -\frac{23 \pm \sqrt{337}}{64} \sqrt{\pi} \sigma^{-\frac{3}{2}} W_{2D}^{SO}$ $W_{02}^- = -\frac{\sqrt{\pi}}{4} \sigma^{-\frac{3}{2}} W_{2D}^{SO}$	$f_{01,3}^+ = \frac{\sqrt{337} \pm 11}{8\sqrt{337}} \sqrt{\pi} \sigma^{-\frac{3}{2}} \alpha_{SO}$ $f_{02}^- = \frac{\sqrt{\pi}}{4} \sigma^{-\frac{3}{2}} \alpha^{SO}$
n=1	$W_{11,3}^+ = -\frac{24}{4(19 \pm \sqrt{41})} \sqrt{\pi} \sigma^{-\frac{3}{2}} W_{2D}^{SO}$ $W_{12}^- = -\frac{3\sqrt{\pi}}{8} \sigma^{-\frac{3}{2}} W_{2D}^{SO}$	$f_{11,3}^+ = \frac{3(\sqrt{41} \pm 1)}{16\sqrt{41}} \sqrt{\pi} \sigma^{-\frac{3}{2}} \alpha_{SO}$ $f_{12}^- = \frac{3\sqrt{\pi}}{8} \sigma^{-\frac{3}{2}} \alpha^{SO}$

will increase by one, and new bound states will appear with the binding energies and oscillator strengths proportional to σ^{-2} . Omitting highly cumbersome computations, we adduce only final formulas for the binding energies and the oscillator strengths at $n = 0$ of higher order in σ^{-1} :

for the PO phonon assisted bound states

$$W_{0r}^\pm = (-1)^r \left(\frac{\pi}{12} + \frac{5}{8\pi} \right) r! \delta^{\frac{1}{2}} \sigma^{-r-1} W_{2D}^{PO}, \quad (2.55)$$

$$f_{0r}^\pm = \left(\frac{\pi}{12} + \frac{5}{8\pi} \right) \left\{ \begin{matrix} r+1 \\ r \end{matrix} \right\} (r!)^2 \delta^{\frac{1}{2}} \sigma^{-2r} \alpha_{PO}, \quad (2.56)$$

for the SO phonon assisted bound states

$$W_{0r}^\pm = (-1)^r \sqrt{\pi} \frac{(2r-1)!!}{2^{r+1}} \left\{ \begin{matrix} \frac{2r+1}{2(r+1)} \\ 1 \end{matrix} \right\} \sigma^{-r-\frac{1}{2}} W_{2D}^{SO}, \quad (2.57)$$

$$f_{0r}^\pm = \sqrt{\pi} \frac{[(2r-1)!!]^3}{2^{3r-1} r!} \left\{ \begin{matrix} \left[\frac{2r+1}{2(r+1)} \right]^3 \\ r \end{matrix} \right\} \sigma^{-2r+\frac{1}{2}} \alpha_{SO}. \quad (2.58)$$

In these formulas $r = 2, 3, 4, \dots$. The upper and lower values in the figure brackets pertain to the right- and left-hand polarization of the light. Recall that $W_{2D} = \alpha \hbar \omega_0$ denotes the characteristic binding energy scale for the 2DEG. Now it is seen

that upon increasing the bound state index r , the binding energies and oscillator strengths fall sharply both for PO and SO phonons. Furthermore, in weak fields, this decrease of W and f is faster than that of in the strong fields. In the weak fields, the following relation takes place

$$f_{nr}^{\pm} \sim \frac{1}{\hbar\omega_0} W_{nr}^{\pm}. \quad (2.59)$$

In the strong fields, this relation holds at $n = 0$ only for the right-hand polarization. The corresponding expression for the left-hand polarization at $n = 1$ as well as for both polarizations at $n \geq 2$ are

$$f_{nr}^{\pm} \sim \frac{1}{\hbar\omega_0} \sigma^2 W_{nr}^{\pm} \quad (2.60)$$

and at $n = 0$

$$f_{nr}^{\pm} \sim \frac{1}{\hbar\omega_0} \sigma W_{nr}^{\pm}, \quad (2.61)$$

i.e. in these cases the oscillator strengths are essentially weaker.

From the results of the calculations for W and f , thus, it becomes clear that the absorption spectrum in both the right- and left-hand polarization should constitute an "asymmetric doublet" (Fig. 2.7). In the strong fields this asymmetry is with respect to a numerical parameter of type ρ and in the weak fields – with respect to the large parameter σ .

2.5 Discussion of results

2.5.1 Numerical estimates

Both from the fundamental and technological point of view, the most important nanostructures are based on GaAs/Al_xGa_{1-x}As heterojunction. Therefore, for numerical estimates, we choose a GaAs/Al_xGa_{1-x}As single-heterostructure or quantum well as our calculation model. The values of physical and material [130] parameters for these structures are given in Table A.1 in Appendix A. The energies and coupling constants for the SO phonons arising at the GaAs/Al_xGa_{1-x}As heteroface for $x = 0.3$ and $x = 1$ are obtained from formulas (2.7)-(2.9). There exist two, GaAs and AlGaAs like SO phonon modes for a given x with energies below the GaAs like and AlGaAs like bulk PO phonon energies, respectively. The

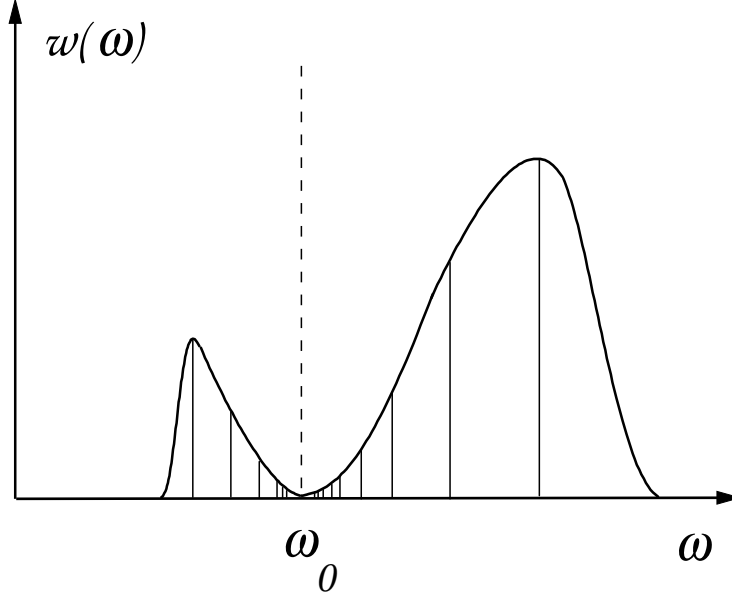


Figure 2.7: Cyclotron phonon resonance spectrum. The dashed line shows the absorption spectrum when no bound states are taken into account. The bold line is the skirt.

coupling constant α_{SO} for the electron interaction with GaAs like SO phonons is much greater than that of for the AlGaAs like SO modes. Therefore we ignore the electron coupling to such AlGaAs like SO phonons. Notice that the SO phonon energies and coupling constants for each mode are changed weakly in x .

Let discuss in more detailed the bulk PO phonon localization effect across the GaAs/ $\text{Al}_x\text{Ga}_{1-x}\text{As}$ heteroface. Using the experimental results [131], we find that the PO phonon dispersion law in GaAs can be described by

$$\omega_{LO}(q) = \omega_{LO} \left(1 - \frac{q^2}{q_0^2} \right), \quad \omega_{LO} = 295 \text{ cm}^{-1}, \quad q_0 = 18.5 \text{ nm}^{-1}. \quad (2.62)$$

The phonon momenta important in the formation of bound states obey to the restrictions, $q_{\perp} \lesssim a_B^{-1}$ and $q_{\parallel} \lesssim \pi/d$. Even in strongest fields ($B = 20 \text{ T}$) and for narrow wells ($d = 2.5 \text{ nm}$) we have $q \lesssim 1 \text{ nm}^{-1}$ so that $|\omega_{PO}(q) - \omega_{PO}| \lesssim 1 \text{ cm}^{-1}$. However, the GaAs like PO mode in $\text{Ga}_{0.7}\text{Al}_{0.3}\text{As}$ has the frequency 284 cm^{-1} . Therefore, the PO vibrations in GaAs are localized in a well with walls of height

$\delta\omega_{PO} = 11 \text{ cm}^{-1}$ which is considerably greater than the dispersion $|\omega_{PO}(q) - \omega_{PO}|$. The depth of penetration of the PO vibrations of GaAs into $\text{Ga}_{0.7}\text{Al}_{0.3}\text{As}$ can be estimated as $q^{-1}\sqrt{\omega_{PO}/\delta\omega_{PO}} \approx 0.3 \text{ nm}$. This means that the bulk PO phonons are strongly localized in quantum wells. This result is in full agreement with the experimental Raman scattering data. [132, 133, 134].

The assumption of the narrow well, $\Delta E_d \equiv E_2 - E_1 \gg \hbar\omega_B, \hbar\omega_0$, is well justified for the well width d less than 20 nm. Par example, at $d = 10 \text{ nm}$, the transverse quantization separation between the first and second highest levels is $\Delta E_d = 170 \text{ meV}$ which is notably greater than the phonon energies, $\hbar\omega_{PO} = 36.62 \text{ meV}$, $\hbar\omega_{SO} = 34.57 \text{ meV}$ at $x = 0.3$, and $\hbar\omega_{SO} = 34.82 \text{ meV}$ at $x = 1$. In the GaAs/ $\text{Al}_x\text{Ga}_{1-x}\text{As}$ quantum wells and heterostructures, the resonance fields are $B_{PO} = 20.87 \text{ T}$, $B_{SO} = 19.70 \text{ T}$ at $x = 0.3$, and $B_{SO} = 19.85 \text{ T}$ at $x = 1$ so that we usually obtain the situation $\omega_B \lesssim \omega_0$ and, therefore, in estimates we use formulas obtained in the case of the weak magnetic fields. Thus, for GaAs/ $\text{Al}_x\text{Ga}_{1-x}\text{As}$ quantum wells and heterostructures using formulas in Tables 2.2 and 2.3, as well the numerical values from Table A.1, we obtain ultimately the W and f . The results for the most removed states bound to the PO and GaAs like SO phonons ($x = 0.3$) in the case of $n = 1$ are collected in Table 2.4. One can see that for $d \sim 10 \text{ nm}$ and $B \sim B_0$ the binding energies are $W \sim 1 \text{ meV}$.

For actual estimates of the absorbed energy fraction, w , we have to allow for the Landau level broadening, *i.e.*, for the smearing of the delta-function in Eq. (2.36). In rough estimates we can replace the delta-function with a Lorentzian characterized by the total width \hbar/τ , where τ is the relaxation time deduced from the mobility. At the absorption maximum we have then $\pi\delta(\omega) \rightarrow \tau$, so that

$$w = 4\pi N \frac{e^2}{m_c c^2} \frac{c}{\sqrt{\kappa(\nu_n)}} f \tau. \quad (2.63)$$

In quantum wells of good (but not exceptional) quality we have $\mu = 10^5 \text{ V s m}^{-1}$ which corresponds to $\tau = 4 \text{ ps}$ and a line width $\hbar/\tau = 0.15 \text{ meV}$. Therefore, in a field of $B = 4 \text{ T}$ and for $d = 10 \text{ nm}$ the bound states from Table 2.4 can hardly be resolved. However, if the field is increased up to 10 T and the well width up to 15 nm, we can increase the binding energies and oscillator strengths by an order of magnitude, *i.e.* we can obtain $W \approx 1 \text{ meV}$ and $f \approx 10^{-2}$. We

Table 2.4: Binding energies and oscillator strengths in the weak magnetic fields for the PO phonon assisted bound states in quantum wells. In these formulas d , B and W should be taken in nm, T, and meV, respectively.

Phonon mode	Binding energies	Oscillator strengths
PO	$W_{11,3}^+ = \left\{ \begin{array}{c} 4.4 \\ 1.2 \end{array} \right\} (d/10) (B/20.87)^2$ $W_{12}^- = 1.9 (d/10) (B/20.87)^2$	$f_{11,3}^+ = 2.6 \cdot 10^{-2} (d/10) (B/20.87)^2$ $f_{12}^- = 5.2 \cdot 10^{-2} (d/10) (B/20.87)^2$
SO	$W_{11,3}^+ = - \left\{ \begin{array}{c} 0.6 \\ 0.3 \end{array} \right\} (B/19.7)^{\frac{3}{2}}$ $W_{12}^- = 0.5 (B/19.7)^{\frac{3}{2}}$	$f_{11,3}^+ = \left\{ \begin{array}{c} 0.8 \\ 0.6 \end{array} \right\} \cdot 10^{-2} (B/19.7)^2$ $f_{12}^- = 1.4 \cdot 10^{-2} (B/19.7)^{\frac{3}{2}}$

will estimate the absorption under these conditions on the basis of Eq. (2.63). Assuming that $N = 4 \cdot 10^{15} \text{ m}^{-2}$, we find that $w = 5 \cdot 10^{-3}$. This means that a ten-layer superlattice can give rise to the fully perceptible absorption amounting to few percent. Recalculation to the bulk absorption coefficient $\gamma = w/d$ yields $\gamma \approx 10^7 \text{ m}^{-1}$ (at a bulk density $N/d = 5 \cdot 10^{23} \text{ m}^{-3}$).

The above estimates for the phonon dispersion $|\omega_{PO}(q) - \omega_{PO}|$ and for the binding energies W shows that $|\omega_{PO}(q) - \omega_{PO}| \ll W$ at the phonon momenta important in the bound state formation. This means that the neglect of the phonon dispersion is justified in this theory.

2.5.2 Conclusion

From the results of the calculations it follows that the branches of the spectrum of two-particle elementary excitations in the 2DEG exposed to the quantizing magnetic field normal to the electron sheet plane describe the bound states of the electron and the optic phonon and there are infinite number of them. The

bound states are characterized by the total angular momentum $l = 0, \pm 1, \pm 2, \dots$ of rotating around \mathbf{B} . The states with a given l are additionally numbered by indexes n and r . Index n indicates the number of the "threshold" near which an infinite sequence of the bound states numbered by the index r is located. Upon increasing r , causing the binding energy W_{nr}^l to fall, there is a simultaneous fall also in the oscillator strength f_{nr}^l , approaching to zero at $r \rightarrow \infty$. The absorption is governed by the bound states with $l = \pm 1$. The binding energies, generally speaking, can be of any sign. Therefore the absorption concentrated not at the "threshold" but below and above it at the separation of $W_{nr}^{\pm 1}$. The characteristic scale of the binding energies $W_{2D} = \alpha\omega_0$ is essentially greater than corresponding scale in the massive samples, $W_{2D} = \alpha^2\omega_0$.

The bound states and the cyclotron phonon resonance are determined by the density of states of a system of two particles: an electron at the level n and an optic phonon. Since the phonon dispersion is ignored, it follows that both particles have an infinite mass so that this system does not have a continuous spectrum. All the electron and phonon states are bound and rigorously stationary. This is the fundamental difference between the cyclotron phonon resonance in a 2DEG and that in a 3D electron gas. For this reason the absorption coefficient for the 2D cyclotron phonon resonance cannot be calculated from perturbation theory.

In strong fields, the binding energies and the oscillator strengths of the states above the threshold are of the same order of magnitude as for the states below the threshold. Therefore, the absorption spectrum should consist of two groups of peaks, which are of approximately the same amplitude and are located approximately asymmetrically relative to the "threshold". The separation between these two groups of peaks is of the same order of magnitude for the right- and left-hand polarizations. The absorption depends on the number n of the final Landau level. The maximal absorption is for the right-hand polarization for the bound states arising near the $n = 1$ level. The absorption for left-hand polarization at $n = 1$ and for both left- and right-hand polarizations at $n \geq 2$ are $(B/B_0)^2$ times less. At $n = 0$, the absorption is suppressed for both polarizations in (B/B_0) times. In weak fields the bound states with the maximum binding energies and oscillator strengths lie above the thresholds, because the peaks below the threshold (at

$\nu < \nu_n$) should be weaker and closer to the "threshold". However, in contrast to the case of strong fields in the weak fields, the absorption is of the same order of magnitude irrespective of the polarization and of the index n . In the 2DEG, all bound states in the case of $n \geq 1$ and part of states at $n = 0$ lie above the PO phonon energy, hence their observation should not be hindered by strong lattice reflection.

From comparison the binding energies for PO and SO phonons in Tables 2.2 and 2.3 it is clear that

$$\frac{W_{LO}}{W_{SO}} \sim \delta \sigma^{-\frac{1}{2}} \left(\frac{\omega_B}{\omega_d} \right)^{\frac{1}{2}} \ll 1, \quad (2.64)$$

In this estimate the difference between the numerical values of the coupling constants α , the phonon frequencies ω_0 for the PO and SO phonons are ignored. The relationship (2.64) applies in strong and weak fields. A similar relationship describes the oscillator strengths. Thus, the states bound to SO phonons should be easier to observe experimentally.

Chapter 3

Electron-phonon relaxation.

Interface effect

3.1 Introduction

Scattering of electrons in massive samples by lattice vibrations in metals and semiconductors has been intensively investigated in the last several decades and at present it is well studied. Comprehensive reviews for a variety of scattering phenomena are given in [135] and [136]. In the last years semiconductor nanoscale systems with carrier confinement in one, two, and all three dimensions are attracting increasing interest (see reviews [6, 7, 8, ?]). The wave functions compressed by the lateral confinement may lead to a substantial enhancement in the optical properties of device nanostructures because the quantum effects can be used to concentrate the optical oscillator strengths at the active transitions. Furthermore, these structures under different new environments exhibit discrete charging effects and give promise of devices operating in the limit of single electron transport. In GaAs/AlGaAs type heterostructures, Coulomb scattering of electrons on the ionized impurities can be suppressed by concentrating the impurities in layers with wide bands while charge carriers — in narrow bands. Such a spatial separation of the impurities and charge carriers is attained by use of a modulated doping technique [137]. This leads to the strong enhancement of the carriers mobility. Even more higher mobilities can be achieved separating the carrier and impurities with an additional non-doped spacer [138]. A comparison of experimental results with

theories of electron scattering in modulated doped heterostructures with spacers shows [139] that in temperatures some below 77K, the acoustic phonon scattering dominates while at helium temperatures – Coulomb scattering. In the higher temperature range, the electron scattering goes mainly due to the electron-optic phonon interaction [140]. In the intermediate temperature range 4.22 – 77 K, the piezoelectric scattering of acoustic phonons is suppressed [141] hence the scattering of the 2DEG on the deformation potential of acoustic phonons becomes more important. Investigations of the carrier scattering in the 2DEG have been carried out by many authors [142, 143, 144, 145, 146]. The electron scattering has been considered in inversion layers [142] and heterostructures [143, 144]. Various relaxation times verified experimentally have been calculated [145, 146]. However, the effect of the phonon reflection from various interfaces on the scattering of the 2DEG from acoustic phonons has not been considered. Interfaces always exist in real structures such as inversion layers, heterostructures, and quantum wells. (The only exceptions are [147, 148, 149, 150]. All these treatments will be discussed later.)

It is usually accepted that the reflection is unimportant and contributes at most a correction factor of the order of unity. However, it will be shown here that this is not the case. Actually, there are situations when the reflection of phonons alters the energy dependence of the electron relaxation times and even can change the order of magnitude of the relaxation times.

It is very difficult to include the phonon reflection using the traditional methods. Consider the following situation: electrons in an inversion layer in the vicinity of a semiconductor surface. If we adopt the usual method, a semi-infinite crystal should be replaced by a finite volume L^3 (see Fig. 3.1), the phonon field should be quantized, the scattering probability from each phonon mode should be obtained, and then all these probabilities should be combined, which is followed by going to the limit $L \rightarrow \infty$. It is necessary in the calculation of the phonon modes to impose on the surface $z = 0$ near which electrons are located, the correct boundary condition, *i.g.*, the absence of a stress on the free surface. Arbitrary boundary conditions can be applied to the far surface at $z = L$. However, irrespective of the choice of the boundary conditions, the vector nature of the phonon field makes it practically impossible to calculate the complex normal

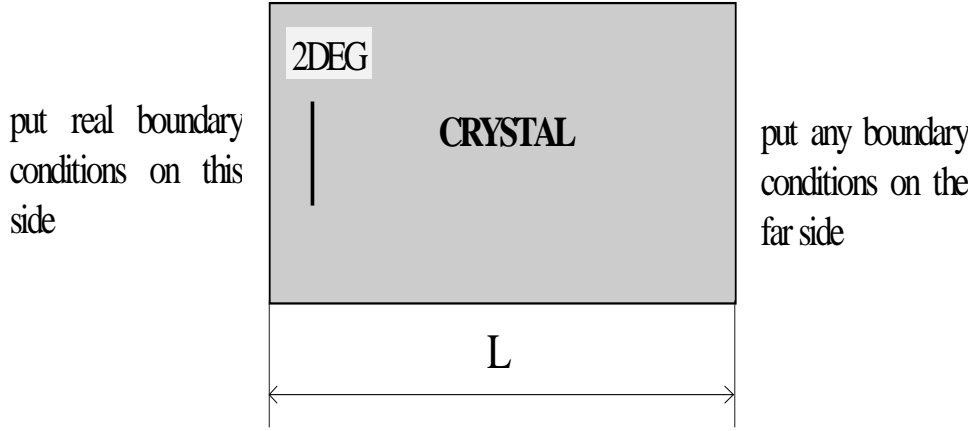


Figure 3.1: In usual method for calculating the transition probability an infinite crystal is replace by finite box of length L .

modes of a plate in the limit $L \rightarrow \infty$. We can bypass this problem by focusing our attention directly on the scattering probability summed over all the phonon modes. *Such a probability evaluated in the Born approximation can be expressed in terms of the phonon field correlation function* [151] *and the correlation function itself is given in terms of the elasticity theory Green function* [152]. The limit $L \rightarrow \infty$ can be then reached for such a function without any difficulties.

In this chapter, the effect of interfaces separating elastic semi-spaces on the scattering of the 2DEG from the deformation potential of acoustic phonons is studied [41, 43, 42]. This problem is sufficiently multiplex, in the sense, that it contains a number of interesting particular cases of the free and rigid surfaces, the solid-liquid interfaces *etc.*. Study of these limiting cases favors more complete understanding of the interface effect on the electron scattering. On the other hand, they have their own significance for device structures in each concrete case. Par example, the case of the solid-liquid contact is applicable directly to the electrolyte-semiconductor device structures which are attracting increasing interest in the last years in connection with a developing of new devices for the solar energy transformation [153, 154]. The model of rigid boundary can be applied to situations when the second medium is sufficiently heavy, for example

metal-insulator-semiconductor (MIS) structures with a heavy gate and a thin oxide layer. If in the rough approximation, differences between acoustic properties of the dielectric and semiconductor are ignored, and a metal mass density account for infinity, then the system can be described in the frames of this model. The model of a free surface applies directly to inversion layers which are formed on natural semiconductor surfaces (for example, Ge or InAs) and to heterojunctions located at distances of the order of 10 nm from the surface. Our model is most applicable to systems where an insulator in the MIS structure is not deposited on the surface, but simply clamped (*Mylar foil*). The acoustic contact is then poor and phonons in the semiconductor are reflected from the semiconductor-insulator interface as if it were a free surface. We also wish to mention MIS structures with a thin oxide layer and a thin (optically transparent) gate. The reflection coefficient for the semiconductor-insulator and insulator-metal interfaces are relatively small. Neglecting, in the first approximation, the differences between the acoustic properties of various media, we can describe such a system using our free surface model.

In Sec. 3.2 a new method for calculating the probability of electron scattering from the deformation potential of acoustic phonons is developed [41] which is applicable to an arbitrary geometry of the sample. Using this method, it is possible to treat the reflection of phonons from a crystal surface and from interfaces separating different materials. To illustrate the method, in Secs. 3.5 and 3.6 the energy (and electron temperature) [41, 43] and the momentum [42] relaxation rates for the Fermi 2DEG in the vicinity of an interface separating semi-infinite elastic spaces are calculated. Our results and conclusions are summarized in Sec. 3.7.

3.2 Interface effect on the electron-phonon interaction

We consider the deformation interaction of electrons with acoustic phonons. Assuming a non-degenerate band, we can write the interaction Hamiltonian in the

lowest order of atomic displacements in the form

$$H_{int} = \frac{1}{2} \Xi_{ij} \{ \partial_i u_j(\mathbf{r}) + \partial_j u_i(\mathbf{r}) \}. \quad (3.1)$$

where, $i, j = 1, 2, 3, \dots$ label Cartesian coordinates ($x = 1, y = 2, z = 3$), Ξ_{ij} is the deformation potential tensor, $u_j(\mathbf{r})$ are the displacement vector components. Summation over repeated indices is assumed to be carried out. It is easy to show that the probability of an electron transition from a state $\Psi_v(\mathbf{r})$ with an energy ε_v to a state $\Psi_{v'}(\mathbf{r})$ with an energy $\varepsilon_{v'}$ due to the perturbation defined by Eq. (3.1) in the first Born approximation is given by the following expression:

$$\begin{aligned} W_{v \rightarrow v'} &= \int d^3 r_1 \int d^3 r_2 \Psi_{v'}^*(\mathbf{r}_1) \Psi_v^*(\mathbf{r}_2) \Psi_{v'}(\mathbf{r}_2) \Psi_v(\mathbf{r}_1) \\ &\times \Xi_{ii'} \Xi_{jj'} \partial_{1i} \partial_{2j} \langle u_{i'}(\mathbf{r}_1) u_{j'}(\mathbf{r}_2) \rangle_\omega. \end{aligned} \quad (3.2)$$

Here $\langle \dots \rangle_\omega$ is the Fourier transform of the correlation function of the displacement field operators in the Heisenberg representation. It is necessary to set $\omega = \varepsilon_v - \varepsilon_{v'}$ in the calculation of the probability.

The elasticity theory Green function $G_{ij}(\mathbf{r}_1, \mathbf{r}_2 | \omega)$ is defined as the displacement along the i axis at a point \mathbf{r}_1 due to a force density

$$- \delta(\mathbf{r}_1 - \mathbf{r}_2) e^{-i\omega t} \quad (3.3)$$

applied in the direction of the j axis.

Assuming an equilibrium phonon field at temperature T , we find that the correlation function in Eq. (3.2) can be expressed in terms of the above retarded Green function [152]

$$\langle u_{i'}(\mathbf{r}_1) u_{j'}(\mathbf{r}_2) \rangle_\omega = -2[N_T(\omega) + 1] \text{Im} G_{ij}(\mathbf{r}_1, \mathbf{r}_2 | \omega) \quad (3.4)$$

where N_T is the Bose factor

$$N_T(\omega) = [\exp(\hbar\omega/T) + 1]^{-1}. \quad (3.5)$$

The Green function $G_{ij}(\mathbf{r}_1, \mathbf{r}_2 | \omega)$ includes naturally all the boundary conditions at the interface and at the surface of a sample. When some of the boundary conditions are replaced by the boundary conditions at infinity then the retarded Green function $G_{ij}(\mathbf{r}_1, \mathbf{r}_2 | \omega + i0) = G_{ret}(\omega)$ should be replaced by the Green function corresponding to outgoing waves $G_{out}(\omega)$.

Eqs. (3.2) and (3.4) solve, in principle, the problem of calculating the electron transition probability between arbitrary electron states in the case of deformation scattering of electrons from equilibrium acoustic vibrations and they apply to an arbitrary geometry of the sample. This approach is especially efficient at the calculating of scattering in lower dimensional systems (in systems with the 2DEG, in quantum wires and dots) when the presence of various interfaces, separating different materials, distorts phonon modes. This method advances an easier way to account for the phonon reflection from various interfaces and to calculate the transition probability summed over all the phonon modes, including the surface phonons. Recently, this method has been used to calculate the electron scattering on surfaces of cryogen crystals (solid hydrogen, deuterium, and neon) from lattice vibrations [155]. It should be noted also that the Green functions of the elasticity theory are sufficiently well studied for several interesting sample geometries (for a review *quod vide* [156]), which makes easier their use and notably shorts calculations of the transition probability.

3.3 Scattering in a Fermi 2DEG near interfaces separating elastic semi-spaces

In most cases, the elastic properties of a sample are those of a layered medium (for example, a semi-infinite semiconductor or a system consisting of oxide and metal layers) and electrons move in a plane parallel to the interface. We shall assume that the plane $z = 0$ near which the 2DEG is located in a medium 1 represents the interface between two elastic media and the z -axis is directed away from a medium 2. Such systems have the translation invariance in x and y directions so that it is convenient to make the Fourier transformation

$$G_{ij}(\mathbf{r}_1, \mathbf{r}_2|\omega) = \int \frac{d^2q}{(2\pi)^2} g_{ij}(\omega, \mathbf{q}|z_1, z_2) \exp[i\mathbf{q} \cdot (\mathbf{R}_1 - \mathbf{R}_2)] \quad (3.6)$$

where $\mathbf{r} = (\mathbf{R}, z)$, \mathbf{q} and \mathbf{R} are two-dimensional vectors in the (x, y) -plane. In the absence of a magnetic field, the electron wave functions are given by

$$\Psi_{n\mathbf{k}}(\mathbf{r}) = \frac{1}{L} \exp[i\mathbf{k} \cdot \mathbf{R}] \psi_n(z). \quad (3.7)$$

Here, \mathbf{k} is the electron momentum in the (x, y) -plane, n labels states describing the electron motion in the direction of the z -axis, L^2 is the area of the structure in the (x, y) -plane. Substituting Eqs. (3.6) and (3.7) in Eqs. (3.2) and (3.4) we obtain

$$W_{n\mathbf{k} \rightarrow n'\mathbf{k}'}^\pm = \frac{2}{L^2} [N_T(\omega) + \frac{1}{2} \pm \frac{1}{2}] \int dz_1 \int dz_2 \psi_{n'}^*(z_1) \psi_n^*(z_2) \psi_{n'}(z_2) \psi_n(z_1) \mathcal{D}(\omega, \mathbf{q} | z_1, z_2) \quad (3.8)$$

where

$$\begin{aligned} \mathcal{D}(\omega, \mathbf{q} | z_1, z_2) = & -\text{Im}[\Xi_{ii'} \Xi_{jj'} q_i q_j g_{i'j'} - \Xi_{33} \Xi_{jj'} q_j i \frac{\partial}{\partial z_1} g_{3j'} + \Xi_{ii'} \Xi_{33} q_i i \frac{\partial}{\partial z_2} g_{i'3} \\ & + \Xi_{33}^2 \frac{\partial^2}{\partial z_1 \partial z_2} g_{33}]. \end{aligned} \quad (3.9)$$

Here the indices i, j take only values 1, 2. For brevity, we have omitted in Eq. (3.9) the dependence of g_{ij} on their arguments. It is necessary to set $\mathbf{q} = \mathbf{k} - \mathbf{k}'$ in the transition probability defined by Eq. (3.8). The $+$ and $-$ signs in Eq. (3.8) refer to transitions involving an energy loss, $\hbar\omega = \varepsilon_{n\mathbf{k}} - \varepsilon_{n'\mathbf{k}'} > 0$ and an energy gain, $\hbar\omega = \varepsilon_{n'\mathbf{k}'} - \varepsilon_{n\mathbf{k}} > 0$, respectively.

We can further simplify the problem assuming that the scattering takes place in an isotropic band with an energy minimum at the center of the Brillouin zone

$$\Xi_{ij} = \Xi \cdot \delta_{ij}. \quad (3.10)$$

We further assume that all the layers are elastically isotropic, which means that the dependence of g_{ij} on the orientation of \mathbf{q} is trivial and is determined by the matrices describing rotations in the (x, y) plane [156]. We then can exploit this isotropy in the (x, y) -plane and obtain

$$\mathcal{D}(\omega, \mathbf{q} | z_1, z_2) = \Xi^2 K(\omega, q | z_1, z_2) \quad (3.11)$$

where the kernel K is given

$$K(\omega, q | z_1, z_2) = -\text{Im} \left[q_i q_j g_{ij} - q_j i \frac{\partial}{\partial z_1} g_{3j} + q_i i \frac{\partial}{\partial z_2} g_{i3} + \frac{\partial^2}{\partial z_1 \partial z_2} g_{33} \right]. \quad (3.12)$$

Since the kernel K is independent of the orientation of vector \mathbf{q} , we may choose $\mathbf{q} \parallel \hat{\mathbf{x}}$, which yields

$$K(\omega, q | z_1, z_2) = -\text{Im} \left[q^2 g_{11} - iq \frac{\partial}{\partial z_1} g_{31} + iq \frac{\partial}{\partial z_2} g_{i3} + \frac{\partial^2}{\partial z_1 \partial z_2} g_{33} \right]. \quad (3.13)$$

Recall that the notation $\mathbf{q} \equiv (q_x, q_y)$ is used.

Further we require the kernel K for the contact of the semi-infinite elastic spaces. The Green function of the elasticity theory for this case have been calculated in [157]. Substituting in Eq. (3.13) the obtained results for g_{ij} from [157], it is straightforward although somewhat tedious to derive an expression for K . We use following notations

$$r_{\pm} = (\alpha_t^2 + q^2)^2 \pm 4q^2\alpha_l\alpha_t, \quad h_{\pm} = \alpha_t^2 + q^2 \pm 2\alpha_l\alpha_t, \quad \gamma = \frac{\rho'c'^2}{\rho c^2}, \quad (3.14)$$

$$\alpha = \sqrt{q^2 - \frac{(\omega + i0)^2}{s^2}}, \quad \beta = \sqrt{q^2 - \frac{(\omega + i0)^2}{c^2}} \quad (3.15)$$

where s and c are the velocities of the longitudinal LA and the transverse TA acoustic waves, ρ is the mass density in the medium 1 where the 2DEG is located. Quantities r', h', α' are defined according to (3.14) and (3.15) with parameters s', c', ρ' of the medium 2. In Eq. (3.15), the branch cut for the square root is assumed to lie along the negative real axis. We then obtain

$$K(\omega, q|z_1, z_2) = \frac{\omega^2}{\rho s^4} \text{Im} \frac{1}{2\alpha_l} \{ \exp[-\alpha_l(z_1 - z_2)] - \mathcal{R} \exp[-\alpha_t(z_1 + z_2)] \} \quad (3.16)$$

where

$$\mathcal{R} = \frac{r_+(\alpha'_l\alpha'_t - q^2) - \gamma^2 r'_-(\alpha_l\alpha_t + q^2) + \gamma[2q^2 h_+ h'_- + \frac{\omega^4}{c^2 c'^2}(\alpha'_l\alpha'_t - \alpha_l\alpha'_t)]}{r_-(\alpha'_l\alpha'_t - q^2) + \gamma^2 r'_-(\alpha_l\alpha_t - q^2) + \gamma[2q^2 h_- h'_+ + \frac{\omega^4}{c^2 c'^2}(\alpha'_l\alpha'_t + \alpha_l\alpha'_t)]}. \quad (3.17)$$

In the kernel (3.16), the quantity \mathcal{R} accounts for the contribution to the scattering by the phonon modes reflected at the interface. In the range where $\omega > sq$ and $\omega > s'q$, expressing \mathcal{R} in terms of the sound velocities and the phonon incidence angles, we can easily show that \mathcal{R} is the reflection coefficient describing the LA \rightarrow LA reflection at the interface separating elastic semi-spaces. It can be easily seen that Eq. (3.16) at $\mathcal{R} = 0$ yields the kernel K for the case when phonons occupy the whole infinite space. In this case, phonons of the TA type, naturally, do not contribute to K and the condition $K \neq 0$ is satisfied only for $sq < \omega$. In the range $\omega < cq$ and $\omega < c'q$, the poles of \mathcal{R} yield the dispersion law of the interface Stoneley waves [158] and, therefore in this region, the kernel K is nonzero only on the line $\omega = csq$ where cs is the velocity of the Stoneley waves. This is consistent with the result that the Green function used in the elasticity

theory to describe the scattering probability has simple poles as a function of ω at the frequencies of the normal phonon modes of the system. Notice that for such layered systems, we have no normal modes corresponding to the LA and TA vibrations. The Green function of the elasticity theory has only branch cut singularities corresponding to the frequencies $\omega = sq$, $s'q$ and $\omega = cq$, $c'q$. In general, the condition for the existence of the Stoneley waves is quite complex and cannot be investigated analytically for an arbitrary ratio of the parameters of the two contacted media [159]. It is, therefore, reasonable taking into account the scattering kinematics to analyze the kernel K separately for different ranges of the electron energy typical for the scattering in the Fermi 2DEG. This will be done in the next section. *Vide infra* we consider limiting cases of the kernel K .

In the case of the contact between solid and liquid semi-spaces taking the imaginary part in Eq. (3.16), beforehand tending $c' \rightarrow 0$ in Eq. (3.17), we obtain for the kernel

$$K(\omega, q|z_1, z_2) = \frac{\omega^2}{\rho s^4} \frac{1}{2a} \{ \cos[a(z_1 - z_2)] - \mathcal{R}_{s-l} \cos[a(z_1 + z_2)] \}, sq < \omega \quad (3.18)$$

$$K(\omega, q|z_1, z_2) = \frac{\omega^2}{\rho s^4} \frac{[4bq^2 + \frac{\rho' \alpha \omega^4}{\rho \alpha' c^4}](b^2 - q^2)^2}{[4\alpha bq^2 + \frac{\rho' \alpha \omega^4}{\rho \alpha' c^4}]^2 + (b^2 - q^2)^4} e^{-\alpha(z_1 + z_2)}, cq < \omega < s'q \quad (3.19)$$

$$K(\omega, q|z_1, z_2) = \frac{\omega^2}{\rho s^4} \frac{\frac{\rho' \alpha \omega^4}{\rho \alpha' c^4}(\beta^2 + q^2)^2}{[4\alpha bq^2 + \frac{\rho' \alpha \omega^4}{\rho \alpha' c^4}]^2 + \frac{\rho' \alpha^2 \omega^8}{\rho \alpha' c^8}} e^{-\alpha(z_1 + z_2)}, s'q < \omega < cq, \quad (3.20)$$

$$K(\omega, q|z_1, z_2) = \frac{\omega^2}{\rho s^4} [4\beta q^2 - \frac{\rho' \alpha \omega^4}{\rho \alpha' c^4}] \times \pi \delta \left(4\alpha \beta q^2 - (\beta^2 + q^2)^2 - \frac{\rho' \alpha \omega^4}{\rho \alpha' c^4} \right) e^{-\alpha(z_1 + z_2)}, \omega < s'q \quad (3.21)$$

where

$$\mathcal{R}_{s-l} = - \frac{4abq^2 - (b^2 - q^2)^2 + \frac{\rho' \alpha \omega^4}{\rho \alpha' c^4}}{4abq^2 + (b^2 - q^2)^2 + \frac{\rho' \alpha \omega^4}{\rho \alpha' c^4}} \quad (3.22)$$

is the LA \rightarrow LA reflection coefficient at the solid-liquid interface. Following notation is used here

$$a = \sqrt{\frac{\omega^2}{s^2} - q^2}, \quad b = \sqrt{\frac{\omega^2}{c^2} - q^2}, \quad (3.23)$$

$$\alpha = \sqrt{q^2 - \frac{\omega^2}{s^2}}, \quad \beta = \sqrt{q^2 - \frac{\omega^2}{c^2}}, \quad (3.24)$$

and a' and α' are defined using the parameters of the liquid medium. In the majority of cases the sound velocity s' in a liquid is less than the velocity of the TA waves in a solid, which we assume to be true here. The bulk acoustic phonon contribution to the scattering is determined by formulas (3.18) and (3.19). Moreover, the LA phonons contribute to the scattering only in the range $\omega > sq$ while the TA phonons – in the whole range $\omega > cq$. Therefore, it is impossible to distinguish the LA and TA phonon contributions. This is natural, as far as, in strict sense, there exist no LA and TA normal modes in this case. They are mixed in the reflection at the interface and form a single bulk wave. It follows from the formulas (3.18)-(3.21) that in the range $\omega < s'q$ the kernel K differs from zero only if the argument of the delta function in Eq. (3.21) vanishes. In contrast to the boundary between the two solid semi-spaces, this condition is satisfied for any ratio of the parameters of solid and liquid media [160] and yields the dispersion law of the Stoneley waves [161]. The energy of the surface Stoneley waves is then concentrated mainly in the liquid medium on the distance of some phonon wavelengths. In the range $s'q < \omega < cq$ the value of K differs from zero because of the interaction of electrons with surface *leaky waves* [161]. These *leaky waves* are actually damped surface Rayleigh waves modified somewhat by the response of the liquid medium. This type of wave transfers energy continuously to the liquid forming an inhomogeneous wave moving away from the interface. This is due to the fact that, strictly speaking, *leaky waves* are not of the surface type. It follows from Eq. (3.20) that the *leaky waves* correspond to a pole on a nonphysical sheet of the Green function of the elasticity theory for the solid-liquid contact. As the differences between the elastic properties of the two contacted semi-spaces decrease, the *leaky wave* becomes even more strongly damped, so that we cannot regard it as a surface wave.

The kernel K for the semi-infinite space with free surface is easy to obtain from formulas (3.18)-(3.21) taking the limit $\rho' \rightarrow 0$. This gives

$$K(\omega, q|z_1, z_2) = \frac{\omega^2}{\rho s^4} \frac{1}{2a} \{ \cos[a(z_1 - z_2)] - \mathcal{R}_{fr} \cos[a(z_1 + z_2)] \}, sq < \omega \quad (3.25)$$

$$K(\omega, q|z_1, z_2) = \frac{\omega^2}{\rho s^4} \frac{4bq^2(b^2 - q^2)^2}{16\alpha^2 b^2 q^4 + (b^2 - q^2)^4} e^{-\alpha(z_1 + z_2)}, cq < \omega < sq, \quad (3.26)$$

$$K(\omega, q|z_1, z_2) = \frac{\omega^2}{\rho s^4} 4\beta q^2 \pi \delta \left(4\alpha\beta q^2 - (\beta^2 + q^2)^2 \right) e^{-\alpha(z_1 + z_2)}, \omega < cq \quad (3.27)$$

where

$$\mathcal{R}_{fr} = -\frac{4abq^2 - (b^2 - q^2)^2}{4abq^2 + (b^2 - q^2)^2} \quad (3.28)$$

is the LA \rightarrow LA reflection coefficient at the free crystal surface. Comparison of Eqs. (3.18)-(3.21) with Eqs. (3.25)-(3.27) shows that only surface waves are qualitatively changed: the Stoneley waves disappear while *leaky waves* transform into the rigorously stationary Rayleigh waves. Therefore in the range $\omega < cq$, the kernel K differs from zero only on the line $\omega = c_R q$, c_R is the velocity of the Rayleigh waves.

In the case of the rigid boundary, the kernel K can be obtained taking the imaginary part in Eq. (3.16), beforehand in Eq. (3.17) tending $\rho' \rightarrow \infty$. This gives

$$K(\omega, q|z_1, z_2) = \frac{\omega^2}{\rho s^4} \frac{1}{2a} \{ \cos[a(z_1 - z_2)] - \mathcal{R}_{rgd} \cos[a(z_1 + z_2)] \}, \quad sq < \omega < cq \quad (3.29)$$

$$K(\omega, q|z_1, z_2) = \frac{\omega^2}{\rho s^4} \frac{bq^2}{q^4 + \alpha^2 b^2} \exp[-\alpha(z_1 + z_2)], \quad cq < \omega < sq \quad (3.30)$$

where the LA \rightarrow LA reflection coefficient at the rigid crystal surface is given by

$$\mathcal{R}_{rgd} = -\frac{ab - q^2}{ab + q^2}. \quad (3.31)$$

As it was to be expected, the scattering is determined only by the bulk waves in this case.

3.4 Scattering probability in a Fermi gas

It is assumed that all the electrons occupy a single level of transverse motion, *i.e.* $\varepsilon_F \ll \hbar\omega_d$, $\hbar\omega_d \equiv \pi^2 \hbar^2 / m_c d^2$ (or $k_F \ll \pi/d$), where d is the thickness of the region of the electron transverse motion in the direction of the z -axis. The scattering takes place between states with different k but all belonging to the same transverse level. The electron gas is separated from the surface by a distance \bar{z} (see Fig. 3.2). For clarity, we first discuss the situation when the lattice temperature T and the electron temperature T_e are zero. Neglecting the reflection of phonons from the surface, it is easy to determine the phonon momenta which dominate in the scattering. A typical normal wave vector component $q_\perp \equiv q_z$

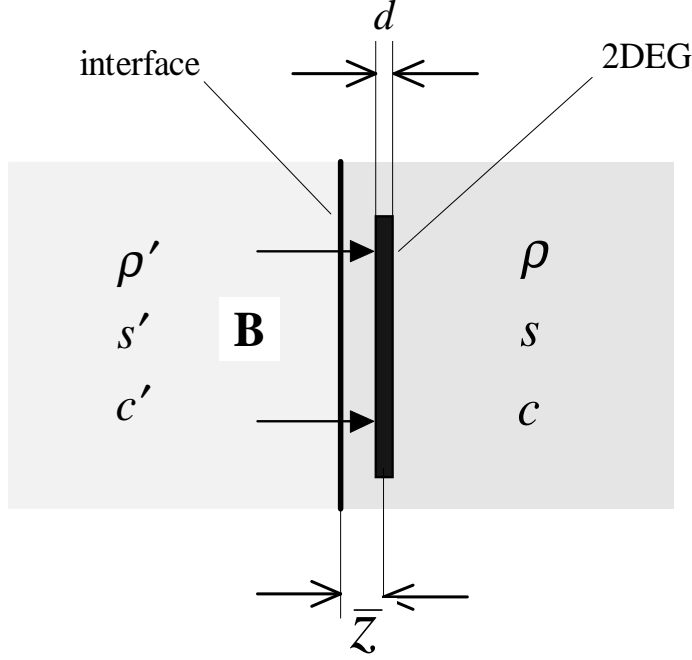


Figure 3.2: The Fermi 2DEG located near the interface separating elastic semi-spaces.

and a typical tangential wave vector component $\mathbf{q}_{\parallel} \equiv (q_x, q_y)$ may generally be different. According to [162] there are three energy ranges $\varepsilon - \varepsilon_F$ for a test electron in which the scattering is qualitatively different. The boundaries of these ranges are determined by the following two energies:

$$\varepsilon_1 = \hbar s k_F = \sqrt{2m_c s^2 \varepsilon_F}, \quad \varepsilon_2 = \pi \hbar s / d = \sqrt{2m_c s^2 \hbar \omega_d}, \quad \varepsilon_1 / \varepsilon_2 = k_F d / \pi \ll 1. \quad (3.32)$$

We now list the characteristic phonon momenta and energies corresponding to the scattering in the three ranges defined above:

range A – $\varepsilon - \varepsilon_F \ll \varepsilon_1$, in which small-angle inelastic scattering takes place

$$q_{\perp} \sim q_{\parallel} \sim \frac{\varepsilon - \varepsilon_F}{\hbar s} \ll k_F; \quad \hbar \omega \sim \varepsilon - \varepsilon_F, \quad (3.33)$$

range B – $\varepsilon_1 \ll \varepsilon - \varepsilon_F \ll \varepsilon_2$, in which large-angle inelastic scattering is dominant

$$q_{\perp} \sim \frac{\varepsilon - \varepsilon_F}{\hbar s} \gg q_{\parallel} \sim k_F; \quad \hbar \omega \sim \varepsilon - \varepsilon_F, \quad (3.34)$$

range C - $\varepsilon_2 \ll \varepsilon - \varepsilon_F$, in which large-angle quasi-elastic scattering takes place

$$q_{\perp} \sim \pi/d \gg q_{\parallel} \sim k_F; \hbar\omega \sim \hbar\pi s/d \ll \varepsilon - \varepsilon_F. \quad (3.35)$$

Now we discuss the interface effect on the scattering probability W in the Fermi 2DEG. For simplicity we first consider the free surface effect. It is clear that the boundary has no effect on the scattering probability W for $q_{\perp}\bar{z} \gg 1$ and should modify W for $q_{\perp}\bar{z} \lesssim 1$. We shall show below that a free boundary suppresses strongly the scattering in the range B for $q_{\perp}\bar{z} \ll 1$.

Consider now only longitudinal LA phonons (*i.e.*, assume that the shear modulus is zero). The dilatation on a free surface satisfies $u \equiv \mathbf{div} \mathbf{u} = 0$ and scattering from the deformation potential is strongly suppressed when electrons are located near a dilatation node, *i.e.*, for $q_{\perp}\bar{z} \ll 1$. Since the condition $\bar{z} \gtrsim d$ is satisfied, this cannot occur in the range C. However, we may expect suppression of scattering in the ranges A and B provided for

$$\frac{\varepsilon - \varepsilon_F}{\hbar s} \bar{z} \ll 1. \quad (3.36)$$

Now we account for the TA phonons. We find that $u \neq 0$ holds on a free surface and it would be incorrect to conclude quite generally that the scattering is suppressed. We shall now consider q_{\parallel} . The inequality $q_{\parallel} \ll q_{\perp}$ holds in the range B, *i.e.*, LA phonons traveling in a direction almost perpendicular to the surface contribute mainly to the scattering. When such LA phonons are reflected from the boundary, TA phonons do not participate in the scattering and, therefore, suppression of the scattering takes place. A strong mixing of LA and TA modes occurs in the region A where the condition $q_{\parallel} \sim q_{\perp}$ is not a sufficient requirement for the scattering to be suppressed. It follows that strong suppression of the scattering in the vicinity of a free surface should occur only in the range B. The effect of the reflection of phonons from a free surface in the ranges A and C, when $\bar{z}(\varepsilon - \varepsilon_F)/\hbar s \lesssim 1$, should lead only to a numerical factor of the order of unity.

Now we consider in which way situation is changed for the interface between elastic semi-spaces. In this case because of the response of the second medium $\mathbf{div} \mathbf{u} \neq 0$ even if the mixing of the TA phonons do not take into account. The measure of the second medium response at $q_{\parallel} = 0$ is the parameter $\lambda = \rho s/\rho' s'$

where ρs is a medium normal impedance. Therefore in those cases when the elastic semi-space is contiguous with a rarefied medium, *i.e.* $\lambda \ll 1$ then one can expect that in the range B, the scattering suppression takes place as before.

We have assumed that $T = 0$. This condition is essentially equivalent to the requirement $T \ll \varepsilon - \varepsilon_F$. It is, therefore, clear that our estimates of q_{\parallel} and q_{\perp} remain also valid for $T \neq 0$ provided the inequality $T \lesssim \varepsilon - \varepsilon_F$ holds. We shall now consider scattering in the range B. It is then possible to expand the kernel K in powers of a small parameter $s^2 q^2 / \omega^2$. Such an expansion yields

$$K(\omega, q|z_1, z_2) = \frac{\omega}{2\rho s^3} \left\{ \cos \left[\frac{\omega}{s}(z_1 - z_2) \right] - \mathcal{R}_{s-l} \cos \left[\frac{\omega}{s}(z_1 + z_2) \right] \right\}, \quad (3.37)$$

$$\mathcal{R}_{s-l} = \mathcal{R}_0 - \frac{s^2 q^2}{\omega^2} \mathcal{R}_1, \quad \mathcal{R}_0 = \frac{1 - \lambda}{1 + \lambda}, \quad (3.38)$$

$$\begin{aligned} \mathcal{R}_1 = & \frac{1}{(1 + \sigma)(1 + \lambda)^2} \left[\left(\frac{2c}{s} \right)^3 - \lambda \left(1 - \frac{s'^2}{s^2} + \frac{2s'c'}{s^2} - \frac{8c^2}{s^2} - \frac{8cc'}{s^2} + \frac{16cc'^2}{s^2 s'} \right) \right. \\ & \left. - \lambda \sigma \left(1 - \frac{s'^2}{s^2} + \frac{4s'c}{s^2} - \frac{8cc'}{s^2} - \frac{8c'^2}{s^2} + \frac{8c'^3}{s^2 s'} \right) - 2\lambda^2 \sigma \frac{c}{s} \right], \quad \sigma = \frac{\rho c}{\rho' c'}. \end{aligned} \quad (3.39)$$

In the region C, the arguments of the cosines in Eq. (3.37) are of the order of π so that we can simplify K by dropping out low-order terms. This gives

$$K(\omega, q|z_1, z_2) = \frac{\omega}{2\rho s^3} \left\{ \cos \left[\frac{\omega}{s}(z_1 - z_2) \right] - \mathcal{R}_0 \cos \left[\frac{\omega}{s}(z_1 + z_2) \right] \right\}. \quad (3.40)$$

Substituting Eqs. (3.40) and Eq. (3.11) into Eq. 3.8, we obtain the scattering probability in the range C between states belonging to the same level of the electron transverse motion

$$\begin{aligned} W_{\mathbf{k} \rightarrow \mathbf{n}'\mathbf{k}'}^{\pm} &= \frac{1}{\bar{\tau}_F} \frac{\pi}{L^2} \frac{\hbar \omega}{m_c (s k_F)^2} \left[N_T(\omega) + \frac{1}{2} \pm \frac{1}{2} \right] \int dz_1 dz_2 \rho(z_1) \rho(z_2) \\ &\times \left\{ \cos \left[\frac{\omega}{s}(z_1 - z_2) \right] - \mathcal{R}_0 \cos \left[\frac{\omega}{s}(z_1 + z_2) \right] \right\}. \end{aligned} \quad (3.41)$$

where $\rho(z) = |\psi(z)|^2$ is the probability to find an electron on a level of the transverse quantization, and

$$\frac{1}{\bar{\tau}_F} = \frac{1}{\pi} \frac{m_c k_F^2}{\hbar^2} \frac{\Xi^2}{\rho s} \quad (3.42)$$

is the characteristic scattering time in the Fermi gas of electrons by the deformation potential of acoustic phonons [136]. It is seen from Eq. (3.41) that W does

not depend on the TA phonon velocity in the medium 2, therefore this expression is true for the solid-liquid contact too. It is easy to find the scattering probability for the cases of free and rigid surfaces taking, respectively, the limits $\rho \rightarrow 0$ and $\rho \rightarrow \infty$ in Eq. (3.41).

In region B, we can use the condition $\omega d/s \ll 1$ and represent the kernel K in the form

$$K(\omega, q|z_1, z_2) = \frac{\omega}{2\rho s^3} \left\{ \sin \frac{\omega}{s} z_1 \sin \frac{\omega}{s} z_2 - \left[\frac{\lambda}{1+\lambda} + \frac{s^2 q^2}{\omega^2} \mathcal{R}_1 \right] \cos \left[\frac{\omega}{s} (z_1 + z_2) \right] \right\}. \quad (3.43)$$

Provided the scattering takes place between states of the same level of the transverse motion n , it follows from Eq. (3.8) that this kernel K should be averaged over the functions $\rho(z)$ describing the transverse motion. The first term then involves integrals

$$\int dz \rho(z) \sin \frac{\omega}{s} z. \quad (3.44)$$

We set $z = \bar{z} + \zeta$, where

$$\bar{z} = \int dz z \rho(z), \quad (3.45)$$

then the inequality $(\omega/s)\zeta \sim (\varepsilon - \varepsilon_F)d/s \ll 1$ holds and the sinus in the integral (3.44) can be expanded in powers of ζ (for any \bar{z} including small values of this quantity). Bearing in mind the definition of \bar{z} , we find the integral in Eq. (3.44) is equal to $\sin(\omega/s)\bar{z}$. As for the cosine in the second term, we can replace $z_1 + z_2$ in this function by $2\bar{z}$. As a result for the scattering probability in the region B, we obtain

$$W_{\mathbf{k} \rightarrow n' \mathbf{k}'}^{\pm} = \frac{1}{\bar{\tau}_F} \frac{2\pi}{L^2} \frac{\hbar \omega}{m_c (s k_F)^2} \left[N_T(\omega) + \frac{1}{2} \pm \frac{1}{2} \right] \times \left\{ \sin^2 \frac{\omega}{s} \bar{z} - \left[\frac{\lambda}{1+\lambda} + \frac{s^2 q^2}{\omega^2} \mathcal{R}_1 \right] \cos 2 \frac{\omega}{s} \bar{z} \right\}. \quad (3.46)$$

The first term in the brackets in Eq. (3.46) appears because electrons are far from a node of the deformation potential which occurs at $z = 0$ for LA phonons. The second term is due to an admixture of TA phonons at the boundary due to the reflection of LA phonons and eliminates the deformation potential node. If the elastic properties of contacting media differ slightly, *i.e.* $\lambda \approx 1$, one can

neglect the second term in the square bracket in Eq. (3.46). Moreover, consider the 2DEG located in the immediate vicinity from the interface, *i.e.* $\bar{z} \sim d$, the first term in Eq. (3.46) also can be neglected. Then, the scattering probability W only by a factor $2\lambda/(1+\lambda)$ differs from the scattering probability W_{3D} calculated without taking into account the phonon reflection at the interface. For the latter case W_{3D} can be obtained by omitting the terms in Eq. (3.46) which oscillate rapidly in the limit $\bar{z} \rightarrow \infty$, *i.e.* the figure bracket is replaced by $1/2$. This fully correspond also to the rigid surface case: in this case we have $\mathcal{R}_1 \rightarrow 2c/s$ and $2\lambda/(1+\lambda) \rightarrow 2$ when $\rho' \rightarrow \infty$.

The situation is changed for $\lambda \ll 1$. In this case neither term in the Eq. (3.46) can be neglected and the scattering probability is determined by "competition" of all terms. Notice, that Eq. (3.46) is valid also for the case of the solid-liquid contact for which

$$\mathcal{R}_1 = \frac{1}{(1+\lambda)^2} \left[\left(\frac{2c}{s} \right)^3 - \lambda \left(1 - \frac{s'^2}{s^2} - 8 \frac{c^2}{s^2} \right) \right]. \quad (3.47)$$

Consider now the third range A representing inelastic low-angle scattering. In view of the absence in this region of a corresponding small parameter, further simplifications of Eq. (3.16) for the kernel K is not generally possible. Therefore, we restrict our analysis to two limiting cases of a contact between a solid and a liquid and their rigidity fixed boundary. Making use that in the region A, $ad \ll 1$ and $\alpha d \ll 1$, the kernel K can be averaged over the functions $\rho(z)$ in the way that the scattering probability in the region A can be represented in the form

$$W_{\mathbf{k} \rightarrow \mathbf{n}'\mathbf{k}'}^{\pm} = \frac{1}{\bar{\tau}_F} \frac{2\pi}{L^2} \frac{\rho s}{m_c k_F^2} \left[N_T(\omega) + \frac{1}{2} \pm \frac{1}{2} \right] K(\omega, q | \bar{z}, \bar{z}). \quad (3.48)$$

Here the kernel K is given either by Eqs. (3.18)-(3.21), 3.25-(3.27) or (3.29)-(3.30). The scattering rate without allowance for the phonon reflection at the interface can be obtained by taking the limit $\bar{z} \rightarrow \infty$ in the above equation, *i.e.* by replacing $K \rightarrow \omega^2/2a\rho s^4$.

3.5 Energy and momentum relaxation of a test electron

We calculate the energy and momentum relaxation rates for a test electron which can be measured accurately in a wide range of temperatures T and T_e [163, 164]. According to [136], the energy relaxation time for the test electron in the Fermi gas is defined as

$$\mathcal{Q}_{n \rightarrow n'}(\varepsilon) = \frac{\varepsilon - \varepsilon_F}{\bar{\tau}(\varepsilon)} = \mathcal{Q}_{n \rightarrow n'}^+(\varepsilon) - \mathcal{Q}_{n \rightarrow n'}^-(\varepsilon), \quad (3.49)$$

$$\mathcal{Q}_{n \rightarrow n'}^{\pm}(\varepsilon) = \sum_{\mathbf{k}'}^{(\pm)} \hbar \omega W_{n\mathbf{k} \rightarrow n'\mathbf{k}'}^{\pm} \frac{1 - f_T(\varepsilon \mp \hbar \omega)}{1 - f_T(\varepsilon)}. \quad (3.50)$$

Here $\mathcal{Q}_{n \rightarrow n'}(\varepsilon)$ is the energy-loss power, f_T is the Fermi factor. The summation (+) is over the final states $\varepsilon(k') < \varepsilon(k)$, the summation (-) is over the final states $\varepsilon(k') > \varepsilon(k)$.

Substituting Eq. (3.41) in Eq. (3.50), we find that $\mathcal{Q}_{n \rightarrow n'}(\varepsilon)$ in the range C is described by

$$\mathcal{Q}(x) = \frac{1}{\bar{\tau}_F} J_1 \frac{(\pi s/d)}{2(k_F d)^2} \text{th} \frac{x}{2}, \quad x = \frac{\varepsilon - \varepsilon_F}{T} \quad (3.51)$$

where the dimensionless integral

$$J_1 = d^3 \int_0^\infty dz [\partial_z \rho(z)]^2 \quad (3.52)$$

is of the order of unity. Hence, it is clear that the energy relaxation rate in the region C is just the same (apart from a numerical factor) with that of considered without the phonon reflection [162] and this is true for any parameters of the medium 2. This result is explained by the fact that in the region C, the interface is always distant, *i.e.* \bar{z} is greater or of the order of the characteristic phonon wavelength along $\hat{\mathbf{z}}$. Notice also that for hot electrons, $x \gg 1$, the relaxation rate does not depend on the electron energy

$$\mathcal{Q}(x) = \frac{1}{\bar{\tau}_F} J_1 \frac{(\pi s/d)}{2(k_F d)^2}. \quad (3.53)$$

As far as in the region C, the scattering is quasi-elastic (see Eq. (3.35)) then the momentum relaxation time is defined by

$$\frac{1}{\bar{\tau}_1(\varepsilon)} = \sum_{\mathbf{k}'} (1 - \cos \theta) W_{\mathbf{k} \rightarrow \mathbf{k}'} \frac{1 - f_T(\varepsilon - \hbar \omega)}{1 - f_T(\varepsilon)}, \quad (3.54)$$

where θ is the scattering angle between \mathbf{k} and \mathbf{k}' . Substituting Eq. (3.41) into Eq. (3.54), we obtain

$$\frac{1}{\bar{\tau}_1(\varepsilon)} = \frac{1}{\bar{\tau}_F} J_0 \frac{(\pi s/d)}{2(k_F d)^2} T, \quad J_0 = d \int_0^\infty dz \rho^2(z). \quad (3.55)$$

It is easy to check that this expression for the momentum relaxation time is in agreement with that of obtained in [162] without allowance for the phonon reflection. Thus in the range C, the interface effect on the energy and momentum relaxation rates is practically absent.

Making use the scattering probability (3.46), we find the following result for the energy relaxation rate in the range B:

$$\frac{\varepsilon - \varepsilon_F}{\bar{\tau}(\varepsilon)} = \frac{1}{\bar{\tau}_F} \left\{ \frac{T^3}{2(\hbar s k_F)^2} [\mathcal{F}_2^-(0|x) - \mathcal{R}_0 \mathcal{F}_2^-(\xi|x)] + \mathcal{R}_1 \mathcal{F}_0^-(\xi|x) \right\} \quad (3.56)$$

where

$$\mathcal{F}_m^-(\xi|x) = \int_0^\infty dy y^m \cos \xi y \left\{ \frac{1}{1 + \exp(y-x)} + \frac{1}{1 + \exp(y+x)} \right\}, \quad \xi = 2 \frac{T}{\hbar(s/\bar{z})}. \quad (3.57)$$

For hot electrons taking the limit $T \rightarrow 0$ in Eq. (3.56), we can obtain

$$\frac{1}{\bar{\tau}(\varepsilon)} = \frac{1}{\bar{\tau}_F} \left\{ \frac{(\varepsilon - \varepsilon_F)^2}{6(\hbar s k_F)^2} \mathcal{I}(\eta, \lambda) + \mathcal{R}_1 \frac{\sin \eta}{\eta} \right\} \quad (3.58)$$

where

$$\mathcal{I}(\eta, \lambda) = 1 - 3 \frac{1 - \lambda}{1 + \lambda} \left[\left(1 - \frac{2}{\eta^2} \right) \frac{\sin \eta}{\eta} + \frac{2}{\eta^2} \cos \eta \right] \quad (3.59)$$

Here $\eta = 2(\varepsilon - \varepsilon_F)\bar{z}/(\hbar s)$ is a parameter describing the distance of a hot electron from the surface. It can be seen that the energy relaxation rate for the test electron is an oscillatory function of the separation \bar{z} of the electron gas from the surface. When the 2DEG is far from the surface, *i.e.* $\bar{z} \gg d$ ($\eta \gg 1$), we obtain

$$\frac{1}{\bar{\tau}(\varepsilon)} = \frac{1}{\bar{\tau}_F} \frac{(\varepsilon - \varepsilon_F)^2}{6(\hbar s k_F)^2} \quad (3.60)$$

The condition $\bar{z} \sim d$ is satisfied for a 2DEG near the surface and the inequality $\eta \lesssim 1$ holds, which yields

$$\frac{1}{\bar{\tau}(\varepsilon)} = \frac{1}{\bar{\tau}_F} \left\{ \mathcal{R}_1 + \frac{\lambda}{1 + \lambda} \frac{(\varepsilon - \varepsilon_F)^2}{3(\hbar s k_F)^2} + \frac{(\varepsilon - \varepsilon_F)^4}{5(\hbar s k_F)^2 (\hbar s / \bar{z})^2} \right\} \quad (3.61)$$

From this equation for the free surface ($\lambda = 0$ and $\mathcal{R}_1 = (2c/s)^3$), it is easy to find

$$\frac{1}{\bar{\tau}(\varepsilon)} = \frac{1}{\bar{\tau}_F} \left\{ \left(\frac{2c}{s} \right)^3 + \frac{(\varepsilon - \varepsilon_F)^4}{5(\hbar s k_F)^2 (\hbar s / \bar{z})^2} \right\} \quad (3.62)$$

Both terms become comparable for $\varepsilon - \varepsilon_F \sim \sqrt{\varepsilon_1 \varepsilon_2}$. The first term is dominant for small $\varepsilon - \varepsilon_F$, *i.e.*, mixing of LA and TA vibrations is important whereas, for large $\varepsilon - \varepsilon_F$, the second term predominates, *i.e.*, we have the effect corresponding to large distances of electrons from the surface. It can be seen from Eqs. (3.60) and (3.62) that a free surface modifies the energy dependence of the energy relaxation rate and leads to the strong suppression of the relaxation since

$$\frac{\bar{\tau}(\varepsilon)|_{\bar{z} \rightarrow \infty}}{\bar{\tau}(\varepsilon)|_{\bar{z} \sim d}} \sim \frac{(\varepsilon - \varepsilon_F)^2}{\varepsilon_2^2} + \frac{\varepsilon_1^2}{(\varepsilon - \varepsilon_F)^2} \ll 1. \quad (3.63)$$

There is no suppression of the relaxation at the boundaries of the range B: for $\varepsilon - \varepsilon_F \sim \varepsilon_1$ because of the strong mixing of LA and TA vibrations and for $\varepsilon - \varepsilon_F \sim \varepsilon_2$ because the distance from the surface becomes of the order of the effective phonon wavelength π/q_\perp .

From comparison of Eqs. (3.61) and (3.62), we obtain the criterion

$$\lambda \ll \frac{\varepsilon_1}{\varepsilon_2} \quad (3.64)$$

which allows us to determine when the interface near which the Fermi 2DEG is located, can be regarded as free. Actually, if inequality (3.64) is obeyed, we can ignore the second term in parentheses in Eq. (3.61). Then, Eq. (3.61) reduces to Eq. (3.62) for the free surface. In the case if

$$\frac{\varepsilon_1}{\varepsilon_2} \sim \lambda \ll 1 \quad (3.65)$$

the boundary can no longer be regarded as free, but we can easily see that the reduction in the relaxation rate still occurs. If the condition (3.65) is satisfied, comparison of Eqs. (3.60) and (3.61) yields

$$\frac{\bar{\tau}(\varepsilon)|_{\bar{z} \rightarrow \infty}}{\bar{\tau}(\varepsilon)|_{\bar{z} \sim d}} \sim \frac{(\varepsilon - \varepsilon_F)^2}{\varepsilon_2^2} + \lambda + \frac{\varepsilon_1^2}{(\varepsilon - \varepsilon_F)^2} \ll 1. \quad (3.66)$$

Now it is seen, if $\lambda \gtrsim 1$, the suppression of the relaxation vanishes because of the strong response of the second medium. In this case we ought to retain only the

second term in Eq. (3.61). Then the energy relaxation rate differs only by the factor $2\lambda(1+\lambda)$ from that of when the phonon reflection is not taken into account. It therefore follows that for the rigid boundary, the relaxation of a test electron is twice as fast as in the case when phonons are three dimensional.

For thermal electrons ($x \sim 1$), ξ is the parameter describing the separation between the interfaces and 2DEG. For remote boundary, $\xi \gg 1$, integrals containing a rapidly oscillating factor $\cos \xi y$ are small, and according to [162] we obtain

$$\frac{\varepsilon - \varepsilon_F}{\bar{\tau}(\varepsilon)} = \frac{1}{\bar{\tau}_F} \frac{T^3}{2(\hbar s k_F)^2} \mathcal{F}_2^-(0|x). \quad (3.67)$$

Consider now a nearby boundary when the condition $\xi \ll 1$ is satisfied. Expanding $\cos \xi y$, we obtain

$$\frac{\varepsilon - \varepsilon_F}{\bar{\tau}(\varepsilon)} = \frac{1}{\bar{\tau}_F} \left\{ \mathcal{R}_1 T + \frac{\lambda}{1+\lambda} \frac{T}{(\hbar s k_F)^2} \mathcal{F}_2^-(0|x) + \frac{T^5}{(\hbar s k_F)^2 (\hbar s / \bar{z})^2} \mathcal{F}_4^-(\xi|x) \right\} \quad (3.68)$$

We have used the result $\mathcal{F}_0^-(0|x) = x$. It can be seen that the criteria (3.64) holds for thermal electrons too. For T in the range B, provided for Eq. (3.65) holds, the relaxation is suppressed even for thermal electrons. For $x \sim 1$, we obtain $\mathcal{F}_m^-(0|x) \sim 1$ and the ratio of the results defined by Eqs. (3.67) and (3.68) is again determined by Eq. (3.66) where $\varepsilon - \varepsilon_F$ should be replaced by T .

In the case when $\lambda \gtrsim 1$, making use Eq. (3.67), we can write

$$\frac{1}{\bar{\tau}(\varepsilon)} = \frac{2\lambda}{1+\lambda} \frac{1}{\bar{\tau}(\varepsilon)|_{\bar{z} \rightarrow \infty}}. \quad (3.69)$$

It should be noticed that both in the ranges C and B, the electron relaxation is mainly due to the bulk acoustic waves. In these energy ranges $\varepsilon - \varepsilon_F \gg \varepsilon_1$ and the scattering due to surface phonons is always quasi-elastic:

$$q_{\parallel} \sim k_F; \quad \omega = c_S q \sim \varepsilon_1 \ll \varepsilon - \varepsilon_F \quad (3.70)$$

therefore their contribution to $\bar{\tau}(\varepsilon)$ is small.

The scattering on the bulk waves is neither quasi-elastic nor small-angle, therefore the momentum relaxation time $\bar{\tau}_1(\varepsilon)$ is of the same order of the energy relaxation time $\bar{\tau}(\varepsilon)$ given by Eq. (3.56). To estimate the role of the surface phonons in the momentum relaxation, we calculate $\bar{\tau}_1(\varepsilon)$ conditioned by the Rayleigh waves

in the free surface case and by the Stoneley waves for the solid-liquid contact. Substituting Eqs. (3.21) and (3.27) into Eqs. (3.8), (3.11), and (3.54), we obtain at $T = 0$

$$\frac{1}{\bar{\tau}_1(\varepsilon)|_{R,S}} = \frac{3\pi}{4} \frac{1}{\bar{\tau}_F} \left(\frac{c_{R,S}}{s} \right)^3 \bar{\Phi}_0^{R,S} \quad (3.71)$$

where the dimensionless factors $\bar{\Phi}_0^{R,S}$ are of the order of unity and determined by parameters of the contacted elastic media (*vide infra* in Appendix (B)). Indices R, S pertain to the Rayleigh and Stoneley waves, respectively. From Eqs. (3.61) and (3.71), one can see that the surface phonon contribution to momentum relaxation is of the order of the bulk phonon contribution in the energy interval $\varepsilon_1 \ll \varepsilon - \varepsilon_F \ll \lambda^{-1/2}\varepsilon_1$ of the range B while in the energy interval $\lambda^{-1/2}\varepsilon_1 \ll \varepsilon - \varepsilon_F \ll \varepsilon_2$, the surface phonon contribution to $\bar{\tau}_1(\varepsilon)$ is small. Thus, in the energy range B if the relations (3.64) and (3.65) hold, the interface suppresses both the energy and momentum relaxation rates.

Now we consider the range A. Substituting Eq. (3.48) into Eq. (3.50), the energy relaxation rate can be represented in the form

$$\frac{\varepsilon - \varepsilon_F}{\bar{\tau}(\varepsilon)} = \frac{1}{\bar{\tau}_F} \frac{T^4}{\pi(\hbar s k_F)^3} \int_0^\infty dt dy y^3 \left\{ \frac{1}{1 + \exp(y - x)} - \frac{1}{1 + \exp(y + x)} \right\} \Phi(t|\xi y) \quad (3.72)$$

where

$$\Phi(t|\xi y) \equiv K(\omega, q|\bar{z}, \bar{z}), \quad y = \frac{\hbar\omega}{T}, \quad t = \frac{sq}{\omega}. \quad (3.73)$$

For the remote interface neglecting in the above formula rapidly oscillating and exponentially small terms at $\xi \gg 1$, we obtain in agreement with [162]

$$\frac{\varepsilon - \varepsilon_F}{\bar{\tau}(\varepsilon)} = \frac{1}{\bar{\tau}_F} \frac{T^4}{4(\hbar s k_F)^3} \mathcal{F}_3^-(0|x). \quad (3.74)$$

For the adjacent interface, tending $\xi \rightarrow 0$ in Eq. (3.72), we find

$$\frac{\varepsilon - \varepsilon_F}{\bar{\tau}(\varepsilon)} = \frac{1}{\bar{\tau}_F} \frac{T^4}{4(\hbar s k_F)^3} \hat{\Phi}_0 \mathcal{F}_3^-(0|x). \quad (3.75)$$

where

$$\hat{\Phi}_m = \frac{2^{2+m}}{\pi} \int_0^\infty dt t^{2m} \Phi(t|0). \quad (3.76)$$

For hot electrons using an asymptotics of the function $\mathcal{F}_3^-(0|x)$ for large x , we obtain

$$\frac{1}{\bar{\tau}(\varepsilon)} = \hat{\Phi}_0 \frac{1}{\bar{\tau}(\varepsilon)|_{\bar{z} \rightarrow \infty}}, \quad \frac{1}{\bar{\tau}(\varepsilon)|_{\bar{z} \rightarrow \infty}} = \frac{1}{\bar{\tau}_F} \frac{\varepsilon - \varepsilon_F}{16(\hbar s k_F)^3}. \quad (3.77)$$

As far as $|\varepsilon - \varepsilon_F| \ll \varepsilon_F$, the scattering in the Fermi gas always is kinematically quasi-elastic, $k = k' = k_F$, therefore in the region A too, the momentum relaxation rate can be calculated by the formula (3.54). Using the scattering probability (3.48), for the momentum relaxation time we obtain:

for the remote interface ($\xi \gg 1$)

$$\frac{1}{\bar{\tau}_1(\varepsilon)} = \frac{1}{16} \frac{1}{\bar{\tau}_F} \frac{T^5}{(\hbar s k_F)^5} \mathcal{F}_4^+(0|x), \quad (3.78)$$

for the adjacent interface ($\xi \ll 1$)

$$\frac{1}{\bar{\tau}_1(\varepsilon)} = \hat{\Phi}_1 \frac{1}{\bar{\tau}_1(\varepsilon)|_{\bar{z} \rightarrow \infty}}. \quad (3.79)$$

From comparison of the above two formulas, it is clear that in the region A, the relaxation rates, obtained allowing and ignoring the phonon reflection from interfaces, differ only in respect of the factor $\hat{\Phi}_m$ which is of the order of unity. This result is due to the strong mixing of LA and TA waves at the reflection in this range.

The integrals $\hat{\Phi}_m$ cannot be calculated analytically. Explicit formulas for functions $\hat{\Phi}_m$ in the case of the solid-liquid contact, the free and rigid boundary, as well as some numerical estimates for particular values of parameters and asymptotic expressions are given in Appendix B. Notice only that in the case of the solid-liquid contact we find that $\hat{\Phi}_m$ is governed by both the bulk and surface wave contributions to the scattering:

$$\hat{\Phi}_m = \hat{\Phi}_m^{B_1} + \hat{\Phi}_m^{B_2} + \hat{\Phi}_m^L + \hat{\Phi}_m^S \quad (3.80)$$

where $\hat{\Phi}_m^B$, $\hat{\Phi}_m^L$ and $\hat{\Phi}_m^S$ correspond to the bulk phonon, *leaky* and Stoneley wave contributions, respectively. Moreover, the range A is the only region where the surface wave contribution is comparable with that of the bulk modes. In the case of a rigid boundary we find, naturally, that $\hat{\Phi}_m$ includes only the bulk phonon contributions.

3.6 Relaxation of electron temperature

When the distribution of hot electrons can be described by an electron temperature $T_e > T$, we can determine the energy relaxation rate for the whole electron

gas. Following [136], we find that the relaxation rate per electron is given by

$$\begin{aligned}\bar{\mathcal{Q}}(T_e, T) &= \frac{1}{NL^2} \sum_{\mathbf{k}} f_{T_e}(\varepsilon) \left\{ \sum_{\mathbf{k}'}^{(+)} \hbar\omega W_{n\mathbf{k} \rightarrow n'\mathbf{k}'} [1 - f_{T_e}(\varepsilon - \hbar\omega)] \right. \\ &\quad \left. - \sum_{\mathbf{k}'}^{(-)} \hbar\omega W_{n\mathbf{k} \rightarrow n'\mathbf{k}'} [1 - f_{T_e}(\varepsilon + \hbar\omega)] \right\}\end{aligned}\quad (3.81)$$

Straightforward calculations show that $\bar{\mathcal{Q}}(T_e, T)$ can be written as the difference between two functions depending only on T_e and T [165], *i.e.*,

$$\bar{\mathcal{Q}}(T_e, T) = \bar{\mathcal{Q}}(T_e) - \bar{\mathcal{Q}}(T) \quad (3.82)$$

Moreover for $\bar{\mathcal{Q}}$ in the corresponding regions, the following expressions are obtained.

In the region C

$$\bar{\mathcal{Q}}(T) = \bar{\mathcal{Q}}(T)|_{\bar{z} \rightarrow \infty} = \frac{1}{\bar{\tau}_F} \frac{(\pi \hbar s/d)}{2(k_F d)^2} \frac{T}{\varepsilon_F} J_1. \quad (3.83)$$

In the region B

$$\bar{\mathcal{Q}}(T) = \frac{1}{\bar{\tau}_F} \left\{ \frac{T^4}{2(\hbar s k_F)^2 \varepsilon_F} [\mathcal{F}_4(0) - \mathcal{R}_0 \mathcal{F}_4(\xi)] + \mathcal{R}_1 \mathcal{F}_2(\xi) \right\} \quad (3.84)$$

where

$$\mathcal{F}_m(\xi) = \frac{1}{2} \Gamma(m) [\zeta(1, 1 + i\xi) + \zeta(1, 1 - i\xi)] \quad (3.85)$$

and $\zeta(m, z)$ is the generalized Riemann zeta function. Now it is easy to obtain the relaxation rate for the distant interface ($\xi \gg 1$):

$$\bar{\mathcal{Q}}(T)|_{\bar{z} \rightarrow \infty} = \frac{\pi^4}{30} \frac{1}{\bar{\tau}_F} \frac{T^4}{(\hbar s k_F)^2 \varepsilon_F}, \quad (3.86)$$

while for adjacent interface, $\xi \ll 1$, we obtain

$$\bar{\mathcal{Q}}(T) = \frac{1}{\bar{\tau}_F} \left\{ \frac{\pi^2}{6} \mathcal{R}_1 \frac{T^2}{\varepsilon_F} + \frac{\pi^4}{15} \frac{\lambda}{1 + \lambda} \frac{T^4}{(\hbar s k_F)^2 \varepsilon_F} + \frac{8\pi^6}{63} \frac{T^6}{(\hbar s k_F)^2 (\hbar s/\bar{z})^2 \varepsilon_F} \right\}. \quad (3.87)$$

Follow to the above method, we can easily show that the criterias (3.64) and (3.65) hold for electron temperature relaxation too. The fulfillment of them implies that the interface separating elastic semi-spaces suppresses the electron temperature

relaxation in the range B. If $\lambda \gtrsim 1$ then the interface changes the relaxation rate only by a numerical factor:

$$\bar{\mathcal{Q}}(T) = \frac{2\lambda}{1+\lambda} \bar{\mathcal{Q}}(T)|_{\bar{z} \rightarrow \infty}. \quad (3.88)$$

Finally, in the region A, the cooling of the Fermi 2DEG for small ξ is given

$$\bar{\mathcal{Q}}(T) = \bar{\Phi}_0 \bar{\mathcal{Q}}(T)|_{\bar{z} \rightarrow \infty}. \quad (3.89)$$

where

$$\bar{\mathcal{Q}}(T)|_{\bar{z} \rightarrow \infty} = \frac{1}{\bar{\tau}_F} \Gamma(5) \zeta(5) \frac{T^4}{4(\hbar s k_F)^2 \varepsilon_F} \quad (3.90)$$

is the electron temperature relaxation rate without allowance for the phonon reflection in agreement with the previous result [162].

3.7 Discussion of results

From the results of calculations in this chapter, it becomes clear that the interface between elastic semi-spaces in different ways influences the electron scattering in the various characteristic energy ranges of the Fermi 2DEG. In the ranges of the inelastic small-angle A ($\varepsilon - \varepsilon_F \ll \hbar s k_F \equiv \varepsilon_1$) and of the elastic large-angle C ($\varepsilon - \varepsilon_F \gg \pi \hbar s / d \equiv \varepsilon_2$), the interface effect is slight. In the region A, it reduces simply to multiplication of the energy and momentum relaxation times by the coefficient $\bar{\Phi}$, whereas in the region C there is no changes at all. In the range A, the weak interface effect is conditioned by the strong conversion effect of the LA and TA phonon modes at the interface reflection. In the range C, the interface is always distant, *i.e.*, the effective wavelength of the interacting phonons, π/q_\perp , is much small than the distance between the 2DEG and interface. However, we can demonstrate that the reflection of phonons affects in higher orders of the small parameter that occurs in the region C. The range A is the only region where the surface phonon contribution to the scattering is essential both for the energy and momentum relaxation. The temperature dependencies obtained for the energy and momentum relaxation have been observed experimentally both in the low temperature range A [146, 164, 166] and the high temperature range C [145, 146, 144]. Recall that in both ranges, the temperature dependencies of

the relaxation times do not differ from that of for the bulk three dimensional phonons.

The large-angle inelastic scattering region B ($\varepsilon_1 \ll \varepsilon - \varepsilon_F \varepsilon_2$) limited from both sides. Therefore, the existence of the energy range B is ensured by the condition $\pi/(k_F d)$, *i.e.* by sufficiently low electron concentrations, $N \approx 10^{15} \text{ m}^{-2}$, and if the localization of the transverse motion of an electrons in the 2DEG is sufficiently strong, $d \approx 3 \text{ nm}$. We then find for GaAs nanostructures (see Table 2.4) that $k_F = 8 \cdot 10^7 \text{ m}^{-1}$, $\varepsilon_1 = 3 \text{ K}$ and $\varepsilon_2 = 40 \text{ K}$. It now follows that the criteria (3.65) is satisfied if $\lambda \ll 0.1$, *i.e.* in the situations when the elastic semi-space is in contact with a small mass density medium, such as gas. In this case the maximum interface effect is achieved in the middle of the energy interval $(\varepsilon_1, \varepsilon_2)$, *i.e.* for $\varepsilon - \varepsilon_F$, $T_e \approx 10 \text{ K}$. Therefore, according to Eq. (3.63), the presence of a free surface increases $\bar{\tau}$ and $\bar{\tau}_1$ in $\varepsilon_2/\varepsilon_1$ times, *i.e.* by a factor of the order of 10. Moreover, for the temperature range below 10 K (in this range, the surface waves also contribute to the momentum relaxation) we have $\bar{\tau}, \bar{\tau}_1 \propto T_e^0$ while for the temperature range above 10 K, $\bar{\tau}, \bar{\tau}_1 \propto T_e^4$, *i.e.* the free surface also alters the dependence of relaxation rates on the electron energy or temperature. Recall that if do not take into account the phonon reflection then $\bar{\tau}, \bar{\tau}_1 \propto T^2$. Estimates of the parameter λ indicate that in the majority of cases for a solid-liquid contact $\lambda \sim \varepsilon_1/\varepsilon_2$, therefore according to (3.66), the solid-liquid interface also strongly suppresses the electron relaxation rate: $\varepsilon_1/\varepsilon_2$ times if $\lambda \lesssim \varepsilon_1/\varepsilon_2$ and λ^{-1} times if $\lambda \gtrsim \varepsilon_1/\varepsilon_2$. In the latter case, the temperature dependence of the relaxation rate is altered in comparison with free surface case. In the middle of the interval $(\varepsilon_1, \varepsilon_2)$, the new mini interval $(\lambda^{-1/2}\varepsilon_1, \lambda^{1/2}\varepsilon_2)$ appears where $\bar{\tau}, \bar{\tau}_1 \propto T^2$. As the parameter λ increases the interval $(\lambda^{-1/2}\varepsilon_1, \lambda^{1/2}\varepsilon_2)$ becomes broader and for $\lambda \gtrsim 1$ covers all the range B. In this case $\bar{\tau}, \bar{\tau}_1$ only by the factor $2\lambda/(1+\lambda)$ differ from the relaxation times when the phonons are three dimensional. The dependence of the energy-loss power \bar{Q} on the electron temperature in the all temperature range is shown schematically in Fig. 3.3.

Notice that the characteristic distance which is required for an interface to have an effect on the electron relaxation is $\hbar s/T_e$. In the middle of the range B this for GaAs gives $\hbar s/T_e \approx 10 \text{ nm}$. In [164], the dependence of the energy relaxation on the electron temperature in inversion layers Si (100) has been measured. It

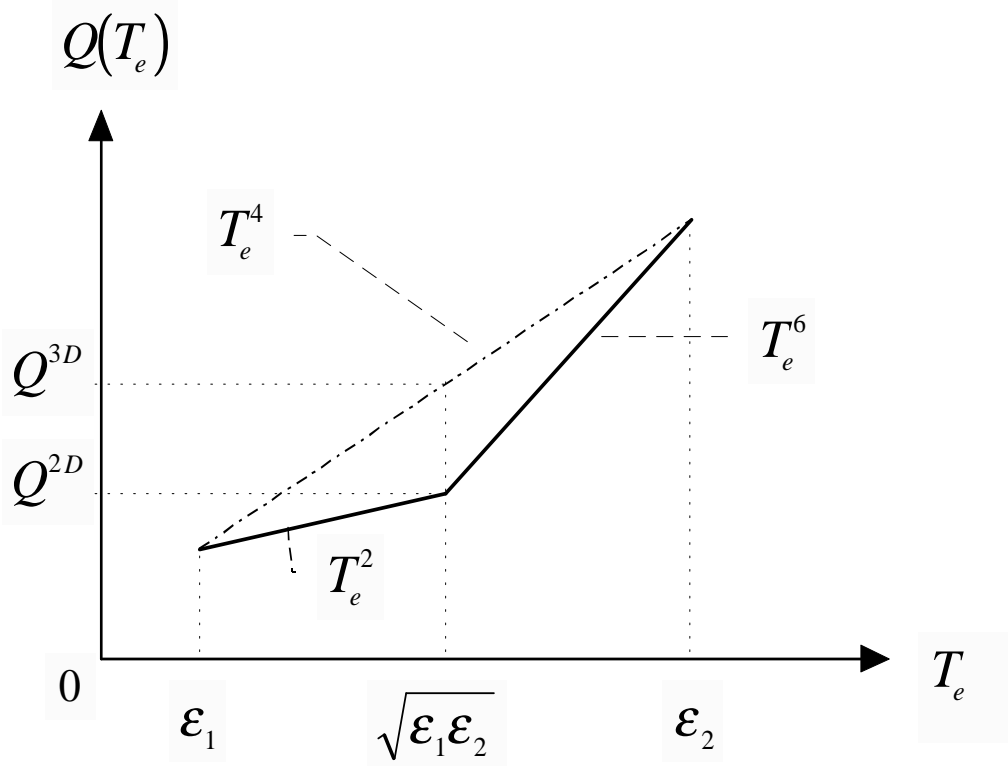


Figure 3.3: The energy-loss power \bar{Q} of the Fermi 2DEG located near the free crystal surface. The dashed line corresponds to the case of the infinitely distant, ($\bar{z} \rightarrow \infty$), boundary.

has been shown that the $\bar{Q} \propto T_e^4$ temperature dependence is realized in the range $T_e \gtrsim \hbar s k_F$. This dependence is explained by the fact that in the samples under the study, the interfaces separating different elastic materials are remote, $\bar{z} \sim 100$ nm, so that their effect on the scattering is negligible. In the temperature dependence of the average momentum relaxation time $\bar{\tau}_1$ deducted from the total mobility measurements [146], between low and high temperature ranges where $\bar{\tau}_1 \propto T_e^{4-5}$ and $\bar{\tau}_1 \propto T_e$, respectively, a sharp dip has been observed in the temperature range near 10 K. The authors suppose that this dip can be caused by other vibration modes of the surface layer which has been not described in the theory of surfons [147, 167]. However, it is possible that this dip is connected by the interface effect on the electron scattering which leads to the analogous behavior of the temperature dependence in this temperature range (*quod vide* in Fig. 3.3).

Now we discuss the results of works [147, 148, 149, 150]. In [147] and [148], the electron scattering in Si inversion layers has been calculated in the high, $T_e = 200 \div 300$ K, and low, $T_e = 1 \div 30$ K, temperature ranges, respectively. In both works, the scattering probability has been expressed in terms of the phonon field correlation function. Assuming that the scattering is quasi-elastic, the authors consider that the static correlator can be used, *i.e.* the Fourier component $\omega = 0$ can be taken. However, this is not the case. From the explicit expressions (3.25)-(3.27) it is seen that to take $\omega = 0$ in the correlator is justified if only ω is small in comparison with sq_{\parallel} . Meanwhile, it follows from Eqs. (3.33)-(3.35) that such situation is never realized: in the range A, we have $\omega \sim sq_{\parallel}$ while in the ranges B and C, $\omega \gg sq_{\parallel}$. Therefore, we suppose that the results of these works are not correct.

Although no assumption of elastic scattering has been made in the work [150], its results in the range B do not agree with our results. However, the authors have also obtained that reflection of bulk phonon modes from the interface is important in the range B and leads to a reduction of relaxation while in the range A, the surface phonon contribution to relaxation is important.

In the work [149], in particular, the conversion process $LA \rightarrow TA$ has been assumed to take place at the sample surface. The dependence $\bar{Q} \propto (T_e^2 - T^2)$ has been obtained which corresponds to the second term in Eq. (3.87). (It appears that the approximation adopted in this reference corresponds to $\bar{z} = 0$.) However, it follows from Eq. 12 of [149] that \bar{Q} does not vanish in the limit $c \rightarrow 0$ when the process $LA \rightarrow TA$ is not allowed. (It is conceivable that this is a misprint since the dimensions on the right-hand side of Eq. 12 after substitution of Eq. 13 are incorrect.)

Chapter 4

Phonon emission by Landau states

4.1 Introduction

Interaction of a 2DEG with acoustic phonons in a magnetic field normal to the electron plane is essential in a number of physical phenomena. One may mention as examples the breakdown of the quantum Hall effect due to phonon-assisted transitions and the steady-state power absorption for a GaAs heterojunction (see Refs. [168, 169], and also the review paper [170]), the thermalization of the heated 2DEG [171, 172, 173], as well as the absorption and emission of ballistic phonon pulses by the bulk Landau states (see the reviews [174, 175]).

The 2DEG is always located near a free crystal surface or near a various interfaces separating different materials. In previous section it has been shown that these boundaries affect electron-acoustic-phonon interaction, and a free surface has the highest effect. Interaction of the 2DEG with acoustic phonons in the magnetic field has been calculated in a number of papers [171, 173, 176]. However in all these papers it has been assumed that crystal boundaries have no effect on interaction. One may easily appreciate the free surface effect if an electron is considered as an acoustic wave emitter. Schematically phonon emission from the 2DEG with account of the phonon reflection is shown in Fig. 4.1. Due to the reflection there appear two new effects in phonon emission. The LA waves emitted into the crystal bulk interfere with the LA waves reflected from the crystal

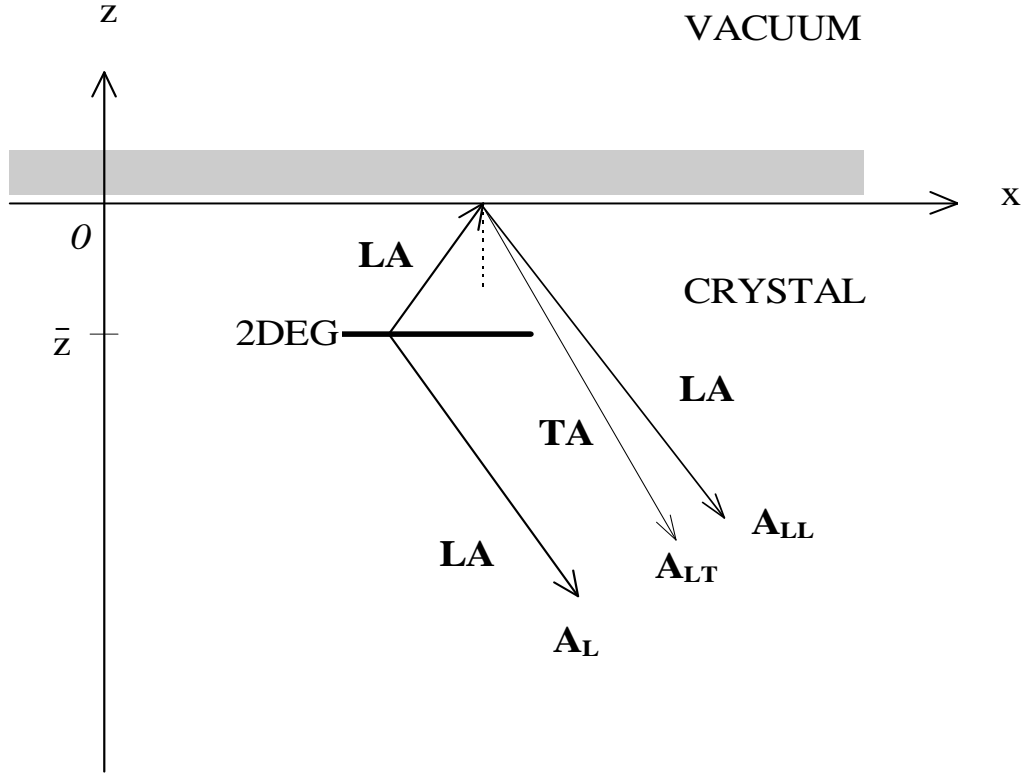


Figure 4.1: Schematic representation of phonon emission from the 2DEG with account of the phonon reflection. A_L and A_{LL} are the amplitudes of LA phonons emitted, respectively, directly into the bulk of crystal and to the crystal surface side then reflected from it. A_{LT} is the amplitude of TA phonons converted from the emitted LA phonons at the reflection from the crystal surface.

surface. As a result the emission efficiency depends on the distance between the 2DEG and the surface. The phonon reflection also affects essentially the composition of the emitted phonon field. Detector records the TA phonons converted from the emitted LA phonons at interfaces separating different materials. Thus, for full interpretation of experimental results, the conversion of various phonon modes and interference between reflected and non-reflected phonons of the same mode should be taken into account.

The 2DEG emits acoustic phonons with wave-vectors predominantly within a narrow cone near the normal to the plane of electrons. At $B = 0$ the frequencies of these phonons are $\omega \sim T_e/\hbar$ where T_e is the electron temperature. The frequencies are spread in a broad band, the frequency dispersion being of the order of the

frequency itself, *i.e.* $\Delta\omega \sim \omega \sim T_e/\hbar$. Such a wave packet with momentum dispersion $\Delta q \sim T_e/\hbar s$. (where s is the sound velocity) attenuates at a distance of the order of $\hbar s/T_e$. If the distance \bar{z} between the 2DEG and the surface is large ($\bar{z} \gg \hbar s/T_e$), the emitted phonon field will not reach the surface and the latter has no effect on electron-phonon interaction. However, the situation is drastically changed if the electrons are in a strong magnetic field B normal to the 2DEG plane. In this case the frequencies of the emitted phonons are close to the cyclotron frequency ($\omega \approx \omega_B$) while the width of the frequency band is of the order of the cyclotron resonance line width, *i.e.* $\Delta\omega \sim 1/\tau$ where τ is the momentum relaxation time [45]. This corresponds to the phonon wave packet attenuation length equal to $s\tau$. In high-quality heterostructures even at liquid helium temperatures, the length $s\tau$ is larger than $\hbar s/T_e$. Therefore, in quantizing magnetic fields electron-phonon interaction can be modified by a free surface far more distant from the 2DEG.

Study of emission and absorption processes for ballistic phonons in systems with the 2DEG gives the most detailed information about the character and specific features of electron-phonon interaction. In this case one may easily trace contributions of separate phonon modes to the interaction characteristics. An experiment of ballistic phonon emission is schematically shown in Fig. 4.2. The 2DEG is heated by passing a current along it. Then emitted phonons travel ballistically from the 2DEG until they reach the opposite face of the sample. Usually it is measured: the intensity distribution on the reverse face of the sample, *i.e.* the angular distribution (travel is ballistic), and a relative proportion of LA and TA phonons using time-of-flight techniques. However, previous works [176, 177, 178, 179, 180], analyzing these effects, both in the presence and absence of the quantizing magnetic field, did not take into account the ballistic phonon reflection from the interfaces near which the 2DEG is placed. The exception is [178] in which it has been shown that the absorption of ballistic thermal phonons by the 2DEG has the correct order of magnitude in the absence of the magnetic field only when the reflection of these phonons from the interfaces is taken into account. The results obtained in the previous chapter also indicate directly the importance of the interface effect. The energy and momentum relaxation of the 2DEG have been calculated [41, 43, 42] and it has been shown that there are

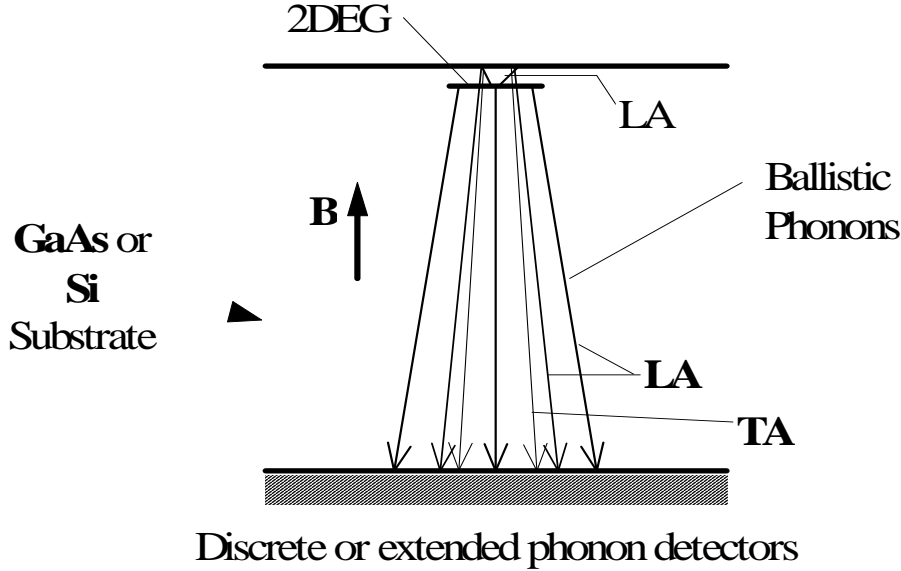


Figure 4.2: Schematic view of the ballistic acoustic phonon emission.

situations when interfaces strongly suppress the relaxation rates. Recently the acoustic phonon emission from the heated 2DEG in Si-metal-oxide nanostructure has been studied theoretically by taking into account of the phonon reflection from Si-SiO₂ interface and it has been shown that the interface plays an important role in the observed phonon intensity. Below it will be shown that the interface effect is highest in the case when the 2DEG is exposed to the quantizing magnetic field. This is conditioned by the fact that in this case, the interface interacts with almost monochromatic phonons.

The previous experimental results (see review [174, 175]) show that the angular distribution of phonon emission has a distinctly expressed peak at small angles and the signal detected on the reverse face of the sample consists of both longitudinal acoustic (LA) and transverse acoustic (TA) phonons. Giving their interpretation of these experimental data for the GaAs/AlGaAs heterostructure, the authors suggest that the presence of TA phonons in the detected signal is only due to a piezoelectric electron-phonon interaction. They proceed from the assumption that in a parabolic energy band, emission of TA phonons is forbidden in the case of deformation electron-phonon interaction. However, this is not the

case. As it can be seen later, the reflection of phonons emitted by the 2DEG only due to the deformation coupling results in the presence of both LA and TA phonons in the detected signal. The position and height of the peak in the angular distribution of phonon emission are also significantly different from those obtained in the case when the phonon reflection from interfaces is not taken into account.

In recent years there has been much success in using of electron-optical phonon interaction to probe the various electronic properties of the 2DEG (see [112] and references cited therein). The electron-longitudinal optical (LO) phonon scattering rates of the 2DEG in the magnetic field free case have been calculated both for usual bulk LO phonons [181, 182, 183, 184, 143, 185, 186, 187] as well as for bulk-like confined LO and surface optical (SO) modes [112, 106, 188, 189, 190, 109, 110, 191]. If the magnetic field is applied normal to the electron layer, the electron motion is fully quantized. In this quantum Hall effect (QHE) geometry, there have been considerable experimental and theoretical interests in the various LO phonon assisted effects of 2D-(resonant)-magneto-polarons, cyclotron resonances [86, 192, 85, 90, 84, 93, 193, 194, 195, 187], 2D-electron-phonon bound states [39], cyclotron-phonon resonances [40], magneto-phonon [196, 197, 198, 199, 200] and energy loss [171, 201, 202] effects.

In various recent experiments of light radiation [203, 204, 205] or Auger [55] processes in the QHE geometry, phonon emission remains the basic mechanism which ensures the relaxation of electrons firstly created in higher Landau states. However, in such effectively zero dimensional (0D) systems with rather thin electron layers and subjected to rather strong magnetic fields, a large separation between Landau levels cannot be covered by an acoustical LA phonon [45] so that the multiphonon 2LA phonon emission processes become more efficient [47]. Meanwhile an optical phonon emission requires a precise resonance $\Delta l \omega_B = \omega_{LO}$, $\Delta l = 1, 2, 3, \dots$ in this regime (ω_B and ω_{LO} are the cyclotron and the LO phonon frequencies). As far as it moves off from the resonance, the efficiency of this process is steeply falls so that out of resonance, LO phonon emission becomes possible in accompaniment of LA phonon emission via the two-phonon emission mechanism. Possibly for this reason, except for the work [173], calculations of the electron-optical phonon relaxation rates have been restricted thus

far to the zero magnetic field case where LO phonon emission is the dominant relaxation mechanism with subpicosecond emission time. In Ref. [173] the direct calculation of the electron-phonon scattering rates have been carried out for a quantum well structure with infinitely high confining wells. It has been obtained, however, that in the case of polar optical (PO) phonon scattering, the relaxation rate diverges. This divergence has been physically attributed to the complete quantization of the electron spectrum although it does not make clear why the relaxation rate diverges only for polar interaction. We suppose that this divergence can be caused by use of the momentum-conservation-approximation [143, 185] in the extreme quantum limit. Whereas this approximation fails in this limit [143, 185]. It can be seen later that calculations without using of the momentum-conservation-approximation allow us to avoid this divergence.

Recently, to estimate the intensity of infrared cyclotron radiation from the 2DEG in a double barrier quantum well structure, the LA, 2LA phonon, photon emission and Auger processes happening in the QHE geometry have been analyzed [206]. Although, the LO+LA phonon emission processes have not been considered, one may expect that in some experimental situations, electron relaxation from a higher Landau level directly into the lowest one can turn out crucial either due to LO phonon emission or, if it is far from the resonance, due to LO+LA phonon emission.

The LO phonon assisted electron relaxation in quantum dots has been studied in [32, 36]. The multiphonon relaxation rate calculation in a GaAs quantum dot [36] has indicated the significance of LO+LA processes in such 0D systems which create a window of rapid subnanosecond relaxation.

Up to now, however, the study of the LO phonon assisted multiphonon processes in effectively 0D systems of the QHE geometry is missing from the literature.

The aim of the present chapter is to study theoretically the deformation acoustic DA phonon and the polar optical PO phonon interaction with the 2DEG in the QHE geometry. The calculations incorporate one DA or PO phonon and two DA+PO phonon emission processes for electron relaxation between bulk Landau states. In Sec. 4.2 the transition probability between two Landau levels

with acoustic phonon emission via a deformation potential is calculated taking into account phonon reflection from the free crystal surface near which the 2DEG is located [45]. This probability is shown to be an oscillating function of the magnetic field B and of the distance \bar{z} from the 2DEG to the free surface. The oscillation period is given by the condition that \bar{z} is a multiple of the half-wavelength of the emitted phonons $\lambda/2 = \pi s/\omega_B$. In Sec. 4.3 the emission spectrum of ballistic acoustic phonons in quantizing magnetic fields normal to the plane of the 2DEG is calculated when the reflection of these phonons from a GaAs/AlGaAs type interface is taken into account [49]. Phonon emission only due to the deformation electron-phonon interaction is considered. It is shown that the interface affects essentially the intensity and the composition of the emitted phonon field. The emission spectrum of surface acoustic phonons is calculated in Sec. 4.3.2 [50]. Strong exponential suppression of emission of surface acoustic phonons occurs in a wide range of the magnetic field variation, $\omega_B \gg 2mc_R^2$ (m_c is the electron mass and c_R is the surface wave velocity). Therefore, cooling of the heated 2DEG is only at the expense of bulk longitudinal and transverse acoustic phonons. In Sec. 4.4 the longitudinal optical phonon assisted electron relaxation is investigated in the 2DEG in the quantum Hall effect geometry [48]. The phonon emission rates versus inter-Landau-level separations are calculated. Electron interaction with bulk PO and interface SO phonons are considered. In quantizing magnetic fields, emission of LA phonons via piezoelectric interaction is suppressed in comparison with deformation interaction [46]. Therefore, the calculations of LO+LA phonon emission are carried out for the deformation potential of DA phonons and for the Frölich coupling of PO phonons. To obtain a finite relaxation rate associated with one-phonon emission, the allowance for the Landau level broadening or for the LO phonon dispersion is made. Below the LO phonon energy, $\hbar\omega_{LO}$, within an energy range of the order of $\hbar\sqrt{\omega_B/\tau}$, the one-phonon relaxation rate exceeds 1 ps^{-1} , τ is the relaxation time deduced from the mobility. In GaAs/AlGaAs heterostructure with the mobility $\mu = 25 \text{ V}^{-1} \text{ s}^{-1} \text{ m}^2$, this range makes up 0.7 meV . The two-phonon emission has a significant contribution to relaxation above $\hbar\omega_{LO}$. At energy separations of the order of sa_B^{-1} (a_B is the magnetic length), LO+LA phonon emission provides a mechanism of subpicosecond relaxation while in a wide energy range of the order of

$\hbar\omega_B$, subnanosecond relaxation can be achieved.

Particular attention is given to the comparison of electron relaxation going on in two different ways: first, relaxation in two consecutive emission acts (emission of a PO phonon with subsequent emission of a LA or 2LA phonons) and, second, PO+DA phonon relaxation via the multiphonon emission mechanism between the same Landau levels. Particularly, emission processes in magnetic fields up to 10 T are considered. On the one hand in such fields, the resonance $\Delta l\omega_B = \omega_{PO}$ can be achieved for small values of $\Delta l = 1, 2, 3$. On the other hand, acoustical phonon emission at electron transitions between such distant Landau levels is still a rather efficient effect [45, 47, 176] observable in experiment [203, 204, 205, 55, 56]. Numerical results are illustrated for PO phonon assisted relaxation between Landau levels $l = 3$ and $l = 0$. The last section contains concluding remarks.

4.2 Electron transition probability between Landau levels: Free surface effect on electron-acoustic phonon interaction

In what follows we evaluate the probability of electron transitions between two Landau levels due to electron-acoustic-phonon interaction via the deformation potential. Implying the 2DEG in a GaAs/AlGaAs heterostructure, the electron effective mass is considered to be isotropic. In this case, according to [41], the transition probability from the state $\Psi_i(\mathbf{r})$ with energy ε_i to the state $\Psi_f(\mathbf{r})$ with energy ε_f with lattice temperature $T = 0$ is given by

$$W_{i \rightarrow f} = \frac{2\Xi^2}{\hbar L^2} \sum_{\mathbf{q}_\perp} \int d^3r_1 \int d^3r_2 \Psi_f^*(\mathbf{r}_1) \Psi_f(\mathbf{r}_2) \Psi_i(\mathbf{r}_1) \Psi_i^*(\mathbf{r}_2) \times \exp[i\mathbf{q}_\perp \cdot (\mathbf{R}_1 - \mathbf{R}_2)] K(\omega, \mathbf{q}_\perp | z_1, z_2). \quad (4.1)$$

Here we have used following notations: Ξ is the deformation potential constant, L^2 is the normalization area in the (x, y) -plane occupied by the 2DEG, \mathbf{q}_\perp and \mathbf{R} are vectors in the (x, y) -plane. The kernel K is given in terms of the force-displacement Green function, calculated for elastic media, composed from GaAs and AlGaAs layers (and a metallic layer, if present). The frequency ω entering

this Green function satisfies $\hbar\omega = \varepsilon_f - \varepsilon_i$. When the temperature $T \neq 0$, the probabilities of the downward transitions $\varepsilon_f < \varepsilon_i$ are obtained from expression (4.1) by multiplying the latter by a Bose factor $N_\omega + 1$ and a Fermi factor $f_i(1 - f_f)$ while for the upward transitions $\varepsilon_f > \varepsilon_i$ the probabilities are calculated from the detailed balance principle. The elastic properties of the crystals GaAs and AlGaAs differ very little. Therefore, in the absence of a metallic gate the Green function of interest is the half-space Green function. In the isotropic approximation the latter has been calculated in Ref. [152], and the corresponding kernel K was calculated in Ref. [41]. A metallic gate changes the kernel K : however, in a rough approximation this fact can be ignored (since the reflection factor for longitudinal acoustic wave energy at the Ni/GaAs interface is less than 10%). The electron wave functions Ψ in (4.1) are of the following form:

$$\Psi_{nlk_x}(\mathbf{r}) = \chi_{lk_x}(\mathbf{R})\psi_n(z) \quad (4.2)$$

where χ is the Landau wave function (l is the Landau level number, k_x is the x -component of the electron momentum), and ψ is the spatial quantization wave function (n is the subband quantum number). Inserting the wave functions (4.2) into (4.1) and performing the integration over \mathbf{R} , we obtain

$$\begin{aligned} W_{nlk_x \rightarrow n'l'k'_x} &= \frac{2\Xi^2}{\hbar L^2} \sum_{\mathbf{q}_\perp} \delta_{k_x, k'_x - q_x} Q_{ll'}^2(q_\perp) \\ &\times \int dz_1 \int dz_2 \psi_f(z_1)^* \psi_f(z_2) \psi_i(z_1) \psi_i(z_2)^* K(\omega, \mathbf{q}_\perp | z_1, z_2). \end{aligned} \quad (4.3)$$

where the modulus squared of the form factor $Q_{ll'}$ is given by Eq. (2.12) [207]. The form factor $Q_{ll'}$ does not depend on momenta k and k' apart but depends only on q_\perp which is bound up with the axial symmetry of the magnetic field. We shall consider only transitions between Landau levels corresponding to the ground state of spatial quantization omitting the subband index n . Summation over the final values k'_x and averaging over the initial values k_x gives

$$\begin{aligned} W_{l \rightarrow l'} &= \text{Av}_{k_x} \sum_{k'_x} W_{nlk_x \rightarrow n'l'k'_x} \\ &= \frac{\Xi^2}{\pi \hbar} \int_0^\infty dq_\perp q_\perp Q_{ll'}^2(q_\perp) \int dz_1 \int dz_2 |\psi(z_1)|^2 |\psi(z_2)|^2 K(\omega, q_\perp | z_1, z_2) \end{aligned} \quad (4.4)$$

Here we have made use of the fact that in the case of the isotropic approximation the kernel K is independent of the direction of the vector \mathbf{q}_\perp . It follows from

(2.12) that the integration in (4.4) is limited by values $q_\perp \lesssim a_B^{-1}$. On the other hand, $\omega = \omega_B, 2\omega_B, 3\omega_B, \dots$. Therefore for the most important transitions with $\omega \sim \omega_B$ we have $(sq_\perp/\omega)^2 \lesssim ms^2/\hbar\omega_B$. Since in GaAs $ms^2 = 0.11$ K, we may conclude that in the quantizing magnetic fields always the $sq_\perp/\omega \ll 1$ inequality takes place. Thus, we can expand the kernel K in q_\perp and use the simplified expression

$$K(\omega, q_\perp | z_1, z_2) = \frac{\omega}{2\rho s^3} \{ \cos[a(z_1 - z_2)] - \cos[a(z_1 + z_2)] \}, \quad a = \sqrt{\frac{\omega^2}{s^2} - q_\perp^2}. \quad (4.5)$$

Recall that here ρ is the crystal mass density, s is the longitudinal sound velocity. The value $z = 0$ refers to the free surface position. The quantity a , which represents the component of the phonon wave vector normal to the surface, is not expanded in q_\perp , since z_1 and z_2 can be large if the 2DEG is far from the surface. Now let us choose a certain point \bar{z} inside the 2DEG (e.g. the "center of gravity" of the distribution $|\psi(z)|^2$ or the GaAs/AlGaAs interface) and substitute: $z = \bar{z} + \zeta$ into the integral (4.4) and the kernel (4.5). Then carrying the intergration over ζ_1 and ζ_2 , we obtain

$$W_{l \rightarrow l'} = \frac{\Xi^2 \omega}{2\pi \hbar \rho s^3} \text{Re} \int_0^\infty dq_\perp q_\perp Q_{ll'}^2(q_\perp) \left[|I(a)|^2 - \exp(2ia\bar{z}) I(a)^2 \right]. \quad (4.6)$$

The form factor $I(a)$ is given by

$$I(a) = \int d\zeta |\psi(z)|^2 \exp(ia\zeta) \equiv |I(a)| \exp\{i\varphi(a)\}. \quad (4.7)$$

Since in the latter integral the integration range is limited due to the localization of the distribution $|\psi(z)|^2$, we can put $q_\perp = 0$, *i.e.* take $a = \omega/s$. However, this approximation can be invalid in the exponential factor $\exp(2ia\bar{z})$, since \bar{z} can be large. But still, for values \bar{z} not too large we may use the expansion

$$a = \frac{\omega}{s} \left[1 - \frac{1}{2} \frac{s^2 q^2}{\omega^2} - \dots \right]. \quad (4.8)$$

Inserting this expansion in the exponential factor, we obtain

$$\begin{aligned} W_{l \rightarrow l'} &= \frac{\Xi^2 \omega}{2\pi a_B^2 \hbar \rho s^3} \text{Re} \left\{ 1 - \exp \left[i \left(\frac{2\omega}{s} \bar{z} + \varphi \left(\frac{\omega}{s} \right) \right) \right] F_{ll'}(\xi) \right\}, \quad (4.9) \\ F_{ll'}(\xi) &= \int_0^\infty dt Q_{ll'}^2(t) \exp(-i\xi t) \end{aligned}$$

$$= \frac{l!}{l'!(l-l')!} \frac{(i\xi)^{2l'}}{(1+i\xi)^{l+l'+1}} {}_2F_1(-l', -l'; l-l'+1; -\xi^{-2}), \quad (4.10)$$

$$\xi = \frac{\bar{z}}{\Delta l \Lambda_1}, \quad \Lambda_1 = \frac{\hbar}{2ms}, \quad \Delta l = l - l'. \quad (4.11)$$

Here ${}_2F_1$ is the Gauss hypergeometric function. The integrals $F_{ll'} \rightarrow 0$ when $\bar{z} \rightarrow 0$ so that the probability W has a definite limit corresponding to the infinitely distant free surface, as one should expect. We list explicit formulae for F for the most important transitions,

$$F_{10}(\xi) = (1+i\xi)^{-2}, \quad F_{20}(\xi) = (1+i\xi)^{-3}, \quad (4.12)$$

$$F_{21}(\xi) = 2 \frac{(i\xi)^2}{(1+i\xi)^4} {}_2F_1(-1, -1, 2; -\xi^{-2}). \quad (4.13)$$

It follows from the integrals (4.11) that one can neglect the free surface effects when $\bar{z} \gg \Lambda_1$. For GaAs $\Lambda_1 = 170$ nm while typical values of \bar{z} are in the interval 50 to 150 nm. The expansion (4.8) can be used in $\exp(2ia\bar{z})$ if the quantity

$$\bar{z} \frac{\omega}{s} \left(\frac{sq_{\perp}}{\omega} \right)^4 \approx \bar{z} \frac{a_B^2}{\Lambda_1^3} \quad (4.14)$$

is small. This condition is usually satisfied in the quantizing fields. Equally with the momentum spread, there exists another reason why the effect of the free surface becomes weaker with distance, namely, the spread of the frequencies of the emitted phonons due to the Landau level broadening. To take this broadening into account, we average the transition probability (4.11) over ω using a Lorentzian distribution with its center at the transition frequency $\Delta l \omega_B$ and width $1/\tau$. Only the fast oscillating factor containing \bar{z} should be averaged, and as a result this factor is substituted as follows

$$\exp\left(i \frac{2\omega}{s} \bar{z}\right) \rightarrow \exp\left(-\frac{\bar{z}}{\Lambda_2} + i \frac{2\omega}{s} \bar{z}\right), \quad (4.15)$$

$$\Lambda_2 = \frac{1}{2} \frac{\hbar s}{\Gamma} \quad (4.16)$$

where Γ is the Landau level width. Before comparing the two attenuation lengths Λ_1 and Λ_2 , we discuss what sort of Landau level width is to be used in averaging. In high-quality heterostructures the Landau level width being determined from the de Haas-van Alphen effect, is a factor of about 10 larger than the width $\Gamma = \hbar/\tau$, with τ determined from mobility or from cyclotron resonance [208]. This is

because the scattering potential has a smooth component with a large amplitude. The smooth potential produces an inhomogeneous broadening of the Landau levels seen in the de Haas-van Alphen effect. However, the smooth potential gives no contribution to scattering, since its correlation length exceeds the electron Fermi wavelength [209]. Neither does the smooth component contribute to the cyclotron resonance linewidth, since the absorption occurs without change of k_x , *i.e.* with a fixed position of the center of the Landau oscillator.

It follows from (4.3) that phonon emission is accompanied by a change of k_x , the change being of the order of a_B^{-1} . In other words, when a phonon is emitted, the center of the Landau oscillator is shifted by a distance of the order of a_B . Since in quantizing magnetic fields $a_B \ll \Lambda$, no contribution is made by the smooth potential component to the frequency spread of the emitted phonons. Therefore the $\Gamma = \hbar/\tau$ in (4.16) should be deduced from the momentum relaxation time.

Even in high-quality heterojunctions with mobility $\mu = 100 \text{ m}^2 \text{ V}^{-1} \text{ s}^{-1}$ the length $\Lambda_2 = 100 \text{ nm}$ is comparable with the distance \bar{z} . Therefore the Landau level broadening is essential.

With the model wave function [125]

$$|\psi(\zeta)|^2 = \frac{1}{2d^3} \zeta^2 \exp(-\zeta/d), \quad (4.17)$$

where $\zeta = 0$ corresponds to the interface position, one obtains

$$\left| I \left(\frac{\omega}{s} \right) \right|^2 = \frac{1}{(1+\eta)^3}, \quad \tan \varphi \left(\frac{\omega}{s} \right) = \frac{\eta(3-\eta)^2}{(3\eta-1)^2}, \quad \eta = \frac{\omega^2}{(s/d)^2}. \quad (4.18)$$

For a GaAs/AlGaAs heterojunction the typical value is $d = 3 \text{ nm}$ (see Ref. [210]), and $\omega_B = s/d$ when $B = 0.66 \text{ T}$. With the wave function (4.17), the probability of the most important transition from $l = 1$ to $l = 0$ is

$$\begin{aligned} W_{1 \rightarrow 0} &= \frac{1}{\bar{\tau}} \left(\frac{\omega_B}{s/d} \right)^2 \left[1 + \left(\frac{\omega_B}{s/d} \right)^2 \right]^{-3} \\ &\times \left\{ 1 - \frac{\exp(-\bar{z}/\Lambda_2)}{1 + (\bar{z}/\Lambda_1)^2} \cos \left(2 \frac{\omega_B}{s} \bar{z} + 6 \tan^{-1} \frac{\omega_B}{s/d} - 2 \tan^{-1} \frac{\bar{z}}{\Lambda_1} \right) \right\} \\ \frac{1}{\bar{\tau}} &= \frac{m \Xi^2}{2\pi \hbar^2 \rho s d^2}. \end{aligned} \quad (4.19) \quad (4.20)$$

Here $\bar{\tau}$ is a nominal relaxation time, depending only on the heterojunction. For a GaAs/AlGaAs heterojunction with $d = 3 \text{ nm}$ we have $\bar{\tau} = 0.20 \text{ ns}$. One may

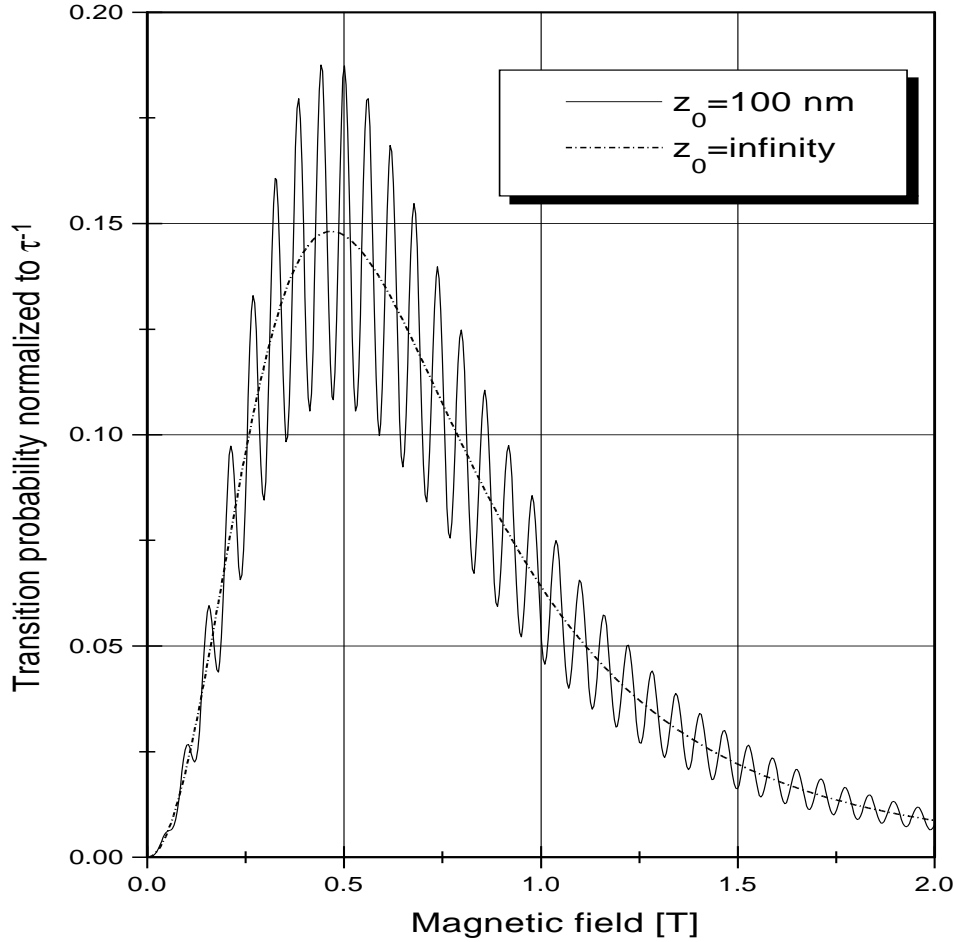


Figure 4.3: Transition probability $W_{1 \rightarrow 0}$ between Landau levels $l_1 = 1$ and $l_2 = 0$ versus magnetic field B for the distance $\bar{z} = 100$ nm and $\bar{z} = \infty$ from the 2DEG to the free surface.

see from (4.19) that when the 2DEG is not too far from the free surface, the transition probability W has an oscillatory dependence on the magnetic field B and on the distance \bar{z} from the free surface. For illustration we calculate from (4.19) $W_{1 \rightarrow 0}$ (normalized to $1/\bar{\tau}$) versus B for $\bar{z} = 100$ nm and $\bar{z} = \infty$ (Fig. 4.3) and also versus \bar{z} for $B = 0.5$ T (Fig. 4.4).

4.3 Ballistic acoustic phonon emission by Landau states

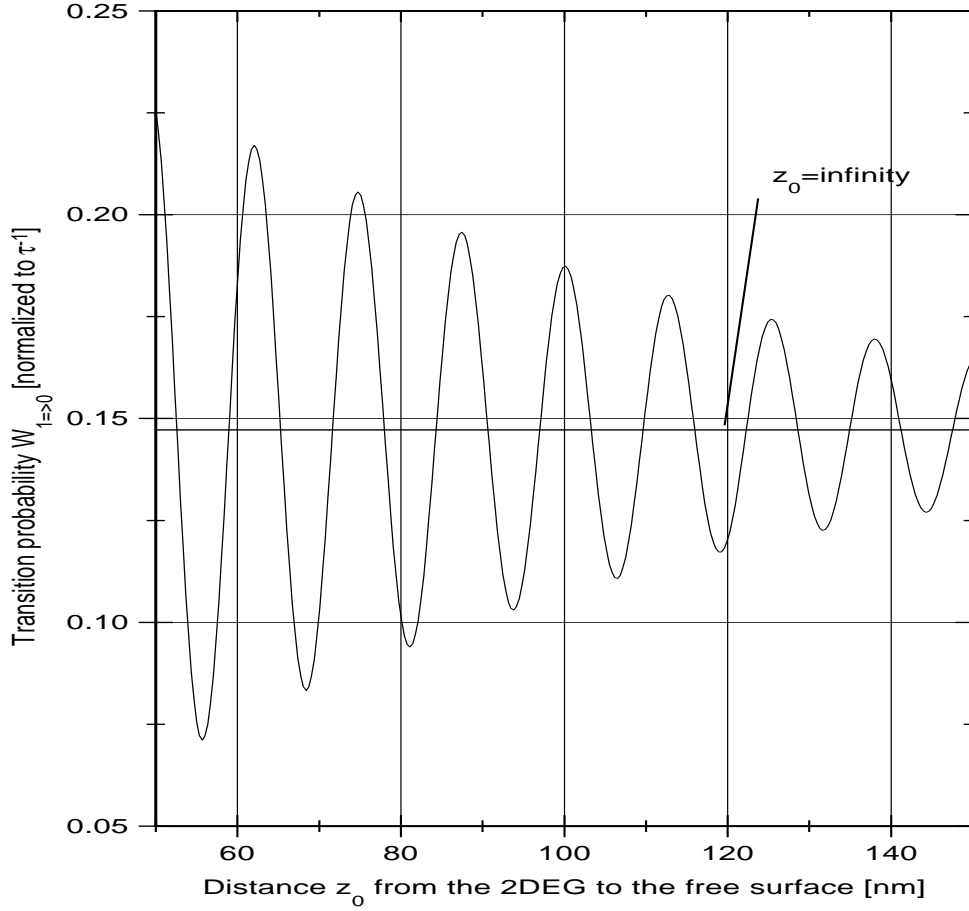


Figure 4.4: Transition probability $W_{1 \rightarrow 0}$ between Landau levels $l_1 = 1$ and $l_2 = 0$ versus distance from the 2DEG to the free surface for the magnetic field $B = 0.5$ T. The transition probability is also shown when no phonon reflection is taken into account.

4.3.1 Acoustic energy flux density

For deformation electron-phonon interaction in the non-degenerate isotropic energy band, with the energy minimum in the Brillouin zone center, the interaction Hamiltonian density can be represented in the following form

$$H_{int} = \Xi |\Psi(\mathbf{r}, t)|^2 \mathbf{div} \mathbf{u}(\mathbf{r}, t). \quad (4.21)$$

Here Ξ is the deformational potential constant, $\Psi(\mathbf{r}, t)$ and $\mathbf{u}(\mathbf{r}, t)$ are respectively the electron and phonon field operators in the Heisenberg representation. It can be shown by a straightforward calculation that the spectral density of the acoustic

energy flux at the frequency ω has the form

$$\mathcal{W}_\alpha = \text{Re} \left[-i \frac{\omega}{2\pi} \langle \sigma_{\alpha\beta}^+(\mathbf{r}_0) u_\beta(\mathbf{r}_0) \rangle_\omega \right], \quad (4.22)$$

$$\sigma_{\alpha\beta}(\mathbf{r}_0) = 2\mu u_{\alpha\beta} + \lambda u_{\gamma\gamma} \delta_{\alpha\beta}, \quad u_{\alpha\beta} = \frac{1}{2}(\partial_\alpha u_\beta + \partial_\beta u_\alpha). \quad (4.23)$$

Here $\sigma_{\alpha\beta}$ and $u_{\alpha\beta}$ are the stress and deformation tensors of the elastic medium, μ and λ are the Lamé coefficients, $\langle \dots \rangle_\omega$ is the Fourier transform of the correlator of the operators σ and u . Repeated Cartesian indices imply summation over the values $\alpha, \beta = 1, 2, 3$, and $\partial_\alpha \equiv \partial/\partial_\alpha$ is the partial derivative operator.

As follows from expressions (4.21) and (4.22), in order to obtain the flux density \mathcal{W}_α we have to calculate the correlator for the phonon field operators

$$K_{\alpha\beta}(\mathbf{r}, \mathbf{r}') = \langle u_\alpha^+(\mathbf{r}) u_\beta(\mathbf{r}') \rangle_\omega. \quad (4.24)$$

With that purpose we note that the deformational displacement $u_\alpha(r, t)$ is caused by the force

$$F_\alpha(\mathbf{r}, t) = -\frac{\delta}{\delta u_\alpha} H_{int} = \Xi \partial_\alpha |\Psi(\mathbf{r}, t)|^2. \quad (4.25)$$

Therefore, making use of the Green function $G_{\alpha\beta}$ from elasticity theory, for the displacement under the force (4.25) we can write

$$u_\alpha(\mathbf{r}) = \int d^3r_1 dt_1 G_{\alpha\beta}(\mathbf{r}, \mathbf{r}_1 | t - t_1) F_\beta(\mathbf{r}_1, t_1) \quad (4.26)$$

The electron field operators in the occupation number representation are expressed through the anti-commutative Fermi operators a_s in the following form,

$$\Psi(\mathbf{r}, t) = \sum_s a_s \psi_s(\mathbf{r}) \exp(-i\varepsilon_s t) \quad (4.27)$$

where ε_s and ψ_s are, respectively, energies and wavefunctions of electrons in the single-particle states which are characterized by a set of quantum number s . Substituting expressions (4.25)-(4.27) into (4.24) we can represent the correlator K in the following form

$$\begin{aligned} K_{\alpha\beta}(\mathbf{r}, \mathbf{r}') &= 2\pi\Xi^2 \sum_{s,s'} f_s(1-f_{s'}) \delta(\varepsilon_s - \varepsilon_{s'} - \hbar\omega) \int d^3r_1 d^3r_2 \\ &\times \psi_s^*(\mathbf{r}_1) \psi_{s'}(\mathbf{r}_1) \psi_s(\mathbf{r}_2) \psi_{s'}^*(\mathbf{r}_2) D_\alpha^*(\mathbf{r}, \mathbf{r}_1 | \omega) D_\beta(\mathbf{r}', \mathbf{r}_2 | \omega) \end{aligned} \quad (4.28)$$

in which

$$D_\alpha(\mathbf{r}, \mathbf{r}' | \omega) = \partial'_\beta G_{\alpha\beta}(\mathbf{r}, \mathbf{r}' | \omega) \quad (4.29)$$

and the f_s are the electronic occupation numbers.

Now, in order to obtain the energy flux, we have to find the Green function for a layered elastic medium consisting of GaAs and AlGaAs, and a metallic gate. As was shown in previous section, such a layered medium can be described for our purposes in the framework of a semi-infinite elastic medium, *i.e.* we can consider the elastic waves to be reflected only from a surface adjacent to the vacuum. In this case it is assumed that the 2DEG is at a distance \bar{z} from the free surface.

The Green function for an isotropic semi-infinite elastic medium in the momentum representation in the plane of the translation invariance has been obtained in [156]. Using these results, we have calculated the Green function in the coordinate representation. As far as phonon emission is detected in an infinitely distant point on the reverse face of the sample, we are interested in obtaining the Green function $G(\mathbf{r}_0, \mathbf{r}_1|\omega)$ when $\mathbf{r}_0 \rightarrow \mathbf{n}\infty$, \mathbf{n} is a unit vector directed towards the detector.

The result of calculations shows that the acoustic energy flux density is represented as a sum of the flux densities of the bulk LA and TA phonons:

$$\mathcal{W}_\alpha^{Bulk} = \mathcal{W}_\alpha^L + \mathcal{W}_\alpha^T \quad (4.30)$$

where

$$\mathcal{W}_\alpha^L = \frac{1}{\pi} \rho s^2 q_\alpha^L \hbar \omega K_{\beta\beta}^L(\mathbf{r}_0, \mathbf{r}_0), \quad (4.31)$$

$$\mathcal{W}_\alpha^T = \frac{1}{\pi} \rho c^2 q_\alpha^T \hbar \omega K_{\beta\beta}^T(\mathbf{r}_0, \mathbf{r}_0), \quad (4.32)$$

in which s (c) and $q_\alpha^L = n_\alpha \omega / s$ ($q_\alpha^T = n_\alpha \omega / c$) are the velocities and momenta for the LA (TA) phonons, respectively. Further, the kernel of the correlator K^L in expression (4.28) is given by

$$D_\alpha^*(\mathbf{r}_0, \mathbf{r}_1|\omega) D_\beta(\mathbf{r}_0, \mathbf{r}_2|\omega) = \frac{\omega^2}{16\pi^2 r_0^2 \rho^2 s^6} \mathcal{H}^{L*}(\mathbf{r}_1) \mathcal{H}^L(\mathbf{r}_2) \quad (4.33)$$

where

$$\mathcal{H}^L(\mathbf{r}) = \exp(-i\mathbf{q}_\perp^L \mathbf{R}) \left[\exp(-iq_z^L z) + \mathcal{R}_{LA \rightarrow LA} \exp(iq_z^L z) \right]. \quad (4.34)$$

Similarly, in calculating K^T we have exploited

$$D_\alpha^*(\mathbf{r}_0, \mathbf{r}_1|\omega) D_\beta(\mathbf{r}_0, \mathbf{r}_2|\omega) = \frac{\omega^2}{16\pi^2 r_0^2 \rho^2 c^4 s^2} \mathcal{H}^{T*}(\mathbf{r}_1) \mathcal{H}^T(\mathbf{r}_2) \quad (4.35)$$

where

$$\mathcal{H}^L(\mathbf{r}) = \mathcal{R}_{LA \rightarrow TA} \exp(-i\mathbf{q}_\perp^L \mathbf{R} - i\alpha^L z). \quad (4.36)$$

The following notations were used in expressions (4.34) and (4.36): $\mathbf{r} = (\mathbf{R}, z)$ and $\mathbf{q} = (\mathbf{q}_\perp, q_z)$, where \mathbf{R} and \mathbf{q}_\perp are two dimensional vectors in the (x, y) -plane. The reflected-to-incident LA wave amplitude ratio $\mathcal{R}_{LA \rightarrow LA}$ is given by the following expression

$$\mathcal{R}_{LA \rightarrow LA} = \frac{c^2 \sin(2\theta) \sin(2\theta_T) - s^2 \cos^2(2\theta_T)}{c^2 \sin(2\theta) \sin(2\theta_T) + s^2 \cos^2(2\theta_T)}, \quad \sin \theta_T = \frac{c}{s} \sin \theta \quad (4.37)$$

where θ is the angle between the vector \mathbf{n} and the normal to the plane of incidence.

The amplitude ratio of the reflected TA wave to the incident LA wave as well as the momentum α^L are determined differently in various ranges of the angle θ , $\theta < \theta < \theta_c$ and $\theta_c < \theta < \pi/2$, where $\theta_c = \arcsin(c/s)$ is the critical angle of the TA wave total reflection.

When $\theta < \theta < \theta_c$ then the momentum $\alpha^L = -i(\omega/s) \cos \theta_L$ where $\sin \theta_L = (s/c) \sin \theta$ and

$$\mathcal{R}_{LA \rightarrow TA} = \frac{2cs \sin(2\theta) \cos(2\theta)}{c^2 \sin(2\theta) \sin(2\theta_L) + s^2 \cos^2(2\theta)}. \quad (4.38)$$

When $\theta_c < \theta < \pi/2$ then the momentum $\alpha^L = (\omega/s) sh\vartheta_L$ where $ch\vartheta_L = (s/c) \sin \theta$ and

$$|\mathcal{R}_{LA \rightarrow TA}|^2 = \frac{4c^2 s^2 \sin^2(2\theta) \cos^2(2\theta)}{c^4 \sin^2(2\theta) sh(2\vartheta_L) + s^4 \cos^4(2\theta)}. \quad (4.39)$$

Since we are interested in emission taking place in the magnetic field, we have to take in the correlator (4.28) the electron wave functions given by Eq. (4.2). Substituting expressions (4.28), (4.33)-(4.36) and (4.2) into the relation (4.31), we finally obtain the following expression for the LA phonon energy flux density emitted from a unit area of the 2DEG into a solid angle element do around the direction θ :

$$d\mathcal{W}^L(\theta) = [1 + \mathcal{R}_{LA \rightarrow LA}^2 + 2\mathcal{R}_{LA \rightarrow LA} \cos 2\varphi] \mathcal{W}^{3D}(\theta) do \quad (4.40)$$

where

$$\mathcal{W}^{3D}(\theta) = \mathcal{W}_0 Q_{l_1 l_2}^2 \left(\frac{\omega}{s} \sin \theta \right) \left| I \left(\frac{\omega}{s} \cos \theta \right) \right|^2, \quad \mathcal{W}_0 = \frac{\Xi^2 \omega_B^4}{8\pi^3 \rho s^5 a_B^2} f_{l_1} (1 - f_{l_2}) \quad (4.41)$$

is the LA phonon acoustic energy flux when the phonon reflection is not taken into account. The form factors $Q_{l_1 l_2}$ and $I(q_z)$ are given by Eq. (2.12) and Eq. (4.7). The phase φ in Eq. (4.7) can be represented in the form

$$\varphi(\theta, \bar{z}) = \frac{\omega}{s} \bar{z} \sin \theta + \varphi_0, \quad (4.42)$$

a_B is the magnetic length. It is assumed that the interacting electrons stay at the same spatial quantization level. It is also taken into account the spin degeneration factor $g_s = 2$.

For TA phonons in the same way, we obtain in the angular range $0 < \theta < \theta_c$

$$d\mathcal{W}^T(\theta) = \frac{s^3}{c^3} |\mathcal{R}_{LA \rightarrow TA}|^2 \mathcal{W}^{3D}(\theta_L) d\theta \quad (4.43)$$

while in the range $\theta_c < \theta < \pi/2$

$$d\mathcal{W}^T(\theta) = \frac{s^3}{c^3} |\mathcal{R}_{LA \rightarrow TA}|^2 \mathcal{W}^{3D}(\pi/2 - i\vartheta_L) d\theta \quad (4.44)$$

Notice that in the range $0 < \theta < \theta_c$, \mathcal{W}^T does not depend on the distance \bar{z} while in the range $\theta_c < \theta < \pi/2$, there appears a strong exponential dependence via a factor $\exp[-2(\omega/s)\bar{z}sh\vartheta_L]$.

4.3.2 Suppression of surface acoustic phonon emission

In the previous section, the emission spectrum for the bulk ballistic acoustic phonons has been calculated when the reflection of these phonons from the interface near the 2DEG has been taken into account. It is clear that, in spite of the considered deformational electron-phonon coupling, the detected signal consists of both longitudinal LA and transverse TA phonons. However, the emitted phonon field, in general, must also include surface acoustic SA phonons. Over the last few years the interaction between the 2DEG and surface acoustic waves in the quantum Hall regime have been widely investigated [211, 212, 213, 214, 215].

In order to find the emission spectrum of the ballistic surface phonons, we have to complement our calculations of the previous section also for the energy range $\omega < cq_\perp$, where c is the TA phonon velocity, ω and q_\perp are the energy and in-plane momentum of the phonons. Recall that the elasticity theory Green function has the pole in this energy range corresponding to the normal surface

mode of the elastic layered medium. Straightforward calculations show that the spectral density of the acoustic energy flux \mathcal{W} at frequency ω is represented as a sum of the flux densities of the bulk and surface SA phonons,

$$\mathcal{W} = \mathcal{W}^{Bulk} + \mathcal{W}^S. \quad (4.45)$$

Moreover, if one describes the layered medium of the GaAs/AlGaAs heterostructure in the framework of a semi-infinite elastic medium which is an acceptable approximation for our purposes [45] then for the flux density of the Rayleigh waves emitting from a unit area of the 2DEG we obtain

$$\mathcal{W}^R|_{1 \rightarrow 0} = g \mathcal{W}_0 \kappa_R^2 \exp(-\kappa_R^2) \left(1 + \frac{\eta_R d}{\bar{z}}\right)^{-6} \exp(-2\eta_R), \quad (4.46)$$

$$\kappa_R^2 = \frac{1}{2}(q^R a_B)^2 = \frac{\omega_B}{2m_c c_R^2}, \quad \eta_R = \gamma_1 \frac{\omega_B}{c_R / \bar{z}}. \quad (4.47)$$

where the dimensionless quantity g is given

$$g(\xi_1, \xi_2) = 2\pi \left[\frac{1}{2\gamma_1} \left(1 - \frac{\gamma_1}{\gamma_1} (1 + \gamma_2^2) + \frac{\gamma_1^2}{\gamma_2^2} \right) - (\gamma_1 - \gamma_2) \frac{1 + \gamma_2^2}{1 - \gamma_2^2} \right] \\ \times \left\{ \sqrt{1 - \gamma_2} \left[2(\gamma_1 - \gamma_2) + \gamma_1 \left(\frac{1}{\gamma_1} - \frac{1}{\gamma_2} \right)^2 \right]^2 \right\}^{-1}, \quad (4.48)$$

$$\gamma_1 = \sqrt{1 - \xi_1^2}, \quad \gamma_2 = \sqrt{1 - \xi_2^2}, \quad \xi_1 = \frac{c_R}{s}, \quad \xi_2 = \frac{c_R}{c}. \quad (4.49)$$

Here c_R is the velocity of the Rayleigh waves. For GaAs with $c/s = 0.59$ and $c_R/c = 0.92$ (see Table 2.4), we obtain $g = 2.51$. This surface acoustic energy flux is isotropic and concentrated in the 2DEG plane. The factor \mathcal{W}_0 is given by 4.41 and depends on the parameters of the problem which are the same for both bulk and surface phonons. Moreover, we have $\mathcal{W}^B \sim \mathcal{W}_0$ at the peak of the bulk phonon emission (*cf.* Eq. (4.41)). However, in magnetic fields $B = 1$ T taking $d = 3$ nm and $\bar{z} = 100$ nm one can be convinced that $\kappa_R^2 = 303$ and $2\eta_R = 157$. This means that the emission of SA phonons is extremely weak. The first exponent in Eq. (4.47) is also present in the corresponding expression for the bulk phonon emission intensity. However, in contrast with the bulk phonon case where for the same transition energy $\hbar\omega_B$, the emission is almost normal to the 2DEG plane, the momentum of the Rayleigh waves completely lies in the 2DEG plane. That is why in this case $\kappa_R^2 \gg 1$ and the interaction matrix element rapidly

decreases. This is a direct consequence of the fact that the electron states in this magnetic field regime constitute a plane wave packet, and in this packet there is an exponentially small number of waves for which the momentum conservation law is fulfilled for interaction with surface phonons with $q = \omega_B/c_R \gg p_B \equiv a_B^{-1}$. The second exponent appears because the SA phonons propagate along the free surface and exponentially attenuate if departing from this surface. It is easy to see that for typical values of $\bar{z} = 50 - 150$ nm the surface is always distant: $\eta_R \gg 1$. Thus one can confirm that the strong exponential suppression of the SA phonon emission occurs in the wide range of the magnetic field variation, $\hbar\omega_B \gg 2m_e c_R^2$ so the cooling of the heated 2DEG is only at the expense of emission of the bulk phonons.

4.3.3 Interference and conversion effects

The relations obtained in previous section show that in spite of deformation electron-phonon interaction, and though the energy band has a parabolic shape, the phonon field emitted by the 2DEG consists of both bulk LA and TA phonons. On the other hand, it is clear that the electrons interact directly only with LA phonons (*cf.* Eq. (4.21)). This situation can be explained as follows (see Fig. 4.1). The electrons of the 2DEG emit only LA phonons in all directions. Therefore the detector at the point \mathbf{r}_0 will record all the LA phonons which are emitted in the direction of negative z -axes at the angle of θ . Only such phonons were taken into account in the 3D case. However, the detector will also respond to all those phonons which have been primary emitted in the direction of positive z -axes at the angles of θ and θ_L to the free surface. Such LA phonons, upon their reflection and conversion at the free surface, propagate backwards in the form of LA and TA phonons, respectively, in the negative z -direction both at the same θ angle. The reflected LA phonons interfere with the initial LA phonons. Thus the detector will respond to the *interference* field of the LA phonons and to the *conversion* field of the TA phonons. Now, since the phase difference of the initial and reflected LA phonons is the function of the angle θ and the distance \bar{z} (*cf.* Eq. 4.42), the intensity of the detected interference of the LA phonons should also depend on θ and \bar{z} (see expressions (4.40)). At the same time, one should expect that the

intensity of the conversion field of the TA phonons should be independent of the distance \bar{z} . This, indeed, is the case when $\theta < \theta_c$. According to Eq. (4.43), the flux of the converted TA phonons depends only on θ but not on the distance \bar{z} . When θ exceeds θ_c , the intensity of the converted TA phonons begins to depend strongly on \bar{z} via the factor $\exp[-2(\omega/s)\bar{z}sh\vartheta_L]$ (*cf.* Eq. (4.44)). The appearance of such a dependence can be most easily understood if we consider the inverse process of the TA→LA conversion at the phonon absorption by the 2DEG. When the TA phonons are incident on the free surface at the angle of $\theta > \theta_c$ due to the total reflection effect, the LA phonons are being created in the (x, y) -plane (one should not confuse them with surface phonons). The amplitude of such phonons decreases exponentially with the distance from the surface. Therefore, their interaction with the 2DEG is effective and the absorption of the TA phonons incident at angles of $\theta > \theta_c$ takes place when the distance \bar{z} is of the order of the LA phonon wavelength λ . Usually in real structures this is not the case. Therefore, in terms of the phonon emission, one can state that for $\bar{z} \gg \lambda$, the conversion field of the TA phonons is concentrated inside a cone $\theta < \theta_c$. Recall that if the reflection of phonons from the free surface is not taken into account then according to relation (4.41), the emission of the phonon field is concentrated in a narrow cone around the magnetic field direction. As can be seen from expression (4.40), the presence of the free surface changes the LA phonon flux magnitude by a factor of $[1 + \mathcal{R}_{LA \rightarrow LA}^2 + 2\mathcal{R}_{LA \rightarrow LA} \cos 2\varphi]$. This factor varies between the values 0 and 4 (see insets in Figs. 4.5-??). Therefore, there can be situations when the effect of the free surface on the magnitude of the acoustic energy flux can be very strong. Due to oscillations of this factor, new peaks can originate in the dependence of \mathcal{W}^L on θ , *i.e.* the initial and reflected LA phonons can cancel each other in the interference when their phase difference is close to π . This can take place, for example, at small angles θ and at distances $\bar{z} \sim d$ (Fig. 4.6) where d is the electron layer thickness. One should observe, however, that the Landau level broadening, the account of which requires the following substitution in (4.40)

$$\cos 2\varphi \rightarrow \exp\left[-\frac{\bar{z}}{\Lambda_2}\right] \cos 2\varphi \quad (4.50)$$

where the characteristic damping length Λ_2 is given by Eq. (4.16), will somewhat spoil the monochromatic character of the emitted phonons and, thus, smooth the

oscillations (Fig. 4.8). Therefore it will be difficult to observe the interference peaks on the background of the main peak for large values of $\bar{z} \gtrsim \Lambda_2$. Note also that the factor $\exp(-\bar{z}/\Lambda_2)$ ensure that the Landau level broadening diminishes the effect of the free surface when $\bar{z} \rightarrow \infty$. This effect, however, is not eliminated *completely*. When $\bar{z} \rightarrow \infty$ the interference between the LA phonons disappears, and so does the TA phonons in the range $\theta_c < \theta < \pi/2$ while in the range $0 < \theta < \theta_c$, the conversion effect remains active. If we take into account that the main emission is concentrated near small angles θ , then $\mathcal{R}_{L \rightarrow L} \approx 1$ and, therefore, $\mathcal{W}^L|_{\bar{z} \rightarrow \infty}$ is nearly twice as large as \mathcal{W}^{3D} . This result is natural, since the detector in this case will respond to the LA phonons emitted both in positive and negative z -directions. However, the most intriguing for experiment is that due to the conversion effect of the LA phonons into the TA, it becomes possible under the deformational electron-phonon interaction to detect the TA phonons on the reverse side of the sample. Moreover, the intensity of these TA phonons is independent on \bar{z} and by its order of magnitude is comparable with \mathcal{W}^{3D} .

4.3.4 Angular distribution of the emitted phonon field

In this section the angular distribution of the emitted phonon field is calculated under the condition that the electrons occupy only the ground level of the size quantization. Therefore, to obtain the form-factor I we use the model function (4.17) in which $\bar{z} = 0$ corresponds to the free surface position. Usually for a GaAs/AlGaAs heterojunction the characteristic distance $d = 3$ nm while typical values of \bar{z} vary between 50 and 150 nm. Calculations carried out for the electron transitions between the Landau levels $l = 1$ and $l = 0$ in the magnetic field with $B = 0.5$ T. It is assumed the Fermi level is to be midway between these Landau levels and the electron temperature $T_e = 7$ K.

In Figs. 4.5-4.8 the angular dependence of phonon emission is shown for two values of the distance \bar{z} . The thin curve shows the emission intensity when the phonon reflection is not taken into account. From Figs. 4.5-4.8 one can see that the phonon emission is practically absent for angles larger than 30° . The TA phonon field is concentrated in a narrower cone around the magnetic field than the LA phonon field. Note that the total inner reflection angle $\theta_c = 36^\circ$. As one

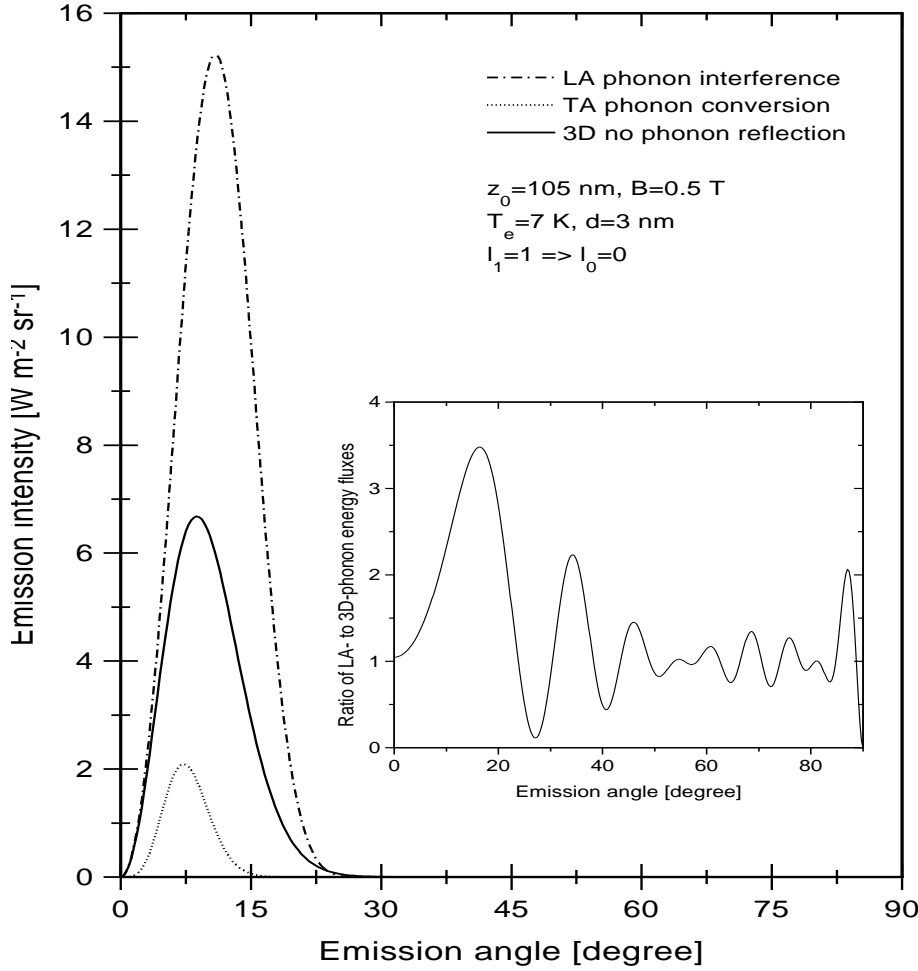


Figure 4.5: Angular distribution of the phonon emission intensity at $\bar{z} = 105$ nm when the Landau level broadening is not taken into account. Inset shows dependence of the ratio $\mathcal{W}^L/\mathcal{W}^{3D}$ on the emission angle.

can see from the diagrams in Figs. 4.5 and 4.6, the angular pattern of the LA phonon emission is very much different for $\bar{z} = 105$ nm and $\bar{z} = 109$ nm when the Landau level broadening is not taken into account. Namely, for $\bar{z} = 105$ nm, LA phonon emission has a peak at $\theta \approx 11^\circ$ while for $\bar{z} = 109$ nm, emission is strongly suppressed at the same angle so that there appear two other peaks. This is due to the interference oscillations discussed above. These oscillations are more distinctly demonstrated on insets of Figs. 4.5 and 4.6 where the dependence of the ratio $\mathcal{W}^L/\mathcal{W}^{3D}$ on the angle θ is shown. The oscillations almost preserve their form with varying \bar{z} , they are simply shifted along the θ -axis, so that emission

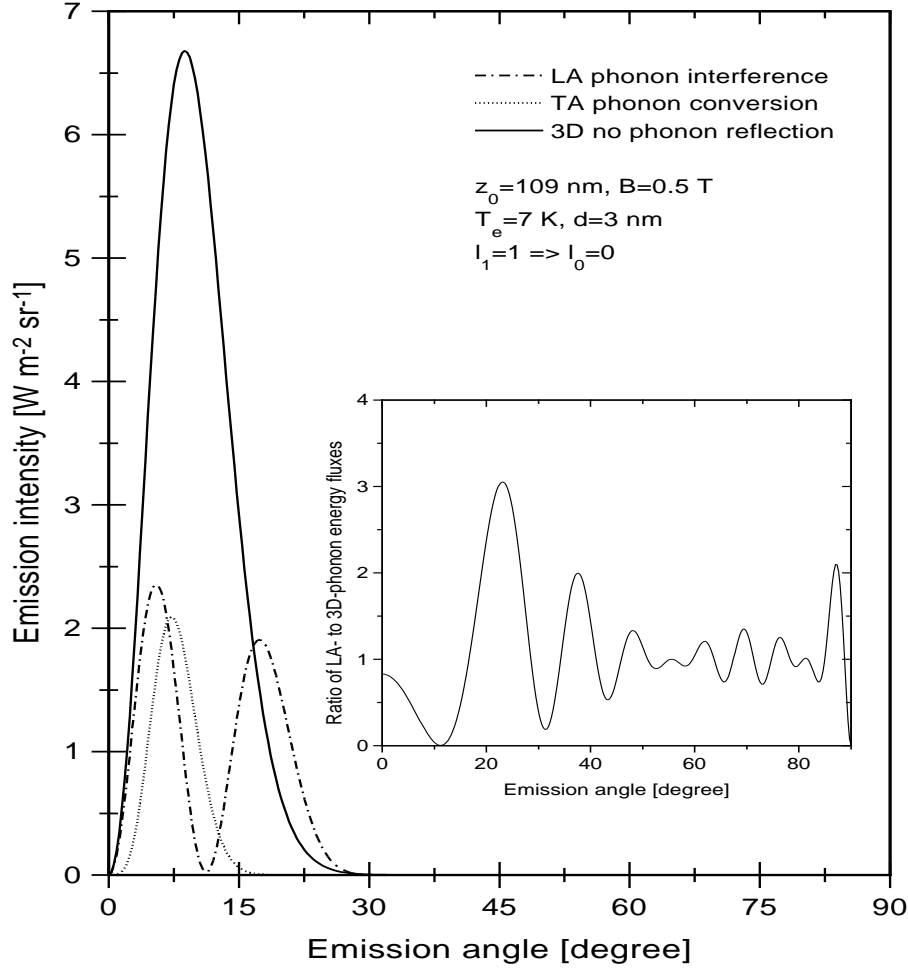


Figure 4.6: Angular distribution of the phonon emission intensity at $\bar{z} = 109$ nm when the Landau level broadening is not taken into account. Inset shows the interference oscillations.

can be strongly suppressed by choosing a proper \bar{z} . However, for large values $\bar{z} \gtrsim \Lambda_2$ (even for high-quality heterostructures with mobility $\mu = 100$ m² V⁻¹ s⁻¹ we have $\Lambda_2 \approx 100$ nm), the Landau level broadening smoothes these oscillations, as it is shown on inset of Figs. 4.7 and 4.8. So the emission character will not be impressively different for different values of \bar{z} (*quod vide* Figs. 4.5 and 4.6). Finally, note that the intensity of TA phonon emission is nearly 3 – 6 times smaller than that of LA phonons but still remains a quite measurable quantity for experiment.

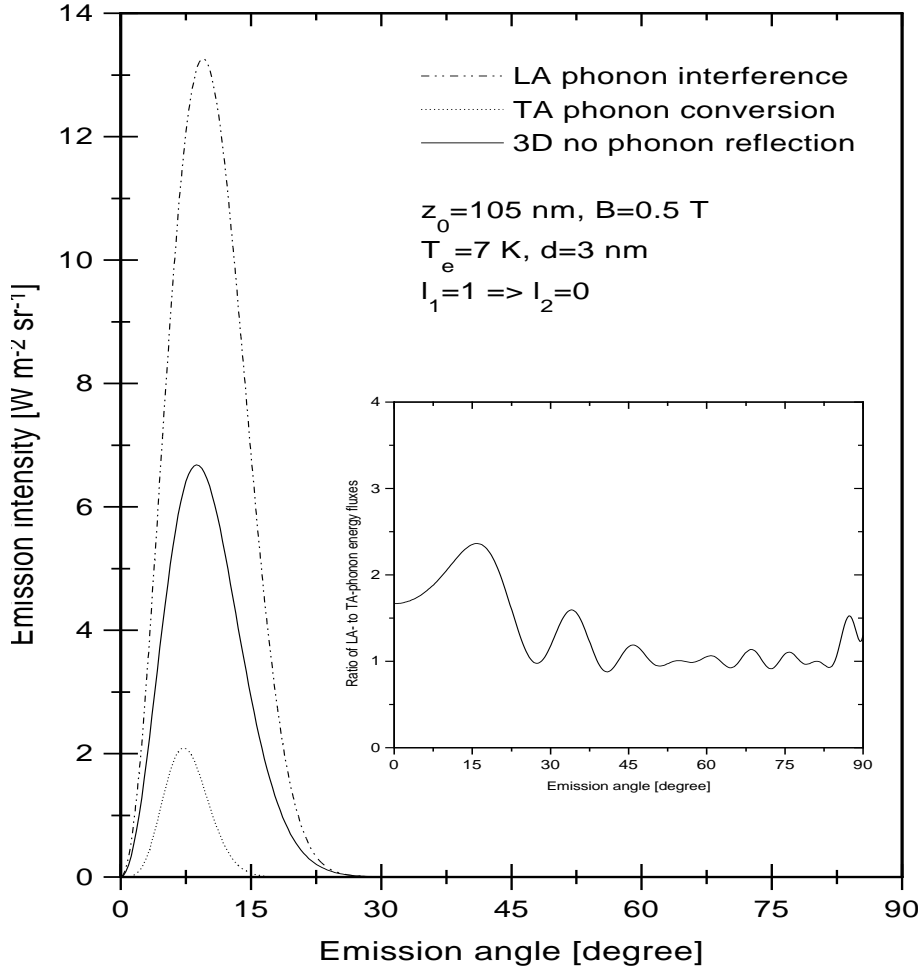


Figure 4.7: Angular distribution of the phonon emission intensity at $\bar{z} = 105$ nm when the Landau level broadening is taken into account.

4.4 Optical phonon emission: One phonon processes

The 2DEG embedded in an elastic medium of a single heterostructure and subjected to the quantizing magnetic field in z -direction normal to the electron layer is considered in this section. The scattering probability at which one phonon of a given mode Υ and a 3D-wavevector $\mathbf{q} = (\mathbf{q}_\perp, q_z)$ is emitted by an electron of the 2DEG is given by Fermi's golden rule as

$$W_{nlk_x \rightarrow n'l'k'_x}^{\Upsilon \mathbf{q}} = \frac{2\pi}{\hbar} |M_{nlk_x \rightarrow n'l'k'_x}^{\Upsilon \mathbf{q}}|^2 \delta(\varepsilon_{nl} - \varepsilon_{n'l'} - \hbar\omega_\Upsilon(q)) \quad (4.51)$$

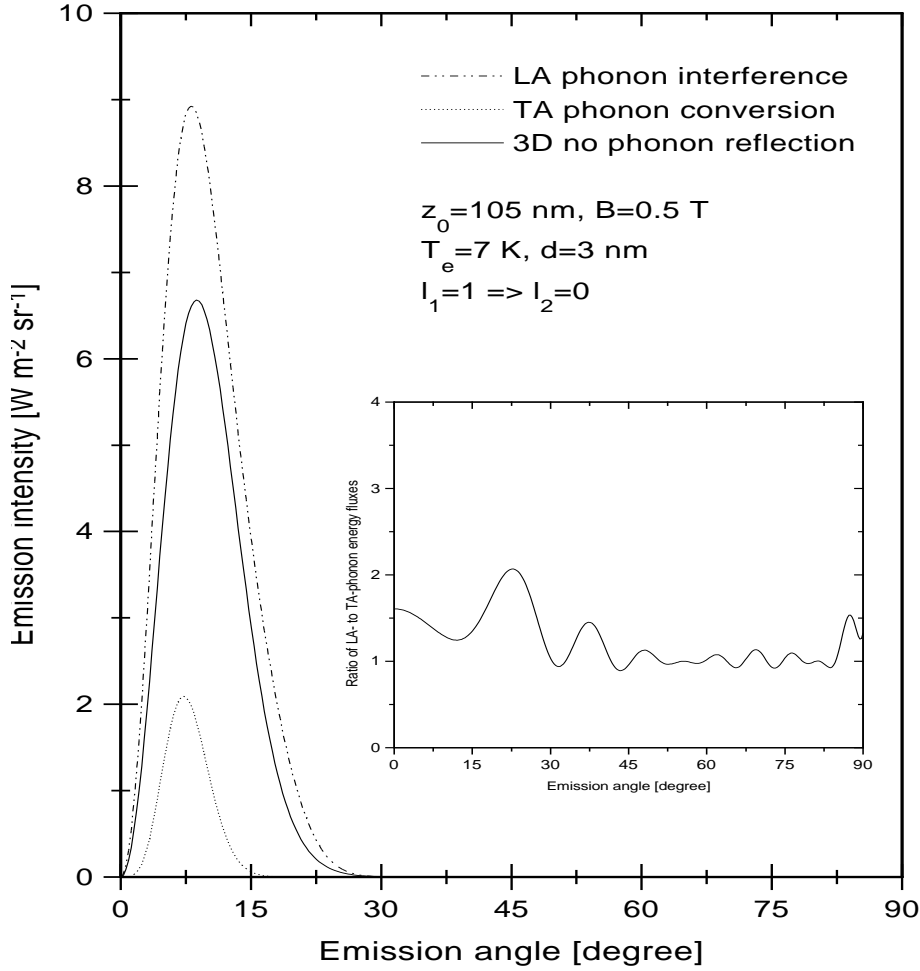


Figure 4.8: Angular distribution of the phonon emission intensity at $\bar{z} = 109$ nm when the Landau level broadening is taken into account.

The electron eigenstate $|nlk_x\rangle$ is labeled by a subband index n corresponding to the quantization of electron motion in z -direction, by a Landau index l and an electron momentum x -component k_x . In the case of the bulk Landau states the eigenenergy ε_{nl} does not depend on the quantum number k_x which counts the degeneracy of a Landau level. The frequency of a phonon in a given mode is $\omega_{\Upsilon}(\mathbf{q})$. Because corresponding wave functions $|nlk_x\rangle$ are factored into a subband function $|n\rangle$ and a Landau oscillator function $|lk_x\rangle$ the matrix element can be represented in the form

$$M_{nlk_x \rightarrow n'l'k'_x}^{\Upsilon} = B^{\Upsilon}(q) Q_{ll'}(q_{\perp}) I_{nn'}^{\Upsilon}(q_{\Upsilon}) \delta_{k'_x, k_x - q_x} \quad (4.52)$$

where the form factor $Q_{ll'}$ is given by Eq. (2.12). In the case of $n = n' = 0$, using the model wave function (4.17), one can obtain the following explicit forms for the subband part of the matrix element

$$|I_{00}^{PO,DA}(q_z)|^2 = (1 + q_z^2 d^2)^{-3}, \quad |I_{00}^{SO}(q_\perp)|^2 = (1 + q_\perp d)^{-6} \quad (4.53)$$

where d is the length scale of the 2DEG in z -direction. It is assumed that d is the smallest parameter of the problem so that the electron relaxation between Landau levels of the lowest subband should be considered.

In Eq. (4.52) the factors $B^\Upsilon(q)$ characterize the electron-phonon interaction and are given by

$$B^{DA}(q) = iq^{1/2} \frac{B_{DA}^{1/2}}{L^{3/2}}, \quad \frac{1}{\bar{\tau}_{DA}} = \frac{m_c B_{DA} p_{PO}^3}{\pi \hbar^2 s} = \frac{\Xi^2 p_{PO}^3}{2\pi \hbar \rho s^2} = \frac{1}{4 \text{ ps}}, \quad (4.54)$$

$$B^{PO}(q) = \frac{1}{iq} \frac{B_{PO}^{1/2}}{L^{3/2}}, \quad \frac{1}{\bar{\tau}_{PO}} = \frac{m_c B_{PO}}{\pi \hbar^3 p_{PO}} = 2\alpha_{PO}\omega_{PO} = \frac{1}{0.14 \text{ ps}}, \quad (4.55)$$

$$\begin{aligned} B^{SO}(q_\perp) &= \frac{1}{iq_\perp^{1/2}} \frac{B_{SO}^{1/2}}{L}, \quad \frac{1}{\bar{\tau}_{SO}} = \frac{m_c B_{SO}}{\pi \hbar^3 p_{SO}} = \frac{\alpha_{SO}\omega_{SO}}{\alpha_{PO}\omega_{PO}} \frac{1}{\bar{\tau}_{PO}} \\ &= \begin{cases} (0.50 \text{ ps})^{-1} & \text{for } x = 0.3, \\ (0.34 \text{ ps})^{-1} & \text{for } x = 1. \end{cases} \end{aligned} \quad (4.56)$$

Here L is the normalization length, m_c is the electron effective mass, s is the sound velocity and $\hbar p_\Upsilon = \sqrt{2m_c \hbar \omega_\Upsilon}$. The constants B_{DA} , B_{PO} [136] and B_{SO} are bound up, respectively, with the deformation potential constant Ξ , the usual Frölich constant α_{PO} and the electron-SO phonon coupling α_{SO} . The constant α_{SO} for interface modes in a single heterostructure is defined according to Eq. (2.7).

In Eqs. (4.55)-(4.56) instead of the constants B_Υ , the nominal times $\bar{\tau}_\Upsilon$ [136] are defined which give a visual view of scattering rates. It can be seen that $\bar{\tau}_{SO}$ is $2.5 \sim 3.5$ times larger than $\bar{\tau}_{PO}$, *i.e.*, generally speaking, the interaction with interface modes should be weaker than with bulk modes.

4.4.1 Polar optical phonon scattering

The scattering rate of an electron between two Landau levels l and l' interacting with PO phonon can be represented in the form

$$\frac{1}{\tau_{l \rightarrow l'}^{PO}} = \sum_{\mathbf{q}, k'_x} W_{nlk_x \rightarrow n'l'k'_x}^{PO\mathbf{q}} = \frac{2\pi^2 v_{PO}}{L^3 \bar{\tau}_{PO}} \sum_q \frac{1}{q^2} Q_{ll'}^2(q_\perp)$$

$$\times |I_{00}(q_z)|^2 \delta(\Delta l \omega_B - \omega_{PO}(q)) = \frac{\sqrt{\omega_B \omega_{PO}}}{\bar{\tau}_{PO}} D_{ll'}^{PO}(\gamma) \quad (4.57)$$

where the overlap integral $D_{ll'}^{PO}(\gamma)$ is given as

$$\begin{aligned} D_{ll'}^{PO}(\gamma) &= \int_0^\infty dx dt \frac{Q_{ll'}^2(t)}{(t+x^2)(1+\gamma^2 x^2)^3} \\ &\times \delta(\Delta l \omega_B - \omega_{PO}(\mathbf{q})), \quad \gamma^2 = 2 \frac{d^2}{a_B^2}. \end{aligned} \quad (4.58)$$

The PO phonon emission is governed by the density of final states of a two-particle system: an electron at the level l' and a PO phonon. If the PO phonon dispersion be ignored then both particles have an infinite mass so that this system does not have a continuous spectrum. Thus, to obtain the finite relaxation rate the Landau level broadening or the PO phonon dispersion is to be taken into account.

Allowance for the Landau level broadening

For actual calculations of the scattering rate (4.57) we have to smear the δ -function in Eq. (4.58). Replacing the δ -function by a Lorentzian

$$\delta(\dots) \rightarrow \frac{\tau}{\pi[1 + \tau^2(\omega_{PO} - \Delta l \omega_B)^2]} \quad (4.59)$$

characterized by the total width \hbar/τ where τ is the relaxation time deduced from the mobility (*e.g.* $\mu = 25 \text{ V}^{-1} \text{ s}^{-1} \text{ m}^2$ corresponds to $\tau = 10 \text{ ps}$), it is easy to obtain

$$D_{ll'}^{PO}(\gamma) = \frac{\tau}{1 + \tau^2(\omega_{PO} - \Delta l \omega_B)^2} d_{ll'}^{PO}(\gamma), \quad (4.60)$$

$$d_{ll'}^{PO}(\gamma) = \frac{1}{16} \int_0^\infty dt Q_{ll'}^2(t) \frac{8 + 9\gamma\sqrt{t} + 3\gamma^2 t}{\sqrt{t}(1 + \gamma\sqrt{t})^3}, \quad (4.61)$$

$$d_{l0}^{PO}(0) = \sqrt{\pi} \frac{(2l-1)!!}{2^{l+1} l!}. \quad (4.62)$$

One can see that $x^2 \simeq t \simeq 1$, *i.e.* $q_z \simeq q_\perp \simeq a_B^{-1}$, have the main contribution to the integral (4.58). This isotropic distribution in momenta of emitted phonons is conditioned by the long-range nature of the polar interaction. It forces the scattering time to be governed by the minimum scale in the momentum space,

$\min\{a_B^{-1}, d^{-1}\}$. Recall that in the case of DA phonon scattering, phonon emission is anisotropic in the momentum space: $q_z \simeq d^{-1} \gg q_\perp \simeq a_B^{-1}$ [176, 45, 216].

In magnetic fields below 10 T using $d = 3$ nm as a typical value for a GaAs/AlGaAs heterostructures we have $\gamma^2 \ll 1$. Therefore, in rough estimates, the value of $d_{ll'}^{PO}$ at $\gamma = 0$ can be used.

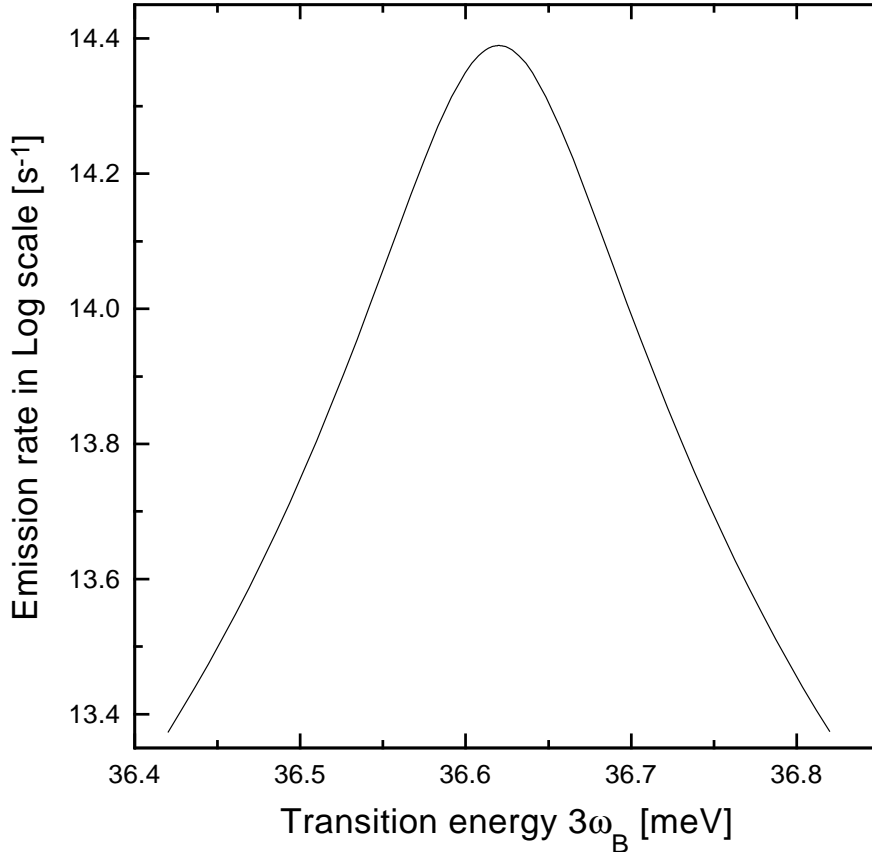


Figure 4.9: The Landau level broadening contribution to the PO phonon emission rate versus on the inter-level-spacing $\Delta l\omega_B$ for the electron transitions between $l = 3$ and $l' = 0$ levels in the vicinity of the PO phonon energy ω_{PO} .

The result of numerical calculations according to Eqs. (4.57) and 4.62 at $\gamma \neq 0$ and $\tau = 10$ ps is shown in Fig. 4.9. The diagram of the scattering rate dependence on the inter-Landau-level separation for $l = 3$ and $l' = 0$ represents a narrow peak at the PO phonon energy with peak value exceeding 10^2 ps⁻¹. One may see that for detuning 0.2 meV the scattering time $\tau_{3 \rightarrow 0}^{PO}$ increases by an order.

Note that in the case of the relaxation between Landau levels $l = 1$ and $l' = 0$ the scattering rate dependence on the inter-level spacing is also represented as a Lorentzian with approximately the same width and with the peak value 1.17 times larger than that of for the relaxation between levels $l = 3$ and $l' = 0$.

Allowance for the PO phonon dispersion

In this case taking $\omega_{PO}(q) = \omega_{PO}(1 - q^2/2q_0^2)$ with $\omega_{PO} = 36.62$ meV and $q_0 = 18.5 \text{ nm}^{-1}$ the overlap integral (4.58) can be reduced to a one-dimensional integral of the form

$$\begin{aligned} D_{ll'}^{PO}(\gamma) &= \int_0^\infty dx dt \frac{Q_{ll'}^2(t)}{(t+x^2)(1+\gamma^2 x^2)^3} \delta\left(\Delta\omega_B - \omega_{PO} + \frac{t+x^2}{2x_0^2}\omega_{PO}\right) \\ &= \frac{a}{\omega_{PO} - \Delta\omega_B} \int_0^1 dx \frac{Q_{ll'}^2(y)}{(1+b^2 x^2)^3}, \quad a^2 = \left(1 - \frac{\Delta\omega_B}{\omega_{PO}}\right) q_0^2 a_B^2, \\ x_0^2 &= \frac{1}{2} q_0^2 a_B^2, \quad y = a^2(1-x^2), \quad b^2 = a^2 \gamma^2 \end{aligned} \quad (4.63)$$

which is evaluated numerically for the electron transitions between $l = 3$ and $l' = 0$ Landau levels (Fig. 4.10). Because of the energy conservation, electron relaxation via this mechanism is possible only on the low magnetic field side, $3\omega_B < \omega_{PO}$. The scattering rate has a sharp and strongly asymmetric peak immediately below ω_{PO} with the peak value exceeding 10 fs^{-1} . It can be seen from Esq. 4.57 and 4.63 that the scattering rate decreases exponentially for energies below the peak value while it drops more strongly for energies above the peak value (Fig. 4.10). As following from the comparison of diagrams of Figs. 4.9 and 4.10, the PO phonon dispersion contribution at the relaxation peak by an order of magnitude is greater than the Landau level broadening contribution. The former remains significant even for samples of exceptional quality ($\mu > 100 \text{ V}^{-1} \text{ s}^{-1} \text{ m}^2$). On the other hand the allowance for the Landau level broadening gives rise to a symmetric peak at ω_{PO} thereby providing the one-phonon relaxation on the upper side of the resonance.

Note that the electron-PO phonon relaxation rate calculated for a GaAs quantum dot [36] as a function of a dot diameter or, that is the same, of an inter-level-spacing has an approximately 3 ~ 4 times narrow peak than the peak of the PO phonon dispersion contribution obtained here in the QHE geometry. Both have approximately the same peak value.

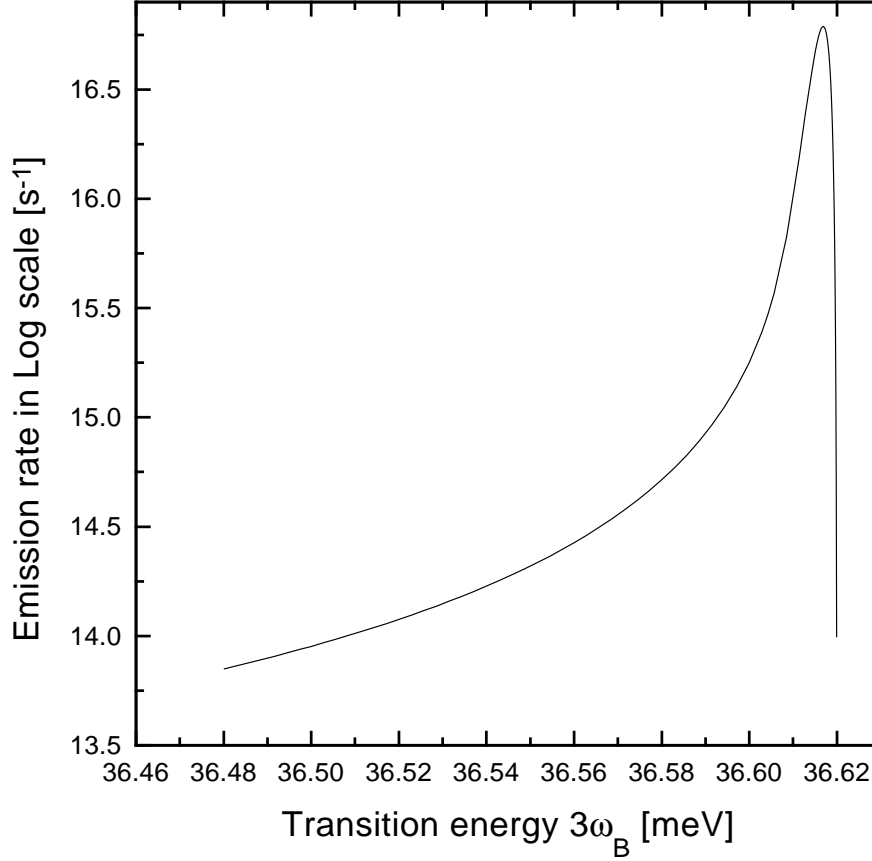


Figure 4.10: The PO phonon dispersion contribution to the PO phonon emission rate as a function on the inter-level-spacing $\Delta l\omega_B$ for the electron transitions between $l = 3$ and $l' = 0$ levels.

4.4.2 Surface optical phonon scattering

In the case of a single heterostructure, the surface optical SO phonons do not exhibit dispersion. Therefore for SO phonons we consider only the Landau level broadening contribution to the relaxation. To obtain the scattering rate we have to replace all indexes *PO* by *SO* and to take the overlap integral $D_{ll'}^{SO}$ in the form

$$D_{ll'}^{SO}(\gamma) = \frac{\tau}{1 + \tau^2(\omega_{SO} - \Delta l\omega_B)^2} d_{ll'}^{SO}(\gamma), \quad (4.64)$$

$$d_{ll'}^{SO}(\gamma) = \int_0^\infty dt \frac{Q_{ll'}^2(t)}{\sqrt{t}(1 + \gamma\sqrt{t})^6}, \quad (4.65)$$

$$d_{l0}^{SO}(0) = \sqrt{\pi} \frac{(2l-1)!!}{2^l l!}. \quad (4.66)$$

Note that $t \simeq 1$, *i.e.* $q_\perp \simeq a_B^{-1}$ have contributed heavily to both integrals in Eqs. (4.62) and 4.65. It is clear that the SO phonon relaxation peak is shifted on the low energy side by $\omega_{PO} - \omega_{SO} \approx 2$ meV. Taking $d = 3$ nm and $B = 7$ T it is easy to obtain $d_{30}^{SO} = 0.023$ and $d_{30}^{PO} = 0.1$. Therefore at the relaxation peak, the PO phonon scattering rate is to the SO phonon scattering rate as

$$\max \frac{\tau_{3 \rightarrow 0}^{SO}}{\tau_{3 \rightarrow 0}^{PO}} = \frac{\bar{\tau}_{SO}}{\bar{\tau}_{PO}} \sqrt{\frac{\omega_{PO}}{\omega_{SO}}} \frac{d_{30}^{PO}}{d_{30}^{SO}} = \begin{cases} 15.9 & \text{if } x = 0.3, \\ 10.8 & \text{if } x = 1. \end{cases} \quad (4.67)$$

Thus SO phonon relaxation at least by an order is weaker than relaxation via PO phonon emission.

4.5 Phonon emission: Two-phonon processes

To calculate the electron transition probability due to the two-phonon emission mechanism, the quasiparticle approach has been exploited. Therefore, the two-phonon contribution to electron relaxation in the first order of the perturbation theory arising from the interaction Hamiltonian expanded up to second order in the phonon displacement operators can be neglected [136]. The second order contribution to the probability of an electron transition from a bulk Landau state $|lk_x\rangle$ into a state $|l'k'_x\rangle$ of the same lowest subband (for brevity the subband index will be omitted) at which one PO phonon with a 3D-wavevector \mathbf{q} and one DA phonon with a 3D-wavevector \mathbf{q}' are emitted is given by

$$\begin{aligned} W_{lk_x \rightarrow l'k'_x}^{+\mathbf{q},+\mathbf{q}'} &= \frac{2\pi}{\hbar^4} \frac{B_{PO}B_{DA}}{L^6} \frac{q'}{q^2} \delta_{k'_x, k_x - q_x - q'_x} \delta(\Delta l \omega_B - \omega_{PO} - sq') \\ &\times \left| \sum_{\bar{l}, \bar{k}_x} \left\{ \frac{\langle l'k'_x | \exp(-i\mathbf{q}'\mathbf{r}) | \bar{l}\bar{k}_x \rangle \langle \bar{l}\bar{k}_x | \exp(-i\mathbf{q}\mathbf{r}) | lk_x \rangle}{(l - \bar{l})\omega_B - \omega_{PO}} \right. \right. \\ &\left. \left. + \frac{\langle l'k'_x | \exp(-i\mathbf{q}\mathbf{r}) | \bar{l}\bar{k}_x \rangle \langle \bar{l}\bar{k}_x | \exp(-i\mathbf{q}'\mathbf{r}) | lk_x \rangle}{(l - \bar{l})\omega_B - sq'} \right\} \right|^2. \quad (4.68) \end{aligned}$$

The PO+DA phonon emission rate at electron transitions between Landau levels l and l' can be obtained after summing up over the phonon and the final electron momenta, \mathbf{q}, \mathbf{q}' and k'_x ,

$$\frac{1}{\tau_{l \rightarrow l'}^{PO+DA}} = \sum_{k'_x, \mathbf{q}, \mathbf{q}'} W_{lk_x \rightarrow l'k'_x}^{+\mathbf{q},+\mathbf{q}'}. \quad (4.69)$$

Note that after summation over k'_x the result cannot depend on gauge non-invariant quantum number k_x . The explicit calculation of the emission rate can be carried out by consideration separately the following two situations: $(\Delta l\omega_B - \omega_{PO}) \ll \omega_B, \omega_{PO}$ and $(\Delta l\omega_B - \omega_{PO}) \lesssim \omega_B, \omega_{PO}$, where the relaxation is qualitatively different.

4.5.1 Low magnetic fields

$(\Delta l\omega_B - \omega_{PO}) \ll \omega_B, \omega_{PO}$ In this energy range the main contribution to the sum over intermediate states \bar{l} in Eq. 4.68 have the state $\bar{l} = l'$ in the first term and the state $\bar{l} = l$ in the second term. Therefore, the emission rate can be rewritten as

$$\begin{aligned} \frac{1}{\tau_{l \rightarrow l}^{PO+DA}} &= \frac{2\pi}{\hbar^4} \frac{B_{PO}B_{DA}}{L^6 c^2} \sum_{\mathbf{q}, \mathbf{q}'} \delta(\Delta l\omega_B - \omega_{PO} - sq') \\ &\times \frac{Q_{ll'}^2(q_\perp)}{q^2 q'} |Q_{l'l'}(q'_\perp) - Q_{ll}(q'_\perp)|^2 |I_{00}(q_z)|^2 |I_{00}(q'_z)|^2 \end{aligned} \quad (4.70)$$

which again can be reduced to a one-dimensional integral of the form

$$\begin{aligned} \frac{1}{\tau_{l \rightarrow l}^{PO+DA}} &= \frac{1}{\bar{\tau}_{PO+DA}} \frac{\omega_B}{sp_{PO}} d_{ll'}^{PO}(\gamma) \int_0^{\beta^2} dt' \exp(-t') \\ &\times \frac{[L_{l'}(t') - L_l(t')]^2}{\sqrt{\beta^2 - t'} [1 + \gamma^2(\beta^2 - t')]^3}, \beta = \frac{\Delta l\omega_B - \omega_{PO}}{\sqrt{2}s} a_B \end{aligned} \quad (4.71)$$

where a nominal relaxation time is introduced for the DA+PO phonon emission mechanism

$$\frac{1}{\bar{\tau}_{PO+DA}} = \frac{1}{4sp_{PO}\bar{\tau}_{PO}\bar{\tau}_{DA}} \quad (4.72)$$

which depends only on a heterojunction parameters. For a GaAs/AlGaAs heterojunction with $d = 3$ nm we have $\bar{\tau}_{PO+DA} \approx 2.9$ ps.

Actually in this energy range of $\Delta l\omega_B$, the electron transitions take place in following two ways. (i) Remaining on the level l , an electron emits a DA phonon thereby the electron-phonon system is forced to transit into a virtual intermediate state. Then the electron emits a second PO phonon so that the electron-phonon system turns out in the final state with the real electron on the Landau level l' and with two real DA and PO phonons. (ii) In the second way, the electron emits firstly the PO phonon and simultaneously makes a transition to the level l' . By

emission of the second DA phonon, the created virtual intermediate state is forced to transit into the same final state. In both cases 3D-wavevectors of emitted PO- and DA phonons are not correlated. The 3D-wavevectors of emitted PO phonons have the same isotropic distribution in the momentum space as in the one-phonon emission case. While the momentum distribution of the emitted DA phonons is different in different ranges of $\Delta l \omega_B$. Immediately above the PO phonon energy for $\beta \ll 1$ (this corresponds to the energies $(\Delta l \omega_B - \omega_{PO}) \ll s/a_B$), electrons emit DA phonons with $q'_\perp \simeq q'_z \simeq a_B^{-1}$. In this case the following asymptotic expression is obtained for the emission rate

$$\frac{1}{\tau_{l \rightarrow l'}^{PO+DA}} = \frac{16(l-l')^2}{15} \frac{\beta^5}{\bar{\tau}_{PO+DA}} \frac{\omega_B}{sp_{PO}} d_{ll'}^{PO}(\gamma). \quad (4.73)$$

The essential part of the magnetic field dependence in this range is given by

$$\frac{1}{\tau_{l \rightarrow l'}^{PO+DA}} \propto (B - B_{\Delta l})^5, \quad (4.74)$$

i.e., relaxation is enhanced as a fifth power of $B - B_{\Delta l}$ with increase in the magnetic field. Here $B_{\Delta l}$ is the magnetic field for which $\Delta l \omega_B = \omega_{PO}$.

In opposite limiting case of $\beta \gg 1$, actually for energies $s/d \lesssim (\Delta l \omega_B - \omega_{PO}) \ll \omega_B, \omega_{PO}$, electrons emit DA phonons with $q'_\perp \simeq a_B^{-1} \ll q'_z \simeq d^{-1}$, *i.e.*, DA phonon emission is heavily concentrated in a narrow cone around the magnetic field. In this case for the emission rate we obtain

$$\frac{1}{\tau_{l \rightarrow l'}^{PO+DA}} = \frac{1}{\bar{\tau}_{PO+DA}} \frac{2}{\beta(1 + \gamma^2 \beta^2)^3} \frac{\omega_B}{sp_{PO}} d_{ll'}^{PO}(\gamma). \quad (4.75)$$

The essential part of the magnetic field dependence is given by

$$\frac{1}{\tau_{l \rightarrow l'}^{PO+DA}} \propto (B - B_{\Delta l})^{-1}, \quad (4.76)$$

i.e., in this range relaxation becomes linearly weaker with increase in the magnetic field.

Results of numerical evaluation of the emission rate as a function of the inter-Landau-level separation $\Delta l \omega_B$ in the whole energy range (4.5.1) are illustrated for transitions between Landau levels $l = 3$ and $l' = 0$ in Fig. 4.11. So far as the two-phonon processes contain the small electron-phonon coupling in the second order, PO+DA emission gives rise to a peak which is lower than that of for one-phonon

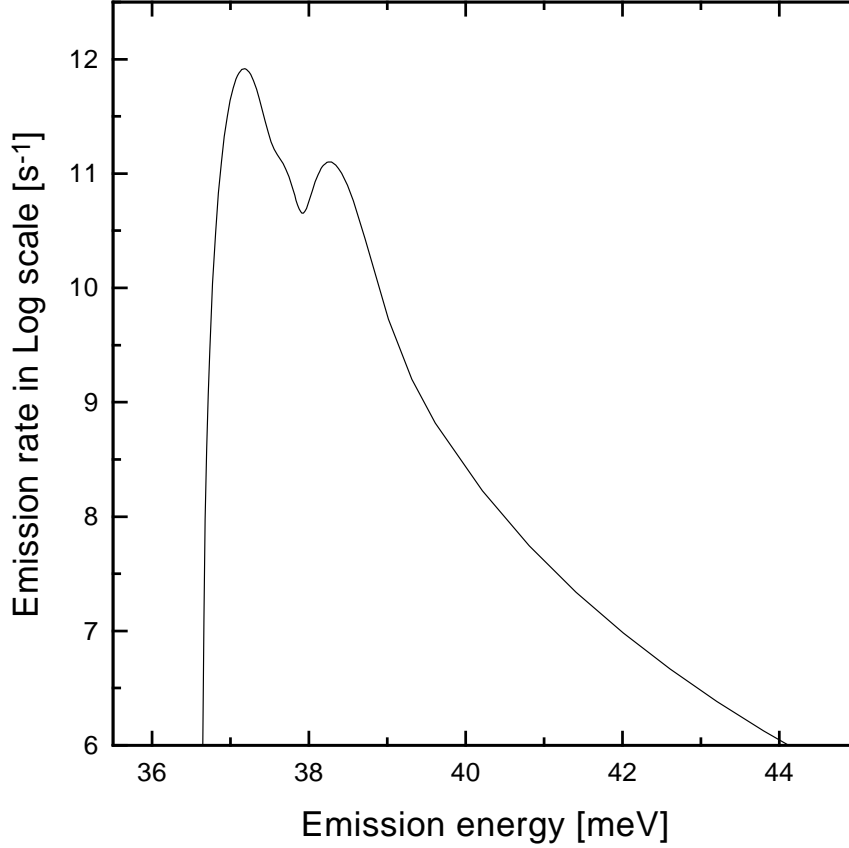


Figure 4.11: The PO+DA phonon emission rate versus on the inter-Landau-level separation $\Delta l \omega_B$ for the electron transitions between $l = 3$ and $l' = 0$ levels in the energy range $(3\omega_B - \omega_{PO}) \ll \omega_B, \omega_{PO}$.

emission. PO+DA phonon relaxation has a sharp onset at low magnetic fields corresponding to energies immediately above $\hbar\omega_{PO}$ where the peak increases as a fifth power in the magnetic field achieving the peak value exceeding 1 ps^{-1} . At high magnetic fields the peak decreases much slowly, linearly in $B - B_{\Delta l}$, so that the PO+DA phonon emission mechanism gives rise to a rather broad peak than the PO phonon emission peak.

4.5.2 High magnetic fields

$(\Delta l \omega_B - \omega_{PO}) \simeq \omega_B, \omega_{PO}$. As it follows from the energy conservation, the energy of an emitted DA phonon is $sq' \simeq \omega_B$ so that $q' \simeq \omega_B/s \gg a_B^{-1}$. On the other

hand, electrons in the states with Landau indexes $l \simeq 1$ have momenta of the order of a_B^{-1} . Therefore for more important electron transitions with $l, l' \simeq 1$ the momentum transmission to the phonon system is also of the same order of a_B^{-1} . Hence in this energy range, electrons should emit phonons with almost oppositely directed momenta of approximately equal absolute values to avoid an additional suppression of the two-phonon emission. The large momentum transferred to each phonon results in the large Landau index \bar{l} for intermediate states in Eq. (4.68). As far as the quasiclassic description takes place for $\bar{l} \gg 1$, the intermediate state energies are

$$\bar{l}\omega_B \approx \frac{(\Delta\bar{l}\omega_B - \omega_{PO})^2}{2ms^2} \gg l\omega_B, \omega_{PO}, sq'. \quad (4.77)$$

Therefore for the emission rate in the range (4.5.2) we obtain

$$\frac{1}{\tau_{l \rightarrow l'}^{PO+DA}} = \frac{3}{2\bar{\tau}_{PO+DA}} \frac{(2ms^2/\hbar)^2 \omega_B}{(\Delta l\omega_B - \omega_{PO})^3} \frac{1}{p_{PO}d}. \quad (4.78)$$

The magnetic field dependence is given by

$$\frac{1}{\tau_{3 \rightarrow 0}^{PO+DA}} \propto (B - B_{\Delta l})^{-3}. \quad (4.79)$$

Because in the range (4.5.2), B is of the order of $B_{\Delta l}$ one can replace $B - B_{\Delta l}$ by $B_{\Delta l}$ so that the emission rate dependence on the magnetic field is weak in a rather wide energy range above ω_{PO} .

It is interesting also to compare the PO+DA phonon emission rate for transitions between Landau levels $l = 3$ and $l' = 0$ with the 2LA phonon emission rate at transitions between levels $l = 1$ and $l' = 0$. Using the result obtained in [47] it is easy to obtain

$$\frac{1}{\tau_{3 \rightarrow 0}^{PO+DA}} = 8 \frac{\tau_{DA}}{\tau_{PO}} \frac{\omega_{PO}^2 (2mc^2/\hbar)}{(3\omega_B - \omega_{PO})^3} \frac{1}{\tau_{1 \rightarrow 0}^{2DA}}. \quad (4.80)$$

Taking $B = 8.4$ T and $d = 3$ nm for a GaAs/AlGaAs heterojunction we have $2ms^2 \approx 0.02$ meV and $\omega_B = 2\omega_{PO}/5 \approx 14.65$ meV. So as it follows from Eq. (4.78) at transitions between Landau levels $l = 3$ and $l' = 0$ one can use $\tau_{3 \rightarrow 0}^{PO+DA} = 100$ ns as a characteristic relaxation time in the range (4.5.2). Under the same conditions at transitions between levels $l = 1$ and $l' = 0$ for the LA and 2LA phonon emission times we have, respectively, $\tau_{1 \rightarrow 0}^{DA} = 5.4$ μ s [45] and $\tau_{1 \rightarrow 0}^{2DA} = 15.6\tau_{3 \rightarrow 0}^{PO+DA}$. Thus comparison of these times shows the importance of the PO+DA emission

processes in the QHE geometry. In some experimental arrangements the PO+DA phonon emission mechanism is much more efficient than relaxation in the following two consecutive emission acts: PO phonon emission (even under the sharp resonance) + either LA or 2LA phonon emission.

4.6 Summary

In conclusion, PO phonon assisted electron relaxation is calculated as a function of the inter-Landau-level spacing in the 2DEG in the QHE geometry. The PO, SO and PO+DA phonon emission processes via polar optical and deformation acoustical interactions are considered. The interface SO phonon relaxation is at least by an order weaker than the relaxation via PO phonon emission. To obtain a finite relaxation rate associated with one-phonon emission, the allowance for the Landau level broadening and for the PO phonon dispersion is made. Immediately below the phonon energy $\hbar\omega_{PO}$, the PO phonon dispersion contribution gives rise to a sharp peak with the peak value approximately 0.17 fs^{-1} . The Landau level broadening contribution has a rather broad peak with the relatively lower peak value. Below ω_{PO} within an energy range of the order of $\hbar\sqrt{\omega_B/\tau}$, the one-phonon relaxation rate exceeds 1 ps^{-1} (τ is the relaxation time deduced from the mobility). In GaAs/AlGaAs heterostructures with the mobility $\mu = 25 \text{ V}^{-1} \text{ s}^{-1} \text{ m}^2$ this range makes up 0.7 meV .

Two-phonon emission is a controlling relaxation mechanism above $\hbar\omega_{PO}$. For $\Delta\omega_B$ immediately above ω_{PO} , PO+DA phonon relaxation has a sharp onset. The relaxation rate increases as a fifth power in the magnetic field achieving to the peak value exceeding 1 ps^{-1} at energy separations of the order of s/a_B (in GaAs at $B = 7 \text{ T}$ we have $\hbar(s/a_B) \approx 0.4 \text{ meV}$). At higher magnetic fields in the energy range $sa_B^{-1} \lesssim \Delta\omega_B - \omega_{PO} \lesssim sd^{-1}$ (in GaAs with $d = 3 \text{ nm}$ we have $\hbar(s/d) \approx 1.2 \text{ meV}$), the two-phonon peak decreases linearly in the magnetic field. Above ω_{PO} within the wide energy range (in GaAs this range makes up to 5 meV), the magnetic field dependence of the relaxation rate is rather weak and the subnanosecond relaxation between Landau levels $l = 3$ and $l' = 0$ can be achieved via two-phonon emission mechanism.

Our analysis demonstrates also that in some experimental situations, the

PO+DA phonon emission mechanism is more efficient than relaxation in two consecutive emission acts: PO phonon emission (even under the sharp resonance) with the subsequent emission of either LA- or 2LA phonon.

Chapter 5

Edge state scattering

5.1 Introduction

The single particle energy spectrum in a 2DEG exposed to a homogeneous magnetic field normal to the electron plane is separated into the quasibulk Landau and edge states. The edge states correspond to the classical skipping orbits. Their location with respect to the boundary of the sample depends on the wave vector k . When the $k \rightarrow \infty$, the edge state number l transforms into a quasibulk Landau state (see Fig. 5.1). The confining potential in the plane of electrons removes the degeneracy of the Landau levels so that, in contrast to the bulk Landau states, the edge state energy exhibits a finite dispersion $\varepsilon_l(k)$ with $\varepsilon_l(k) \rightarrow \varepsilon_l = \hbar\omega_B(l+1/2)$ if $k \rightarrow \infty$ (ω_B is the cyclotron frequency). There exist edge states also in quantum wires (QWs) in the magnetic field normal to the wires. If wire width L is much greater than the magnetic length, $L \gg a_B$, ($a_B = \sqrt{\hbar/m_c\omega_B}$ is the magnetic length, m_c is the electron effective mass), then the backscattering between edge states moving in opposite directions on the opposite sides of the wire is strongly suppressed. So in sufficiently strong magnetic fields, the edge states in the 2DEG and QW can be treated in the same way as one dimensional system structures. Currently semiconductor nanostructures with such one dimensional electron systems attract considerable interest both to study in them novel physical phenomena as well as for possible device applications such as QW lasers (see review [26]).

To explain the quantum Hall effect (QHE) in high mobility samples with a

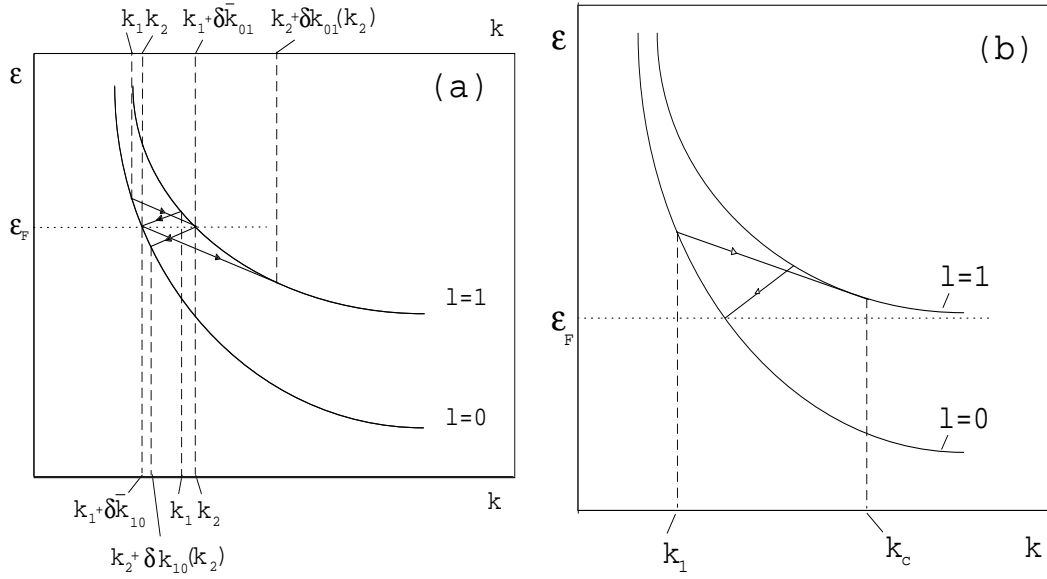


Figure 5.1: A schematic diagram of the edge state energy spectrum. (a) Transitions $0 \rightarrow 1$ and $1 \rightarrow 0$ due to acoustic phonon emission are shown. At low temperatures, states close to the $0k_1$ are important. (b) If the Fermi level is close to the bulk Landau level, the transitions $0 \rightarrow 1$ involving states above the threshold k_c are only possible. At high temperatures, states disposed at the separations of T_e above and below ϵ_F are important.

2DEG of submicron dimensions, since shortly after its discovery [13], a new concept based on the Büttiker-Landauer quantum edge state transport formalism has been advanced [217, 218, 219, 220]. In this description the conducting properties of the 2DEG are determined by the edge states at the Fermi level, ϵ_F , which are propagated along the sample boundaries. Within the sample, electrons occupy N quasibulk Landau levels below ϵ_F , but near the boundary of the sample, the confining potential bent up these energy levels so that they rapidly increase and intersect ϵ_F . Thus each quasibulk Landau level below ϵ_F gives rise to a quasi-one dimensional transport edge channel at ϵ_F on either side of the sample. If the 2DEG is coupled to two large electron reservoirs with applied potential $\Delta\mu$ and with ideal contacts, *i.e.*, they transmit every electron without reflection, then the edge states are equally populated and each edge channel carries an equal fraction of the current on a given side of the sample. On opposite sides of the sample, the current flows in opposite directions resulting in a total

current $I = N(2e/h)\Delta\mu$ and a Hall voltage $V_H = \Delta\mu/e$ so that we have the QHE with the Hall conductance $G_H = N(2e^2/h)$. Under these conditions G_H does not depend on the properties of the contacts and is determined by the number N of the quasibulk Landau levels. Kent *et al.* in their recent experiment [221] have obtained qualitative agreement with such theoretical description of the QHE.

On the other hand, electrons can be selectively injected into different edge channels and selectively detected using non-ideal probes. As a result we can have a non-equal population of the edge states and significant deviation from the normal integer QHE. In this case, as it has been theoretically shown by Büttiker [217], G_H depends on the properties of the current and voltage contacts and is not related to the number of bulk Landau states below ε_F . While flowing along an edge of samples, the current tends to redistribute so that an equal fraction of the current is to be carried by each edge channel. Such a re-establishment of the current equilibrium can be achieved via electron scattering processes by phonons and impurities. If spatial separation between edge channels is not much greater than the magnetic length then the equilibrium is expected to occur after the current travels a distance of the order of the zero-field inelastic and elastic scattering length, 10 μm . However, recently van Wees *et al.* [222] and Komiyama *et al.* [223], involving high mobility 2DEG systems with non-ideal current probes separated more than 200 μm from one another, have observed that a long distance in excess of 100 μm is necessary to equilibrate the populations between different edge channels. It has been shown in these works that under the conditions of strong magnetic fields and low temperatures, the quantization of the Hall conductance is determined *only* by the number of the quantum edge channels which are coupled to the non-ideal probes and is independent of the total number of the occupied quasibulk edge states. This effect, usually referred to as the anomalous integer QHE, has also been revealed in a number of recent experiments [224, 225, 223, 226, 227, 222, 228]. Data of these experiments, being analyzed with the help of Landauer-Büttiker formalism, provide some information about the inter-edge-relaxation that leads to the re-establishment of the equilibrium. In the course of such analyses two important features were revealed which indicate the importance of the analogous theoretical investigations. Firstly, the characteristic scattering length $\mathcal{L}_{l \rightarrow l'}$ between states l and l' exceeds significantly the

transport scattering length obtained from zero-field mobility. It points out the significant suppression of the scattering compared to the case of zero magnetic field. Secondly, a strong temperature dependence of $\mathcal{L}_{l \rightarrow l'}$ was revealed [225, 227].

In their experiment Alphenaar *et al.* [229] have further clarified the long range of non-equilibrium distribution of electrons. The carrier source contact has been adjusted in such a way that the current has been injected into the sample from the non-ideal current probe reservoir through only the lowest of edge channels. The authors have studied in detail the dependence of the inter-edge-state equilibration length on different pairs of edge states, on the magnetic field and filling factors. The result indicates that the $N - 1$ outermost edge states equilibrate but these states are decoupled from the innermost edge state. A clear understanding of the reason for this effect has not been achieved yet. In principle, it is impossible to do this in the framework of the theories with a parabolic confining potential. Such potential has no flat domain corresponding to the interior of the sample. Therefore, there are no quasibulk edge states and one cannot reveal properties of the scattering which appear when the Fermi level is close to a bulk Landau level. Thus, it is important to carry out calculations for the scattering length for transitions between outermost and the innermost quasibulk edge states for an arbitrary shape of the confining potential. The efficiency of such an interaction is chiefly determined by the form of the edge state spectrum. As it follows from the energy and momentum conservation laws, there are two threshold-like points on the innermost quasibulk Landau level so that transitions from outermost to innermost edge state after emission of acoustic phonons are restricted by the final states between of these two points. As we can see below, these states, the velocity of which is approximately equal to the sound velocity, play an important role in the scattering processes.

Theoretically, inter-edge-state relaxation has been addressed in several works [227, 230, 231, 232, 233]. Scattering by irregularities of the boundary is discussed in Refs. [230, 231] and scattering by delta-function impurities and phonons in [227, 232]. A two-phonon scattering mechanism has been suggested recently [233]. Although significant progress has been achieved the problem still cannot be considered as solved. Results of Refs. [230, 231] are difficult to compare with experiment because little is known about the actual profile of the boundaries.

The application of the delta-function impurity model to the GaAs/Ga_{1-x}Al_xAs heterostructures which have been used in the experiments [222, 223, 224, 225, 226, 227, 228, 229] is somewhat questionable since it is known (*cf.*, *e.g.*, Refs. [234, 208, 235]) that in these systems at least zero-field scattering is determined by the long-range potential fluctuations due to the remote ionized donors.

One of the aims of the present chapter is to calculate the inter-edge-state scattering length due to phonons and impurities under more general assumptions than used previously, for realistic models of the electron-phonon and electron-impurity interaction and for a realistic confining potential.

In contrast to the above conventional transport measurement experiments, in this chapter we study the inter-edge-state relaxation also in the phonon emission experimental technique. The phonon emission or absorption experiments (see review papers [174, 175] measure directly the total energy flux from the 2DEG interacting with different phonon modes and, in some cases, are more powerful tools to investigate the electron-phonon interaction in the 2DEG systems. The basic difference between the conventional energy-loss experiments and the phonon emission experiments is that in the latter case, the phonon signal is measured in the certain phonon emission angle and at the fixed excitation energy. Therefore, to have a knowledge of the frequency and angular distributions of the emitted phonon field is very important for the detection of the phonon signal. These distributions are determined both by the energy and momentum conservation laws during a scattering act. At inter-Landau-state transitions, the phonon emission energy is fixed by the cyclotron energy, therefore the angular dependence of the emitted phonons remains as the sole important characteristic of emission in this case.

Till recently theoretical investigations of the phonon emission in the 2DEG under the quantizing magnetic field have been limited only to the considerations of the bulk Landau states which have been the main subject of the previous chapter. However, equally with the bulk Landau states, the quantum edge states also give contribution to the emission and absorption of ballistic phonons by the 2DEG. In the recent experiment [221], the absorption of nonequilibrium phonon pulses has been already used to investigate a backscattering of electrons between edge states on opposite sides of the sample. Possibly, absorption of ballistic

acoustic phonons by edge states play an important role in the phonon-drag effect in the QHE regime observed in experiments [236, 237]. The frequency spectrum and angular distribution of the total energy-loss rate due to LA phonon emission have been obtained in a QW [238].

Electron-optical phonon interaction in a polar semiconductor controls such phenomena as the cooling of photoexcited hot carriers on the picosecond time scale as well as transport and optical properties at relatively high temperatures. To date, however, this aspect of electron-phonon scattering remains the least investigated when either the 2DEG or QW subjected to the quantizing magnetic field. The polar optical PO phonon assisted edge state relaxation in the 2DEG has not been given. Recent studies have been reported for cylindrical QWs where the axial magnetic field effect on the electron-PO phonon interaction has been discussed [239]. In rectangular QWs, scattering processes involving only one transverse subband have been considered [240] using the delta-function approximation for electron wave functions along the magnetic field [?].

The second goal of present chapter is to calculate the ballistic acoustic (both deformation and piezoelectric interaction) and polar optical phonon emission by quantum edge states.

This chapter is organized as follows. First in Sec. 5.2 we consider the inter edge state relaxation due to electron-phonon and electron impurity interactions. Results of this section have been reported in [51, 52]. Then in Secs. 5.3 and 5.4 we discuss emission of acoustic and optic phonons by quantum edge states [54, 53].

Sect. 5.2.1 is devoted to the impurity scattering. We use the standard model of the heterostructures [6, 241] which takes into account long-range potential fluctuations due to the layer of ionized donors as well as short-range fluctuations due to the uniformly distributed acceptors. Analytical expressions for the scattering length are derived for an arbitrary confining potential. In Sect. 5.2.2 phonon scattering is discussed. We consider deformation acoustic (DA) and piezoelectric (PA) interactions and again derive analytical expressions for an arbitrary confining potential. As follows from energy and momentum conservation, only phonons with frequencies above some threshold can participate in the transitions between edge states. As a result, phonon scattering is exponentially suppressed

at low temperatures. According to our numerical evaluations, the observed temperature dependence of the scattering length cannot be attributed to phonon scattering.

The impurity-assisted phonon scattering suggested by Y B Levinson and D L Maslov [52] is discussed in Sect. 5.2.3. The difficulty with the exponential suppression of the scattering does not exist in this mechanism, since the impurity takes up the momentum and thermal phonons are able to participate in the process. Thus, one can expect a significant enhancement of the scattering. Actually, it is found that impurity-assisted phonon scattering can dominate over ordinary phonon scattering only at very low temperatures (in the hundred mK range). The temperature dependence associated with this kind of scattering is non-exponential: the scattering rate goes like T^2 below some crossover point and after that like T . A similar temperature dependence has been observed recently in the hundred mK range [225]. In Sect. 5.2.4 it is found that the experimental temperature dependence of the scattering can be explained solely by the thermal averaging of the long-range impurity scattering rate while short-range and phonon scattering play a minor role.

In the Sec. 5.3.1 an analytic expression for the ballistic acoustic energy flux emitted by quantum edge states is derived. Detailed analysis of the phonon emission intensity distribution is made in the low and high regimes of electron temperature T_e as well as different positions of the Fermi level ε_F are considered in Sec. 5.3.2. It is shown that at low temperatures the phonon emission is predominantly concentrated within a narrow cone around the direction of the edge state propagation while at high temperatures – around the magnetic field normal to the electron plane. The emission intensity decreases when the Fermi level falls down. This diminution is exponential at low temperatures. In Sec. 5.3.3 phonon emission due to the piezoelectric interaction is discussed. In contrast to the case of bulk Landau states where piezoelectric interaction is always suppressed in comparison with deformation interaction, in the edge state case, the relative contributions of the piezoelectric and deformation interactions depend on the magnetic field. The angular distribution of emitted phonons is presented in Sec. 5.3.4.

In Sec. 5.4 the LO-phonon assisted edge state relaxation is investigated in

QWs with rectangular cross sections exposed to the normal magnetic field. The energy and momentum relaxation rates for a test electron and electron temperature are calculated. Detailed results are given for the intrasubband and intersubband scattering rates as a function of the initial electron energy and of the magnetic field. By considering different limiting cases of the ratio of the cyclotron frequency to the strength of the lateral confinement, it is obtained results for the edge state relaxation both in the 2DEG and QW as well as for the magnetic field free case.

5.2 Inter-edge-state relaxation

5.2.1 Impurity scattering

Consider a 2DEG in a uniform perpendicular magnetic field B . Let the z -axis be parallel to the magnetic field and the x -axis be parallel to the sample boundary. Positive values of y -coordinate correspond to the interior of the sample. In the following we assume that the edge-states are spin-degenerate.

The wave function and the spectrum of the edge state is

$$\Psi_{nlk}(\mathbf{r}) = \exp(ikx)\chi_{lk}(y)\psi_n(z) \varepsilon_{nl}(k) = \varepsilon_l(k) + \varepsilon_n. \quad (5.1)$$

Here $\varepsilon_l(k)$ and χ_{lk} are the energy and wave function of the quantum edge state in the plane of electrons specified by the Landau index l and momentum k (Fig. 5.1). The energy and wave function of the spatial quantization of the 2DEG are ε_n and ψ_n .

In the Born approximation one can calculate the elastic scattering length for transition $l \rightarrow l'$ according to this formula

$$\frac{1}{\mathcal{L}_{l \rightarrow l'}} = \frac{1}{\hbar^2 v_l v_{l'}} \int \frac{dp_y}{2\pi} |Q_{ll'}|^2 < UU >_p, \quad (5.2)$$

where $< UU >_p$ is the 2D Fourier component of the scattering potential correlation function taken at the 2DEG plane, $\mathbf{p} = (p_x, p_y)$, v_l is the group velocity of the edge state l and the form factor

$$Q_{ll'}(p_y, k, k') = \int dy \chi_{l'k'}(y) e^{-ip_y y} \chi_{lk}(y) \quad (5.3)$$

In (5.2) one should put $p_x = \delta k_{ll'} = |k_l(\varepsilon) - k_{l'}(\varepsilon)|$ with ε being the energy of the initial state. Here the velocities v and functions χ for states l and l' correspond to the energy ε . Note that $\mathcal{L}_{l \rightarrow l'} = \mathcal{L}_{l' \rightarrow l}$.

We assume that the ionized donors are situated in a narrow layer separated from the 2DEG plane by the undoped spacer of the thickness z_0 . Due to the electroneutrality the density of donors (per cm^{-2}) equals $N_s + N_d$, where N_s is the density of the 2DEG and N_d is the density of the depletion charge layer on the GaAs side, the latter is assumed to be uniformly doped by the acceptors with the net density (per cm^3) N_{AC} . Then the correlation function $\langle UU \rangle_q$ can be written in the form [6, 241]

$$\langle UU \rangle_p = \left(\frac{2\pi e^2}{\epsilon \epsilon_s(p)p} \right)^2 [(N_s + N_d) \exp(-2pz_0) + \frac{1}{2p} N_{AC}], \quad (5.4)$$

where ϵ is the lattice dielectric constant taken to be the same for GaAs and GaAlAs, $\epsilon_s(p) = 1 + q_s/p$ is the dielectric function of the 2DEG, q_s is the screening parameter. To determine q_s in a quantizing magnetic field constitutes a special problem, and we will discuss it later (Sect. 5.2.4). The first term in (5.4) corresponds to the long-range part of the scattering, while the second does to the short-range part.

For the long-range scattering one can proceed further assuming that $\delta k_{ll'} z_0 \gg 1$. In this case only small values of $p_y \simeq (\delta k_{ll'}/z_0)^{1/2}$ contribute to the integral (5.2). Using this simplification one can calculate the scattering length due to the long-range potential

$$\frac{1}{\mathcal{L}_{l \rightarrow l'}^L} = \frac{1}{\mathcal{L}_L} \exp(-2\delta k_{ll'} z_0) A_{ll'}^2, \quad (5.5)$$

where $A_{ll'} = Q_{ll'}(0)$ and the nominal scattering length is defined as

$$\frac{1}{\mathcal{L}_L} = 2\pi^{3/2} \left[\frac{2\pi e^2}{\hbar \epsilon (v_l v_{l'})^{1/2}} \right]^2 (N_s + N_d) \frac{1}{(\delta k_{ll'} + q_s)^2} \left(\frac{\delta k_{ll'}}{z_0} \right)^{1/2}. \quad (5.6)$$

Note that due to the small factor $\exp(-2\delta k_{ll'} z_0)$ in (5.5), scattering can be strongly suppressed compared to the case of zero magnetic field. It can happen even in the case when the spatial separation between edge channels $\delta y_{ll'} = a_B^2 \delta k_{ll'}$, where a_B is the magnetic length, is not large compared to a_B . For the short-range scattering Eq. (5.2) cannot be reduced to a more simple form without any assumption on the confining potential.

Now we consider the case of the smooth potential $V(y)$, with $V'(y)a_B \ll \hbar\omega_B$. In this case

$$\begin{aligned}\chi_{lk}(y) &= \Phi_l(y - ka_B^2), \\ \varepsilon_{lk} &= \varepsilon_l + V(ka_B^2),\end{aligned}\tag{5.7}$$

where Φ_l is the harmonic oscillator wave function. In the smooth potential the overlap integral (5.3) can be calculated explicitly. Using (5.7) we have

$$A_{ll'}^2 = (2^{l+l'} l! l'!)^{-1} \sigma^{2l+2l'} \exp(-\sigma^2/2),\tag{5.8}$$

where $\sigma = (\delta y_{ll'}/a_B)^2 \gg 1$. The short-range scattering length $\mathcal{L}_{l \rightarrow l'}^S$ becomes

$$\frac{1}{\mathcal{L}_{l \rightarrow l'}^S} = (2\pi)^{-1/2} \left[\frac{2\pi e^2}{\hbar \varepsilon (v_l v_{l'})^{1/2}} \right]^2 \frac{N_{AC}}{a_B \delta k_{ll'} (\delta k_{ll'} + q_s)^2} A_{ll'}^2.\tag{5.9}$$

The group velocity in the smooth potential is

$$v_{lk} = a_B^2 V'(ka_B^2).\tag{5.10}$$

It follows from (5.8) that in the smooth potential the dominant transitions are $l \rightarrow l + 1$.

The inverse scattering lengths (5.5), (5.9) are to be averaged near the Fermi energy

$$\left\langle \frac{1}{\mathcal{L}_{l \rightarrow n'}} \right\rangle = \int d\varepsilon \left(-\frac{\partial f_0}{\partial \varepsilon} \right) \frac{1}{\mathcal{L}_{l \rightarrow n'}(\varepsilon)}.\tag{5.11}$$

where f_0 is the equilibrium Fermi distribution. Averaging (5.11) plays a minor role for the impurity scattering of free electrons when $T \ll \varepsilon_F$ and reduces usually to the substitution $\varepsilon = \varepsilon_F$ in scattering lengths. However, for inter-edge-state relaxation, the averaging (5.11) results in a pronounced temperature dependence appearing in a comparatively low temperature range. This can be seen from the following arguments. When integrating in (5.11), each value of ε corresponds to some value of $\delta k_{ll'}(\varepsilon)$ entering scattering lengths (5.5), (5.9). The gap between any two branches of the spectrum corresponding to different Landau levels, say ε_{lk} and $\varepsilon_{l'k}$ decreases as $k \rightarrow \infty$. This means that $\delta k_{ll'}(\varepsilon)$ decreases with ε (cf. Fig. 5.1). Therefore, the main contribution to (5.11) stems from $\varepsilon \simeq \varepsilon_F + T$ or $\delta k_{ll'}(\varepsilon) = \delta k_{ll'}(\varepsilon_F) + \delta \hbar v_{ll'}^{-1} T$ where $\delta v_{ll'}^{-1} = |v_l^{-1} - v_{l'}^{-1}|$. Due to the

exponential factors in (5.5) and (5.9), corrections to $\delta k_{ll'}$ can become significant even if $\delta \hbar v_{ll'}^{-1} T \ll \delta k_{ll'}(\varepsilon_F)$.

If the confining potential is smooth, the temperature dependence is determined mainly by the $\delta y_{ll'}$ dependence of the overlap integral (5.8). The onset temperature is

$$T_1 \simeq \frac{\hbar \delta v_{ll'}}{a_B^2 \delta k_{ll'}(\varepsilon_F)}. \quad (5.12)$$

For smooth potentials $T_1 \ll \hbar \omega_B$, while in the typical experimental conditions $\hbar \omega_B \simeq \varepsilon_F$. However, even if $V(y)$ is not smooth, the long-range scattering length (5.5) can strongly depend on T due to the exponential factor containing thickness of the spacer z_0 . The onset temperature for this kind of dependence is

$$T_2 = \frac{\hbar \delta v_{ll'}}{z_0}. \quad (5.13)$$

Again, if the impurity potential is smooth, *i.e.* $z_0 \gg a_B$, then $T_2 \ll \hbar \omega_B$. Results of the numerical calculation of (5.11) will be given in Sect. 5.2.4.

To learn what is the dominant mechanism of impurity scattering,, it is sufficient to put all of the characteristic lengths entering the pre-exponential factors in (5.5) and (5.9) to be the same: $a_B = z_0 = k_F^{-1} = q_s^{-1} \equiv \bar{k}^{-1}$ and $N_d = N_s = \bar{k}^2$. Comparing (5.5) and (5.9) one can see that the long-range scattering dominates, if the thickness of the spacer z_0 is less than

$$z_0^* = \frac{1}{2\delta k_{ll'}} \ln \frac{\bar{k}^3}{N_{AC}}. \quad (5.14)$$

For instance, taking $k_{ll'} = 1.5/a_B$ at $B = 2$ T, $\bar{k}^{-1} = 10$ nm and $N_{AC} = 10^{14}$ cm⁻² we get $z_0^* \approx 60$ nm.

5.2.2 Acoustic phonon scattering

The scattering length due to phonon scattering is

$$\frac{1}{\mathcal{L}_{l \rightarrow l'}} = \frac{2\pi}{\hbar v_l} \sum_{k'} \sum_{\mathbf{q}} [|M_{lk \rightarrow l'k'}^{+\mathbf{q}}|^2 \delta(\varepsilon_{lk} - \varepsilon_{l'k'} - \hbar \omega_q) (N_{\mathbf{q}} + 1) (1 - f_0(\varepsilon_{l'k'})) + \quad (5.15)$$

$$|M_{lk \rightarrow l'k'}^{-\mathbf{q}}|^2 \delta(\varepsilon_{lk} - \varepsilon_{l'k'} + \hbar \omega_q) N_{\mathbf{q}} (1 - f_0(\varepsilon_{l'k'}))],$$

where \mathbf{q} is the phonon wavevector, $\omega_q = sq$, with s being the sound velocity, $N_{\mathbf{q}}$ and $f_0(\varepsilon)$ are the equilibrium Bose and Fermi distributions, respectively.

The emission matrix element $M_{lk \rightarrow l'k'}^{+\mathbf{q}}$ is calculated with the phonon perturbation potential [136]

$$W^+(\mathbf{r}) = B(q)e^{-i\mathbf{q}\mathbf{r}}, \quad (5.16)$$

where for the deformation potential scattering (DA), B^{DA} is given by Eq. (??) while for the piezoacoustic scattering (PA)

$$B^{PA}(q) = e\beta \left(\frac{\hbar}{2\rho\omega_q L^3} \right)^{1/2}. \quad (5.17)$$

Here L^3 is the normalization volume, β is an effective piezoelectric modulus, ρ is the crystal mass density. For absorption processes $W^- = (W^+)^*$.

Since $s \ll v_l, v_{l'}$, the scattering is quasielastic, *i.e.*, the energy of the emitted or absorbed phonons $\hbar\omega_q \ll \hbar\omega_B$. Hence, in the transition $l \rightarrow l'$ (cf. Fig. 5.1) the change of k is $\delta k_{ll'}$. The minimal energy of the phonon is $\Delta_{ll'} = \hbar s \delta k_{ll'}$. In the following we consider low temperatures $T \ll \Delta_{ll'}$. In this case, due to the phonon Bose factor and the Pauli exclusion principle, the phonon energy $\hbar\omega_q$ is close to the threshold $\Delta_{ll'}$. As a result the calculations of the scattering length is greatly simplified. In the Born approximation we get for DA scattering

$$\frac{1}{\mathcal{L}_{l \rightarrow n'}} = \frac{\Xi^2}{2\pi\hbar\rho s^2} A_{ll'}^2 \frac{\delta k_{ll'}^2}{\hbar v_l v_{l'}} T F\left(\frac{\varepsilon - \varepsilon_F}{T}, \frac{\Delta_{ll'}}{T}\right), \quad (5.18)$$

where

$$F(\xi, \eta) = (1/2)[\ln(1 + \exp(\xi - \eta)) + \exp(\xi) \ln(1 + \exp(-\xi\eta))] \quad (5.19)$$

The velocity $v_{l'}$ and function $\chi_{l'}$ of the final state correspond to the energy of this state $\varepsilon = \varepsilon'$. Equation (5.18) is valid if $\exp(\varepsilon - \varepsilon_F - \Delta_{ll'}/T) \ll \exp(\Delta_{ll'}/T)$ or, in other words, if $|\varepsilon - \varepsilon_F| < \Delta_{ll'}$ and if $\varepsilon - \varepsilon_F - \Delta_{ll'} \ll \Delta_{ll'}$. In the first case $\hbar\omega - \Delta_{ll'} \simeq T$, while in the second case $\hbar\omega - \Delta_{ll'} \simeq \varepsilon - \varepsilon_F - \Delta_{ll'}$. It has been also assumed that $T \gg ms^2$ and $\Delta_{ll'} \ll \hbar s/d$, where d is the scale of the electron wave function $\psi(z)$. For GaAs/AlGaAs heterostructure $d = 3$ nm, $s = 5 \times 10^3$ m s⁻¹, $ms^2 = 0.1$ K and $\hbar s/d = 13$ K. Taking $\delta k_{ll'} = a_B^{-1}$, we have for $B = 2$ T: $a_B = 18$ nm, $\Delta_{ll'} = 2$ K and $\hbar\omega_B = 39$ K. The inverse scattering length (5.18) is to be averaged near Fermi energy according to (5.11). Since the function F grows exponentially with $\varepsilon - \varepsilon_F$ for $\varepsilon - \varepsilon_F > 0$, the average value is rather due to hot electrons ($\varepsilon - \varepsilon_F \simeq \Delta_{ll'} \gg T$) than to thermal ones ($\varepsilon - \varepsilon_F \simeq T$). Until

$\Delta_{ll'} \ll \hbar\omega_B$, one can put $\varepsilon = \varepsilon_F$. With the above mentioned assumptions for DA scattering we get

$$\left\langle \frac{1}{\mathcal{L}_{l \rightarrow n'}} \right\rangle_{DA} = \frac{1}{\mathcal{L}_{DA}} A_{ll'}^2 (\delta k_{ll'} a_B)^3 \frac{s^2}{v_l v_{l'}} \exp\left(-\frac{\Delta_{ll'}}{T}\right). \quad (5.20)$$

For piezoelectric PA scattering calculations are similar:

$$\left\langle \frac{1}{\mathcal{L}_{l \rightarrow n'}} \right\rangle_{PA} = \frac{1}{\mathcal{L}_{PA}} A_{ll'}^2 (\delta k_{ll'} a_B) \frac{s^2}{v_l v_{l'}} \exp\left(-\frac{\Delta_{ll'}}{T}\right). \quad (5.21)$$

Here we defined nominal scattering lengths

$$\frac{1}{\mathcal{L}_{DA}} = \frac{\Xi^2}{4\pi\hbar\rho s^3 a_B^3}, \quad (5.22)$$

$$\frac{1}{\mathcal{L}_{PA}} = \frac{(e\beta)^2}{4\pi\hbar\rho s^3 a_B}. \quad (5.23)$$

For GaAs at $B = 2$ T we have $(\bar{\tau}_{DA})_B = 800$ ps and $(\bar{\tau}_{PA})_B = 75$ ps (Ξ^2 and β^2 taken from Ref. [136]). The exponential suppression of the scattering rate is because of the deficit of the superthermal phonons for absorption and deficit of the free final states below ε_F for emission.

To consider the case of the smooth potential one has to substitute Eq. (5.8) for $A_{ll'}$ into (5.20) and (5.21). Comparing (5.20) or (5.21) with Eq. (7) in Ref. [232] one can see that the corresponding equations agree only in the exponential factors from the overlap integral and from the deficit of the final states.

The results presented above are valid provided that the chemical potential difference $|\Delta\mu|$ between edge levels is small compared to temperature. If this condition is not satisfied, then Eqs. (5.20) and (5.21) should be multiplied by the additional factor $\exp(|\mu|/T)$ [233].

5.2.3 Impurity-assisted phonon scattering

According to Eqs. (5.20) and (5.21), phonon scattering is strongly suppressed at $T \ll \Delta_{ll'}$ due to the exponential factors. The origin of the threshold $\Delta_{ll'}$ entering this factors is momentum conservation. If one considers a three-body collision, namely, impurity-assisted phonon scattering, the momentum $\delta k_{ll'}$ is taken up by the impurity, and no exponential suppression of the scattering appears.

The matrix element of the impurity-assisted transition of the electron from state (n, k) to the state (l', k') accompanied by the emission of a phonon with momentum q can be written in the form

$$M_{lk \rightarrow l'k'}^{+q} = \sum_{l''k''} \frac{\langle l'k'q|U|l''k''q \rangle \langle l''k''q|W|nk \rangle}{\varepsilon_{lk} - \varepsilon_{l''k''} - \hbar\omega_q + i\gamma} + \quad (5.24)$$

$$+ \frac{\langle l'k'q|W|l''k'' \rangle \langle l''k''|U|nk \rangle}{\varepsilon_{lk} - \varepsilon_{l''k''} + i\gamma}$$

where $1/2\gamma$ is the decay time of the intermediate state (l'', k'') due to all possible scattering processes. The absorption matrix element $M_{lk \rightarrow l'k'}^{-q}$ is obtained in a similar way. The calculations in (5.24) are greatly simplified by using the arguments given below.

Although the summation in (5.24) is presumed to be over all intermediate values of l'' , the main contribution to (5.24) comes from the transition $l = l''$ corresponding to the smallest value of the denominator. In the first term of (5.24) $k'' = k - q_x$, in the second $k'' = k + q_x$, thus, in general, the impurity first-order matrix elements $\langle \dots |U| \dots \rangle$ entering (5.24) depends on q_x . But, if q_x is small enough, one can neglect it in $\langle \dots |U| \dots \rangle$. The condition for this simplification is different for short- and long-range impurity potentials. For the former case this condition is

$$q_x \ll \delta k_{ll'}, \quad (5.25)$$

while for the latter

$$q_x z_0 \ll 1. \quad (5.26)$$

If

$$\max\{q_x a_B, k q_x a_B^2\} \ll 1 \quad (5.27)$$

and

$$q_y a_B \ll 1 \quad (5.28)$$

one can put the overlap integrals (5.3) stemming from the first-order phonon matrix elements to be equal to unity. When substituting (5.24) into (5.15), it is convenient to express $\langle \dots |U| \dots \rangle$ through the first-order impurity scattering length $\mathcal{L}_{l \rightarrow l'}^i$ calculated in Sect. 5.2.1 (*cf.* Eq. (5.2)). This can be done by using the relation

$$\frac{1}{\mathcal{L}_{l \rightarrow l'}^i} = \frac{L}{\hbar^2 v_l v_{l'}} |\langle l'k'|U|lk \rangle|^2. \quad (5.29)$$

Using (5.16) and (??), we have for DA phonon scattering after some manipulations

$$\frac{1}{\mathcal{L}_{l \rightarrow l'}} = \frac{1}{2(2\pi)^3} \frac{1}{\mathcal{L}_{l \rightarrow l'}^i} \frac{\Xi^2}{\hbar \rho s} \int d^3 q q |a^+ + a^-|^2 [(N_q + 1)(1 - f_0(\varepsilon - \hbar \omega_q)) + (5.30) \\ + N_q(1 - f_0(\varepsilon + \hbar \omega_q))],$$

where $a^+ = (v_l q_x - s q + i\gamma)^{-1}$ and $a^- = (q s - v_{l'} q_x + i\gamma)^{-1}$. Eq. (5.30) includes contributions from two types of transitions: from real and from virtual ones [136]. For real transitions the energy conservation takes place: $\varepsilon_{l''k''} = \varepsilon_{lk}$. These transitions can be imagined as proceeding through the successive scatterings – first, by impurities and, second, by phonons or vice versa – and are not of interest here. The contribution of the real transitions to (5.30) comes from the terms $|a^\pm|^2$ which reduce to the δ -functions reflecting energy conservation at $\gamma \rightarrow +0$. Hence, these terms should be omitted. The true second-order transitions proceed through the virtual states with $\varepsilon_{l''k''} \neq \varepsilon_{lk}$. Virtual transitions are related to the terms $a^+(a^-)^* + c.c.$. The principal value of the integral over $d\Omega_q$ is

$$J = v.p. \int d\Omega_q (a^+(a^-)^* + c.c.) = \frac{4\pi}{v_l v_{l'} q^2} \frac{1}{x - x'} \ln \left(\frac{1 - x}{1 + x} \frac{1 + x'}{1 - x'} \right), \quad (5.31)$$

where $x = s/v_l$, $x' = s/v_{l'}$. As in the Sect. 5.2.2, we assume that $s \ll v_l, v_{l'}$. Then (5.31) reduces to $J = 8\pi/(v_l v_{l'} q^2)$. Finally, substituting (5.31) into (5.30) and integrating over dq , we have

$$\frac{1}{\mathcal{L}_{l \rightarrow l'}} = \frac{1}{\mathcal{L}_{DA}^i} \frac{s^2}{v_l v_{l'}} \Phi \left(\frac{\varepsilon - \varepsilon_F}{T} \right), \quad (5.32)$$

where

$$\frac{1}{\mathcal{L}_{DA}^i} = \frac{1}{\mathcal{L}_{l \rightarrow l'}^i} \frac{\pi^2 \Xi^2}{\hbar^3 \rho s^3} \frac{T^2}{\hbar^2 s^2} \quad (5.33)$$

and

$$\Phi(x) = \int_0^\infty dy y ((N(y) + 1)(1 - f_0(y - x)) + N(y)(1 - f_0(y + x))). \quad (5.34)$$

To make the conditions (5.26)-(5.28) more explicit we assume that the confining potential is not smooth, *i.e.* $\delta k \simeq a_B^{-1}$, $k \simeq a_B^{-1}$ and $v_l \simeq v_{l'}$. One can see that the main contribution to (5.32) comes from $q \simeq q_y \simeq q_z \simeq q_T \equiv T/\hbar s$ and $q_x \approx q_T s/v_l$. Then, instead of (5.26)-(5.28), we have $T \ll \hbar s/a_B$, if the

short-range impurity scattering dominates, and $T \ll \min\{\hbar s/a_B, \hbar v_l/z_0\}$, if the long-range one does.

For PA scattering the calculations proceed in a quite similar way up to the integration over dq . At this point we faced the problem: if $B^{PA}(q)$ is taken in the form (5.17), the integral over dq diverges at $q \rightarrow 0$ as $\int dq/q^2$. Since PA interaction is interaction of an electron with the electrostatic potential induced by the phonon waves, the divergence at $q \rightarrow 0$ means that the screening of this interaction by free electrons has not been taken into account. In our case the screening problem is somewhat specific, since we must take into account the screening of three-dimensional phonons by two-dimensional electrons. The solution of this problem is given in the Appendix ???. The result is quite obvious: $B^{PA}(q)$ entering (5.16) and given by (5.17) should be replaced by $B^{PA}(q)/\epsilon_s(q_{||})$ where $q_{||}$ is the component of the phonon vector parallel to the 2DEG plane. The remaining calculations are straightforward. Explicit results can be obtained in two limiting cases: $q_T \ll q_s$ or $q_T \gg q_s$. In the former case

$$\frac{1}{\mathcal{L}_{l \rightarrow l'}} = \frac{1}{4\pi^2} \frac{1}{\mathcal{L}_{PA}} \left(\frac{T}{\hbar s q_s} \right)^2 \frac{s^2}{v_l v_{l'}} \Phi \left(\frac{\varepsilon - \varepsilon_F}{T} \right). \quad (5.35)$$

In the latter

$$\frac{1}{\mathcal{L}_{l \rightarrow l'}} = \frac{2}{\pi^3} \frac{1}{\mathcal{L}_{PA}^i} \frac{T}{\hbar s q_s}, \quad (5.36)$$

where

$$\frac{1}{\mathcal{L}_{PA}^i} = \frac{1}{\mathcal{L}_{l \rightarrow l'}^i} \frac{(e\beta)^2}{\hbar \rho s^3}. \quad (5.37)$$

Averaging of the inverse scattering lengths (5.32) and (5.35) according to Eq. (5.11) reduces to the averaging of function $\Phi(x)$. Numerical calculation gives $\langle \Phi \rangle \approx 5.2$.

5.2.4 Discussion

As far as we are aware, the temperature dependence of the inter-edge-state relaxation rate has been measured only in three works [229, 225, 227]. Measurements in Ref. [229] were carried out only at two values of temperature. High magnetic fields and low temperatures were used in Ref. [225] and, as a result, spin-splitting of the edge states was observed. Thus, results of Ref. [225] cannot be compared directly to the present theory because we assume that the edge states are

spin-degenerate. Fortunately, the experimental conditions of Ref. [227], lower magnetic fields, higher temperatures, and the Fermi level lying far away from the adjacent Landau levels, allow us to make such a comparison. To obtain some numerical evaluations using the results of Secs. 5.2.1- 5.2.3 one needs to choose the confining potential $V(y)$ in some specific form. *Ab initio* calculation of $V(y)$ constitutes a very complicated problem and is beyond the framework of the present work. We take $V(y)$ in the model form

$$V(y) = V_0 \exp\left(-\frac{y}{a_0}\right) \quad (5.38)$$

where V_0 and a_0 are free parameters to be determined from the fit to the experimental data. To make our heterostructure model consistent with the experimental value of the zero-field mobility we found it necessary to consider the spacer thickness z_0 as free parameter also.

Another subtle question is the choice of the screening parameter q_s entering the expressions for impurity scattering length (5.5) and (5.9) and for impurity-assisted phonon scattering length (5.35) and (5.36). For impurity-assisted phonon scattering we assume that $q_T \ll a_B^{-1}$. If the confining potential is not smooth, the edge states are located at the distance $\bar{y} \simeq a_B$ near the sample boundary. For typical experimental conditions, the width of the sample channel is much larger than \bar{y} . This means that the screening of the electron-phonon interaction potential is provided rather by the wide domain of bulk electrons filling the Landau levels than by the narrow strips of width \bar{y} where the electrons filling the edge states are situated. Thus, to learn what is q_s entering Eqs. (5.35) and (5.36) one can consider the infinite 2DEG in a quantizing magnetic field. The screening problem for these conditions is very complicated and is not well understood. It is known [6, 242] that in a quantizing magnetic field the usual Thomas-Fermi expression connecting q_s with the density of states (DOS) at the Fermi level ν_F holds

$$q_s = \frac{2\pi e^2}{\epsilon} \nu_F, \quad (5.39)$$

but ν_F differs from the DOS for zero-field case ν_F^0 . At $T = 0$ and in the absence of any scattering, ν_F is a sum of δ -functions centered at Landau levels. If a short-range scattering is taken into account, then each δ -function is smoothed

and becomes Gaussian-shaped [6, 242]. In this case ν_F is extremely small compared with ν_F^0 unless the Fermi level is very close to one of the adjacent Landau levels. As a result, for short-range scattering, screening is very weak. However, as was shown in a number of experimental works [243, 244, 245, 246], the observed behavior ν_F has no relation to the theory that assumes short-range scattering. For GaAs/GaAlAs heterostructures the value of ν_F in the center of the gap between two Landau levels where DOS has its minimum was found to be $(0.1 - 0.2) \times \nu_F^0$ [243, 244, 245]. Such high values of DOS unequivocally point at the long-range character of the scattering, as was confirmed also by independent experiments on the determination of the quantum decay lifetime and its comparison with the transport time entering the mobility [208, 235]. Unfortunately, no quantitative theory for DOS under the long-range scattering conditions exists at present. This is why to estimate roughly q_s entering (5.35) and (5.36) we use the above-mentioned experimental values of ν_F in (5.39).

For impurity scattering the momentum transfer is $\delta k_{ll'}$. If the potential is not smooth, $\delta k_{ll'}^{-1} \simeq a_B \simeq \bar{y}$. Thus, the screening of electron-impurity interaction is provided by the same electrons that fill the edge states. The proper accounting of the screening in this situation constitutes a very complicated problem. We do not know the solution of this problem. Nevertheless, one can assume that the screening properties of edge states do not differ drastically from those of the 2DEG without the magnetic field. This assumption is based on the fact that the specific features of the screening by Landau electrons are caused by the gaps in the DOS, while the DOS of edge states is gapless. Thus, to estimate roughly q_s entering Eqs. (5.5) and (5.9) we use ν_F^0 instead of ν_F in (5.39).

According to the results of numerical calculations, the main contribution to the total inverse scattering lengths due to phonons (Eqs. (5.20) and (5.21)) and impurities (Eqs. (5.5) and (5.9) averaged according to Eq. (5.11)) is given by the long-range impurity scattering. The scattering rates due to the short-range impurities and both the DA and PA phonons underestimate the experimental data, taken from Ref. [227] and corresponding to the transition $0 \rightarrow 1$ at $B = 3.7$ T, by at least a factor of 50. According to calculations by Komiyama *et al.* [227], phonon scattering dominates while impurity scattering plays a minor role. Thus, using a more realistic model than the delta-function impurity model

used in Ref. [227] leads to different conclusions. One can note also that the DA phonon scattering length estimated in Ref. [232] is much shorter than ours. The reason of the difference is mainly attributed to the another choice of the electron-phonon interaction constant. The constant used in Ref. [232] is not related to the deformation potential constant Ξ .

The contribution of the impurity-assisted phonon scattering essentially depends on temperature. The impurity-assisted phonon scattering lengths (5.32), (5.35) and (5.36) do not contain the small exponential factors that the first-order scattering lengths (5.20) and (5.21) do, since only thermal phonons are involved in the process. However, there are two other reasons that do not allow the impurity-assisted phonon scattering rate to be very high. Firstly, it is a second-order process: the scattering rate is proportional to the product of the electron-impurity and of the electron-phonon interaction constants. Secondly, the phase volume of the thermal phonons is lower than the phase volume of the superthermal phonons involved in the first-order scattering. As a result, gaining in the exponent we yield the smaller pre-factors than before. The impurity-assisted phonon scattering rate exceeds the first-order one if the temperature is low enough, so that the exponential factors in (5.20), (5.21) become very small. Using the list of parameters corresponding to the experiment [227] and taking $\nu_F = 0.1\nu_F^0$ to estimate the screening parameter entering Eqs. (5.35) and (5.36), one can see that the impurity-assisted scattering is stronger than the first-order phonon scattering if $T \lesssim T_{DA} \approx 0.4$ K for DA interaction and at $T \lesssim T_{PA} \approx 0.5$ K for PA interaction, while the measurements in Ref. [227] were carried out at significantly higher temperatures ($T = 1.5 - 12$ K). Since, according to the calculations, even the DA and PA scattering is much weaker than the impurity scattering at these temperatures we did not consider the impurity-assisted phonon scattering when comparing to the results of Ref. [227]. However, at lower temperatures: $T < \min(T_1, T_2, T_{DA}, T_{PA})$, where T_1 and T_2 are defined by Eqs. (5.12) and (5.13) respectively, the impurity-assisted phonon scattering can dominate. The temperature dependence similar to that given by Eqs. (5.32)-(5.36) has been observed recently in Ref. [225], although one must bear in mind that present theory cannot be applied directly to this experiment (*cf.* beginning of the present section).

The strong suppression of the inter-edge-state relaxation scattering compared

to the zero-field case was observed in the majority of the experiments . For example, in Ref. [227] the zero-field transport scattering length is $4.3 \mu\text{m}$ while at $T = 1.5 \text{ K}$ the inter-edge-relaxation length is $500 \mu\text{m}$. Usually this suppression is attributed to the smoothness of the confining potential and, consequently, to the exponential smallness of the overlap integrals. On the other hand, the potential (5.38) with the parameter values given above cannot be considered as being smooth, but we also have strong suppression of the scattering. According to our calculations, the suppression is caused mainly by the exponential smallness of the correlation function (5.4) and not by the smallness of the overlap integrals. As has been shown in Refs. [247], $V(y)$ decreases as $1/y$ at $y \gg a_d$, where a_d is the width of the depletion region.

In order to avoid the contradiction with Refs. [247] we have to assume that Eq. (5.38) is referred to the intermediate region where the confining potential changes drastically whereas long-decaying tail of $V(y)$ is described by asymptotic law obtained in Refs. [247]. However, as follows from the comparison with the experiment, edge channels are situated in the intermediate region where presence of the long-decaying tail is of minor importance. Notice that recent study of the inter edge relaxation due to the multiple impurity scattering by Martin and Feng [248] similarly shows that the impurity assisted scattering gives rise to the linear temperature dependence.

5.3 Phonon Emission by Quantum Edge States

5.3.1 Acoustic energy flux: Deformation Potential

When the 2DEG is embedded in an elastic medium and the phonon displacement is caused by the deformation electron-phonon interaction then the spectral density of the acoustic energy flux \mathcal{P}_α in a point \mathbf{r}_0 and at a frequency ω is given by Eq. (4.22). To obtain \mathcal{P}_α explicitly it is necessary to calculate the correlator of the phonon field operators $K_{\alpha\beta}(\mathbf{r}, \mathbf{r}') = \langle u_\alpha^*(\mathbf{r}) u_\beta(\mathbf{r}') \rangle_\omega$ which can be represented in the form (4.28). If do not take into account the phonon reflection from interfaces separating different materials then it follows from Eq. (4.34) that the following

function should be used as a kernel of the correlator (4.28):

$$D_{\alpha}^*(\mathbf{r}_0, \mathbf{r}_1 | \omega) D_{\alpha}(\mathbf{r}_0, \mathbf{r}_2 | \omega) = \frac{\omega^2}{16\pi^2 r_0^2 \rho^2 s^6} \exp[-i\mathbf{q}(\mathbf{r}_2 - \mathbf{r}_1)] \quad (5.40)$$

where ρ is the mass density of the elastic medium, s and $\mathbf{q} = \mathbf{n}\omega/s$ are the velocity and momentum of LA-phonons. It is clear from experimental situation that the acoustic energy flux emitted from the 2DEG located near one side of the sample is detected in an infinitely distant point on the reverse side of the sample. Therefore, in obtaining the kernel (5.40) we have assumed $\mathbf{r}_0 \rightarrow \mathbf{n}\infty$, \mathbf{n} is a unit vector towards the detector. This kernel is averaged in (4.28) by electron wave functions. In this case ε and Ψ represent, respectively, the electron energy and wave function for edge states. We assume that all electrons occupy a single level n of the spatial quantization and the electron transitions take place between edge states with different Landau index l and momentum k . Substituting Eqs. (5.1) and (5.40) into Eq. (4.28) we obtain the acoustic energy flux density in a frequency range $d\omega$ emitted from an unit length (towards \mathbf{x}) of the 2DEG into a solid angle do around the direction of \mathbf{n}

$$\mathcal{P}_{l \rightarrow l'}^{DA}(\mathbf{q}) = \frac{\Xi^2 \omega^4}{8\pi^3 \rho s^5 \delta v_{ll'}} f(\varepsilon_l(k_0))(1 - f(\varepsilon_{l'}(k_0 + q_x))) |Q_{ll'}(q_x, q_y)|^2 |I_{00}(q_z)|^2 \quad (5.41)$$

where the form factors in directions \mathbf{y} and \mathbf{z} are

$$Q_{ll'}(q_x, q_y) = \int dy \chi_{lk_0}(y) e^{-iq_y y} \chi_{l'k_0+q_x}(y) \quad (5.42)$$

and

$$I_{nn}(q_z) = \int dz |\psi_n(z)|^2 e^{-iq_z z} \quad (5.43)$$

Notice that the confining potential in the plane of the 2DEG violate the axial symmetry of the magnetic field so that the form factor (5.42) depends on the momenta q_x and q_y apart. In Eq. (5.41) $\delta v_{ll'} = |v_l(k_0) - v_{l'}(k_0 + q_x)|$, $v_l(k)$ is the group velocity of the edge state l with the momentum k , $k_0 = k_0(\mathbf{q})$ is determined from the energy and momentum (in the \mathbf{x} -direction) conservation laws, *i.e.* from the following equation

$$\varepsilon_l(k) - \varepsilon_{l'}(k + q_x) = \omega = s \sqrt{q_x^2 + q_y^2 + q_z^2}. \quad (5.44)$$

Actually, despite lack of the momentum conservation in \mathbf{y} - and \mathbf{z} -directions, the phonon momentum \mathbf{q} uniquely determines the initial l , $k_0(\mathbf{q})$ and final l' , $k_0(\mathbf{q}) + q_x$

edge states in an act of the phonon emission. Thus, equation (5.41) gives the distribution of the emission intensity in phonon momenta.

5.3.2 Low and High Temperature Regimes

In this section we will discuss the situation in low and high temperature regimes in which the emission is qualitatively different. From Eq. (5.44) one can see that for a given k , q_x cannot be less than some value $\delta k_{ll'}(k)$ determined from Eq. (5.44) at $q_y = q_z = 0$. Hence, only phonons with frequencies $\omega \geq s\delta k_{ll'}(k)$ can be emitted from the edge state l, k . On the other hand, the effectiveness of each emission act depends on the position of the Fermi level and electron temperature. Due to the deficit of the hot electrons with energies above $\varepsilon_l(k_1) = \varepsilon_F + s\delta k_{ll'}(k_1)$ and deficit of the free final states with energies below $\varepsilon_{l'}(k_2 + s\delta k_{ll'}(k_2)) = \varepsilon_F - s\delta k_{ll'}(k_2)$, emission acts from states l, k with k between k_1 and k_2 are comparatively more efficient (see Fig. (5.1)(a)). The energy spectrum of the edge states is arranged so that for a fixed energy level we always have $v_l > v_{l'}$ if $l < l'$. Therefore $\delta k_{ll'}(k)$ achieves its minimum $\delta \bar{k}_{ll'} = \delta k_{ll'}(k_1)$ at upper edge of the interval (k_1, k_2) . Thus from the Fermi factors as well as form factors (5.42) and (5.43) we have following obvious restrictions on the emission processes:

$$|q_x - \delta \bar{k}_{ll'}| \leq T_e/s, \quad |q_y| \leq \min\{a_B^{-1}, T_e/s\}, \quad |q_z| \leq \min\{d^{-1}, T_e/s\}, \quad (5.45)$$

where a_B is the magnetic length, d is the characteristic length of electron motion in \mathbf{z} -direction. (So far as the electron transitions take place between edge states of one spatial quantization, d is the minimum length scale of the problem). Here q_x is not a free parameter but it should firstly satisfy the momentum conservation in the \mathbf{x} -direction.

At low temperatures, $T_e \ll s\delta \bar{k}_{ll'}$, we have $q_x \approx \delta \bar{k}_{ll'}$, $q_z \sim T_e/s$. If the confining potential is not smooth, $\delta \bar{k}_{ll'} \sim a_B \gg T_e/s$, so that $q_y \sim T_e/s$ and $q_x \gg q_y$. In the case of the smooth potential $\delta \bar{k}_{ll'} \gg a_B^{-1}$ so that T_e/s and a_B^{-1} can be of the same order of magnitude. But in any case, the relation $q_x \gg q_y$ remains true. Thus at low temperatures $q_x \gg q_y, q_z$, *i.e.* phonons are mainly emitted in \mathbf{x} -direction. Therefore one can substitute $q_x = \delta \bar{k}_{ll'}$ and $q_y = q_z = 0$ in the prefactor of (5.41) and form factors (5.42), (5.43). Taking into account

that $I_{nn}(0) = 1$, one can find for the acoustic energy flux distribution in the momentum space

$$\mathcal{P}_{l \rightarrow l'}^{DA}(\mathbf{q}) = \frac{\Xi^2 \delta \bar{k}_{ll'}^4}{8\pi^3 \rho s \delta \bar{v}_{ll'}} Q_{ll'}^2(q_x, 0) \exp \left\{ -\frac{s \delta \bar{k}_{ll'}}{T_e} - \frac{s}{T_e} \left[(q_x - \delta \bar{k}_{ll'}) + \frac{q_y^2 + q_z^2}{2 \delta \bar{k}_{ll'}} \right] \right\} \quad (5.46)$$

where $\delta \bar{v}_{ll'} = \delta v_{ll'}$ at $k = k_1$ and $q_x = \delta \bar{k}_{ll'}$. In the case of the non-smooth potential we have only one length scale a_B in the (x, y) -plane and so $Q_{ll'} \sim 1$ if $q_y \sim a_B^{-1}$. In the case of the smooth potential, $Q_{ll'}$ can be calculated explicitly [223] and is given by

$$Q_{ll'}^2(q_x, 0) = (2^{l+l'} l! l'!)^{-1} (q_x a_B)^{2l+2l'} \exp\{-(q_x a_B)^2/2\}. \quad (5.47)$$

Now one can see that at low temperatures electrons at inter-edge-state transitions emit almost monochromatic acoustic phonons with frequencies $\omega \approx s \delta \bar{k}_{ll'}$. The emission predominantly concentrated within a narrow cone around the edge state propagation. The emission intensity exponentially drops out of the cone. For the non-smooth potential, the emission cone is isotropic in the (y, z) -plane and the cone angle is determined by the length scales $\sqrt{\delta \bar{k}_{ll'} T_e / s}$ in \mathbf{x} -direction (in the case of the smooth potential also by the length scale $\max\{a_B^{-1}, \sqrt{\delta \bar{k}_{ll'} T_e / s}\}$ in the \mathbf{y} -direction) and $\sqrt{\delta \bar{k}_{ll'} T_e / s}$ in \mathbf{z} -direction. A momentum spread in \mathbf{x} -direction is $\Delta q_x \equiv q_x - \delta \bar{k}_{ll'} \sim T_e / s$. It should be noticed that only a part of states from the interval between k_1 and k_2 gives an essential contribution to the phonon emission processes. When k varies in this interval (see Fig. 5.1), $\delta k_{ll'}(k)$ is changed by $\delta \bar{k}_{ll'} s \delta \bar{v}_{ll'} / v_l v_{l'}$ which is much less than $\delta \bar{k}_{ll'}$ even if $\delta \bar{v}_{ll'} \sim v_l, v_{l'}$. However, only states l, k for which $s \delta k_{ll'}(k) s \delta \bar{v}_{ll'} / v_l v_{l'} \sim T_e$, are effective in the emission processes. Because of the velocity asymmetry $v_l > v_{l'}$ if $l < l'$, the number of these states decreases when the Fermi level falls down. Simultaneously $\delta \bar{k}_{ll'}$ increases which leads to the suppression of the phonon emission (*cf.* [229]). If the Fermi level is very close to the topmost bulk Landau level (Fig. 5.1(b)), $v_{l'} \sim s$ and $\delta v_{ll'} \sim v_l$ so that $s \delta k_{ll'}(k)$ is changed by $s \delta \bar{k}_{ll'} s \delta \bar{v}_{ll'} / v_l v_{l'} \sim s \delta \bar{k}_{ll'} \gg T_e$ in the interval (k_1, k_2) . Therefore the main contribution to the phonon emission comes from the single edge state l, k_c where k_c is defined from $v_{l'}(k_c) = s$. The emission processes from states lying below k_c are forbidden by conservation laws, while from states above k_c : due to the strong deficit of the hot electrons. Such critical

point k_e exists only for transitions $l \rightarrow l'$ with $l < l'$. In the case of $l > l'$ there is no critical points in the edge state spectrum and it is possible smooth transition to the case of the phonon emission from the bulk Landau levels [45, 50, 49]. Because of $\delta\bar{k}_{ll'}$ for $l > l'$ is always more than for $l < l'$, there is an asymmetry between emission processes $l \rightarrow l'$ and $l' \rightarrow l$. This asymmetry depends on the Fermi level position and is pronounced when the Fermi level is close to the bulk Landau level: $\mathcal{P}_{l \rightarrow l'} \gg \mathcal{P}_{l' \rightarrow l}$ if $l > l'$.

At high temperatures, $T_e \gg s\delta\bar{k}_{ll'}$, the states, which are more efficient in the emission processes, are disposed above and below the Fermi level at the separation of the order of T_e . Therefore it is clear that $q_x \sim \delta\bar{k}_{ll'}$ and $q_y \sim a_B^{-1}$ are determined, respectively, only by the momentum conservation and by the magnetic length according to (5.45). Correlation between q_x and q_y is determined by the shape of the confining potential just as at the low temperatures. In \mathbf{z} -direction we have $q_z \sim \min\{d^{-1}, T_e/s\}$ so that the relation $q_z \gg q_x, q_y$ takes place for any d and T_e as well as for any shape of the confining potential. Thus in contrast to the low temperature regime, at high temperatures the phonon emission is concentrated within a narrow cone around magnetic field normal to the plane of the 2DEG. Using the variation wave function for the lowest subband $n = 0$ we have $|I_{00}|^2 = [1 + (q_z d)^2]^{-3}$. Taking into account that in this regime $f(\varepsilon_l(k_0))(1 - f(\varepsilon_{l'}(k_0 + q_x))) \sim \exp\{-sq_z/T_e\}$ we obtain for the emission intensity

$$\mathcal{P}_{l \rightarrow l'}^{DA} = \frac{\Xi^2 q_z^4}{8\pi^3 \rho s \delta\bar{v}_{ll'}} \frac{Q_{ll'}^2(q_x, 0)}{[1 + (q_z d)^2]^3} \exp\left\{-\frac{sq_z}{T_e}\right\}. \quad (5.48)$$

By comparing Eqs. (5.46) and (5.48) one may see that at low temperatures the phonon emission is exponentially suppressed. At high temperatures electrons emit phonons with frequencies $\omega \sim T_e$ and the emission is much intense than at low temperatures when $\omega \sim s\delta\bar{k}_{ll'} \gg T_e$. In the high temperature regime, phonon emission is not so sensible with respect to the Fermi level position.

5.3.3 Acoustic Phonon Emission: Piezoelectric Potential

Up to now we considered only the deformation electron-phonon interaction. Direct calculation shows that to find the phonon emission intensity due to the piezoelectric coupling it should be done the following replacement [46] in Eq. (5.41):

$$\Xi^2 \frac{\omega^2}{s^2} \rightarrow (e\beta)^2 \quad (5.49)$$

where β is the piezoelectric modulus of the crystal averaged over directions of a phonon propagation and its polarizations [249, 250]. Therefore, taking the values of Ξ and β from [136], for GaAs we find

$$\frac{\mathcal{P}^{DA}}{\mathcal{P}^{PA}} = \frac{\Xi^2(\omega/s)^2}{(e\beta)^2} = \left(5.6 \frac{\omega}{s} [nm^{-1}]\right)^2. \quad (5.50)$$

At low temperatures $\omega \sim s\delta\bar{k}_{ll'}$. Therefore for the non-smooth confining potential

$$\frac{\mathcal{P}^{DA}}{\mathcal{P}^{PA}} \sim \left(\frac{5.6}{a_B[nm]}\right)^2 = \frac{B[T]}{20.9} \quad (5.51)$$

and DA interaction is suppressed with respect to PA interaction for not so high magnetic fields. In the case of the smooth potential

$$\frac{\mathcal{P}^{DA}}{\mathcal{P}^{PA}} \sim \left(\frac{\delta\bar{k}_{ll'}a_B}{4.6}\right)^2 B[T] \quad (5.52)$$

and because of $\delta\bar{k}_{ll'}a_B \gg 1$, even at $B \sim 1T$, the DA and PA interaction give roughly the same contribution to the phonon emission.

At high temperatures we have $\omega \sim T_e$ so that

$$\frac{\mathcal{P}^{DA}}{\mathcal{P}^{PA}} \sim \left(\frac{T_e[K]}{6.9}\right)^2, \quad (5.53)$$

i.e. at actual temperatures $T_e \sim 10$ K, contributions of the DA and PA interaction are approximately of the same order of magnitude.

To compare the contributions of edge and bulk Landau states to the phonon emission from the 2DEG one has to average Eq. (5.41) in k_0 and to make a substitution $\pi\delta(\dots) \rightarrow \tau$ in Eq. 8 of Ref. 20 where τ determines the Landau level broadening. Proceed in this way, in the high temperature regime one may obtain for magnetic fields $\omega_B \sim T_e$ and for $\delta\bar{v}_{ll'} \sim v_l, v_{l'}$, even in heterojunctions

not so high quality with the mobility $\mu = 10 \text{ m}^2 \text{ V}^{-1} \text{ s}^{-1}$, the contribution of the edge states to the cooling of the 2DEG at least is not less than the contribution of the bulk Landau states. In the regime of low temperatures, because of $\omega_B \gg s\delta\bar{k}_{ll'} \gg T_e$, it is clear that the phonon emission is only due to inter-edge-state transitions while the emission is practically absent at electron transitions between bulk Landau states.

5.3.4 Angular distribution of emitted acoustic phonons

In this section we estimate the acoustic energy flux power emitted by the edge states at the peak of emission for the case of the non-smooth confining potential. In the low temperature regime the emission goes mainly via piezoelectric coupling. At the peak of emission, $q_x = \delta\bar{k}_{ll'}$ and $q_y = q_z = 0$. Therefore, the emission intensity at the emission peak can be represented in the form

$$\mathcal{P}_0^{PA} = \frac{1}{(2\pi)^2} \frac{ms}{\bar{\tau}_{PA}} \frac{v_B}{\delta\bar{v}_{ll'}} \left(\frac{\delta\bar{k}_{ll'}}{p_B} \right)^2 \exp \left(-\frac{s\delta\bar{k}_{ll'}}{T_e} \right) \quad (5.54)$$

where the nominal time of the piezoelectric interaction is defined as

$$\frac{1}{\bar{\tau}_{PA}} = \frac{(e\beta)^2 p_B}{2\pi\hbar\rho s^2} \quad (5.55)$$

and $p_B = a_B^{-1} = mv_B$ is the magnetic momentum. For GaAs we have $ms = 3.1 \cdot 10^{-28} \text{ J s m}^{-1}$ and at $B = 2 \text{ T}$, $\tau_{PA} = 36.4 \text{ ps}$. Taking $\delta\bar{v}_{10} = v_B$ and $\delta\bar{k}_{10} = p_B$ we have $s\delta\bar{k}_{10} = 2.2 \text{ K}$ for $B = 2 \text{ T}$ so that at $T_e = 0.5 \text{ K}$ we obtain $\mathcal{P}_0^{PA} = 3.1 \cdot 10^{-21} \text{ W s m}^{-1}$ for the electron transitions between $l = 1$ and $l = 0$ edge states. For the emission cone angle we find $\theta = \tan^{-1} q_x / \sqrt{q_y^2 + q_z^2} = 25^\circ$ (see Fig. 5.2).

At high temperatures $\mathcal{P}_{l \rightarrow l'}^{DA}$ and $\mathcal{P}_{l \rightarrow l'}^{PA}$ can be represented in the forms

$$\mathcal{P}_{l \rightarrow l'}^{DA} = \frac{1}{(2\pi)^2} \frac{ms}{\bar{\tau}_{DA}} \frac{v_B}{\delta\bar{v}_{ll'}} \left(\frac{T_e}{sp_B} \right)^4 \frac{x^4 e^{-x}}{[1 + \eta^2 x^2]^3} \quad (5.56)$$

where the nominal time of the interaction is defined as

$$\frac{1}{\bar{\tau}_{DA}} = \frac{\Xi^2 p_B^3}{2\pi\hbar\rho s^2} \quad (5.57)$$

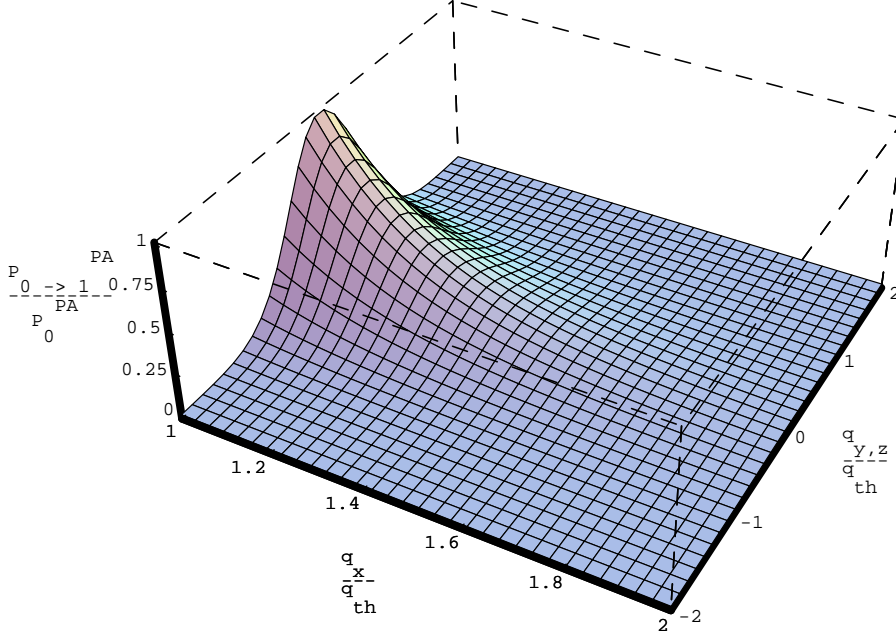


Figure 5.2: Emission intensity distribution (piezoelectric interaction) in phonon momenta at low temperatures $T_e \ll \hbar\omega_{th} \equiv sq_{th} \equiv s\delta k_{10}$ and for the non-smooth confining potential.

and

$$\mathcal{P}_{l \rightarrow l'}^{PA} = \frac{1}{(2\pi)^2} \frac{ms}{\bar{\tau}_{PA}} \frac{v_B}{\delta \bar{v}_{ll'}} \left(\frac{T_e}{sp_B} \right)^2 \frac{x^2 e^{-x}}{[1 + \eta^2 x^2]^3}. \quad (5.58)$$

Here $x = \frac{\hbar sq_z}{T_e}$ and $\eta = \frac{T_e}{\hbar s/d}$. The emission peaks in this temperature regime are defined from conditions that the last factor in Eqs. (5.56) and (5.58) should be maximum. For the GaAs/AlGaAs heterojunction $d = 3$ nm, $s = 5 \cdot 10^3$ m s⁻¹ and so $\hbar s/d = 13$ K. Taking $T = 10$ K we obtain that the emission peaks for DA and PA interaction are determined, respectively, from $x = 1.21$ and $x = 0.85$. This means that at the emission peak, frequencies of phonons emitted due to the deformation coupling are approximately 1.4 times larger than frequencies of phonons emitted due to the piezoelectric coupling. At $B = 2$ T we have $\bar{\tau}_{DA} = 382$ ps so that taking again $\delta \bar{v}_{10} = v_B$ we obtain $\mathcal{P}_0^{DA} = 1.03 \cdot 10^{-18}$ for the electron transitions between edge states $l = 1$ and $l = 0$. W s m⁻¹ and $\mathcal{P}_0^{PA} = 0.53 \cdot 10^{-18}$ W s m⁻¹. For the emission cone angle we find $\theta = \tan^{-1} q_z / \sqrt{q_x^2 + q_y^2} = 10^\circ$ for DA phonons (see Fig. 5.3) and $\theta = 14^\circ$ for PA phonons (see Fig. 5.4).

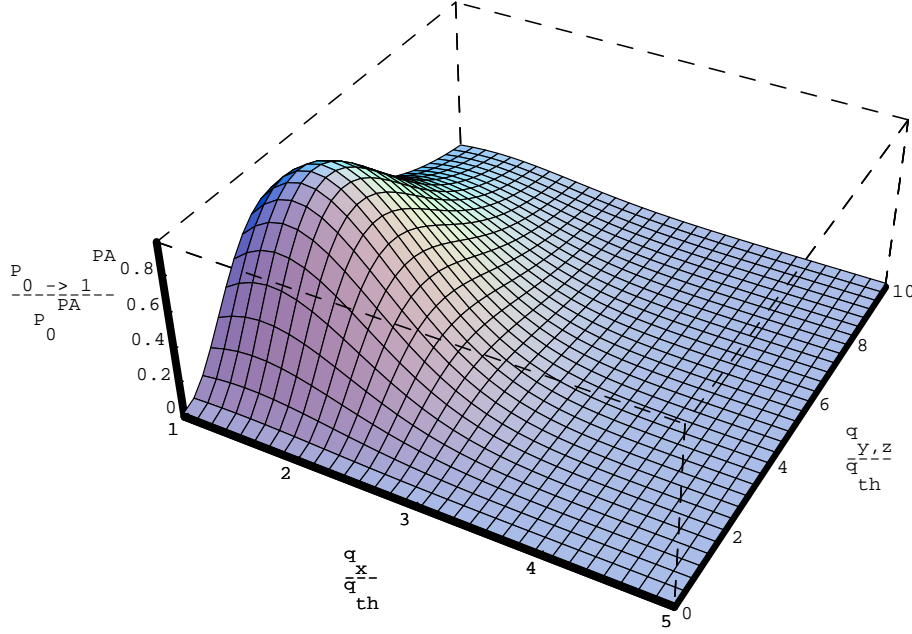


Figure 5.3: Emission intensity distribution (deformation interaction) in phonon momenta at high temperatures $T_e \gg \hbar\omega_{th} \equiv sq_{th} \equiv s\delta k_{10}$ and for the non-smooth confining potential.

It should be observed that in the smooth confining potential, phonon emission is suppressed exponentially. At low temperatures suppression takes place for two reasons. First, because of the threshold nature of emission, electrons are forced to emit phonons with frequencies larger than $\omega_{th} \equiv s\delta\bar{k}_{ll'} \gg sp_B$. Second, because of the exponential smallness of the overlap integral $Q_{ll'}$. While at high temperatures suppression takes place only for the last reason.

5.4 LO-phonon assisted edge state relaxation

5.4.1 Inter edge state transition probability

In this section we consider the edge states in the $z = 0$ plane created by a normal quantizing magnetic field \mathbf{B} applied in z -direction in a rectangular QW formed in x -direction by additional lateral confinement $V(y)$ in y -direction of the 2DEG. The lateral confining potential is assumed to be parabolic, $V(y) =$

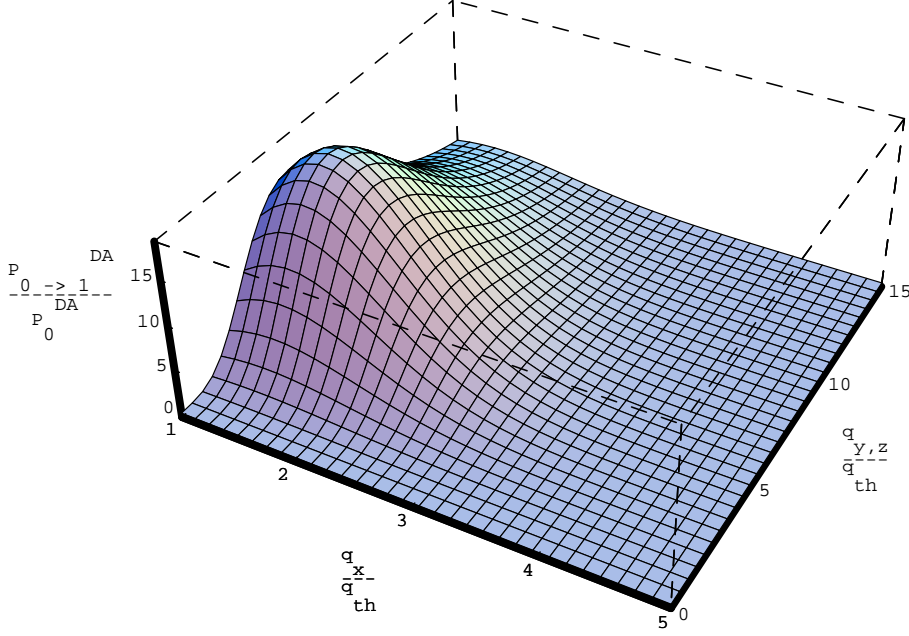


Figure 5.4: Emission intensity distribution (piezoelectric interaction) in phonon momenta at high temperatures $T_e \gg \hbar\omega_{th} \equiv sq_{th} \equiv s\delta k_{10}$ and for the non-smooth confining potential.

$m\omega_0^2 y^2/2$, ω_0 is a characteristic frequency defining the strength of the lateral confinement. Such type of the potential is sufficiently realistic one [251] and allows to carry out more analytical calculation. In such one-dimensional electron system, motion of particles is described by eigenfunctions $|nlk\rangle$ labeled by a subband index n corresponding to the heterojunction quantization in the z -direction, by hybrid index l corresponding to the twofold quantization due to the lateral and magnetic confinement on electrons, and by wave vector k corresponding to the free translation electron motion along the x -direction. Corresponding eigenstates $|nlk\rangle = |n\rangle |lk\rangle$ are factored into a subband function $|n\rangle = \psi(z)$ and a Landau oscillator function $|lk\rangle$. The latter $|lk\rangle = e^{ikx}\chi_{lk}(y)$ are products of plane waves and harmonic oscillator functions centered at $y_k = \lambda ka^2$ ($a = \sqrt{\hbar/m_0\omega}$ is the characteristic length of the hybrid quantization). The dependence of y_k on the quantum number k creates spatial separation of the edge states with different k . Therefore, in order to insure sufficient overlap between the electron wave functions, a transferred momentum in an act of phonon emission

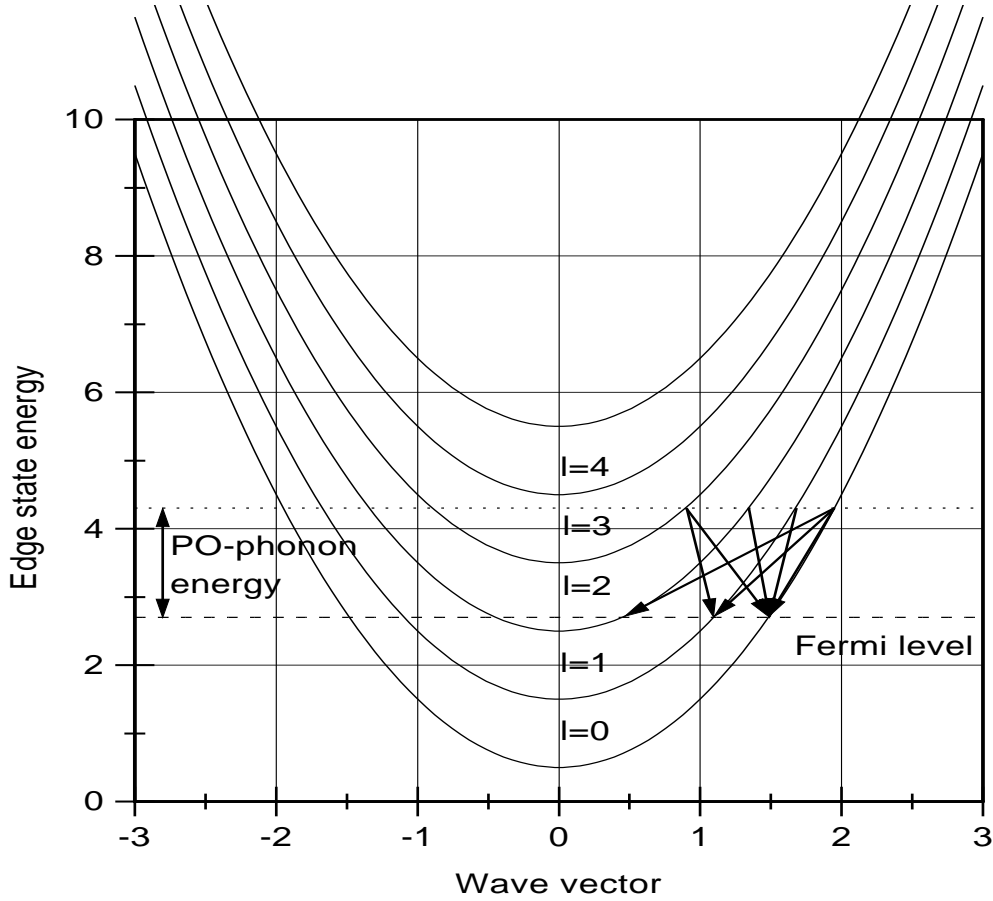


Figure 5.5: Hybrid edge state spectrum in the parabolic lateral confinement. All possible transitions due to polar optical phonon emission are shown.

parabolic lateral confinement is given by

$$\varepsilon_{nl}(k) = \varepsilon(k) + \varepsilon_{nl}, \quad \varepsilon(k) = \frac{\hbar^2 k^2}{2m_B}, \quad \varepsilon_{nl} = \varepsilon_n + \hbar\omega(l + \frac{1}{2}), \quad m_B = \frac{\omega^2}{\omega_0^2} m_k \quad (5.59)$$

where ε_n is the subband energy, the frequency ω and effective renormalized mass m_B determine the hybrid subbands (see Fig. 5.5). The corresponding DOS for the subband nl per unit length is given by

$$g_{nl}(\varepsilon) = \frac{1}{\pi\hbar} \sqrt{\frac{2m_B}{\varepsilon - \varepsilon_{nl}}} \Theta(\varepsilon - \varepsilon_{nl}) \quad (5.60)$$

where $\Theta(x) = 1$ if $x \geq 0$ and zero otherwise is the Heaviside step function. The DOS has a square-root singularity at the bottom of any subband nl . We recall that the DOS exhibits an analogous behavior in the bulk samples exposed to

the quantizing magnetic field. The position of the Fermi level ε_F and the linear electron density ν are related in the following way

$$\nu = \frac{2}{\pi\hbar} \sum_{n,l} \sqrt{2m_B(\varepsilon_F - \varepsilon_{nl})} \Theta(\varepsilon_F - \varepsilon_{nl}). \quad (5.61)$$

Different physical situations corresponding to $\nu = \text{const}$ and $\varepsilon_F = \text{const}$, as well as to the mixture situations when both ν and ε_F vary with field (*e.g.*, the situation when the ratio of ε_F/ω remains constant) can be realized experimentally. Notice that in these different situations the magnetic field dependence of various physical quantities can be differ.

The scattering probability at which one polar optical PO phonon with a wavevector $\mathbf{q} = (q_x, q_y, q_z)$ and frequency ω_{PO} (the PO phonon dispersion is neglected, $\omega_q = \omega_{PO} = 36.62$ meV) is emitted or absorbed by an edge state can be represented as [136]

$$\begin{aligned} W_{nlk \rightarrow l'lk'}^{\pm \mathbf{q}} &= \frac{2\pi^2}{L_x L_y L_z} \frac{\hbar v_{PO}}{\bar{\tau}_{PO}} \frac{1}{q^2} |Q_{ll'}(k', k; q_y)|^2 |I_{nl'}^{PO}(q_z)|^2 \\ &\times (N_T(\omega_{PO}) + 1/2 \pm 1/2) \delta_{k', k \mp q_x} \delta(\varepsilon_{nlk} - \varepsilon_{n'l'k'} \mp \hbar\omega_{PO}) \end{aligned} \quad (5.62)$$

In the above, \pm refer to the emission and absorption of a PO phonon, L_x, L_y , and L_z are wire length, width, and height, respectively, $v_{PO} = \hbar p_{PO}/m_c$, $\hbar p_{PO} = \sqrt{2m_c \hbar \omega_{PO}}$. The nominal time $\bar{\tau}_{PO}^{-1} = 2\alpha_{PO}\omega_{PO} = (0.14 \text{ ps})^{-1}$ characterizes electron-PO phonon interaction ($\alpha_{PO} = 0.07$ is the Frölich coupling constant). $N_T(\omega_{PO})$ is the Bose-Einstein factor at temperature T . If phonon confinement effects are neglected, the form factor $Q_{ll'}$ is given by Eq. 2.12 and, in the parabolic confinement, does not depend on momenta k and k' apart but depends only on the combination $q_\lambda = \sqrt{q_y^2 + \lambda^2 q_x^2}$ ($\lambda \equiv \omega_B/\omega$). To treat the electron relaxation between edge states of the lowest $n = 0$ subband, the variational wave function $\phi_0(z) = (z/\sqrt{2d^3}) \exp(-z/2d)$ [208] is used. Then the form factor in the z -direction, I_{00}^{PO} , is given in the following explicit form

$$|I_{00}^{PO}(q_z)|^2 = (1 + q_z^2 d^2)^{-3} \quad (5.63)$$

where d is the length scale characterizing confinement of the electrons in z -direction. By considering the inter-subband relaxation it is assumed that the electrons in the z -direction are confined in a rectangular potential with infinite

high walls so that the wave functions are $\phi_n(z) = \sqrt{2/d} \sin \pi n z / d$ which give for the form factor $I_{nn'}^{PO}$ following expression

$$|I_{nn'}^{PO}(q_z)|^2 = \frac{n^2 n'^2 \pi^4 \zeta^2}{(\zeta^2 - \alpha^2)^2 (\zeta^2 - \beta^2)^2} \begin{cases} \cos^2 \zeta & \text{if } n + n' = 3, 5, 7, \dots \\ \sin^2 \zeta & \text{if } n' + n = 2, 4, 6, \dots \end{cases},$$

$$\zeta = \frac{q_z d}{2}, \alpha = \frac{\pi}{2}(n + n'), \beta = \frac{\pi}{2}(n' - n) \quad (5.64)$$

Eqs. (5.63) and (5.64) show that the form factor in the z -direction decreases in both cases as a sixth power of ζ for small wavelengths, $q_z \gg d^{-1}$.

5.4.2 Kinematics of PO phonon emission

The kinematics of the PO phonon emission and absorption is determined firstly by the conservation laws. In this system due to quantization of electron motion, the momentum conservation remains only in x -direction so that we have

$$\varepsilon(k) = \varepsilon(k') + \Delta_{nl n' l'}^{\pm}, \quad k = k' \pm q_x,$$

$$\Delta_{nl n' l'}^{\pm} = \varepsilon_{n' l'} - \varepsilon_{nl} \pm \hbar \omega_{PO}. \quad (5.65)$$

These relationships are shown in Fig. 2.1. Electron transitions are possible between edge states with different n, l, k lying on two horizontal lines separated by $\hbar \omega_{PO}$. If $\Delta_{nl n' l'}^{\pm} > 0$ ($\Delta_{nl n' l'}^{\pm} < 0$) electrons gain (lose) the momentum, $q_x^+ > 0$ ($q_x^+ < 0$), at the phonon emission and lose (gain) the momentum, $q_x^+ < 0$ ($q_x^- > 0$), at the phonon absorption processes. All emission (absorption) processes with gain (lose) of the momentum have a threshold nature, *i.e.* only electrons with the energy $\varepsilon(k) \geq \Delta_{nl n' l'}^{\pm}$ ($\varepsilon(k) \leq \Delta_{nl n' l'}^{\pm}$) can emit (absorb) PO phonons. The number of all possible electron transitions increases in Fermi level height. Notice that as it follows from Eqs. 5.65 at fixed electron subband quantum numbers, the electron initial energy uniquely determines the x -component of the emitted or absorbed phonon momentum.

$$q_x^{\pm} = \pm k \left(1 - \sqrt{1 - \Delta_{nl n' l'}^{\pm} / \varepsilon(k)} \right). \quad (5.66)$$

Exact momentum conservation in the y - and z -directions is replaced by the form factors $Q_{ll'}$ and $I_{nn'}$ which require following restrictions for l, l' and n, n' of

the order unity

$$\lambda q_x a \lesssim 1, \quad (5.67)$$

$$q_y a \lesssim 1, \quad (5.68)$$

$$q_z d \lesssim 1. \quad (5.69)$$

Actually, condition (5.67) is the restriction upon the electron initial energy and magnetic fields for which emission and absorption of PO phonons provide a sub-picosecond relaxation between given subbands with quantum numbers nl and $n'l'$. By virtue of the relationship (5.66), the condition (5.67) can be rewritten in the following explicit form

$$2 \frac{\omega_B}{\omega_0} \left(\sqrt{\frac{\varepsilon(k)}{\omega}} - \sqrt{\frac{\varepsilon(k')}{\omega}} \right) \lesssim 1. \quad (5.70)$$

The parameter ω_B/ω_0 determines an extend degree of the inter edge state spatial separation at electron transitions. If $\omega_0/\omega_B \ll 1$ then a slight shift in the electron momentum $k - k' = q_x$ or energy $\varepsilon - \varepsilon' = \Delta_{nl'n'}^\pm$ causes a large inter edge state separation and weak overlap between electron wave functions. Therefore in this case we restrict the present analysis to the magnetic fields for which $\Delta_{nl'n'}^\pm \sim \omega_0 \ll \omega_B$ while electron energy ε can be of the order both $\Delta_{nl'n'}^\pm$ and $\hbar\omega_B$. In the limit of a non-smooth confinement, $\omega_0/\omega_B \gtrsim 1$, even for $\varepsilon - \varepsilon' = \Delta_{nl'n'}^\pm \sim \omega_B$ there exists sufficient overlap between electron wave functions. Therefore, in this case we consider magnetic fields and energies for which $\varepsilon \sim \omega_B \sim \Delta_{nl'n'}^\pm \sim \omega_0$.

Due to the long-range nature of the PO interaction, phonons with minimum momenta $q \equiv \sqrt{q_x^2 + q_y^2 + q_z^2} \sim \min\{q_x, q_y, q_z\}$ are emitted or absorbed at the relaxation processes. Since for the given electron discrete quantum numbers and initial energy, q_x is a fixed quantity then only phonons are essential for which

$$q_y, q_z \lesssim q_x. \quad (5.71)$$

In the limit of high magnetic fields, $d \gg a$, the distribution in phonon momenta is isotropic in the (x,y)-plane of in the inverse space while in z -direction, the restriction (5.69) is more severe than that of (5.71) so that we have $q_z \ll q_y \lesssim q_x$. In the opposite limit of weak magnetic fields, $\omega_B \ll \omega_0$, (*i.e.* $\lambda \ll 1$), the distribution in phonon momenta is isotropic in the (x,z)-plane while in y -direction,

$q_y \sim \lambda q_x$, therefore we have $q_y \ll q_z \lesssim q_x$. In the intermediate range of magnetic fields we have $\lambda \sim 1$ and $d \ll a$ therefore the distribution in phonon momenta is determined only by inequality (5.71).

5.4.3 Energy relaxation of a test electron

The energy relaxation rate for a test electron between two subbands nl and $n'l'$ due to PO phonons can be represented in the form [136]

$$\mathcal{Q}_{nl \rightarrow n'l'}^{PO}(k) = \mathcal{Q}_{nl \rightarrow n'l'}^+(k) - \mathcal{Q}_{nl \rightarrow n'l'}^-(k) \quad (5.72)$$

where

$$\mathcal{Q}_{nl \rightarrow n'l'}^\pm(k) = \frac{\hbar\omega_{PO}}{\bar{\tau}_{PO}} \frac{v_{PO}}{v(k \mp q_x^\pm)} \Phi_{nl}^\pm(k) G_{nl \rightarrow n'l'}^\pm(k) \equiv \frac{\hbar\omega_{PO}}{\tau_{PO}^\pm(\varepsilon)} \quad (5.73)$$

is the energy transferred to the lattice (obtained from the lattice) at the PO phonon emission (absorption) processes, $1/\tau_{PO}^\pm(\varepsilon)$ is the PO phonon emission (absorption) rate. Here $v(k) = 1/\hbar \partial \varepsilon(k)/\partial k$ is the group velocity of the edge state which depends only on the momentum k for the parabolic confinement. The overlap integral $G_{nl \rightarrow n'l'}^\pm(k)$ is given as

$$G_{nl \rightarrow n'l'}^\pm(k) = \frac{1}{4\pi} \int_{-\infty}^{+\infty} \frac{dq_y dq_z}{q_x^2 + q_y^2 + q_z^2} |Q_{l'}(q_\lambda)|^2 |I_{nn'}^{PO}(q_z)|^2 \Big|_{q_x=q_x^\pm}. \quad (5.74)$$

Integration over phonon momenta does not catch on the temperature factor $\Phi_{nl}^\pm(k)$ which is a function of the electron initial quantum numbers,

$$\Phi_{nl}^\pm(k) = (N_T(\omega_{PO}) + 1/2 \pm 1/2) \frac{1 - f_T(\varepsilon_{nl}(k) \mp \hbar\omega_{PO})}{1 - f_T(\varepsilon_{nl}(k))}, \quad (5.75)$$

$f_T(\varepsilon)$ is the Fermi factor. Therefore, any variation of temperature will change only intensity of the phonon emission and absorption while momentum distribution of emitted and absorbed PO phonons by the test electrons does not depend on temperature.

In the case of relaxation between edge states of the lowest subband for actual calculations of the overlap integral $G_{nl \rightarrow n'l'}^\pm(k)$ we use expression (5.63) for the form factor $I_{nn'}$. Then directly taking integration over q_z , Eq. (5.74) can be

reduced to the following one-dimensional integral

$$G_{0l \rightarrow 0l'}^{\pm}(k) = \frac{1}{16} \int_0^{\infty} dy Q_{ll'}^2(t) \frac{8 + 9r + 3r^2}{r(1+r)^3},$$

$$t = \frac{a^2}{2d^2}(y^2 + \lambda^2 x^2), \quad r = \sqrt{x^2 + y^2}, \quad x = q_x d, \quad y = q_y d. \quad (5.76)$$

which we evaluate numerically. The results of numerical calculations in the limit

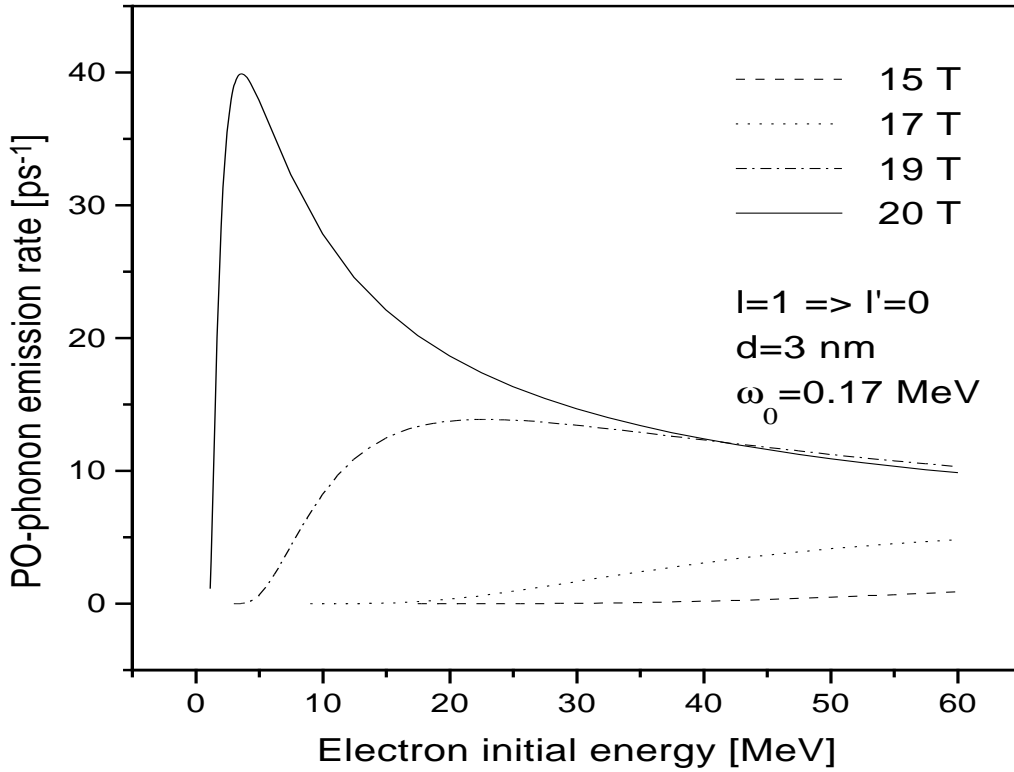


Figure 5.6: The PO phonon emission rate versus the electron initial energy for the $l = 1 \Rightarrow l' = 0$ transition and for different values of the magnetic field.

of the smooth confinement (we take $\omega_0 = 1.754$ meV) for transitions between hybrid subbands $l = 1 \rightarrow l' = 0$ and $l = 2 \rightarrow l' = 0$ are shown in Figs. 5.6 and 5.7, respectively. We use $d = 3$ nm as a typical value for a GaAs/AlGaAs heterostructure. The diagrams represent the PO phonon emission rate dependencies on the electron initial energy at room temperatures for several values of the magnetic field. One can see from Fig. 5.6 that for the transition $l = 1 \rightarrow l' = 0$ at low magnetic fields $B = 15, 17$ T corresponding to the detuning $\Delta_{0100}^+ = 9.89, 6.38$

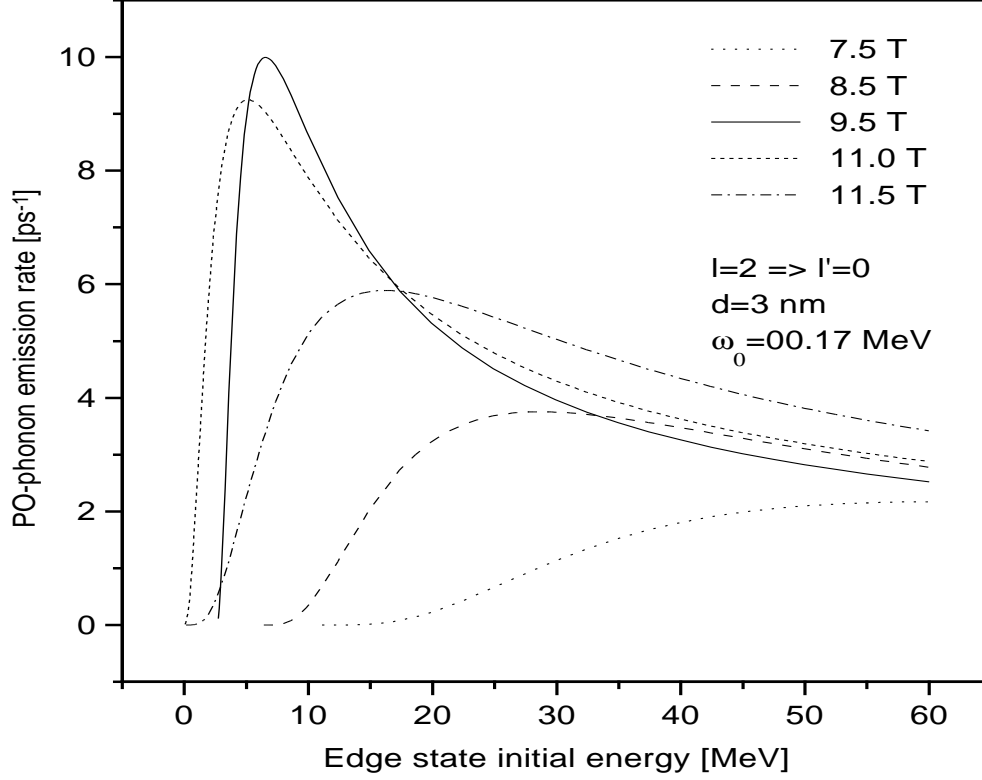


Figure 5.7: The PO phonon emission rate versus the electron initial energy for the $l = 2 \Rightarrow l' = 0$ transition and for different values of the magnetic field.

meV, the emission rate increases slowly but monotonously though it is remaining sufficiently small in the whole range of the electron initial energy variation. It is exceeding the value of 1 ps^{-1} only near the upper edge of the energy variation. Such behavior is conditioned by the sufficiently large value of the transferred momentum q_x (so that the inequality (5.67) is not satisfied) and by its monotonous decrease in the same energy range. The curves of the emission rate for the magnetic fields $B = 19, 20 \text{ T}$ corresponding to the detuning $\Delta_{0100}^+ = 2.87, 1.12 \text{ meV}$ represent peaks at the energies for which the inequality (5.67) starts to take place. The peak values exceeding 40 ps^{-1} and 10 ps^{-1} , respectively. At higher energies, the inequality (5.67) takes place in the strong sense, $\lambda q_x a \ll 1$, therefore the overlap integral (5.74) becomes weakly depending on the energy and the energy dependence of the emission rate is mainly determined by the behavior of the DOS, *i.e.*, it slowly decreases with an energy increase. On the low-energy

side we have $\lambda q_x a \gg 1$ causing an exponential increase of the emission rate with energy increase. The curve with $B = 20.64$ T represents the emission rates corresponding to the very sharp detuning ($\Delta_{0100}^+ < 0.5$ meV). In this case we have $\lambda q_x a \ll 1$ in the whole energy range and features of the emission rate are mainly determined by an energy dependence of the DOS. Particularly, the sharp increase of the emission rate at low energies arises from the divergence of the DOS at the bottom of the electronic subband.

Such kinds of curves with analogous behavior we find also for the electronic transitions between subbands $n = 0, l = 2$ and $n' = 0, l' = 0$ (Fig. 5.7).

Chapter 6

Theory of Auger-upconversion

6.1 Introduction

Auger scattering in semiconductors is well known from investigations of nonradiative recombination [252, 253, 254, 255, 37]. Free electrons and holes are a prerequisite for this process: the energy obtained in the recombination of an electron-hole pair is taken to excite another electron. The latter electron may lose its excess energy by electron-lattice relaxation; thus the recombination energy is converted into heat. More recently two-particle correlation effects in the Auger process [256] have been demonstrated experimentally for p -GaAs and n -Si [257, 258]. In quantum well structures, Auger processes become possible between different subbands and have been investigated both in theory and experiment (see [259] and references therein). The reduction of Auger scattering rate in quantum dots due to the discreteness of the electronic states has been used as an argument to propose quantum dots lasers [260]. Except for an early study of transport in crossed electric and magnetic fields [261], the theory of Auger scattering was restricted so far to the magnetic field free case.

In recent magneto-luminescence experiments by Potemski *et al.* [55, 56] on one-side modulation doped GaAs/AlGaAs quantum wells an up-conversion has been observed and interpreted as being due to an Auger process. These authors studied in photoluminescence and photoluminescence under excitation an asymmetric GaAs/AlGaAs single quantum well of width $d = 25$ nm with an electron

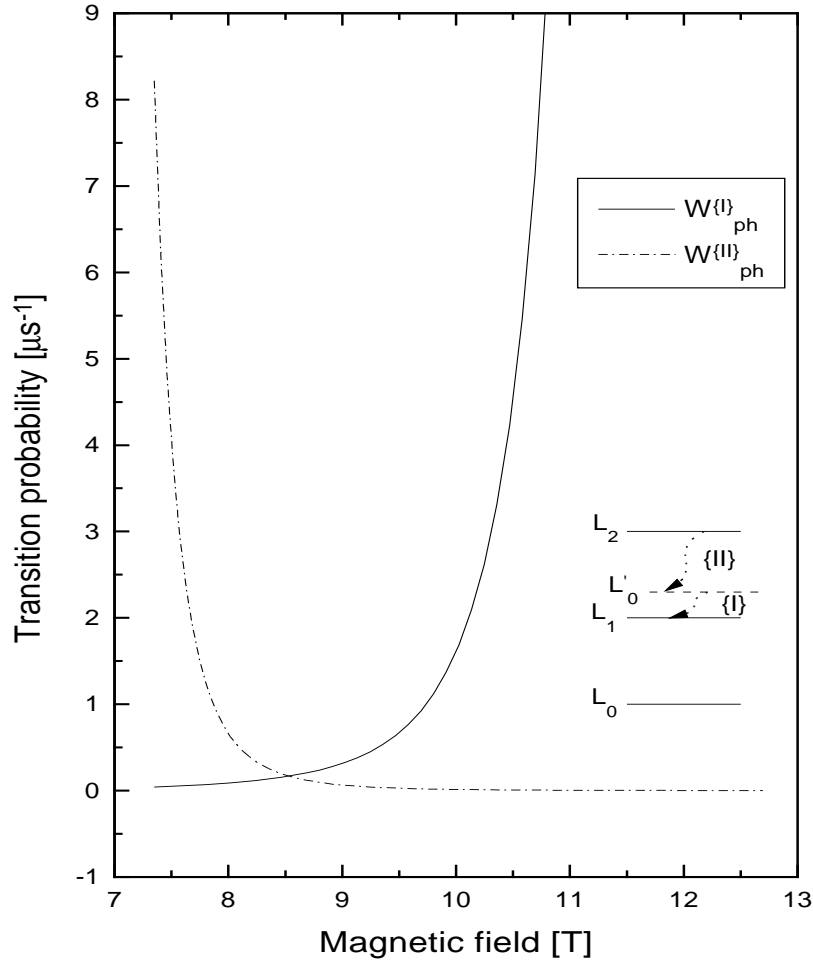


Figure 6.1: Magnetic field dependence of the probabilities for the transitions between Landau levels $L'_0 \rightarrow L_1(\{I\})$ and $L_2 \rightarrow L'_0(\{II\})$ caused by acoustic phonon emission.

density of $N_s = 7.6 \cdot 10^{11} \text{ cm}^{-2}$ with a magnetic field \mathbf{B} applied in growth direction. The characteristic energy level scheme for $7.9 \text{ T} \leq B \leq 12.9 \text{ T}$ is depicted as inset in Fig. 6.1: the lowest Landau level of the second electric subband L'_0 lies between the second L_1 and third L_2 Landau levels of the lowest electric subband (the index refers to the Landau quantum number), while due to the doping concentration the Fermi energy is pinned to the level L_1 . Changing the magnetic field in this interval allows to tune L'_0 between L_1 and L_2 . The luminescence spectrum under interband excitation into L_1 at low temperatures ($T = 1.8 \text{ K}$) and for low excitation power ($P_{exc} \leq 10 \text{ W cm}^{-2}$) shows two peaks (see Fig. 6.2 taken from

Ref. [55]): besides the luminescence due to recombination of an electron from L_0 with a hole in a valence band, a second peak is observed above the exciting laser energy and is related to L'_0 , *i.e.* recombination of an up-converted electron with a hole. In order to explain this second peak, the following processes have been supposed: after an interband excitation of electrons into the partially filled level L_1 (i), a recombination takes place between electrons from L_0 and photo-induced holes (ii), then in an Auger process two electrons in L_1 are scattered to L_2 and L_0 (iii), and a relaxation process brings the electron from L_2 to L'_0 (iv), from where it recombines with a photo-induced hole (v) to give the up-converted luminescence or, emitting a phonon, relaxes into the level L_1 (vi). Potemski *et al.* [55, 56] present the dependence of the luminescence intensity related to L_0 and L'_0 on the magnetic field and the excitation power (see Fig. 6.3 taken from Ref. [55]). The most surprising result is the high intensity of the L'_0 luminescence which can be of the same order as the L'_0 luminescence.

Experimentally, electron-electron interaction has been studied in various phenomena. Besides already mentioned luminescence experiment [55, 56], inter- and intra-Landau level Auger transitions have been observed also in the cyclotron resonance in the 2DEG [262]. As a dephasing mechanism electron-electron interaction is observed in interference of two electron beams in the 2DEG [263]. It can be responsible for the signal decay in four wave mixing experiment [264] and consider as a possible mechanism [265, 266] of the mutual drag between two electron gases, 2D-3D, and 2D-2D [267, 268].

Electron-electron scattering is one of the main mechanisms controlling relaxation, transport and optical properties of electrons. The electron scattering has been firstly calculated by Landau and Pomeranchuk [269] in massive samples. In recent years, intensive effort of many authors has been exhausted to develop theory of electron-electron scattering in low-dimensional nanostructures [6, 7, 9]. In the 2DEG, electron scattering has been calculated by Chaplik [270] at low and by Gulianni and Quinn [271] at high temperatures for free Fermi-liquid electrons. When electrons are strongly scattered by random short range potential of impurities, the Fermi-liquid picture can be no longer valid. In this situation electron-electron scattering has been discussed by Schmid [272] and by Altshuler and Aronov [273] for the magnetic field free case.

As already mentioned, theoretical studies of Auger scattering between Landau levels in a 2DEG are missing in the literature. In this section phenomenological calculations of the electron-electron scattering rate for free electrons of the 2DEG exposed to the normal quantizing field are presented [57, 46].

Quite recently these calculations have been generalized by Levinson [274] for a smooth random potential depending on only one coordinate which allow to calculate Landau level broadening corresponding to heterostructures and narrow quantum wells with a large spacer [275, 276].

In the last few years electron-acoustic phonon interaction in a 2DEG in a quantizing magnetic field has attracted attention because of its role in the breakdown of the dissipationless quantum Hall effect [169, 168] and the cooling of a 2DEG at low temperatures $T \leq 40K$ [173, 171, 172]. The emission and absorption of the ballistic phonon pulses by a 2DEG in MOS-structures and GaAs-heterostructures have been studied in theoretical works [176, 45, 49, 50] as well as in many experiments (see the review paper [277]). In all calculations, however, only acoustic phonon-assisted transitions within Landau levels of the lowest subband are considered.

Therefore in this chapter, we calculate the characteristic times of processes (iii) and (iv), (vi), *i.e.* Auger scattering between Landau levels of the lowest electric subband and electron-acoustic phonon scattering between Landau levels of the two lowest electric subbands ($L_2 \rightarrow L'_0$ and $L'_0 \rightarrow L_1$), as well as the lifetime of a test hole in level L_0 with respect to both the Auger process and the phonon emission. By analyzing rate equations for the processes (i)-(vi) we find an estimate for the time of the Auger process as well as magnetic field and excitation power dependencies of the two luminescence peaks which are consistent with the experimental findings.

6.2 Auger scattering between Landau levels

Due to the combined effect of quantum well confinement and Landau quantization, the energy spectrum of electrons in a quantum well with magnetic field in growth direction (parallel z) is discrete. The single particle energy ε_{nl} is characterized by a subband index n and a Landau level index l (the spin degeneracy is not

removed and is taken into account in the occupation factors). The corresponding wave functions $\Psi(\mathbf{r})$ ($\mathbf{r}=(\mathbf{R}, z)$) are factored into an oscillator function $\chi_{lk}(\mathbf{R})$ for the Landau oscillator and a subband function $\psi_n(z)$. The single particle energy does not depend on the quantum number k which results from the asymmetric gauge of the vector potential and counts the degeneracy of the Landau levels.

The scattering time for a single electron due to the Auger process, in which two electrons are scattered from single particle states 1, 2 into states 1', 2', is given by

$$\frac{1}{\tau_{Auger}^e} = \sum_{k_2, k'_1, k'_2} W_{1,2 \rightarrow 1',2'} f_2 (1 - f_{1'}) (1 - f_{2'}) \quad (6.1)$$

where the occupation probabilities f take into account the Pauli exclusion principle. In detail the transition probability is given by

$$W_{1,2 \rightarrow 1',2'} = \frac{2\pi}{\hbar} |M_{1,2 \rightarrow 1',2'}|^2 \delta(\varepsilon_{n_1 l_1} + \varepsilon_{n_2 l_2} - \varepsilon_{n'_1 l'_1} - \varepsilon_{n'_2 l'_2}). \quad (6.2)$$

In Eq. (6.2) we have taken the sum over the momenta k to account for all equivalent scattering processes, which are possible due to the degeneracy for a given set of Landau levels. After the summation the result does not depend on k_1 (and thus on the choice of the gauge, as it should be). Thus τ_{Auger}^e is the relaxation time of a test electron from the level L_1 to L_0 with respect to the Auger process. For later considerations we introduce also the lifetime of a test hole in the level L_0 with respect to the Auger process from the level L_1 as

$$\frac{1}{\tau_{Auger}^h} = \sum_{k_1, k_2, k'_2} W_{1,2 \rightarrow 1',2'} f_1 f_2 (1 - f_{2'}) \quad (6.3)$$

where $1 - f'_2$ is the occupation probability of a hole in L_2 .

The matrix element $M_{1,2 \rightarrow 1',2'}$ to be calculated with functions of Eq. (??) is that of the Coulomb interaction potential after 2D Fourier transformation

$$V_{ee}(\mathbf{r}_1, \mathbf{r}_2) = \frac{1}{A} \sum_{\mathbf{q}} \frac{2\pi e^2}{\kappa_0 q} \exp \{ i\mathbf{q}(\mathbf{R}_1 - \mathbf{R}_2) - q |z_1 - z_2| \} \quad (6.4)$$

where A is the normalization area in the (x, y) -plane, κ_0 is the low-frequency dielectric constant. Here the screening due to free carriers in the electron subband is not considered.

In our special case we are interested in transitions only within the first electric subband ($n = 1$). Therefore, using the form factor

$$F(q) = \int dz_1 dz_2 \psi_1^2(z_1) \psi_1^2(z_2) \exp \{-q | z_1 - z_2 | \} \quad (6.5)$$

the matrix element can be represented in the form

$$\begin{aligned} M_{1,2 \rightarrow 1',2'} &= \frac{1}{A} \sum_{\mathbf{q}} \frac{2\pi e^2}{\kappa_0 q} F(q) Q_{l_1 l'_1}(q) Q_{l_2 l'_2}(q) \delta_{k'_1, k_1 + q_x} \delta_{k'_2, k_2 - q_x} \\ &\times \exp \left[\frac{1}{2} i a_B^2 q_y (k_1 + k'_1 - k_2 - k'_2) - i \phi (l'_1 + l'_2 - l_1 - l_2) \right]. \end{aligned} \quad (6.6)$$

Here $a_B = (\hbar / |e| B)^{1/2}$ is the magnetic length, ϕ is the polar angle of the vector \mathbf{q} . The functions $Q_{ll'}$ are given by Eq. (2.12). Using the model wavefunction (??) [125], the form factor (6.5) can be calculated explicitly

$$F(q) = \frac{10 b^6 e^{-b+q}}{(b+q)^6} + \frac{b(8b^2 + 9bq + 3q^2)}{16(b+q)^3}. \quad (6.7)$$

It is easy to see from Eqs. (6.1)-(6.3) that the momenta k appear only in the matrix element so that using (6.6) one can find

$$\sum_{k_2, k'_1, k'_2} |M_{1,2 \rightarrow 1',2'}|^2 = \frac{1}{A} \frac{1}{2\pi a_B^2} \frac{4\pi^2 e^4}{\kappa_0^2} \sum_{\mathbf{q}} \frac{1}{q^2} F^2(q) Q_{l_1 l'_1}^2(q) Q_{l_2 l'_2}^2(q). \quad (6.8)$$

It should be noted that after performing the summation of the modulus squared of the matrix element over the momenta k no interference between different Fourier components of the Coulomb potential occurs.

So far we have not considered the δ -function in Eq. (6.2) which would give a factor of infinity because of energy conservation. For a realistic 2DEG, impurity scattering results in a broadening of the Landau levels [278]. The same mechanism also limits the mobility of the carriers in the system (see Chapter 4). Therefore, we replace the δ -function by a Lorentzian with a width corresponding to the scattering time $\tau \approx 10$ ps for the mobility $\mu = 25 \text{ V}^{-1} \text{ s}^{-1} \text{ m}^2$ which means $\pi \delta(\varepsilon_{n_1 l_1} + \varepsilon_{n_2 l_2} - \varepsilon_{n'_1 l'_1} - \varepsilon_{n'_2 l'_2}) \rightarrow \tau$. This approach is inconsistent in so far as impurity scattering, in principle, gives k -depended energies, however, we perform the k -sum without taking this into account.

Now from (6.1), (6.2), and (6.8) we obtain

$$\frac{1}{\tau_{Auger}^e} = W_{Auger} f_2 (1 - f_{1'}) (1 - f_{2'}) \Big|_{l_1 + l_2 = l_{1'} + l_{2'}} \quad (6.9)$$

and the probability of the Auger process is

$$W_{Auger} = 2 \left(\frac{e^2}{\hbar} \right)^2 \frac{\tau}{\kappa_0^2 a_B^2} \Phi \left(\frac{a_B}{z_0} \right). \quad (6.10)$$

The overlap integral

$$\Phi \left(\frac{a_B}{z_0} \right) = \int_0^\infty \frac{dq}{q} F^2(q) Q_{l_1 l'_1}^2(q) Q_{l_2 l'_2}^2(q) \Big|_{l_1+l_2=l'_1+l'_2} \quad (6.11)$$

depends on magnetic field via the dimensionless parameter a_B/z_0 where z_0 is a characterizing length parameter of the lowest electric subband. We have calculated the overlap integral $\Phi(a_B/z_0)$ for the Auger process involving Landau levels $l_1 = l_2 = 1$ and $l'_1 = 0, l'_2 = 2$ (Auger process from the level L_1 into the levels L_0 and L_2) using the form factor (6.7) (see the lower part of Fig. 6.4). The value of the parameter $z_0 = 3/b = 10.5$ nm has been chosen to reproduce the separation of the two lowest subbands of the actual quantum well in [55] and [56] by a triangular potential model. The magnetic field dependence of the probability of Auger process W_{Auger} is also plotted in Fig. 6.4. One can see that in the range of magnetic fields between 7.9 T and 12.9 T, the function Φ is slowly varying function in the magnetic field so that the probability W_{Auger} is a *linearly* increasing function in B in the same range. When the magnetic field is varied from 1 to 20 T, the probability W_{Auger} increases approximately from 1 to 10 fs. Notice that, recently, such a fast electron-electron thermalization (faster than 10 fs) has been observed in modulation-doped GaAs quantum wells [279].

However, the occupation factors, which have to be included in order to obtain τ_{Auger}^e , will drastically increase this value. For the case under consideration in the experiment of [55] and [56] (with $N_s = 7.6 \cdot 10^{15} \text{ cm}^{-2}$, $T = 1.8$ K and $B = 9.5$ T) but without pumping, we find by including the occupation factors $\tau_{Auger}^e \simeq 10^{63} W_{Auger}^{-1}$, *i.e.* the Auger process is not possible at all because the lower Landau level L_0 is almost completely filled. It becomes possible only by optical pumping into the level L_1 and subsequent recombination from L_0 , thus creating the empty states required for the Auger process. Without pumping, the Auger process is possible only at much lower magnetic fields (for lower carrier density) or much higher temperatures.

Applying the same considerations to τ_{Auger}^h we obtain an expression as (6.9) but with the factor f_1 instead of the factor $1 - f'_1$. This gives for half-filled L_1

level $\tau_{Auger}^h \approx 2$ fs. In contrast to τ_{Auger}^e we see that τ_{Auger}^h does not depend on available free places in the level L_0 and shows the efficiency of the Auger process in comparison with other processes which add (by emission of phonons) or remove (by interband recombination) electrons in L_0 .

6.3 Electron-acoustic phonon scattering between Landau levels

Transitions between Landau levels of the different electric subbands are possible by emission of acoustic phonons via the deformation (DA) potential. The corresponding relaxation time of a test electron is given by

$$\frac{1}{\tau_{nl \rightarrow n'l'}^{DA}} = (1 - f_{n'l'}) \sum_{k'} W_{nlk \rightarrow n'l'k'}^{DA} \quad (6.12)$$

where the transition probability from the state Ψ_{nlk} to the state $\Psi_{n'l'k'}$ is given by [45]

$$W_{nlk \rightarrow n'l'k'}^{DA} = \frac{1}{A} \frac{\Xi^2}{\hbar \rho s^2} \frac{\omega^2}{s^2} \sum_{\mathbf{q}} \frac{1}{a} \delta_{k', k+q_x} Q_{l'}^2(q) |I_{nn'}(a)|^2, \quad a = \sqrt{\frac{\omega^2}{s^2} - q^2}. \quad (6.13)$$

with the form factors Q and I given by (5.42) and (5.43), respectively. Recall that Ξ is the deformation potential constant, ρ is the mass density of the crystal, s is the velocity of sound and the transferred energy $\hbar\omega = \varepsilon_{nl} - \varepsilon_{n'l'}$.

Direct calculation shows that the probability for the piezoelectric potential (PA) can be obtained from (6.13) by replacing $\Xi^2(\omega^2/s^2)$ by $(e\beta)^2$ where β is the piezoelectric modulus of the crystal averaged over directions of propagation of phonons and its polarizations. Therefore, for GaAs one can find

$$\frac{W^{DA}}{W^{PA}} = \frac{\Xi^2(\omega^2/s^2)}{(e\beta)^2} = \left(\frac{\omega[\text{meV}]}{0.42} \right)^2. \quad (6.14)$$

This means that in strong quantizing magnetic fields ($B \sim 10$ T) when L'_0 is sufficiently far away from L_1 and L_2 , *i.e.* it is far from the crossing point of the magnetic field when $\omega \ll \omega_B$, the PA-interaction is suppressed with respect to the DA-interaction.

From (6.13), taking a sum over the momentum k' of the final states, it is easy to find

$$W_{nl \rightarrow n'l'} = \sum_{k'} W_{nlk \rightarrow n'l'k'}^{DA} = \frac{\Xi^2}{2\pi\hbar\rho s^2} \frac{\omega^2}{s^2} \times \int dz_1 dz_2 \psi_{n_1}(z_1) \psi_{n_2}(z_1) \psi_{n_1}(z_2) \psi_{n_2}(z_2) K\left(\frac{\omega}{s} | z_1 - z_2 \right) \quad (6.15)$$

where the kernel is

$$K\left(\frac{\omega}{s} | z_1 - z_2 \right) = \int_0^{\omega/s} dq \frac{q}{a} Q_{ll'}^2(q) \exp\{ia(z_1 - z_2)\}. \quad (6.16)$$

The following two transitions will be considered below:

$$n = 2, l = 0 \rightarrow n' = 1, l' = 1 \quad (L'_0 \rightarrow L_1) \quad \{I\}$$

with

$$\hbar\omega = \hbar\omega_1 = \varepsilon_{20} - \varepsilon_{11} = \omega_E - \omega_B, \quad Q_{10}^2(q) = t \exp(-t) \quad (6.17)$$

and

$$n = 1, l = 2 \rightarrow n' = 2, l' = 0 \quad (L_2 \rightarrow L'_0) \quad \{II\}$$

with

$$\hbar\omega = \hbar\omega_1 = \varepsilon_{12} - \varepsilon_{20} = 2\hbar\omega_B - \hbar\omega_E, \quad Q_{20}^2(q) = (t^2/2) \exp(-t). \quad (6.18)$$

Here $\omega_B = eB/mc$ is the cyclotron energy and $\hbar\omega_E = \varepsilon_{20} - \varepsilon_{10}$ is the energy separation between first and second electric subband.

The kernel (6.16) for these two transitions can be rewritten

$$K\left(\frac{\omega}{s} | z_1 - z_2 \right) \Big|_{\{I;II\}} = \frac{1}{a_B^2} \int_0^\alpha dt \{t; (t^2/2)\} \frac{1}{a} \exp[ia(z_1 - z_2) - t]. \quad (6.19)$$

where $\alpha = (\omega^2/2s^2)a_B^2$ is an integration parameter. This integration has been evaluated by means of the steepest descent method using the fact that in quantizing magnetic fields the parameter $\alpha = (\omega^2/2s^2)a_B^2 \simeq \omega_B/2ms^2 \gg 1$ is always large. Then we find

$$K\left(\frac{\omega}{s} | z_1 - z_2 \right) \Big|_{\{I;II\}} = \frac{\omega}{s} \frac{1}{2\alpha} \frac{(1 - i\beta)^2}{(1 + \beta^2)^2} \left\{ 1; \frac{1 - i\beta}{1 + \beta^2} \right\} \exp\left[i\frac{\omega}{s}(z_1 - z_2)\right] + o\left(\frac{1}{\alpha}\right) \quad (6.20)$$

where the parameter $\beta = (\omega/s)(z_1 - z_2)/2\alpha$. For $\omega \sim \omega_B$ and for $z_1, z_2 \sim d$ we have $\beta \sim ms(z_1 - z_2) \sim msd$. For GaAs the length $\hbar/ms = 340$ nm so that at $d = 25$ nm we have $\beta \ll 1$. Hence, neglecting the terms of the higher order in β we obtain

$$K \left(\frac{\omega}{s} |z_1 - z_2| \right) \Big|_{\{I;II\}} \approx \frac{\omega}{s} \frac{1}{2\alpha} \exp \left[i \frac{\omega}{s} (z_1 - z_2) \right]. \quad (6.21)$$

One can see that in this approximation the kernel differs for the two transitions only by the different values of the transferred energy ω . This result for K is easy to find from (6.16) by replacing a by ω/s . This means that in a 2DEG in a quantizing magnetic field normal to the electron sheet, electrons due to the DA interact mainly with phonons which propagate along the magnetic field direction **B**. It should be noticed that this statement is true not only for these particular transitions but also in general.

Substituting the kernel (6.21) in (6.15) we obtain the probability for the transitions $\{I\}$ and $\{II\}$

$$W_{ph}^{\{I;II\}} = \frac{1}{\bar{\tau}_B} \frac{\omega}{s} a_B \left| I_{12} \left(\frac{\omega}{s} \right) \right|^2, \quad \omega = \{\omega_1; \omega_2\}. \quad (6.22)$$

Here we define a nominal interaction time

$$\frac{1}{\bar{\tau}_B} = \frac{\Xi^2}{2\pi\hbar\rho s^2 a_B^3} \quad (6.23)$$

which depends on the magnetic field. Since the parameter $(\omega/s)d \gg 1$ (actually, this inequality defines the energy range in which we are interested), the form factor I_{12} can be calculated by the method of a stationary phase [280, 281]. Using Airy functions instead of wave functions $\psi_n(z)$ one can find

$$\left| I_{12} \left(\frac{\omega}{s} \right) \right|^2 = 4 \left(\frac{\omega}{s} \bar{z} \right)^{-6}, \quad \bar{z} = \frac{\hbar}{\sqrt{2m\omega_E/(\alpha_1 - \alpha_0)}} \quad (6.24)$$

where α_i is the i th zero of the Airy function.

Substitute (6.24) in (6.22) we find

$$W_{ph}^{\{I\}} = \frac{1}{\bar{\tau}_B} \frac{a_B}{\bar{z}} \frac{4(s/\bar{z})^5}{(\omega_E - \omega_B)^5} \propto B(B_E - B)^{-5}, \quad (6.25)$$

$$W_{ph}^{\{II\}} = \frac{1}{\bar{\tau}_B} \frac{a_B}{\bar{z}} \frac{4(s/\bar{z})^5}{(2\omega_B - \omega_E)^5} \propto B(2B - B_E)^{-5} \quad (6.26)$$

where B_E is the magnetic field when $\omega_B = \omega_E$. For GaAs at $B = 9.5$ T and $\bar{z} = 6.7$ nm (this corresponds to $\omega_E = 22.4$ meV taken from [55] and [56]), we find $W_{ph}^{\{II\}} = (32.3 \mu s)^{-1}$ and $W_{ph}^{\{I\}} = (1.5 \mu s)^{-1}$. Note, that the relaxation probability calculated in [45] for magnetic fields $B \simeq 1T$ is much greater. Such a suppression of the electron-phonon interaction at $\omega \sim \omega_B$ and $(\omega_B/s)\bar{z} \gg 1$ follows from the conservation laws. The electron states in this regime constitute a wave packet so that the states with $l, n \sim 1$ have momenta of the order of a_B^{-1} in the (x, y) -plane and of the order of \bar{z}^{-1} in z -direction. Therefore, only for a small number of electron states in this packet, the momentum conservation law is fulfilled at the interaction with acoustic phonons with momenta $\omega/s \gg a_B^{-1}, \bar{z}^{-1}$.

The dependence of the probabilities (6.25) and (6.26) on the magnetic fields is plotted in Fig. 6.1. At low fields $B \simeq 8$ T the transition $\{II\}$ ($L_2 \rightarrow L'_0$) is predominant. As B increases, the probability $W_{ph}^{\{II\}}$ rapidly falls while $W_{ph}^{\{I\}}$ (this corresponds to $L'_0 \rightarrow L_1$) slowly increases so that already at $B = 8.6$ T these two transitions are equally probable. At high fields transition $L_2 \rightarrow L'_0$ is suppressed with respect to $L'_0 \rightarrow L_1$ and $W_{ph}^{\{I\}}$ rapidly increases with increasing B so that at fields near B_E achieves to values corresponding to times less than 1 ns.

In order to obtain the relaxation times $\tau_{ph}^{\{I\},\{II\}}$, the occupation factors have to be included according to Eq. (6.9). Noting that for the case under consideration in experiment [55] and [56] the L_1 and L'_0 levels are not fully occupied, we obtain

$$\tau_{ph}^{\{I\},\{II\}} = (1 - f_{11,20})W_{ph}^{\{I\},\{II\}} \sim W_{ph}^{\{I\},\{II\}}. \quad (6.27)$$

To find out which mechanism (the Auger scattering or the phonon emission) is responsible for filling of holes in the level L_0 with electrons, we estimate also the lifetime of a test hole in L_0 with respect to the phonon emission from the higher level L_1

$$\frac{1}{\tau_{ph}^h} = \sum_{k'} W_{11k \rightarrow 10k'}^{DA} f_{11} \equiv W_{1 \rightarrow 0} f_{11}. \quad (6.28)$$

Here the probability $W_{11k \rightarrow 10k'}^{DA}$ is given by Eq. (6.2) for the transferred energy $\omega = \omega_B$. Since always $\omega_B > \omega_1, \omega_2$, the approximations, which have been made above to calculate the kernel K and form factor $I_{nn'}$, are also justified for this case. Therefore one can obtain $W_{1 \rightarrow 0}$ from Eq. (6.21) by substituting $\omega = \omega_B$. It is clear, that the lifetime of a test hole τ_{ph}^h is larger than the relaxation times

$\tau_{ph}^{\{I\},\{II\}} \sim 1 \mu s$ and thus much larger than ($\tau_{Auger}^h \sim 1 fs$). Hence, the Auger process is much more efficient to fill holes in the level L_0 than the phonon emission. This fact makes possible the observation of the Auger-upconversion by interband optical pumping [55] and [56].

6.4 Analysis of the rate equations.

So far we have considered only the processes (iii), (iv) and (vi). In order to correctly describe the experimental situation of [55] and [56], we have to take into account also the processes (i), (ii) and (v), *i.e.* the pumping by interband excitation to the level L_1 and the recombination of electrons from L_0 and L'_0 with the photo-induced holes. As it has been discussed already in Sec. 6.2, the Auger process becomes possible only after processes (i) and (ii). Intensities of the emissions from the levels L_0 and L'_0 are determined by the characteristic times of the processes (i)-(vi) from the following set of rate equations

$$\frac{\partial n_0}{\partial t} = \frac{n_0}{\tau_0} - \frac{n_1}{\tau_{Auger}^e} \quad (6.29)$$

$$\frac{\partial n_1}{\partial t} = \tilde{P}_{exc} + \frac{n'_0}{\tau_{ph}^{\{I\}}} - \frac{2n_1}{\tau_{Auger}^e} \quad (6.30)$$

$$\frac{\partial n'_0}{\partial t} = \frac{n_2}{\tau_{ph}^{\{II\}}} - \frac{n'_0}{\tau_{ph}^{\{I\}}} - \frac{n'_0}{\tau'_0} \quad (6.31)$$

$$\frac{\partial n_2}{\partial t} = \frac{n_1}{\tau_{Auger}^e} - \frac{n_2}{\tau_{ph}^{\{II\}}} \quad (6.32)$$

Here n_l (n'_l) is the areal number density of electrons in the Landau level with index l of the first (second) electric subband including spin degeneracy. The characteristic times of the recombination of electrons from level L_0 and L'_0 with photo-induced holes are τ_0 and τ'_0 which depend on B in the same way and are of same order of magnitude. In Eq. (6.30) we have also defined the flux of electrons created by interband excitation into the level L_1

$$\tilde{P}_{exc} = \frac{P_{exc}}{\omega_{exc}}(1 - f_1) \quad (6.33)$$

where P_{exc} and $\hbar\omega_{exc}$ are the excitation power and energy. The factor $1 - f_1$ takes into account the availability of free states in the level L_1 . In a stationary case we

have $\partial n / \partial t = 0$ and the rate equations reduce to

$$I_0 \equiv \frac{n_0}{\tau_0} = \frac{n_1}{\tau_{Auger}^e} = \frac{n_2}{\tau_{ph}^{\{II\}}} \quad (6.34)$$

$$I'_0 \equiv \frac{n'_0}{\tau'_0} \quad (6.35)$$

$$I_0 - I'_0 = \frac{n'_0}{\tau_{ph}^{\{I\}}} \quad (6.36)$$

$$I_0 + I'_0 = \tilde{P}_{exc} \quad (6.37)$$

$$(6.38)$$

where I_0 and I'_0 are proportional to the luminescence intensities for recombinations from L_0 and L'_0 , respectively. According to Eq. (6.34), the luminescence intensity I_0 is determined both by τ_{Auger}^e and $\tau_{ph}^{\{II\}}$. Because of $\tau_{Auger}^e = (n_1/n_2)\tau_{ph}^{\{II\}} > \tau_{ph}^{\{II\}}$ we find for $B = 9.5$ T that $\tau_{Auger}^e > 30$ μ s. This means that the relaxation time of a test electron in the level L_1 with respect to the Auger scattering is strongly enhanced due to the occupation factors over the characteristic time W_{Auger}^{-1} and the lifetime of a test hole τ_{Auger}^h in the level L_0 which are of the order of 1 fs.

Because τ_{Auger}^h is much smaller than all other characteristic times of this system, the Auger-upconversion mechanism immediately fills all arising holes in L_0 due to the recombination of electrons from L_0 and creates electrons in the level L_2 . Thus the number of the up-converted electrons is always equal to the number of recombining electrons from L_0 . However, the intensity of the up-converted luminescence I'_0 is determined by the competition of the processes (v) and (iv), *i.e.* by the ratio of τ'_0 and $\tau_{ph}^{\{I\}}$ (see Eqs. (6.35) and (6.36)).

In order to obtain the dependencies of I_0 and I'_0 on the magnetic field and the excitation power we consider two different cases. In a case when process (v) is dominant over the process (vi), *i.e.* $\tau_{ph}^{\{I\}} \gg \tau'_0$, we find from equations (6.34)-(6.37) that

$$I_0 \approx I'_0 \approx \frac{\tilde{P}_{exc}}{2} \gg \frac{N_0}{\tau_{ph}^{\{I\}}}, \quad n_0 \sim n'_0 \sim N_0 \quad (6.39)$$

which means

$$I_0, I'_0 \propto P_{exc}, \quad \left(1 - \frac{B_1}{B}\right). \quad (6.40)$$

Here N_0 is the capacity of one Landau level and B_1 corresponds to the full occupation of two Landau levels L_0 and L_1 . With the help of Eqs. (6.25), (6.27), and (6.33) it is seen that the inequality in Eq. (6.39), which is determined by $\tau_{ph}^{\{I\}} \gg \tau'_0$, corresponds to the situation when the magnetic field is close to the lower bound of the considered interval and at the same time the excitation power is high. In opposite case when $\tau_{ph}^{\{I\}} \ll \tau'_0$, which corresponds to magnetic fields close to the upper bound and low powers, we find from Eqs. (6.34)-(6.37)

$$I'_0 = \frac{\tilde{P}_{exc}^2}{N_0/\tau_{ph}^{\{I\}}} \ll I_0 = \tilde{P}_{exc}, \quad n_0 \sim N_0 \gg n'_0 \quad (6.41)$$

This means that

$$I'_0 \propto P_{exc}^2, \quad \left(1 - \frac{B_1}{B}\right) (B_E - B)^5 \quad (6.42)$$

while

$$I_0 \propto P_{exc}, \quad \left(1 - \frac{B_1}{B}\right). \quad (6.43)$$

Now it is clear from Eqs. (6.39) and (6.40) that at B near B_1 both intensities I_0 and I'_0 increase linearly with B . As B increases further, I_0 continues to increase in accordance with (6.43) but not so sharply as near B_1 . However, I'_0 shows another behavior given by Eq. (6.42) and decreases with B as $(B_E - B)^5$ when B is near B_E (Fig. 6.5). At low powers I'_0 depends quadratically on P_{exc} (Eq. (6.42)) while at high powers for I'_0 (Eq. (6.40)) and in the whole range of the power variation for I_0 (Eqs. (6.40) and (6.43)) this dependence is linear.

In conclusion, our calculation provides an understanding of the main features of the experiments reported in [55] and [56]. In the light of our investigations it would be interesting to have detailed experimental information on the intensities I_0 near B_1 and I'_0 near B_E for which also our theory provides definite information.

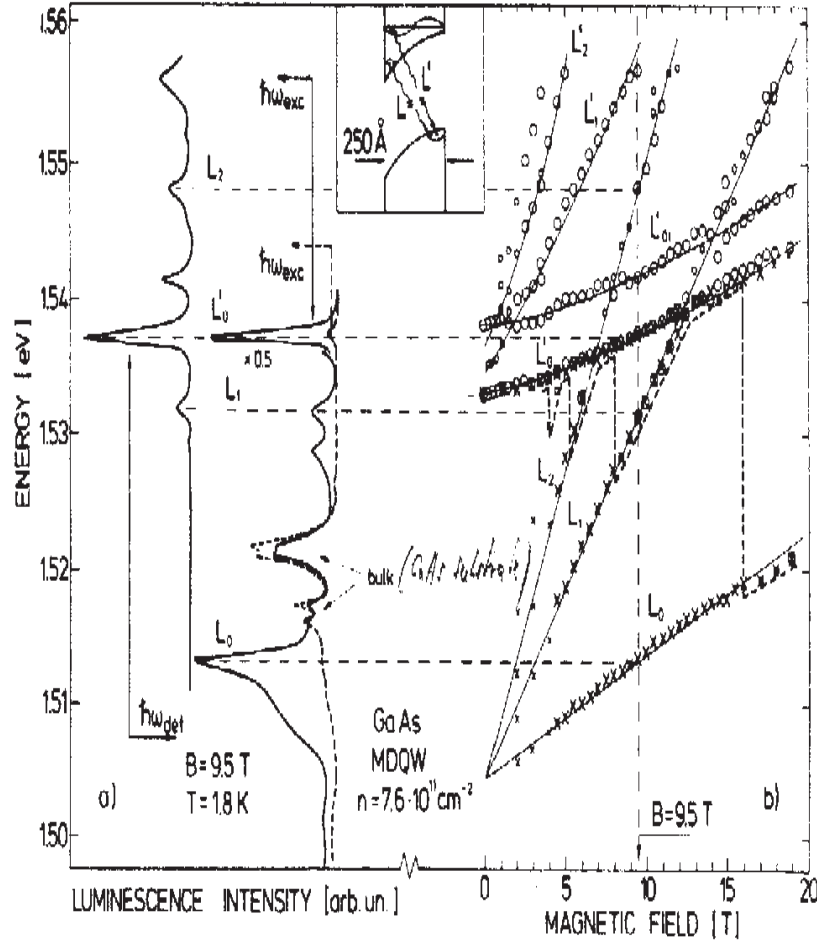


Figure 6.2: (a) Intensity of the luminescence detected at $\hbar\omega_{det}$ as a function of the exciting energy (left) and luminescence spectra at different excitation energies $\hbar\omega_{exc}$ (right). Two-dimensional and bulk structures are observed when the excitation energy corresponds to the peak of the two-dimensional density of states (solid line), and mainly bulk-related luminescence is visible when exciting in the gap between the two-dimensional levels (dashed line). (b) The Landau level fan chart of the optically active transitions observed in luminescence (crosses) and luminescence-excitation (open circles) spectra. The size of the symbol reflects the transition intensity. The L'_0 absorption line involves the light-hole level. The Fermi-level position is shown with the dashed line.

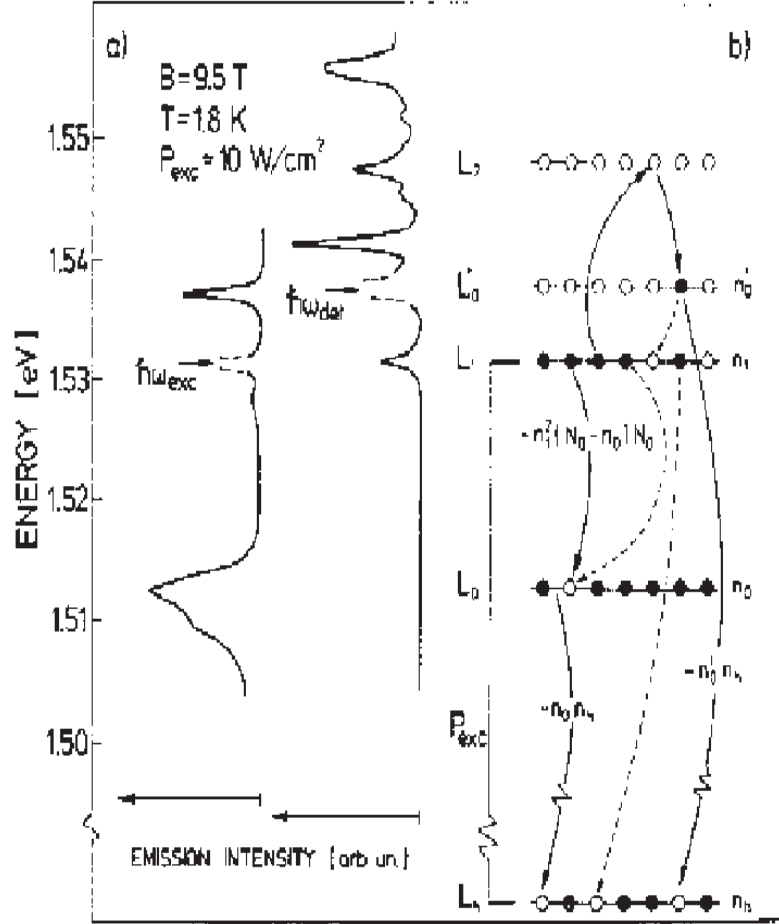


Figure 6.3: (a) Solid circles: variation of the peak intensity (I_0') of the above-laser emission as a function off the magnetic-field-dependent filling factor ν or the separation Δ between the excitation- and the emission-peak energies. The peak intensity of the L_0 -related luminescence (I_0) is shown with open circles. Solid lines are guides for the eye. (b) Power dependence (in relative units) of the I_0' and I_0 when exciting into the L_1 level. Solid lines represent quadratic (for I_0') and linear (for I_0) variations.

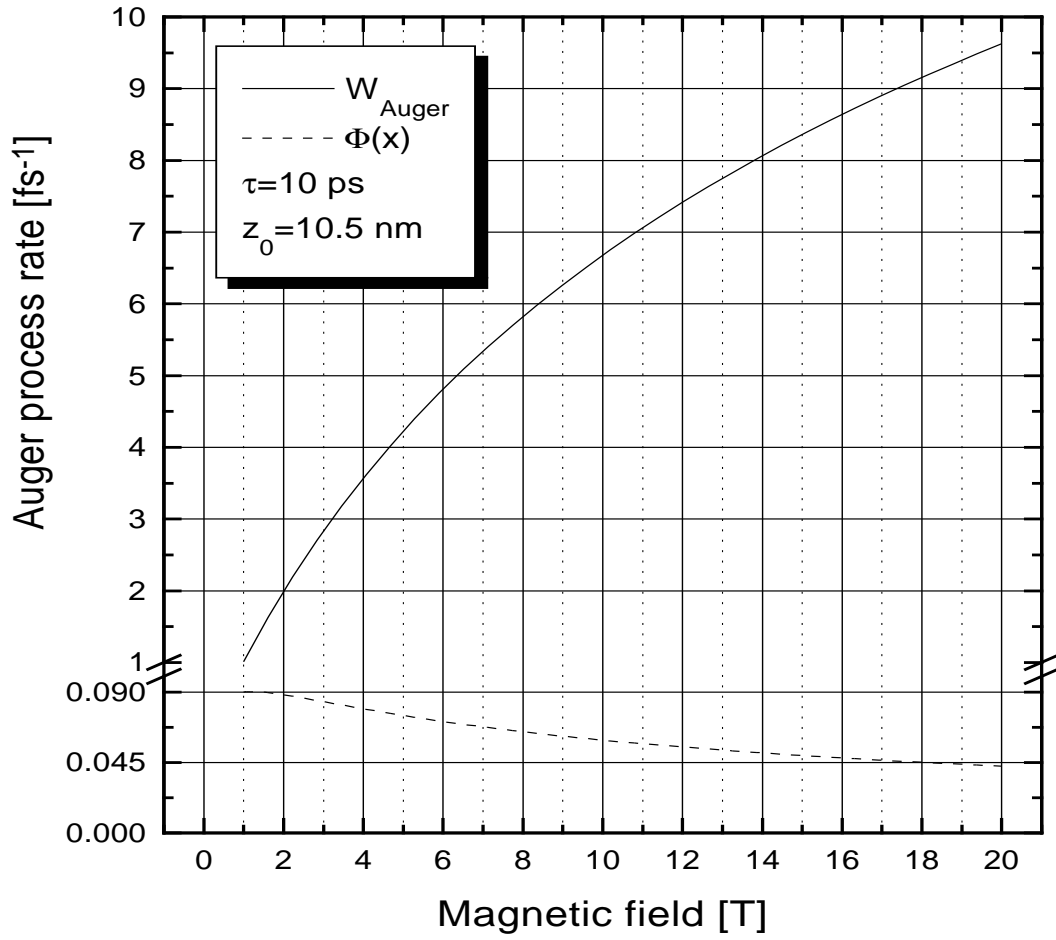


Figure 6.4: Probability of the Auger process W_{Auger} from the level L_1 into the levels L_0 and L_2 . Dashed line shows the overlap integral $\Phi(a_B/z_0)$.

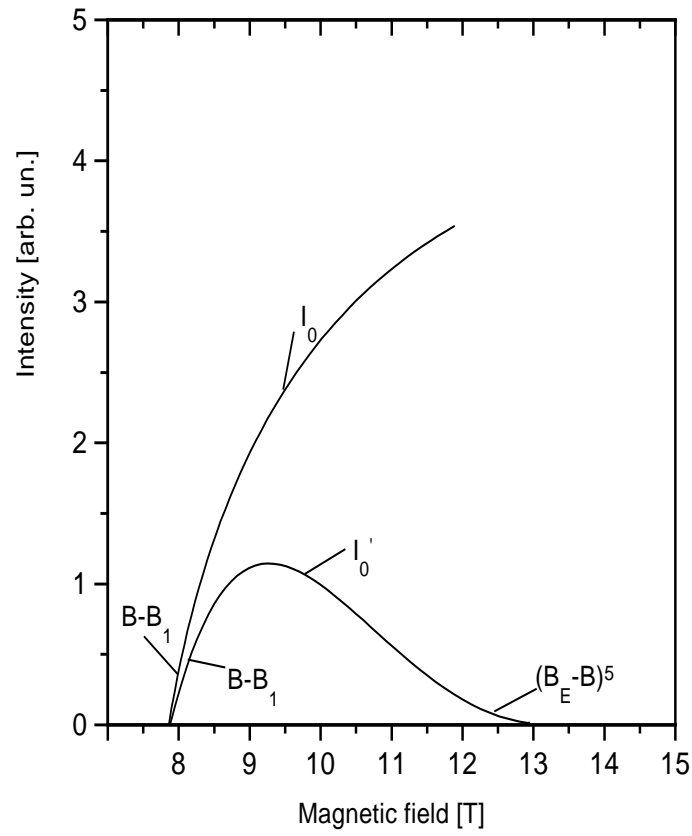


Figure 6.5: Magnetic field dependence of the luminescence intensities I_0 and I'_0 for recombination from the Landau levels L_0 and L'_0 , respectively.

Chapter 7

Magneto-transport in a non-planar 2DEG

7.1 Introduction

The last decade has seen the many of different and creative new environments under which quantum nanosystems with the 2DEG are investigated. Particularly, the 2DEG exposed to a homogeneous magnetic field has proved to be an extremely rich subject for investigations in theory and experiment [19]. In these nanosystems in addition to the lateral confinement, the carrier motion becomes quantized also in the plane normal to the magnetic field. The quantization length is varied with magnetic field which assures an easily way to obtain information on the properties of charge carriers. Considerable efforts have been devoted to study transport properties in such effectively zero dimensional systems [21, 282]. Already, a set of remarkable phenomena such as the integer and the fractional quantum Hall effects [283], the Aharonov-Bohm effect [284, 285], and the magneto-resistance oscillations of the 2DEG subjected to periodic electric field weak modulations along one or two directions, also called *Weiss* oscillations [286, 287, 288] (to mention just a few) has been uncovered.

In the last several years a more complex situation of the 2DEG in a non-uniform magnetic field has attracted considerable interest [289]. Depending on the strength of the local magnetic field, the electron motion in the plane of the 2DEG can be tuned from regular to chaotic [290, 291]. The motion of ballistic

electrons in a periodic magnetic field is also believed to be closely related to the motion of *composite fermions* in a density modulated 2DEG in the fractional QHE regime [292, 293]. Such magnetic supersystems offer the possibility of producing magnetic confinement. In a non-zero magnetic field region, the lowest energy state for an electron is the lowest Landau level with energy $\hbar\omega_B$ (ω_B is the cyclotron frequency). In a zero-field region, the lowest energy state is zero. Therefore, when electrons start to move away from the zero-field region, the non-zero-field region acts as a barrier. Moreover this barrier differs from a usual potential barrier in two ways. First, the barrier is kinetic, *i.e.* the electron gains kinetic energy as the electron overcomes the barrier. Second, tunneling through the magnetic barrier is an inherently two-dimensional process so that the transmission probability depends on the angle at which the electron hits the non-zero-field region. This last property has been exploited to predict a wave-vector selective filter for electrons [294]. Other interesting feature can manifest magnetic "dots" coupled to the 2DEG. These dots could be used to produce magnetic fields that could confine electrons to a disk region. Such magnetic dots could be explored as memory elements in future electronics.

Theoretically the transport properties of a 2DEG subjected to a spatial dependent perpendicular magnetic field have been addressed in several works. The possibilities of the creation of periodic superstructures by a non-homogeneous magnetic field have been investigated in [295, 296, 297]. Distinct theoretical predictions have been achieved for the limit of a weak one-dimensional magnetic modulation. Transport of a 2DEG in a weakly modulated periodic magnetic field normal to the electron sheet and its collective excitation spectra have been studied in [294, 298] and [299]. The single-particle energy spectra of a 2DEG have been calculated in a non-homogeneous magnetic field for different step-like [300], linearly varying with position [301] and other functional magnetic field profiles [302]. The magnetic field dependence of the conductance of a ballistic QWr [296] and of a 2DEG through an orifice [303] has been studied. The properties of wave-vector dependent electron tunneling [294] and electron moving [67] in step-like magnetic structures have been investigated. Analysis of the weak localization and calculation of the Hall and diagonal resistivities of the 2DEG in an inhomogeneous magnetic field have been presented in [304, 305, 306]. Quite recently

it has been shown that the spatial distribution of electron and current densities in a linearly varying magnetic field has very rich structure related to the energy quantization [307].

Until recently experimental attempts to produce non-homogeneous magnetic fields on the micrometer or nanometer scale have failed. Now, however experimental groups in Germany, Japan, and the UK have succeeded in coupling the 2DEG to the non-homogeneous magnetic field. High mobility 2DEGs are formed in standard GaAs/AlGaAs heterojunctions. The spatial modulation of the magnetic field is made possible by depositing patterned gates of superconducting or ferromagnetic materials on the surface of heterostructures.

A group at the Max-Planck-Institute in Stuttgart has used ferromagnetic dysprosium (Dy) metal stripes [308, 309], while a group at Tokyo University has used ferromagnetic nickel gates [310] to modulate the magnetic field. The strength of these micromagnets can be increased via an external magnetic field. A group at Nottingham University has used a superconducting stripes on the surface of the heterostructure [311]. Using this technique of patterned gates, it has become possible to realize experimentally magnetic dots [312, 308].

However, such scheme of creating inhomogeneous magnetic fields has two disadvantages: i) the variation in the magnetic field is very small in the 2DEG plane since gates are a few hundred angströms above the plane of the 2DEG and dies away rapidly a short distance below the gates, ii) the patterned gate layers will also cause strain and electrostatic iii) variations which are in general stronger than the effects of the varying magnetic field which makes it hard to attribute effects unambiguously to the magnetic field.

Recently a research group from the Toshiba Cambridge Research Center Ltd. and Cavendish Laboratory have reported an alternative approach to produce spatially varying magnetic fields [58]. They have proposed to take advantage of the regrowth technology of $III - V$ semiconductors on patterned substrates and offer a more flexible and potentially fruitful solution of this problem. A remotely doped GaAs/ $\text{Al}_x\text{Ga}_{1-x}\text{As}$ heterojunction is grown over wafer previously patterned with series of facet. The electron gas is confined to a sheet at the GaAs/ $\text{Al}_x\text{Ga}_{1-x}\text{As}$ heteroface which is no longer planar but follows the contour of the original wafer. The use of *in situ* cleaning technique enables to regrow

uniform high quality 2DEGs over etched substrates [59, 60].

Application of a homogeneous magnetic field to this structure results a spatially varying field component normal to the 2DEG. This has firstly been demonstrated for samples with a single planar facet [58, 59, 60, 61]. Rotating the plane of the sample allows us to find different non-homogeneous magnetic superstructures: magnetic barriers, magnetic wells and completely novel situations where the normal component of the field changes its sign on the facet (see Fig. 7.1). Improved control over the topography of the electron gas will allow magnetic-

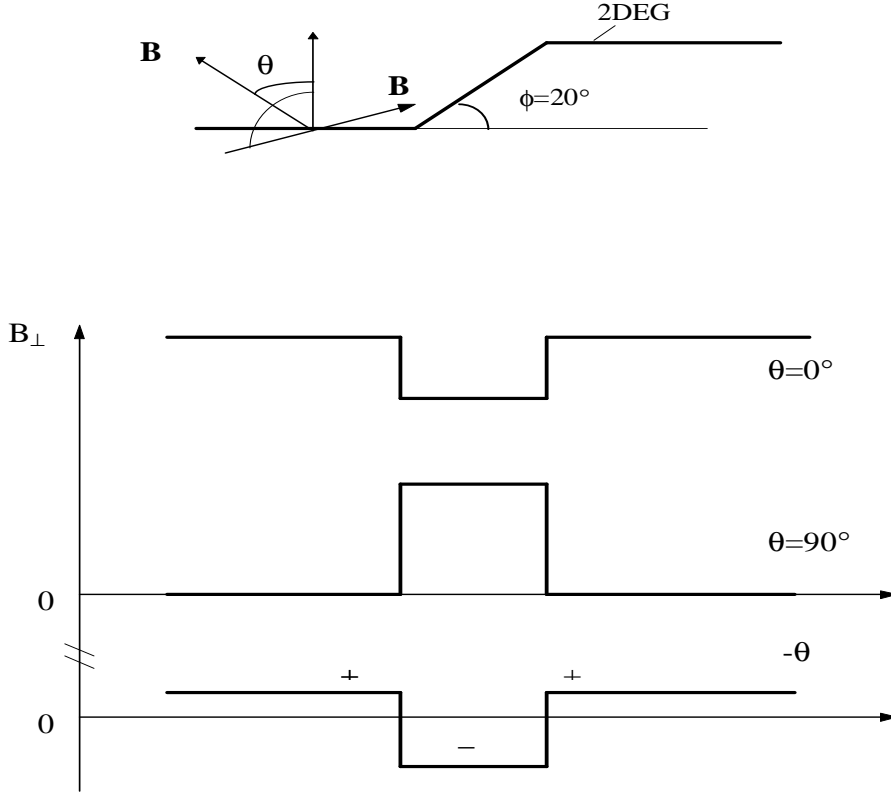


Figure 7.1: Applying a uniform magnetic field produces a spatially non-homogeneous field component normal to the 2DEG. Different magnetic superstructures can be obtained, depending on the θ angle between the magnetic field and the substrate normal, magnetic barriers ($\theta = 90^\circ$), magnetic wells ($\theta = 0^\circ$), and novel situations when the normal component of the field changes its sign on the magnetic interface.

field variations in more than one dimension. In principle, this technique offers the possibility of investigating the behavior of electrons in a curved quasi-two-dimensional space, and the effects of varying that curvature. Quite recently a theoretical study of quantum magnetic confinement and transport of electrons in spherical and hemispherical 2DEGs has been presented [62]

Thus, using this *in situ* cleaning technique, we can now investigate the effect of varying *the topography* of an electron gas in addition to varying the *dimensionality*. This new technology will open up a new dimension for investigations in nanophysics. Characterizing and understanding transport properties of magnetic superstructures with elementary cells containing a 2DEG with well-defined topographical features are crucial both for the basic phenomena and device applications.

The aim of the present chapter is to investigate theoretically the magneto-transport of the non-planar 2DEG [63, 64, 65, 66, 67] to explain recent experimental results obtained in the Toshiba Cambridge Center and Cavendish laboratory [58, 59, 60, 61, 62]. As an example, the electric field distribution has been calculated in the presence of a magnetic tunnel barrier of μm width. The system satisfies the Poisson equation in which line charges develop at the magnetic/non-magnetic-field interface. We have found that most of the electrons are injected at the edges of the magnetic barrier. The magneto-resistances across the facet as well as in the planar regions of the 2DEG have been calculated which provide an understanding of the main features of the magnetic field dependencies observed experimentally by M L Leadbeater *et al* [59]. They have constructed a non-planar 2DEG which has been fabricated by growth of a GaAs/AlGaAs heterojunction on a wafer pre-patterned with facets at 20° to the substrate. Applying a uniform magnetic field, \mathbf{B} , produces a spatially non-uniform field component perpendicular to the 2DEG (see the $\theta = 90^\circ$ case in Fig. 7.1). With the field in the plane of the substrate an effective magnetic barrier has been created located at the facet. The resistance across such an etched facet has shown oscillations which are periodic in $1/B$ and which are on top of a positive magneto-resistance background which increases quadratically with the magnetic field for small fields B and linear in B for large B . In experiment the dimensions of the facet have been $40\ \mu\text{m}$ wide and $3\ \mu\text{m}$ long, the voltage probes close to the facet are situated 10

μm apart across the facet (*quod vide* Ref. [59] for more details). The magneto-resistance has been measured using also the voltage probes on the planar regions of the 2DEG. There is no perpendicular component of the magnetic field in these regions, however, for probes directly adjacent to the facet, a strong magneto-resistance has been observed. Pairs of probes on opposite the sides of the mesa and on the opposite sides of the facet have shown the same symmetry. While there has been a pronounced asymmetry in each of traces with reversal of the magnetic field direction.

Another motivation for our theory is the necessity of reexamining the standard Hall analyses for very small device geometry [313, 314]. As device sizes have shrunk to the submicron scale, it has become harder to make contact probes small relative to the size of the sample to be characterized. Due to the very high current densities involved, point-like contacts come to introduce their own sources of error. Particularly, in the QHE geometry, singularities of the current density associated with the breakdown of the QHE [315, 316]. Hall voltage distribution has been measured in modulation-doped GaAs/AlGaAs heterojunctions while observing the QHE [317] and has been calculated in an ideal 2DEG [318, 319]. The geometric effect of contacts has been studied by many authors [320, 321, 322, 323, 324, 325, 326] (see also the review article [327]). First such a theory has been developed by Wick [320], who assumes that the contacts have a much higher conductivity than the sample being measured. Therefore the contacts can be modeled as an equipotential at the sample boundary which allow to treat many geometries by the method of Schwartz-Christoffel mappings. These results obtained by Wick have been applied directly to the QHE regime by Kawaji [324]. The same approach has been exploited by other authors to analyze geometric contact effects in the QHE regimes [325, 326]. As we are aware, all of the exact treatments except the recent work [328], treat a single isolated contact interface which can be usefully applied to Hall bars with high aspect ratios while for samples with lower aspect ratios this approach does not work.

Our theory presented in this work can be applied for samples with arbitrary aspect ratios and with any number of magnetic interfaces.

7.2 Theoretical model

To explain, qualitatively, the main features of the experimental measurements in Ref. [59], namely the smooth background of the magnetic field dependence of the resistance across the facet and the symmetries of the resistance traces measured between various probes in the planar regions, we rely on a classical model since the width of the magnetic field barrier is much larger than the magnetic length. Recall, that the present situation is different from that of discussed in Ref. [294] where quantum tunneling through magnetic nanostructures was treated.

Due to its topography, the non-planar 2DEG is embedded in ordinary three-dimensional space so that the electron position is determined by three Cartesian coordinates. In reality, however, we are dealing with a two-dimensional problem. By a simple coordinate parameterization, the problem could be reduced to the geometry with 2D-electrons located in a (x, y) -plane and the magnetic field normal component applied in z -direction. We take the magnetic field profile $B(x) = 0$ ($0 < x < a$ and $b < x < L$) and $B(x) = B$ ($a < x < b$) which is appropriate to the experimental situation. Assuming the electric field and the current density to be independent on the z -coordinate, from 2D classical electrostatics we obtain the spatial electric field distribution in the (x, y) -plane which determines the magneto-resistance which we compare with experiment.

In a steady state, the spatial distribution of an electric current density \mathbf{J} is independent of time, and satisfies the discontinuity equation

$$\mathbf{div} \mathbf{J}(x, y) = 0 \quad (7.1)$$

which means that total charge in any volume of the 2DEG remains constant. The electric field \mathbf{E} in the 2DEG in which a steady current flows is constant, and therefore from Maxwell's equations we have

$$\mathbf{curl} \mathbf{E}(x, y) = 0, \quad (7.2)$$

i.e. it is a potential field. Eqs. (7.1) and (7.2) should be supplemented by a system equation relating \mathbf{J} and \mathbf{E} . In a zero magnetic field in the most of cases this relation is linear (Ohm's law). In a normal quantizing magnetic field charge carriers are moved due to the Coulomb and Lorenz forces so that the basic system

equation is given by

$$\mathbf{J}(x, y) = \sigma \mathbf{E}(x, y) - \tan \zeta(x) \mathbf{J}(x, y) \times \mathbf{B}(x) \quad (7.3)$$

where the conductivity $\sigma = ne\mu$ is determined by the sample mobility μ (n is the surface concentration of electrons), the spatial dependent Hall angle $\zeta(x)$ is defined by

$$\tan \zeta(x) = \sigma R_B B(x) \quad (7.4)$$

R_B is the Hall coefficient. The spatial dependent magnetic field can be expressed by the Heaviside step function in the following way

$$\mathbf{B}(x) = \hat{\mathbf{z}}B[\theta(x-a) - \theta(x-b)], \quad \theta(x) = \begin{cases} 1, & \text{if } x > 0, \\ 0, & \text{if } x < 0 \end{cases}. \quad (7.5)$$

Using Eqs. (7.1) and (7.2) it is easy to show that by virtue of Eqs. (7.3), (7.4) and (7.5), the electric field satisfies the following equation at all points within the whole region of the 2DEG

$$\begin{aligned} \mathbf{div} \mathbf{E}(x, y) &= \tan \delta \{ \sin[2\zeta(x)] E_y(x, y) - \cos[2\zeta(x)] \\ &\quad \times E_x(x, y) \} \{ \delta(x-a) - \delta(x-b) \} \\ &\equiv 4\pi\rho_s \{ \delta(x-a) - \delta(x-b) \}. \end{aligned} \quad (7.6)$$

with $\delta(x)$ the Dirac-delta function.

At the boundary of the 2DEG, the normal component of the current density and the tangential component of the electric field must be continuous which follows from Eqs. (7.1) and (7.2), respectively. This means that there be no current flow out the sides ($x = -w$ and $x = w$) and no electric field parallel to the ends ($y = 0$ and $y = L$) of the 2DEG. For the magnetic field configuration given by Eq. (7.5), the system equation (7.2) implies that the current and electric field make an angle 0 and ζ in the regions $B = 0$ and $B \neq 0$, respectively. Therefore the boundary condition $\mathbf{J} = 0$ on the sides of the 2DEG can be replaced by the condition that the electric field makes an angle 0 and ζ with respect to the sides, respectively in the regions $B = 0$ and $B \neq 0$ (see Fig. 7.2). Now it is clear that the problem can be treated as a field problem, *i.e.* in order to solve the problem, it is necessary to obtain the solution of the set of Eqs. 7.3 and 7.6 with boundary conditions shown on Fig. 7.2. Unlike to the usual type electric

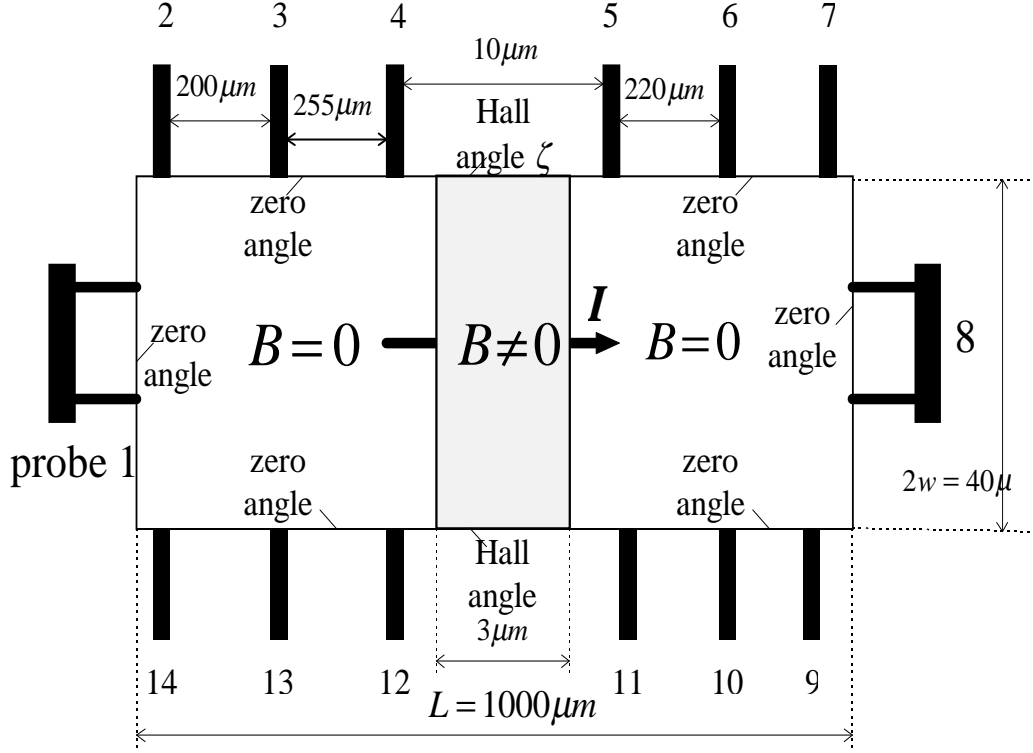


Figure 7.2: A magnetic barrier is created in a non-planar 2DEG exposed to the uniform magnetic field. Dimensions and voltage probe locations correspond to the experimental situation. Boundary conditions are given in terms of angle which makes the electric field with respect to the sides and ends of the 2DEG. The current flows between voltage probes 1 and 8.

potential problem, here boundary conditions do not involve specifications of the potential or its normal derivative but of the electric field angle with respect to the boundary of the 2DEG.

When the electric field represented as the gradient of a potential function it satisfies the 2D Laplace equation in the *separate* planar and non-planar regions of the 2DEG. However, this potential *does not* satisfy the Laplace equation in the whole 2DEG region. It satisfies the Poisson equation with a non-trivial right side part which is determined by the field itself. Thus at the magnetic interfaces $y = a$ and $y = b$ there is an accumulation of linear charges with a charge density

ρ_s .

Direct way to solve the such electric potential problem is to obtain the solutions of three Laplace's equations separately in the both planar and in the non-planar regions, introducing additional four unknown angles which the electric field makes on both sides of the magnetic interfaces with respect to the normal of the interfaces. Then using the continuity of the normal current and the tangential field components we have to match these solutions and eliminate these four angles. However, because of a singularity of the electric field at the magnetic interfaces, inconveniences occur in such procedure (see also Ref. [328]). To get round this difficulty, first we have solved directly Laplace's equation for whole region of the 2DEG, *i.e.* taking $\rho_s = 0$ in Eq. (7.6) with the same boundary conditions specified above on Fig. 7.2. Then, we have included the line charges at $y = a$ and $y = b$ which implies that the electric field exhibits jumps at these points and we have modified the solution of the Laplace equation such that it satisfies the Poisson equation corresponding to Eqs. (7.2) and (7.6). To construct the solution of the 2D Laplace equation, the conformal mapping method [329] has been exploited. From the Cauchy-Riemann conditions it follows that the desired electric field related to the complex field via $\mathbf{E}' = iE'_x + E'_y$ is solenoidal and irrotational, *i.e.* there is a complete correspondence between plane electrostatics field and regular functions. If the geometry of the 2DEG were that of including rectangular shown in Fig. 7.3 then the boundary conditions would be satisfied by a uniform electric field, $\mathbf{E} = \hat{\mathbf{y}}E_0$. Therefore, if we let $-E'(z) = \lambda dw(z)/dz = \exp[f(z)]$ (λ is an arbitrary constant which should be determined by the potential difference between the ends of the 2DEG) then in order to map the rectangle into the such parallelogram in complex plane $w(z)$ shown in the upper picture in Fig. 7.3, it is necessary to find an analytical function $f(z)$ whose imaginary part satisfies the boundary conditions:

$$\begin{aligned} \text{Im}f(z) &= 0 \quad \text{on the ends of the 2DEG,} \\ \text{Im}f(z) &= 0 \text{ or } \zeta \quad \text{on the sides of the 2DEG.} \end{aligned} \quad (7.7)$$

Using the conformal mapping $\xi(z)$, we map the rectangular domain of the 2DEG in the complex $z = x + iy$ plane onto the upper half plane of the $\text{Im}\xi > 0$ such that the boundary of the rectangle goes into the real axis (the lower picture in

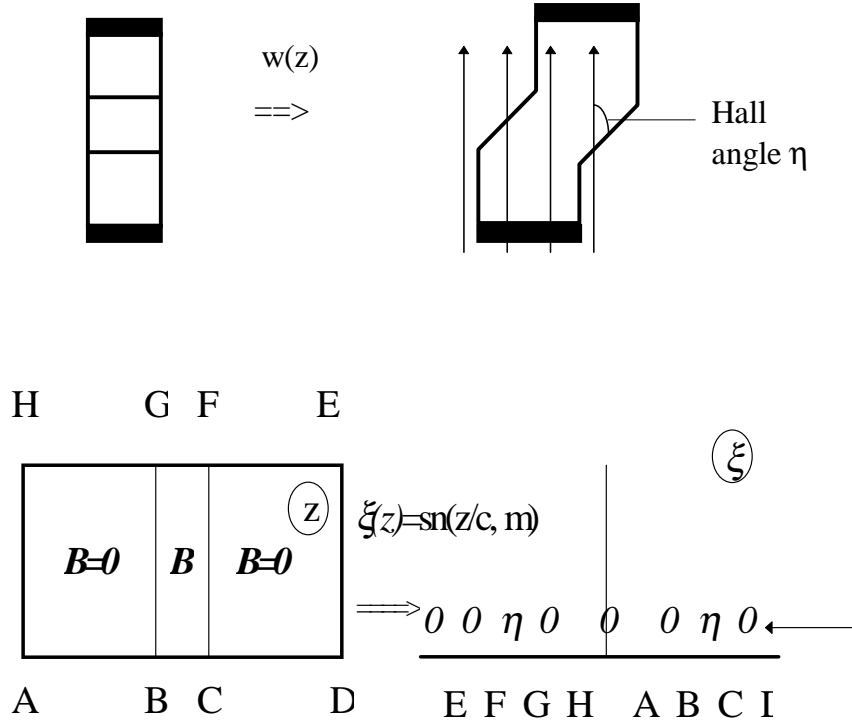


Figure 7.3: Conformal mapping $w(z)$ of the rectangular domain of the 2DEG onto the domain of a parallelogram form where boundary conditions are satisfied by a uniform electric field (the upper picture). Conformal mapping $\xi(z)$ of the rectangular domain of the 2DEG onto the upper half plane of the $\text{Im}\xi > 0$ such that the perimeter of the rectangle goes into the real axis (the lower picture).

Fig. 7.3). This is accomplished by the Jacobi elliptic function, $\xi(z) = \text{sn}(z/c, m)$ where the constant $c = L/K'(m) = w/K(m)$ and m are determined by the sample aspect ratio, K and K' are the complete elliptic integrals of first kind [330], $2w$ is the width of the 2DEG. Thus the problem is reduced to the standard electrostatics problem of finding the potential for the upper half plane bordered by electrodes represented by the open intervals along real axis $\text{Im}\xi = 0$:

$$\begin{aligned}
 &(-\infty, -\text{sn}(1, \beta)); (-\text{sn}(1, \beta), -\text{sn}(1, \alpha)); \\
 &(-\text{sn}(1, \alpha), \text{sn}(1, \alpha)); (\text{sn}(1, \alpha), \text{sn}(1, \beta)); (\text{sn}(1, \beta), \infty)
 \end{aligned} \tag{7.8}$$

where $\alpha = a/L$ and $\beta = b/L$, and

$$sn(x, y) \equiv sn(K(m)x + iK'(m)y, m). \quad (7.9)$$

Here the normalized length and width variables y and x , respectively, are introduced so that $y \div (0, 1)$, $x \div (-1, 1)$. These electrodes are at the respective potentials $0; \zeta, 0, \zeta, 0$ determined by the boundary conditions. Using the Poisson's integral formula of the Dirichlet's problem for the upper half plane, the electric field has been obtained which satisfies to the 2D Laplace equation

$$\mathbf{E}'(x, y) = \left(\frac{[sn(x, y) + sn(1, \alpha)][sn(x, y) - sn(1, \beta)]}{[sn(x, y) - sn(1, \alpha)][sn(x, y) + sn(1, \beta)]} \right)^{\delta/\pi} \quad (7.10)$$

For the $a = 0$ and $b = L$ limiting case, Eq. (7.10) gives the electric field distribution for a uniform magnetic field in terms of the Jacobi elliptic functions which is in agreement with that of obtained in Ref. [325] in the form of an expansion into hyperbolic functions. The field (7.10) has singularities in the corners of the magnetic interfaces. The same behavior exhibits the electric field in the Hall effect regime. In both cases an analytic function changes its phase from 0 to ζ in one point which results a power-law singularity of this function at that point.

The above field E' does not conserve current and the normal component of \vec{J} jumps at the magnetic interfaces. We can remedy this as follows: in the planar regions the real electric field $\vec{E}(x, y)$ is given by Eq. (7.10) while in the non-planar region, due to the jump of the y -component of the field, we have

$$E_y(x, y) = \frac{1}{\cos^2 \zeta} \mathbf{Re} \vec{E}'(x, y) - \tan \zeta \mathbf{Im} \vec{E}'(x, y), \quad E_x(x, y) = \mathbf{Im} \vec{E}'(x, y). \quad (7.11)$$

The above equation together with the auxiliary Eq. (7.10) gives the solution of our problem and satisfies the Poisson equation corresponding to Eqs. (7.2) and (7.6). Now it is clear that in the whole region we have $J_n(\vec{E}) = \sigma E'_n$, and since $\mathbf{div} \vec{E}' = 0$, the current is conserved at the magnetic interfaces.

7.3 Results and Discussion

The spatial distributions of the argument $\mathbf{Arg} \vec{E}(x, y)$ and the absolute value $\mathbf{Abs} \vec{E}(x, y)$ of the electric field $\vec{E}(x, y)$ in the neighborhood of the facet are

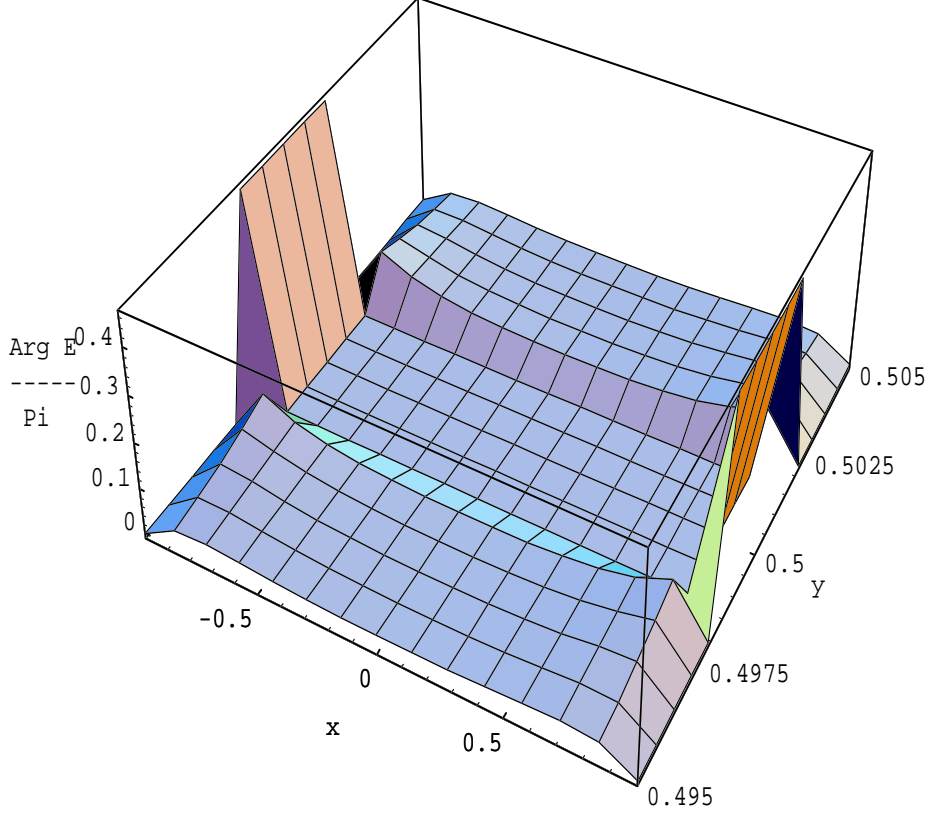


Figure 7.4: Spatial distribution of the argument (in units of π) of \vec{E} for the facet situated between the points 498.5 and 501.5 μm . $L = 1000 \mu\text{m}$, $2w = 40 \mu\text{m}$, $B = 1 \text{ T}$.

shown in Figs. 7.4 and 7.5. One can see that both components of the electric field are small outside the facet region. The field exhibits power law singularity in the diagonally opposite corners of the facet while in the two other corners $\vec{E}(x, y) = 0$. Near the sides of the planar and non-planar regions, $\text{Arg}\vec{E}(x, y)$ is near to zero and ζ , respectively. $\text{Arg}\vec{E}(x, y)$ has local maximum along the y -axis near the edges of the magnetic barrier and sharply drops at the magnetic interface remaining near to zero in the whole non-planar region. The current flows between the ends of the 2DEG crossing the magnetic interfaces mainly in the singular points, *i.e.* it passes along the points for which $\text{Arg}\vec{E}(x, y)$ is close

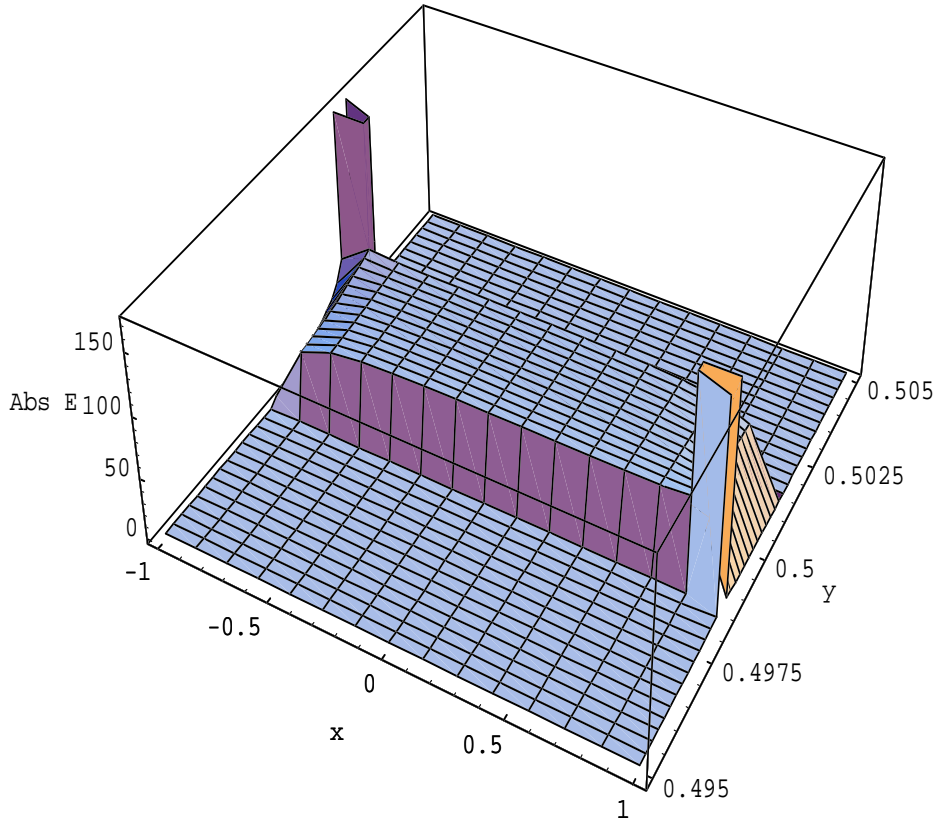


Figure 7.5: Spatial distribution of the absolute value of \vec{E} for the facet situated between the points 498.5 and 501.5 μm . $L = 1000 \mu\text{m}$, $2w = 40 \mu\text{m}$, $B = 1 \text{ T}$.

to zero. Electrons entering or exiting the small regions of the facet corners will have large velocities proportional to the electric field at these locations to account for current conservation with a large number of electrons drifting with slow and uniform velocities in the middle of the facet where the electric field is smaller and uniform. Such an electric field distribution differs from the one in a uniform magnetic field.

The magneto-resistance is determined by the electric field edge profile which is shown in Fig. 7.6 for different values of the magnetic field. The magnetic field dependence of the magneto-resistance across the facet is shown in Fig. 7.7. The classical origin of the positive background has been confirmed experimentally

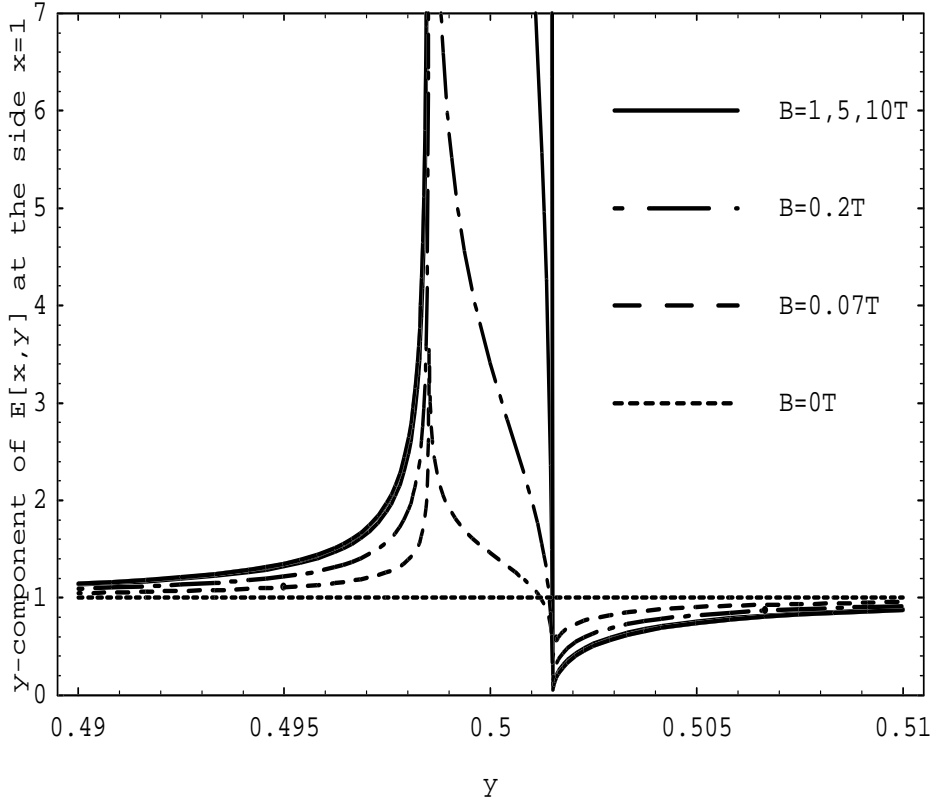


Figure 7.6: The electric field profile at the edge of the 2DEG for different values of the magnetic field.

where it has been found that it persists at temperatures higher than 100 K. Note that experimental configuration is effectively a two terminal measurement where the measured resistance is determined both by the Hall resistance and magneto-resistance. For small magnetic fields the Hall resistance is small and thus the resistance is determined by the magneto-resistance and consequently the resistance increases as B^2 . For larger magnetic fields a quasi-linear behavior of the resistance as a function of B is found which is due to the fact that now it is Hall resistance which mainly limits the current. However, the resistance increases from 13.2 to 1020.8 Ω when $B : 0 \rightarrow 10$ T, which is approximately four times less than observed experimentally. The reason for such a difference could be the low

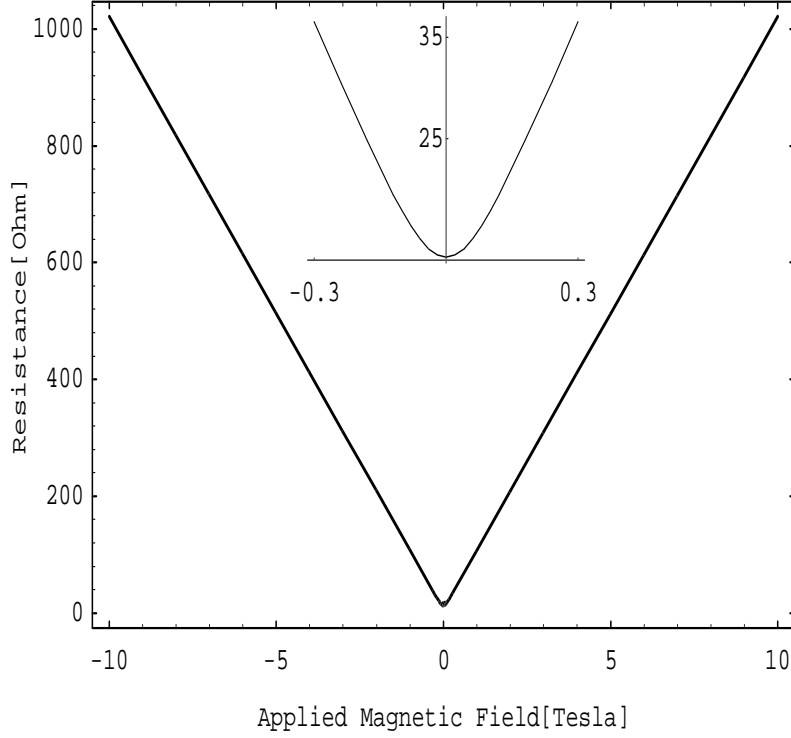


Figure 7.7: Magneto-resistance across the facet corresponding to for $L(3 - 4) = 255 \mu\text{m}$, $L(5 - 6) = 220 \mu\text{m}$, and $L(2 - 3) = 200 \mu\text{m}$.

ratio of the facet ($3 \mu\text{m}$) to the mesa ($1000 \mu\text{m}$) length. The figure Fig. 7.8 shows the magneto-resistance calculated in the planar regions. The top two curves are the resistance for probes above the facet on the left (12-13) and right (3-4) of the mesa and the center two curves show the pairs (10-11) and (5-6) below the facet (see Ref. [59]). In agreement with the experiment, pairs of probes on opposite sides of the mesa and on opposite sides of the facet show the same symmetry while there is a strong asymmetry in each of the traces with reversal of the direction of the magnetic field. These results agree qualitatively with experiment but there are problems with the quantitative values of the resistance. The main variation of the resistance takes place for small B and the magnitude of the variation strongly decreases with distance from the facet. Therefore, in the scale of Fig. 7.8 one

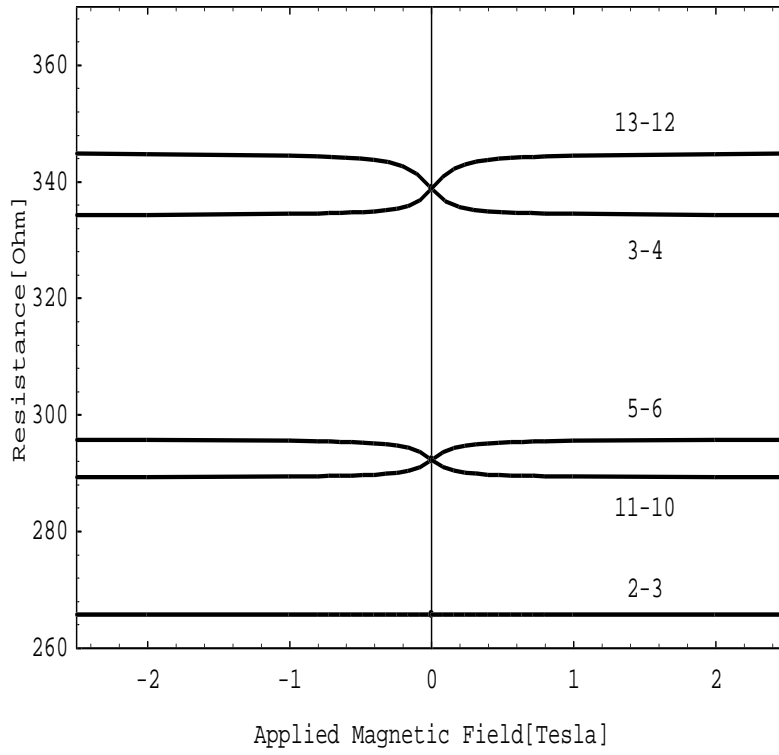


Figure 7.8: Magneto-resistance in the planar regions corresponding to for $L(3 - 4) = 255 \mu\text{m}$, $L(5 - 6) = 220 \mu\text{m}$, and $L(2 - 3) = 200 \mu\text{m}$.

cannot see the resistance variation for probes (2-3) situated $300 \mu\text{m}$ away from the facet.

Chapter 8

Summary

Carrier interaction with phonons, photons, impurities, and electrons have been addressed in semiconductor nanoscale systems with carrier confinement in one and two dimensions subjected to quantizing magnetic fields and without it. Most importantly, our calculations allow to better understand phonon signature in optical, thermalization, and transport experiments that can be used to identify and characterize the basic phenomena of quantum confinement in these quantum nanostructures.

- In the frames of the polaron problem, the peculiarities of the magneto-polaron spectrum near the longitudinal optical phonon emission threshold have been investigated in the 2DEG in the QHE geometry. In spite of weak electron-phonon coupling, an infinite set of new complex quasiparticles, electron-phonon bound states, exists in the magneto-polaron spectrum which is coagulated to the threshold both above and below from it [38, 39].
- The fine structure of cyclotron-phonon resonance due to the electron-phonon bound states has been revealed [40]. Absorption of the electromagnetic field entirely governed by the bound states with the total angular momentum ± 1 . According to the perturbation theory, photon absorption was to be expected at the phonon emission threshold. In reality, the absorption spectrum consists of two groups of peaks which constitute an asymmetric "doublet" relative to the threshold.

- A new method for calculating the probability of electron scattering from the deformation potential of acoustic phonons has been proposed [41]. Such a probability summed over all phonon modes of the layered elastic medium is expressed in terms of the elasticity theory Green function which contains all information about structure geometry.
- Exploiting this method, the relaxation rates for a Fermi 2DEG located in the vicinity of an interface between elastic semi-spaces have been calculated [43]. Analysis of limiting cases for an interface between solid and liquid semi-spaces, for a free and rigid surfaces has shown that there are situations when the phonon reflection from various interfaces alters the energy (or electron temperature) dependence of the relaxation times and leads to a strong reduction of the relation rates.
- The interface effect is obtained to be highest in quantizing magnetic fields [45] since the 2DEG interacts with almost monochromatic cyclotron phonons in this case. The electron transition probability between discrete Landau levels of the 2DEG has an oscillating behavior of the magnetic field and of the distance from the 2DEG to the interface.
- In quantizing magnetic fields, scattering from the piezoelectric potential of acoustic phonons is strongly suppressed with respect to the deformation interaction mechanism [46].
- Emission of ballistic acoustic phonons at electron transitions between fully discrete Landau levels in a 2DEG with account of the phonon reflection from a GaAs/AlGaAs type interface has been studied [49, 50]. In accordance with the experimental results, the angular distribution of emitted phonons has a sharp expressed peak for small angles around the magnetic field. Account for the interface effect affects essentially the intensity and the composition of the detected phonon field. Under the deformation electron-phonon interaction on the sample reverse face, the detector records both the *interference* field of the LA phonons and, which is most intriguing for experiment, the *conversion* field of the TA phonons [49]. Emission of surface acoustic phonons is suppressed exponentially in a wide range of the

magnetic field variation [50].

- Polar optical PO-phonon assisted electron relaxation in the 2DEG in the QHE geometry has been calculated [48]. The surface optical SO phonon relaxation has been obtained to be at least by an order weaker than relaxation via bulk PO phonon emission. Account for the Landau level broadening and for the PO phonon dispersion results to the finite relaxation rates associated with one-phonon emission. The dispersion contribution gives rise to a sharp peak with the peak value approximately 0.17 fs^{-1} . The broadening contribution has a rather broad peak with relatively lower peak value.
- Two-phonon emission is a controlling relaxation mechanism above the phonon energy $\hbar\omega_{PO}$ [48]. Immediately above $\hbar\omega_{PO}$, the PO+DA phonon relaxation rate increases as a B^5 achieving to the peak value exceeding 1 ps^{-1} at energy separations of the order of $\hbar s/a_B$. In the energy range $sa_B^{-1} \lesssim \Delta l\omega_B - \omega_{PO} \lesssim sd^{-1}$, the two-phonon peak decreases linearly in B , so that within the wide energy range of the order of $\hbar\omega_B$, subnanosecond relaxation between Landau levels can be achieved.
- We have calculated the inter edge state scattering length for an arbitrary confining potential [51, 52]. Phonon (deformation acoustic DA and piezoelectric PA interactions) and impurity scatterings are discussed and analytical expressions are derived. As follows from energy and momentum conservation, only phonons with frequencies above some threshold can participate in the transitions between edge states. As a result, phonon scattering is exponentially suppressed at low temperatures. The observed temperature dependence of the scattering length cannot be attributed to phonon scattering.
- Ballistic acoustic phonon emission (both for DA and PA interactions) by quantum edge states has been investigated [54, 53]. At low temperatures the emitted acoustic phonon field is predominantly concentrated within a narrow cone around the direction of the edge state propagation, while at high temperatures – around the magnetic field normal to the electron plane. At low temperatures the emission intensity decreases exponentially with

decreasing filling of Fermi level. The relative contributions of PA and DA interactions depend on the magnetic field, the shape of confining potential, and temperature.

- In recent magneto-luminescence experiments by Potemski *et al.* [55, 56] on one-side modulation doped GaAs/AlGaAs quantum wells, an up-conversion has been observed and interpreted as being due to an Auger process. We have developed a theory of Auger up-conversion in quantum wells in quantizing magnetic fields to explain these experimental results [57, 46]. We have calculated the characteristic times of electron-electron scattering processes between Landau levels of the lowest electric subband and of electron-acoustic phonon scattering between Landau levels of the two lowest electric subbands as well as the lifetime of a test hole with respect to both the Auger process and phonon emission. By analyzing rate equations for these processes as well as for the pumping by interband excitation and the recombination of electrons with photo-induced holes, we have found the Auger process time. As well the magnetic field and the excitation power dependencies of the two luminescence peaks have been obtained which are consistent with the experimental findings. Thus, an understanding of the Auger up-conversion observed in the magneto-luminescence in quantum wells is provided.
- Recently a research group from the Toshiba Cambridge Research Center Ltd. and Cavendish Laboratory have proposed a new technique to produce non-homogeneous magnetic fields [58, 59]. A remotely doped GaAs/Al_xGa_{1-x}As heterojunction is grown over wafer previously patterned with series of facet. The 2DEG is no longer planar but follows the contour of the original wafer. Application of a homogeneous magnetic field to this structure results a spatially varying field component normal to the 2DEG. We have investigated theoretically the magneto-transport of the non-planar 2DEG [63, 64, 65, 66, 67]. The magneto-resistance across the facet as well as in the planar regions of the 2DEG has been calculated which explain the main features of the magnetic field dependence observed experimentally by M L Leadbeater *et al* [59, 60].

Acknowledgements

I thank Prof. Y B Levinson, U Rössler, and F. Peeters for the common work on the problems presented in the dissertation. These were the important stages in my research experience.

I am grateful to Prof. V M Harouthounian for his support during my work in the semiconductor division of YSU.

I am thankful to all my colleagues from Radiophysics and Solid state physics departments of YSU, from the theoretical group of YrPhI, from Institute of Microelectronics in Chernogolovka, from Regensburg and Antwerp Universities. I acknowledge especially to Prof. G W Bryant, L J Challis, A V Chaplik, E M Kazaryan, J Keller, A A Kirakosyan, D L Maslov, A H Melikyan, H R Minasyan, S G Petrosyan, É I Rashba, K F Renk, A G Sedrakyan, and A Shik, for helpful discussions, suggestions, and comments.

Appendix A

In this appendix we collect in a table some physical and material parameters for GaAs/Al_xGa_{1-x}As heterojunction based quantum nanostructures.

Table A.1: Some physical and material parameters used in the dissertation.

Physical and material parameters	GaAs		
Electron effective mass, m_c	$m_c = 0.066m_e$ ¹		
Crystal mass density, ρ [kg m ⁻³]	$\rho = 5.31 \cdot 10^{-3}$		
Long. ac. LA ph. vel. av. in angles, s [m s ⁻¹]	$s = 5.14 \cdot 10^3$		
Trans. ac. TA ph. vel. av. in angles, c [m s ⁻¹]	$c = 3.13 \cdot 10^3$		
Cyclotron energy, $\hbar\omega_B$ [meV]	$1.75B$ [T]		
Magnetic length, a_B [nm]	$25.66B^{-1/2}$ [T]		
Landau level degeneracy, $(2\pi a_B^2)^{-1}$ [m ⁻²]	$2.417 \cdot 10^{14}B$ [T]		
Energy scale, $\hbar s/a_B$ [meV]	$0.13B^{1/2}$ [T]		
Energy scale, $\hbar s/d$ [meV]	$3.37/d$ [nm]		
Subband spacing, $\frac{\hbar^2}{2m_c} \frac{\pi^2}{d^2}$ [meV]	$3.76 \frac{m_e}{m_c} \frac{10}{d[\text{nm}]}^2$		
	Al _x Ga _{1-x} As		
	$x = 0$	$x = 0.3$	$x = 1$
High frequency dielectric constant, κ_∞	10.9	12.0	8.5
Long. opt. LO ph. energy, $\hbar\omega_{LO}$ [meV]	36.62	49.80	50.00
Trans. opt. TO ph. energy, $\hbar\omega_{TO}$ [meV]	33.30	45.10	44.90
Surf. opt. SO ph. energy, $\hbar\omega_{SO}$ [meV]		34.57	34.82
		47.87	47.49
Frölich coupling constant	α_{PO}	α_{SO}/α_{PO}	
	0.07	1.96	1.95
		0.044	0.035

Appendix B

The integrals Φ_m in Eqs. (3.76) are given explicitly by the following formulas.

For the solid state-liquid contact

$$\hat{\Phi}_m(\xi_S, \nu, \mu, \delta, r) = \hat{\Phi}_m^{B_1}(\nu, \mu, \delta) + \hat{\Phi}_m^{B_2}(\nu, \mu, \delta) + \hat{\Phi}_m^L(\nu, \mu, \delta) + \hat{\Phi}_m^S(\xi_S, \nu, \mu, \delta, r) \quad (\text{B.1})$$

where

$$\hat{\Phi}_m^{B_1} = \frac{2^{2+m}}{\pi} \int_0^1 dt t^{2m} \frac{\left(\frac{\delta \nu^4}{\sqrt{\mu^2 - t^2}} + 4 t^2 \sqrt{\nu^2 - t^2} \right)}{(\nu^2 - 2 t^2)^2 + \frac{\delta \nu^4 \sqrt{1 - t^2}}{\sqrt{\mu^2 - t^2}} + 4 t^2 \sqrt{1 - t^2} \sqrt{\nu^2 - t^2}}, \quad (\text{B.2})$$

$$\hat{\Phi}_m^{B_2} = \frac{2^{2+m}}{\pi} \int_1^\nu dt t^{2m} \frac{\left(\frac{\delta \nu^4}{\sqrt{\mu^2 - t^2}} + 4 t^2 \sqrt{\nu^2 - t^2} \right) (\nu^2 - 2 t^2)^2}{\left(\frac{\delta \nu^4 \sqrt{t^2 - 1}}{\sqrt{\mu^2 - t^2}} + 4 t^2 \sqrt{t^2 - 1} \sqrt{\nu^2 - t^2} \right)^2 + (\nu^2 - 2 t^2)^4} \quad (\text{B.3})$$

$$\hat{\Phi}_m^L = \frac{2^{2+m}}{\pi} \int_\nu^\mu dt t^{2m} \frac{\frac{\delta \nu^4}{\sqrt{\mu^2 - t^2}} (\nu^2 - 2 t^2)^2}{\left(4 t^2 \sqrt{t^2 - 1} \sqrt{t^2 - \nu^2} - (\nu^2 - 2 t^2)^2 \right)^2 + \delta^2 \nu^8 \frac{t^2 - 1}{\mu^2 - t^2}} \quad (\text{B.4})$$

$$\hat{\Phi}_m^S = 2^{2+m} \left(\frac{\xi_S}{\nu} \right)^{2m} \frac{\left(q_S - \frac{\delta \xi_S^4}{4r} \right)}{\frac{(p_S - q_S)^2}{p_S q_S} + 2 (p_S - q_S) q_S + \frac{\delta (p_S^2 - r^2) \xi_S^4}{4 p_S r^3}}. \quad (\text{B.5})$$

For the free crystal surface

$$\hat{\Phi}_m(\xi_R, \nu) = \hat{\Phi}_m^{B_1}(\nu) + \hat{\Phi}_m^{B_2}(\nu) + \hat{\Phi}_m^R(\xi_R, \nu) \quad (\text{B.6})$$

where

$$\hat{\Phi}_m^{B_1} = \frac{2^{2+m}}{\pi} \int_0^1 dt t^{2m} \frac{4 t^2 \sqrt{\nu^2 - t^2}}{(\nu^2 - 2 t^2)^2 + 4 t^2 \sqrt{1 - t^2} \sqrt{\nu^2 - t^2}}, \quad (\text{B.7})$$

$$\hat{\Phi}_m^{B_2} = \frac{2^{2+m}}{\pi} \int_1^\nu dt t^{2m} \frac{4 t^2 (\nu^2 - 2 t^2)^2 \sqrt{\nu^2 - t^2}}{(\nu^2 - 2 t^2)^4 + 16 t^4 (\nu^2 - t^2) (t^2 - 1)}, \quad (\text{B.8})$$

$$\hat{\Phi}_m^R = 2^{2+m} \left(\frac{\xi_R}{\nu} \right)^{2m} \frac{p_R q_R^2}{2 p_R (p_R - q_R) q_R^2 + (p_R - q_R)^2}. \quad (\text{B.9})$$

For the rigid boundary

$$\hat{\Phi}_m(\nu) = \hat{\Phi}_m^{B_1}(\nu) + \hat{\Phi}_m^{B_2}(\nu) \quad (\text{B.10})$$

where

$$\hat{\Phi}_m^{B_1} = \frac{2^{2+m}}{\pi} \int_0^1 dt t^{2m} \frac{\sqrt{\nu^2 - t^2}}{t^2 + \sqrt{1 - t^2} \sqrt{\nu^2 - t^2}}, \quad (\text{B.11})$$

$$\hat{\Phi}_m^{B_2} = \frac{2^{2+m}}{\pi} \int_1^\nu dt t^{2m} \frac{t^2 \sqrt{\nu^2 - t^2}}{t^4 + (\nu^2 - t^2)(t^2 - 1)}. \quad (\text{B.12})$$

In formulas (B.1)-(B.12) following notations are introduced

$$\delta = \frac{\rho'}{\rho}, \quad \mu = \frac{s}{s'}, \quad \xi_S = \frac{c_R}{c}, \quad (\text{B.13})$$

$$q = \sqrt{1 - \xi^2}, \quad p = \sqrt{1 - \frac{c^2 \xi^2}{s^2}}, \quad r = \sqrt{1 - \frac{c^2 \xi^2}{s'^2}}. \quad (\text{B.14})$$

In the case of the solid state-liquid contact, when the densities of the contacted semi-spaces differ strongly, we can calculate $\hat{\Phi}_m$ for the extreme value of the parameter $\nu = 1$

$$\hat{\Phi}_0 = 1 + 2\delta(1 - 2\mu^2 + 3\mu^4/2), \quad \hat{\Phi}_0^S = 0, \quad (\text{B.15})$$

$$\hat{\Phi}_0 = 1 + 2\delta\mu^2(1 - 3\mu^2 + 5\mu^4/2), \quad \hat{\Phi}_1^S = 0. \quad (\text{B.16})$$

Notice that in this case, relaxation is determined by the bulk and "leaky" waves. The contribution of the "leaky" waves is proportional to $\delta \ll 1$.

For a free crystal surface taking $\nu = 0.59$ [136] for GaAs, we obtain from the dispersion equation of the Rayleigh waves that $\xi_R \approx 0.917$. Then numerical evaluation of (B.6)-(B.9) gives:

$$\hat{\Phi}_0^{B_1} \approx 0.625, \quad \hat{\Phi}_0^{B_2} \approx 0.297, \quad \hat{\Phi}_0^R \approx 1.706, \quad \hat{\Phi}_0 \approx 2.628, \quad (\text{B.17})$$

and

$$\hat{\Phi}_0^{B_1} \approx 0.873, \quad \hat{\Phi}_0^{B_2} \approx 0.954, \quad \hat{\Phi}_0^R \approx 0.999, \quad \hat{\Phi}_0 \approx 2.826. \quad (\text{B.18})$$

Thus, we see that in the case of energy relaxation, the largest contribution comes from the surface Rayleigh waves while in the case of momentum relaxation, contributions of different phonon modes differ slightly.

Similar calculations for the rigid boundary give

$$\hat{\Phi}_0^{B_1} \approx 1.265, \hat{\Phi}_0^{B_2} \approx 0.452, \hat{\Phi}_0 \approx 1.717, \quad (\text{B.19})$$

and

$$\hat{\Phi}_1^{B_1} \approx 0.852, \hat{\Phi}_1^{B_2} \approx 1.407, \hat{\Phi}_1 \approx 2.259. \quad (\text{B.20})$$

In this case the interface effect is stronger for momentum relaxation.

Bibliography

- [1] *Der Spiegel*, 11:142, 1992.
- [2] L Esaki and R Tsu, editors. *Superlattice and negative conductivity in semiconductors*. RC-2418, IBM Research note, 1969.
- [3] L Esaki. The evolution of semiconductor quantum structures. Do-it-yourself quantum mechanics. In A Stella and L Miglio, editors, *Semiconductor Superlattices and Interfaces*, pages 1–23. North-Holland, Amsterdam, 1993.
- [4] F Capasso, editor. *Physics of Quantum Electron Devices*. Springer-Verlag, Berlin, 1990.
- [5] F Beltram and F Capasso. Artificial semiconductor structures: Electronic properties and device applications. In Paul Butcher, H March Norman, and Mario P Tosi, editors, *Physics of Low-Dimensional Semiconductor Structures*, pages 539–573. Plenum Press, New-York, 1993.
- [6] T Ando, A B Fowler, and F Stern. Electronic properties of two-dimensional systems. *Rev. Mod. Phys.*, 54:437–672, 1982.
- [7] S E Esipov and Y B Levinson. *Adv. Phys.*, 36:331, 1987.
- [8] Paul Butcher, H March Norman, and Mario P Tosi, editors. *Physics of Low-Dimensional Semiconductor Structures*. Plenum Press, New-York, 1993.
- [9] S Chakravarty and A Schmid. Weak localization: The quasiclassical theory of electrons in a random potential. *Phys. Rev.*, 140:193–236, 1986.

- [10] A A Kalfa and A S Tager. Modulation doped heterostructures and their application in shf field transistors. *Electronic technique*, 12(348):26–38, 1982.
- [11] V Karpus. Theoretical limit of mobility of two-dimensional electrons in GaAs. *Semicond. Sci. and Technol.*, 5:691–694, 1990.
- [12] C Weisbuch and B Vinter, editors. *Quantum Semiconductor Structures*. Academic Press, New-York, 1991.
- [13] K von Klitzing, G Dorda, and M Pepper. New method for high-accuracy determination of the fine-structure constant based on quantized Hall resistance. *Phys. Rev. Lett.*, 45:494–497, 1980.
- [14] J Hajdu. Ten years of the quantum Hall effect. In G Landwehr, editor, *High Magnetic Fields in Semiconductor Physics III*, pages 3–16, Berlin, Heidelberg, 1992. Springer-Verlag.
- [15] D C Tsui, H L Störmer, and A C Gossard. Two-dimensional magneto-transport in the extreme quantum limit. *Phys. Rev. Lett.*, 48:1559–1562, 1982.
- [16] H L Störmer, A Chang, D C Tsui, J C M Hwang, A C Gossard, and W Wiegmann. Fractional quantization of the Hall effect. *Phys. Rev. Lett.*, 48:1559–1562, 1982.
- [17] T Chakraborty and P Pietiläinen, editors. *The quantum Hall effects*. Berlin, Berlin, 1995.
- [18] G Landwehr, editor. *High Magnetic Fields in Semiconductor Physics*. Springer-Verlag, Berlin Heidelberg, 1988.
- [19] G Landwehr, editor. *High Magnetic Fields in Semiconductor Physics III*. Springer-Verlag, Berlin Heidelberg, 1992.
- [20] G Landwehr and W Ossau, editors. *High Magnetic Fields in Semiconductor Physics II*. World Scientific, Singapore, 1997.

- [21] R E Prange and S M Girvin, editors. *The Quantum Hall Effect*. Springer-Verlag, New-York Inc., 1990.
- [22] S Komiyama and H Hirai. Two representationd of the current density in charge-transport problems. *Phys. Rev. B*, 54:2067–2090, 1996.
- [23] K von Klitzing. The fine structure constant: A contribution of semiconductor physics to the determination of α . *Festkörperprobleme*, 21:1–23, 1981.
- [24] E Braun, B Schumacher, and P Warnecke. Precision measurements of the quantum Hall effect. In G Landwehr and W Ossau, editors, *High Magnetic Fields in the Physics of Semiconductors II*, pages 1005–1015. World Scientific, Singapore, 1997.
- [25] M Büttiker. The quantum Hall effect in open conductors. In M Reed, editor, *Nanostructured systems*, volume Semiconductors and semimetals V. 35, pages 191–276. Academic Press, New-York, 1989.
- [26] R J Haug. Edge-state transport and its experimental consequences in high magnetic fields. *Semicond. Sci. and Technol.*, 8:131–153, 1993.
- [27] G W Bryant. Electyronic structures of ultrasmall quantum-well boxes. *Phys. Rev. Lett.*, 59:1140–1143, 1987.
- [28] W Wegscheider, L N Pfeiffer, M M Dignam, A Pinczuk, K W West, S L McCall, and R Hull. Lasing from excitons in quantum wires. *Phys. Rev. Lett.*, 71:4071–4074, 1993.
- [29] T Someya, H Akiyama, and H Sakaki. Laterally squeezed excitonic wave functions in quantum wires. *Phys. Rev. Lett.*, 74:3664–3667, 1995.
- [30] Leo Kouwenhoven. Coupled quantum dots as artificial molecules. *Science*, 268:1440–1441, 1995.
- [31] G Lehr, V Harle, F Scholz, and H Schweizer. *Appl. Phys. Lett.*, 68:444–447, 1996.

- [32] U Bockelmann and G Bastard. Phonon scattering and energy relaxation in two-, one-, and zero-dimensional electron gases. *Phys. Rev. B*, **42**:8947–8951, 1990.
- [33] H Benisty, C M Sotomayor-Torres, and C Weisbuch. *Phys. Rev. B*, **44**:10 945–50, 1991.
- [34] E M Shereghii. Role of two-phonon transitions in resonance effects in semiconductors. *Europhys. Lett.*, **18**:325–330, 1992.
- [35] P D Wang and C M Sotomayor Torres. Multiple-phonon relaxation in GaAs-AlGaAs quantum well dots. *J. Appl. Phys.*, **74**:5047–5052, 1993.
- [36] T Inoshita and H Sakaki. Electron relaxation in a quantum dot: Significance of multiphonon processes. *Phys. Rev. B*, **46**:7260–7263, 1992.
- [37] U Bockelmann and T Egeler. Electron relaxation in quantum dots by means of Auger process. *Phys. Rev. B*, **46**:15574–15577, 1992.
- [38] S M Badalyan and A H Melikyan. Threshold anomalies in disintegration of an optic phonon into two acoustic phonons in one dimensional anharmonic crystal. *Sov. Phys. Low Temp.*, **13**:670, 1987.
- [39] S M Badalyan and Y B Levinson. Bound states of electron and optical phonon in a quantum well. *Sov. Phys. JETP*, **67**:641–645, 1988.
- [40] S M Badalyan and Y B Levinson. Cyclotron-phonon resonance in a two dimensional electron gas. *Sov. Phys. Semicond.*, **22**:1278–1281, 1988.
- [41] S M Badalyan and Y B Levinson. Effect of an interface on the scattering of a two dimensional electron gas from acoustic phonons. *Sov. Phys. Solid State*, **30**:1592–1597, 1988.
- [42] S M Badalyan. *Electron-Phonon Interaction in Quasi Two Dimensional Electron Systems*. PhD thesis, Yerevan State University, Yerevan, 1989.
- [43] S M Badalyan. Scattering of electrons in a two dimensional fermi gas by acoustic phonons near an interface between elastic half-spaces. *Sov. Phys. Semicond.*, **3**:1087–1091, 1989.

- [44] S M Badalyan and Y B Levinson. Interface effect on the interaction of a two-dimensional electron gas with acoustic phonons in a quantizing magnetic field. In *Proceedings of 14th All-Union Conference on Theory of Semiconductors*, Donetsk, 1989.
- [45] S M Badalian and Y B Levinson. Free surface effect on the interaction of a two dimensional electron gas with acoustic phonons in a quantizing magnetic field. *Phys. Lett. A*, **140**:62–66, 1989.
- [46] S M Badalian, U Rössler, and M Potemski. Theory of Auger upconversion in quantum wells in a quantizing magnetic field. *J. Physics Cond. Mat.*, **5**:6719–6728, 1993.
- [47] V I Fal’ko and L J Challis. Inter-Landau-level relaxation in two-dimensional electron gases at high magnetic fields. *J. Physics Cond. Mat.*, **5**:3945–3949, 1993.
- [48] S M Badalian. Electron relaxation in the quantum Hall effect geometry: One- and two-phonon processes. *Phys. Rev. B*, **52**:14 781–14 788, 1995.
- [49] S M Badalian and Y B Levinson. Ballistic acoustic phonon emission by a two dimensional electron gas in a quantizing magnetic field with account of the phonon reflection from a GaAs/AlGaAs interface. *Phys. Lett. A*, **155**:200–206, 1991.
- [50] S M Badalian and Y B Levinson. Suppression of the emission of surface acoustic phonons from a two dimensional electron gas a quantizing magnetic field. *Phys. Lett. A*, **170**:229–231, 1992.
- [51] S M Badalian, Y B Levinson, and D L Maslov. Scattering of electron edge states in a magnetic field by impurities and phonons. *Sov. Phys. JETP LETT.*, **53**:595–599, 1991.
- [52] D L Maslov, Y B Levinson, and S M Badalian. Interedge relaxation in a magnetic field. *Phys. Rev. B*, **46**:7002–7010, 1992.

- [53] S M Badalian. Ballistic acoustic phonon emission by quantum edge states. page Abstract 1022, Madrid, 1994. 14th General Conference of the Condensed Matter Division, European Physical Society.
- [54] S M Badalian. Emission of ballistic acoustic phonons by quantum edge states. *J. Physics Cond. Mat.*, **7**:3929–3936, 1995.
- [55] M Potemski, R Stepniewski, J C Maan, G Martinez, P Wyder, and B Etienne. Auger recombination within landau levels in a two-dimensional electron gas. *Phys. Rev. Lett.*, 66:2239–2242, 1991.
- [56] M Potemski, R Stepniewski, J C Maan, G Martinez, P Wyder, and B Etienne. Auger recombination within landau levels in a two-dimensional electron gas. Singapore, 1990. World Scientific.
- [57] S M Badalian, U Rössler, and M Potemski. Theory of Auger up-conversion in quantum wells. In *13th General Conference of the Condensed Matter Division, European Physical Society*, page 1433, Regensburg, Germany, 1993.
- [58] C L Foden, M L Leadbeater, J H Burroughes, and M Pepper. Quantum magnetic confinement in a curved 2deg. *J. Physics Cond. Mat.*, 6:L127–L134, 1994.
- [59] M L Leadbeater, C L Foden, T M Burke, J H Burroughes, M P Grimshaw, D A Ritchie, L L Wang, and M Pepper. Electron transport in a non-uniform magnetic field. *J. Physics Cond. Mat.*, 7:L307–L315, 1994.
- [60] M L Leadbeater, C L Foden, T M Burke, J H Burroughes, M P Grimshaw, D A Ritchie, L L Wang, and M Pepper. Magnetotransport in a non-planar two-dimensional electron gas. *Phys. Rev. B*, 52:R8629–R8632, 1995.
- [61] M L Leadbeater, C L Foden, J H Burroughes, T M Burke, D A Ritchie, and M Pepper. Electron transport in a spatially non-uniform magnetic field. *Phys. Rev. B*, 00:0000–0000, 1996.
- [62] C L Foden, M L Leadbeater, and M Pepper. Quantum magnetic confinement and transport in spherical two-dimensional electron gases. *Phys. Rev. B*, 52:R8646–R8649, 1995.

- [63] S M Badalian, I S Ibrahim, and F M Peeters. Theory of the magneto-transport of electrons in a non-planar two dimensional electron gas. In G Landwehr and W Ossau, editors, *High Magnetic Fields in the Physics of Semiconductors II*, pages 327–330. World Scientific, Singapore, 1997.
- [64] I S Ibrahim, V A Schweigert, S M Badalian, and F M Peeters. Magneto-transport of electrons in a non-homogeneous magnetic field. *Superlattices and Microstructures*, 21, 1997.
- [65] S M Badalian, I S Ibrahim, and F M Peeters. Magneto-transport of electrons in a non-homogeneous magnetic field. In *9th International Conference on the "Superlattices, Microstructures and Microdevices, July 14-19, 1996, (ICSMM-9)*, pages Abstract TuP–52, Liège, Belgium, 1996.
- [66] S M Badalian, I S Ibrahim, and F M Peeters. Theory of the magneto-transport of electrons in a non-planar two dimensional electron gas. In *12th International Conference on the Application of High Magnetic Fields in Semiconductor Physics*, page Abstract TuP 75, Würzburg, Germany, 1996.
- [67] I S Ibrahim, S M Badalian, and F M Peeters. Magneto-transport of electrons through a magnetic barrier. In *Semiconductor-days Meeting in Eindhoven*, Eindhoven, Holland, 1996.
- [68] J T Devreese, editor. *Polarons in Ionic Crystals and Polar Semiconductors*. North-Holland, Amsterdam, 1972.
- [69] J T Devreese and F M Peeters, editors. *Polarons and Excitons in Ionic Crystals and Polar Semiconductors*. Plenum, New-York, 1984.
- [70] T K Mitra, A Chatterjee, and S Mukhoppadhyay. ? *Phys. Reports*, **153**:91, 1987.
- [71] Y B Levinson and É I Rashba. Electron-phonon and exciton-phonon bound states. *Reports on Progress in Phys.*, **36**:1499–1565, 1973.
- [72] Y B Levinson and É I Rashba. Threshold phenomena and bound states in the polaron problem. *Sov. Phys. Usp.*, **111**:683–718, 1973.

- [73] L D Landau and E M Lifshiz. *Quantum Mechanics*. Nauka, Moscow, 1974.
- [74] J Ruwalsds and A Zawadowski. Two-phonon resonances and hybridization of the resonance with single-phonon state. *Phys. Rev. B*, **2**:1172–1175, 1970.
- [75] E J Johnson and D M Larsen. Polaron induced anomalies in the interband magneto-absorption of *InSb*. *Phys. Rev. Lett.*, **16**:655–659, 1966.
- [76] C J Summers, P G Harper, and S D Smith. Polaron coupling and line width studies of cyclotron resonance absorption in *InSb* in the Faraday configuration. *Solid State Commun.*, **55**:615–620, 1967.
- [77] D M Larsen and E J Johnson. Polaron induced anomalies in *InSb*. *J. Phys. Soc. Japan*, **Suppl**, **21**:443–447, 1966.
- [78] P G Harper. The effects of the electron-lattice interaction on the free-carrier magneto-optics of semiconductors. *Proc. Phys. Soc.*, **92**:793–799, 1967.
- [79] L I Korovin. About the role of optic phonons in the interband magneto-optics absorption of semiconductors. *Sov. Phys. JETP*, **53**:1708–1716, 1967.
- [80] P G Harper. Resonant electron-optic mode coupling in polar semiconductors. In J T Devreese, editor, *Polarons in Ionic Crystals and Polar Semiconductors*, pages 301–346. North-Holland, Amsterdam, 1972.
- [81] R A Stradling, P G Harper, and J W Hodby. Electrons and optic phonons in solids – the effects of longitudinal optical lattice vibrations. *Reports on Progress in Phys.*, **36**:1–101, 1973.
- [82] L I Korovin, S T Pavlov, and B E Eshpulatov. The influence of optic phonons on the magneto-optics absorption by two dimensional electron gas. *Sov. Phys. Solid State*, **22**:130–134, 1980.
- [83] S Das Sarma and A Madhukar. Study of electron-phonon interaction and magneto-optical anomalies in two dimensional confined systems. *Phys. Rev. B*, **22**:2823–2836, 1980.

- [84] W Zawadzki. Theory of resonant magneto-polaron in *GaAs/GaAlAs* heterostructure. *Solid State Commun.*, **56**:43–46, 1985.
- [85] F M Peeters and J T Devreese. Energy levels of two and three dimensional polarons in a magnetic field. *Phys. Rev. B*, **31**:3689–3695, 1985.
- [86] M Horst, U Merkt, and J P Kotthaus. Magneto-polarons in a two dimensional electron inversion layer on *InSb*. *Phys. Rev. B*, **50**:754–757, 1983.
- [87] J Singleton, R J Nicholas, and F Nasir. Resonant 2D-magneto-polarons in accumulation layers on *n-Hg_{0.8}Cd_{0.2}Te*. *Solid State Commun.*, **58**:833–838, 1986.
- [88] C C Chang, J G Miches, H H Cheng, R J Nicholas, F M Peeters, X G Wu, W Ossau, J Shen, A Wang, and G Landwehr. A cyclotron resonance study of the resonant polaron coupling in high density CdTe/CdMgTe quantum wells. In G Landwehr and W Ossau, editors, *High Magnetic Fields in the Physics of Semiconductors*, volume 2, pages 809–812, Würzburg, Germany, 29 July-2 August 1996. World Scientific.
- [89] M Horst, U Merkt, W Zawadzki, J C Maan, and K Ploog. Resonant polarons in a *GaAs/GaAlAs* heterostructure. *Solid State Commun.*, **53**:403–405, 1985.
- [90] H Sigg, P Wyder, and J A A J Perenboom. Analysis of polaron effects in the cyclotron resonance of *n*-GaAs and GaAs/GaAlAs heterojunctions. *Phys. Rev. B*, **31**:5253–5261, 1985.
- [91] J Singleton, J A A J Perenboom, and J T. Janssen. Recent high-field investigations of semiconductor nanostructures and other systems at Nijmegen. In G Landwehr, editor, *High Magnetic Fields in Semiconductor Physics III*, pages 686–695, Berlin, Heidelberg, 1992. Springer-Verlag.
- [92] Y J Wang, N A Nickel, B D McCombe, F M Peeters, G Q Hai, Shi J M, and J T Devreese. Resonant magnetopolaron effects in GaAs/AlGaAs MQWs at high magnetic fields. In W Ossau G Landwehr, editor, *High*

- Magnetic Fields in the Physics of Semiconductors*, volume 2, pages 797–800, Würzburg, Germany, 29 July–2 August 1996. World Scientific.
- [93] U Merkt, M Horst, T Evelbauer, and J P Kotthaus. Cyclotron and spin resonance in electron inversion layers on InSb. *Phys. Rev. B*, **34**:7234–7245, 1986.
- [94] Y B Levinson. Electron and phonon bound states in a strong magnetic field. *Sov. Phys. JETP LETT.*, **12**:496–499, 1970.
- [95] Y B Levinson, A Yu Matulis, and L M Shcherbakov. Polaron spectrum in a magnetic field. *Sov. Phys. JETP*, **61**:843–858, 1971.
- [96] L P Pitaevski. On the properties of elementary excitation spectrum near the disintegration threshold of the excitations. *Sov. Phys. JETP*, **366**:1170–1178, 1959.
- [97] F G Bass and Y B Levinson. Cyclotron-phonon resonance in semiconductors. *Sov. Phys. JETP*, **49**:914–924, 1965.
- [98] P K Bakanas, F G Bass, and Y B Levinson. Cyclotron-phonon resonance in semiconductors. *Sov. Phys. Semicond.*, **12**:1457–1481, 1978.
- [99] V I Ivanov-Omskii, L I Korovin, and E M Shereghii. Phonon-assisted cyclotron resonance in semiconductors. *Phys. Stat. Sol. (b)*, **90**:11–32, 1978.
- [100] B D McCombe, S G Bishop, and R Kaplan. Combined resonance and electron g -values in InSb. *Phys. Rev. Lett.*, **18**:748–750, 1967.
- [101] V L Gurevich and Yu A Firsov. On theory of electroconductivity in semiconductors in a magnetic field. *Sov. Phys. JETP*, **40**:199–213, 1961.
- [102] V L Gurevich, Yu A Firsov, and A A Efros. New type of magnetoresistance oscillations of semiconductor and semimetal. *Sov. Phys. Solid State*, **47**:1813–1819, 1962.
- [103] R G Enck, A S Saleh, and H Y Fan. Phonon cyclotron resonance in the infrared absorption in n -type InSb. *Phys. Rev.*, **182**:790–794, 1969.

- [104] B I Bakanas, Y B Levinson, and A Yu Matulis. Fine structure of cyclotron-phonon resonance lines. *Sov. Phys. JETP*, **64**:1065–1070, 1973.
- [105] B Y Kaplan and Y B Levinson. Light absorption by bound states of electrons and phonons in a magnetic field. *Sov. Phys. Solid State*, **14**:1663–1670, 1972.
- [106] R Lassnig. Polar optical interface phonons and Frölich interaction in double heterostructures. *Phys. Rev. B*, **30**:7132–7137, 1984.
- [107] L Wendler. Electron-phonon interaction in dielectric bilayer systems. *Phys. Stat. Sol. (b)*, **129**:513–530, 1985.
- [108] L Wendler and R Pechstedt. Dynamical screening, collective excitations, and electron-phonon interaction in heterostructures and semiconductor quantum well. *Phys. Stat. Sol. (b)*, **141**:129–150, 1987.
- [109] M H Degani and O Hipólito. Electron-phonon interaction effect in a quasi-two-dimensional electron gas in the $GaAs/Ga_{1-x}Al_xAs$. *Phys. Rev. B*, **35**:7717–7720, 1987.
- [110] M H Degani and O Hipólito. Electron-interface-phonon interaction in GaAs-AlAs and InAs-GaSb heterojunctions. *Surf. Sci.*, **196**:459–465, 1988.
- [111] Shi-Wei Gu, Xiao-Jun Kong, and Cheng Wen Wei. Properties of a magnetopolaron at the interface of polar-polar crystals. *Phys. Rev. B*, **36**:7984–7991, 1987.
- [112] N Mori and T Ando. Electron-optical-phonon interaction in single and double heterostructures. *Phys. Rev. B*, **40**:6175–6182, 1990.
- [113] B H Wei, G Z Zhao, and S W Gu. Temperature dependence of cyclotron resonance mass of polaron in a polar crystal slab. *Phys. Rev. B*, **41**:9190–9199, 1991.
- [114] G Q Hai, F M Peeters, and J T Devreese. Polaron-cyclotron-resonance spectrum resulting from interface- and slab-phonon modes in a GaAs/AlAs quantum well. *Phys. Rev. B*, **47**:10358–10374, 1993.

- [115] R J Nicholas, L C Brunel, S Huant, K Karrai, J C Portal, M A Brummel, K Y Cheng, and A Y Cho. Frequency-shifted polaron coupling in $Ga_{0.47}In_{0.53}As$ heterojunction. *Phys. Rev. B*, **55**:883–886, 1985.
- [116] S Das Sarma. Frequency-shifted polaron coupling in GaInAs heterojunction. *Phys. Rev. B*, **57**:651, 1986.
- [117] E M Lifshiz and L P Pitaevski. *Statistical Physics*, volume **2**. Nauka, Moscow, 1978.
- [118] Y B Levinson, A Yu Matulis, and L M Shcherbakov. Gauge invariant diagram technique in a magnetic field. *Sov. Phys. JETP*, **60**:859–866, 1971.
- [119] T Holstein. Theory of transport phenomena in an electron-phonon gas. *Ann. of Phys.*, **29**:410–535, 1964.
- [120] L Dworin. Transverse conductivity of a degenerate system of Landau electrons and optical phonons. *Phys. Rev. A*, **140**:1689–1704, 1965.
- [121] H Frölich. Electrons in lattice fields. *Advances in Phys.*, **3**:325–361, 1954.
- [122] M V Klein. Phonons in semiconductor superlattices. *IEEE J. Quantum Electron.* **QE**, **22**:1760–1770, 1986.
- [123] C Colvard, T A Gant, M V Klein, R Merlin, R Fisher, H Morkoc, and A C Gossard. Folded acoustic and quantized optic phonons in (GaAl)As superlattices. *Phys. Rev. B*, **31**, 1985.
- [124] L I Korovin and B E Eshpulatov. Interband magneto-optic absorption at the surface layer of a semiconductor. *Sov. Phys. Semicond.*, **21**:3703–3712, 1979.
- [125] F F Fang and W E Howard. Negative field-effect mobility on (100) Si surfaces. *Phys. Rev. Lett.*, **16**:797–799, 1966.
- [126] F Stern and W E Howard. Properties of semiconductor surface inversion layers in the electric quantum limit. *Phys. Rev.*, **163**:816–835, 1967.

- [127] B Y Kaplan and Y B Levinson. Electron and phonon bound states in a magnetic field. *Sov. Phys. Solid State*, **14**:1412–1422, 1972.
- [128] I M Gelfand. *Lectures in Linear Algebra*. Nauka, Moscow, 1971.
- [129] A O Gelfond. *Supplement to Y. W. Lovitt's book "Linear Integral Equations"*. GITTL, Moscow, 1957.
- [130] S Adachi. Properties of aluminum gallium arsenide. *J. Appl. Phys.*, **58**:R1, 1985.
- [131] D Levi, Shu-Lin Zhang, M V Klein, J Klem, and H Morcos. Raman study of the effects of annealing on folded LA and confined LO phonons in GaAs/AlAs superlattices. *Phys. Rev. B*, **36**:8032–8037, 1988.
- [132] B Jusserand, D Paquet, and A Regreny. Folded optical phonons in GaAs/GaAlAs superlattices. *Phys. Rev. B*, **30**:6245–6247, 1984.
- [133] A K Sood, J Menéndez, M Cardona, and K Ploog. Resonance raman scattering by confined LO and TO phonons in GaAs/AlAs superlattices. *Phys. Rev. Lett.*, **54**:2111–2118, 1985.
- [134] C Colvard, T A Gant, M V Klein, R Merlin, R Fischer, H Morcos, and A C Gossard. Folded acoustic and quantized optic phonons in GaAs/AlAs superlattices. *Phys. Rev. B*, **31**:2080–2091, 1985.
- [135] A A Abrikosov. *Basics of Metal Theory*. Nauka, Moscow, 1987.
- [136] V F Gantmakher and Y B Levinson. *Carrier Scattering in metals and Semiconductors*. Nauka, Moscow, 1984.
- [137] R Dingle, H L Störmer, A C Gossard, and W Wiegmann. Electron mobilities in modulation-doped semiconductor heterojunction superlattices. *Appl. Phys. Lett.*, **33**:655–667, 1978.
- [138] H L Störmer, A Pinczuk, A C Gossard, and W Wiegmann. Influence of undoped AlGaAs spacer on mobility enhancement in GaAs-AlGaAs superlattices. *Appl. Phys. Lett.*, **38**:691–693, 1981.

- [139] J J Drumond, H Markoc, K Hess, and A Y Cho. Experimental and theoretical electron mobility of modulation doped AlGaAs/GaAs heterostructures grown by molecular beam epitaxy. *J. Appl. Phys.*, **52**:5231–5234, 1981.
- [140] V K Arora and A Naeem. Phonon-scattering-limited mobility in a quantum well heterostructure. *Phys. Rev. B*, **31**:3887–3892, 1985.
- [141] P K Basu and B R Nag. Piezoelectric scattering in quantized surface layers in semiconductors. *J. Physics C*, **14**:1519–1522, 1981.
- [142] F F Fang and A B Fowler. Hot electron effects and saturation velocities in silicon inversion layers. *J. Appl. Phys.*, **41**:1825–1831, 1970.
- [143] B K Ridley. The electron-phonon interaction in quasi-two-dimensional semiconductor quantum well structures. *J. Physics C*, **15**:5899–5917, 1982.
- [144] H Sakaki, K Hirakawa, J Yoshino, and S P Svensson. Effects of electron eating on the two dimensional magneto transport in GaAlAs-GaAs heterostructures. *Surf. Sci.*, **142**:306–313, 1984.
- [145] E E Mendez and P J Price. Temperature of the electron mobility in GaAlAs-GaAs heterostructures. *Appl. Phys. Lett.*, **45**:294–296, 1984.
- [146] Y Kawaguchi and S Kawaji. Lattice scattering mobility of n -inversion layers in Si(100) at low temperatures. *Appl. Phys. Lett.*, **45**:294–296, 1984.
- [147] H Ezawa, S Kawaji, and K Nakamura. Surfons and the electron mobility in silicon inversion layers:. *Jap. J. Appl. Phys.*, **13**:126–155: Errata Jap. J. Appl. Phys. 175. V.14. N.6. P.921–922, 1974.
- [148] Y Shinba, K Nakamura, M Fukuchi, and M Sakata. Hot electrons in Si(100) inversion layers at low lattice temperatures. *J. Phys. Soc. Japan*, **51**:157–163, 1982.
- [149] L I Glazman. Low temperature absorption of the strong electromagnetic wave by electrons of inversion layers. *Sov. Phys. Low Temp.*, **8**:617–625, 1982.

- [150] A L Vartanyan and A A Kirakosyan. Effect of inhomogeneity of an elastic medium on the phonon relaxation mechanism of two-dimensional carriers. *Sov. Phys. Semicond.*, **23**:1146–1151, 1989.
- [151] V F Gantmakher and Y B Levinson. *Carrier Scattering in metals and Semiconductors*. North-Holland, Amsterdam, Oxford, New-York, Tokyo, 1987.
- [152] A A Maradudin and D L Mills. The attenuation of Rayleigh surface waves by surface roughness. *Ann. of Phys.*, **100**:262–309, 1976.
- [153] V M Aroutjounian. Physical properties of the semiconductor-electrolyte boundary. *Sov. Phys. Usp.*, **159**:255–291, 1989.
- [154] A Tardella and J N Chazalviel. Highly accumulated electron layer at a semiconductor/electrolyte interface. *Phys. Rev. B*, **32**:2439–2448, 1985.
- [155] Y B Levinson. Electrons on the surface of the cryogenic crystals: Scattering on the lattice vibrations. *Sov. Phys. JETP*, **95**:698–708, 1989.
- [156] M G Cottam and A A Maradudin. Surface linear response functions. In V M Agranovich and R Laudon, editors, *Surface Excitations*, pages 1–194. Elsevier Science Publ., 1984.
- [157] B Djafari-Rouhani, L Dobrynzki, and R F Wallis. Elastic continuum theory of interface-atom mean-square displacements. *Phys. Rev. B*, **16**:741–749, 1977.
- [158] R Stoneley. Elastic waves at the surface of separation of two solids. In *Proc. Royal Society*, volume **106**, pages 416–445, 1924.
- [159] I A Viktorov. *Sound Surface Waves in Solid States*. Nauka, Moscow, 1981.
- [160] V T Gogoladze. In *Proc. of the Seismology Institute of the Academy of Sciences of the USSR*, pages 31–49, 1948, V. 127.
- [161] L M Brekhovskikh. *Waves in Layered Media*. Nauka, Moscow, 1973.

- [162] V Karpus. Energy and momentum relaxation of two dimensional carriers at the interaction with deformation acoustic phonons. *Sov. Phys. Semicond.*, **20**:12–19, 1986.
- [163] K Hirakawa and H Sakaki. Energy relaxation of two dimensional electrons and deformation potential constant in selectively doped AlGa As/Ga As heterojunctions. *Appl. Phys. Lett.*, **49**:889–891, 1986.
- [164] V T Dolgoplov, A A Shashkin, S I Dorojkin, and E A Vydrov. Energy relaxation time in a two dimensional electron gas at the surface of (001) silicon. *Sov. Phys. JETP*, **89**:2113–2123, 1985.
- [165] P J Price. Hot electrons in a GaAs heterolayer at low temperature. *J. Appl. Phys.*, **53**:6863–6866, 1982.
- [166] K Hess, T Englert, Neugebauer T, G Landwehr, and G Dorda. Hot carrier effects in high magnetic fields in silicon inversion layers at low temperatures: *p*-channel. *Phys. Rev. B*, **16**:3652–3659, 1977.
- [167] H Ezawa. Phonons in a half space. *Ann. of Phys.*, **67**:5438–5460, 1971.
- [168] L Eaves and F W Sheard. Size-dependent quantized break-down of the dissipationless quantum Hall effect. *Semicond. Sci. and Technol.*, **6**:346–349, 1986.
- [169] O Heinonen, P L Taylor, and S M Girvin. Electron-phonon interaction and breakdown of the dissipationless quantum Hall effect. *Phys. Rev. B*, **30**:3016–3019, 1984.
- [170] É I Rashba and V B Timofeev. Quantum hall effect. *Sov. Phys. Semicond.*, **20**:977–1024, 1986.
- [171] H A J M Reinen, T T J M Berendschot, R J H Kappert, and H J A Bluyssen. Electron-phonon interaction of a two-dimensional electron gas in a strong magnetic field. *Solid State Commun.*, **65**:1495–1499, 1988.
- [172] H Kitagawa and S Tamura. Radiation of ballistic phonons from two-dimensional electrons in si-metal-oxide-semiconductor structures: Interference effects of emitted phonons. *Phys. Rev. B*, **46**:4277–4280, 1992.

- [173] M Prasad and M Singh. Electron-phonon scattering in the presence of a magnetic field in quasi-two-dimensional quantum-well structures. *Phys. Rev. B*, **29**:4803–4806, 1984.
- [174] L J Challis, G A Toombs, and F W Sheard. Acoustic phonon interaction with a two-dimensional electron gas (2DEG). In T Paszkiewics, editor, *Physics of Phonons*, pages 348–374. Springer-Verlag, Berlin, 1987.
- [175] L J Challis. Phonon emission, absorption, and reflection from a two-dimensional electron gas. In Paul Butcher, H March Norman, and Mario P Tosi, editors, *Physics of Low-Dimensional Semiconductor Structures*, pages 441–461. Plenum Press, New-York, 1993.
- [176] G A Toombs, F W Sheard, D Neilson, and L J Challis. Phonon emission by a hot two dimensional electron gas in a quantizing magnetic field. *Solid State Commun.*, **64**:577–581, 1987.
- [177] M Rothenfusser, L Köster, and W Dietsche. Phonon emission spectroscopy of a two-dimensional electron gas. *Phys. Rev. B*, **34**:5518–5524, 1986.
- [178] J C Hensel, B J Halperin, and R C Dynes. Dynamical model for the absorption and scattering of ballistic phonons by the electron inversion layer in silicon. *Phys. Rev. Lett.*, **51**:2302–2305, 1983.
- [179] M A Chin, V Narayanamurti, H L Störmer, and J C M Hwang. Phonon emission and electron heating in a two-dimensional electron gas. In *Phonon scattering in condensed matter*, pages 141–144. Springer-Verlag, Berlin, 1984.
- [180] E. Vass. Theory of the spectral acoustic phonon emission intensity of hot 2D electrons in quantized n -inversion layers. *Solid State Commun.*, **61**:127–131, 1987.
- [181] K Hess and P Vogl. Remote polar phonon scattering in silicon inversion layers. *Solid State Commun.*, **30**:807–809, 1979.
- [182] P J Price. Two-dimensional electron transport in semiconductor layers. Phonon scattering. *Ann. Phys. (N.Y.)*, **133**:217–239, 1981.

- [183] P J Price. *Surf. Sci.*, **113**:199, 1981.
- [184] P J Price. *Phys. Rev. B*, **30**:2234, 1984.
- [185] F A Riddoch and B K Ridley. *J. Physics C*, **16**:6971, 1983.
- [186] J Shah, A Pinczuk, A C Gossard, and W Wiegmann. Hotcarrier energy loss rates in GaAs quantum wells: Large differences between electrons and holes. *Physica B+C*, **134**:174–178, 1985.
- [187] S Das Sarma and B A Mason. Degeneracy and screening effects on hot electron relaxation in quantum heterostructures. *Physica B+C*, 134:301–304, 1985.
- [188] F A Riddoch and B K Ridley. Phonon scattering of electrons in quasi-one dimensional quantum wells. *Surf. Sci.*, 142:260–165, 1984.
- [189] B K Ridley. The electron-phonon interaction in quasi-two-dimensional semiconductor quantum well structures. *Phys. Rev. B*, **39**:5282, 1989.
- [190] N Sawaki. Interaction of two-dimensional electrons and polar optical phonons in a superlattice. *Surf. Sci.*, **170**:537–541, 1986.
- [191] S Rudin and T L Reinecke. Electron-LO-phonon scattering rates in semiconductor quantum wells. *Phys. Rev. B*, **41**:7713–7717, 1990.
- [192] S Das Sarma and B A Mason. Screening of polar interaction in quasi-two-dimensional semiconductor microstructures. *Phys. Rev. B*, **31**, 1985.
- [193] X G Wu, F M Peeters, and J T Devreese. *Phys. Rev. B*, **34**:8800, 1986.
- [194] X G Wu, F M Peeters, and J T Devreese. *Phys. Rev. B*, **36**:9765, 1987.
- [195] F M Peeters, X G Wu, and J T Devreese. *Surf. Sci.*, **196**:437, 1988.
- [196] Th Englert, D C Tsui, J C Portal, J Beerens, and A C Gossard. Magneto-phonon resonances of the two-dimensional electron gas in GaAs/AlGaAs heterostructures. *Solid State Commun.*, **44**:1301–1304, 1982.
- [197] R Lassnig and W Zawadzki. *J. Physics C*, **16**:5435, 1983.

- [198] R Lassnig and W Zawadzki. *Surf. Sci.*, **142**:361, 1984.
- [199] P Vasilopoulos. *Surf. Sci.*, **33**:8587, 1986.
- [200] N Mori, H Murata, K Taniguchi, and C Hamaguchi. *Surf. Sci.*, **38**:7672, 1988.
- [201] P Hawker, A J Kent, L J Challis, M Henini, and O H Hughes. Magnetophonon resonance effects in the phonon emission by a hot two-dimensional electron gas in a GaAs-AlGaAs heterojunction. *J. Physics Cond. Mat.*, **1**:1153–1158, 1989.
- [202] P Warmenbol, F M Peeters, X G Wu, and J T Devreese. Magnetophonon effect in the energy relaxation rate of electrons in a GaAs heterostructure. *Phys. Rev. B*, **40**:6258–6264, 1989.
- [203] Y. Galvao Gobato *et al.* *Phys. Rev. B*, **43**:4843, 1991.
- [204] Y. Galvao Gobato *et al.* *Phys. Rev. B*, **44**:13795, 1991.
- [205] W Knap. Private communication. 1995.
- [206] Y Levinson and W Knap. Private communication. 1995.
- [207] R Kubo, S J Miyake, and N Hashitume. In F Seitz and D Turnbull, editors, *Solid State Physics, Vol. 17*. Academic Press, 1965.
- [208] F F Fang, T P Smith, and S L Wright. Landau level broadening and scattering time in modulation doped AlGa As/Ga As heterostructures. *Surf. Sci.*, **196**:310–315, 1988.
- [209] S Das Sarma and F Stern. *Phys. Rev. B*, **32**:8448, 1985.
- [210] F Stern. Self-consistent result for *n*-type Si inversion layers. *Phys. Rev. B*, **5**:4891–4899, 1972.
- [211] A Wixforth and J P Kothaus. In G Landwehr, editor, *High magnetic fields in semiconductor physics*, page 8448. Springer-Verlag, 1988.

- [212] A L Efros and Galperin. Quantization of the acoustoelectric current in a two-dimensional electron system in a strong magnetic field. *Phys. Rev. Lett.*, 64:1959–1962, 1990.
- [213] V W Rampton, K McEnaney, A G Kozorezov, P J A Carter, C D W Wilkinson, M Henini, and O H Hughes. Surface acoustic wave attenuation by localized electrons in a 2DEG at a GaAs/AlGaAs heterojunction. *Semicond. Sci. and Technol.*, **7**:641–647, 1992.
- [214] Seiji Mizuno and Shin ichiro Tamura. Resonant interaction of phonons with surface vibrational modes in a finite size superlattice. *Phys. Rev. B*, **53**:4549–4552, 1996.
- [215] A Knäbchen and Y B Levinson. Surface acoustic wave attenuation by a two-dimensional electron gas in a strong magnetic field. *Phys. Rev. B*, To be published:00–00, 1997.
- [216] S Tamura and H Kitagawa. Two-dimensional electron-acoustic-phonon interaction at high magnetic fields: Thermal conductance in GaAs/AlGaAs heterostructures. *Phys. Rev. B*, **40**:8485–8489, 1989.
- [217] M Buttiker. Absence of backscattering in the quantum Hall effect in multiprobe conductors. *Phys. Rev. B*, 38:9375–9389, 1988.
- [218] R B Laughlin. Quantized Hall conductivity in two dimensions. *Phys. Rev. B*, 23:5632–5633, 1981.
- [219] B I Halperin. Quantized Hall conductance, current-carrying edge states, and the existence of extended states in a two-dimensional disordered potential. *Phys. Rev. B*, 25:2185–2190, 1982.
- [220] A H MacDonald and P Streda. Quantized Hall effect and edge currents. *Phys. Rev. B*, 29:1616–1619, 1984.
- [221] A J Kent, D J McKitterick, L J Challis, P Hawker, C J Mellor, and M Henini. Imaging nonequilibrium phonon-induced backscattering in the quantum Hall regime. *Phys. Rev. Lett.*, 69:1684–1686, 1992.

- [222] B J van Wees, E M M Willems, C J P M Harmans, C W J Bennakker, H van Houten, J G Williamson, C T Foxon, and J J Harris. Anomalous integer quantum Hall effect in the ballistic regime with quantum point contacts. *Phys. Rev. Lett.*, 62:1181–1184, 1989.
- [223] S Komiyama and S Hiyamizu. *Phys. Rev. B*, 40:12566, 1989.
- [224] G Müller, D Weiss, S Koch, K von Klitzing, H Nickel, W Schlapp, and R Losch. *Phys. Rev. B*, 42:7633, 1990.
- [225] G Müller, D Weiss, A V Khaetskii, K von Klitzing, S Koch, H Nickel, W Schlapp, and R Löscher. Equilibration length of electrons in spin-polarized edge channels. *Phys. Rev. B*, 45:3932–3935, 1992.
- [226] S Komiyama, H Hirai, S Sasa, and T Fujii. *Solid State Commun.*, 73:91, 1990.
- [227] S Komiyama, H Hirai, M Oshawa, H Matsuda, S Sasa, and T Fujii. Inter-edge-state scattering and nonlinear effects in a two-dimensional electron gas at high magnetic fields. *Phys. Rev. B*, 45:11085–11107, 1992.
- [228] L P Kowenhoven, F W J Hekking, B J van Wees, , C J P M Harmans, C E Timmering, and C T Foxon. Transport through a finite one-dimensional crystal. *Phys. Rev. Lett.*, 65:361–364, 1990.
- [229] B W Alphenaar, P L McEuen, R G Wheeler, and R N Sacks. Selective equilibration among the current-carrying states in the quantum Hall regime. *Phys. Rev. Lett.*, 64:677–680, 1990.
- [230] L I Glazman and M Jonson. *J. Physics Cond. Mat.*, 1:5547, 1989.
- [231] Y B Levinson and E V Sukhorukov. *Phys. Lett. A*, 149:167, 1990.
- [232] T Martin and S Feng. Suppression of scattering in electron transport in mesoscopic quantum Hall systems. *Phys. Rev. Lett.*, 64:971–974, 1990.
- [233] A V Khaetskii and K A Matveev. *Phys. Rev. B*, 4:3491, 1992.
- [234] S Das Sarma and F Stern. *Phys. Rev. B*, 32:8442, 1985.

- [235] P T Coleridge, R Stoner, and R Fletcher. *Phys. Rev. B*, 39:1120, 1989.
- [236] F Dietzel, W Dietsche, and K Ploog. Electron-phonon interaction in the quantum Hall effect regime. *Phys. Rev. B*, 00:00–00, 1993.
- [237] F Dietzel. *Electron-Phonon-Wechselwirkung im Bereich des Quantum-Hall-Effects*. PhD thesis, Max-Planck-Institut für Festkörperforschung, Stuttgart, 1992.
- [238] A Ya Shik and L J Challis. Electron-phonon energy relaxation in quasi-one-dimensional electron systems in zero and quantizing magnetic fields. *Phys. Rev. B*, 47:2082–2088, 1993.
- [239] M Msale and N C Constantinou. Electron-LO-phonon scattering in a cylindrical quantum wire with an axial magnetic field: Analytic results. *Phys. Rev. B*, 48:11 129–11 134, 1993.
- [240] N Telang and S Bandyopadhyay. Effects of a magnetic field on electron-phonon scattering in quantum wires. *Phys. Rev. B*, 48:18 002–18 009, 1993.
- [241] T Ando. *J. Phys. Soc. Japan*, 51:3900, 1982.
- [242] N J M Horing and M Y Yildiz. Quantum theory of longitudinal dielectric response properties of two-dimensional plasma in a magnetic field. *Ann. Phys. (N.Y.)*, 97:216–241, 1976.
- [243] E Gornik, R Lassnig, G Strasse, H L Stormer, A C Gossard, and W Wiegmann. *Phys. Rev. Lett.*, 54:1820, 1985.
- [244] J P Eisenstein, H L Stormer, V Narayanamurti, A Y Cho, A C Gossard, and C W Tu. *Phys. Rev. Lett.*, 55:875–878, 1985.
- [245] E Stahl, D Weiss, G Weimann, K von Klitzing, and K Ploog. *J. Physics C*, 18:L783, 1985.
- [246] I V Kukushkin and V B Timofeev. magnetic field and screening of the random potential. *Sov. Phys. JETP*, 66:613, 1987.
- [247] L I Glazman and I A Larkin. *Phys. Rev. B*, 6:32, 1991.

- [248] T Martin and S Feng. Edge state scattering. *Phys. Rev. B*, 44:9084–9091, 1991.
- [249] Sh M Kogan. *Sov. Phys. Solid State*, 4:1813, 1962.
- [250] J D Zook. *Phys. Rev. A*, 136:869, 1964.
- [251] S E Laux, D J Frank, and F Stern. Quasi-one-dimensional electron states in a split-gate GaAs/AlGaAs heterostructures. *Surf. Sci.*, 196:101–106, 1988.
- [252] P T Landsberg. The band-band Auger effect in semiconductors. *Solid State Electron.*, 30:1107–1115, 1987.
- [253] A Haug. Auger recombination in quantum well semiconductors: calculation with realistic energy bands. *Semicond. Sci. and Technol.*, 7:1337–1340, 1992.
- [254] C Smith, R A Abram, and M G Burt. Auger recombination in a quantum well heterostructures. *J. Physics C*, 16:L171–L175, 1983.
- [255] Masumi Takeshima. Auger recombination in a quasi-one-dimensional-structure semiconductor. *Phys. Rev. B*, 31:992–999, 1984.
- [256] H Stolz and R Zimmermann. Correlated pairs in two-component fermi systems. *Phys. Stat. Sol. (b)*, 94:135–146, 1979.
- [257] A Hangleiter and R Haecker. Enhancement of band-to-band Auger recombination by electron-hole correlations. *Phys. Rev. Lett.*, 65:215–218, 1990.
- [258] A Hangleiter. In *20th International Conference on Physics of Semiconductors*, page 2566, Thessaloniki, 1990. World Scientific, Singapore.
- [259] S Borenstain and J Katz. Intersubband Auger recombination and population inversion in quantum-well subbands. *Phys. Rev. B*, 39:10852–10857, 1989.
- [260] J L Pan. Reduction of the Auger rate in semiconductor quantum dots. *Phys. Rev. B*, 46:3977–3997, 1992.

- [261] A M Zlobin and P S Zyryanov. Effect of a quantizing magnetic field on electron-electron collisions in semiconductors and nonlinear galvanomagnetic phenomena. *Sov. Phys. JETP*, 31:513–517, 1970.
- [262] I Maran, W Seidenbuch, E Gornik, G Weimann, and M Shayegan. *Semicond. Sci. and Technol.*, 9:700, 1994.
- [263] A Yacoby, U Sivan, C P Umbach, and J M Hong. *Phys. Rev. Lett.*, 64:1938, 1991.
- [264] S Bar-Ad, I Bar-Joseph, Y Levinson, and H Shtrikman. *Phys. Rev. Lett.*, 72:776, 1994.
- [265] P J Price. Hot phonon effects in heterolayers. *Physica*, 134 B:164–168, 1985.
- [266] B Laikhtman and P M Solomon. *Phys. Rev. B*, 41:9921, 1990.
- [267] T J Gramila, J P Eisenstein, A H MacDonald, L N Pfeiffer, and K W West. *Phys. Rev. Lett.*, 66:1216, 1991.
- [268] S A Trugman. *Phys. Rev. B*, 27:7539, 1987.
- [269] L D Landau and Pomeranchuk. *Phys. Z. Sowjetunion*, 10:649, 1936.
- [270] A V Chaplik. *Sov. Phys. JETP*, 33:997, 1971.
- [271] G F Giuliani and J J Quinn. *Phys. Rev. B*, 26:4421, 1982.
- [272] A Schmid. *Z. Phys.*, 271:1974, 1974.
- [273] B L Altshuler and A A Aronov. Electron density of states and energy relaxation time in magnetic fields. *Solid State Commun.*, 38:11–15, 1981.
- [274] Y Levinson. Electron-electron scattering in a two-dimensional electron gas in a strong magnetic field. *Phys. Rev. B*, 51:16 898–16 906, 1995.
- [275] E Gornik. In J T Devreese and F M Peeters, editors, *The Physics of the two-dimensional electron gas*. Plenum-Press, New-York, 1987.

- [276] S Das Sarma and X C Xie. *Phys. Rev. Lett.*, 61:738, 1995.
- [277] L J Challis, A J Kent, and V W Rampton. Phonon emission and scattering in a two-dimensional electron gas in quantizing magnetic fields. *Semicond. Sci. and Technol.*, 5:1179–1185, 1990.
- [278] T Ando. Theory of quantum transport in a two-dimensional electron system under magnetic fields. iii. Many-site approximation. *J. Phys. Soc. Japan*, 37:622–630, 1974.
- [279] W H Knox, D S Chemla, G Livescu, J E Cunningham, and J E Henry. Femtosecond carrier thermalization in dense fermi seas. *Phys. Rev. Lett.*, 61:1290–1293, 1988.
- [280] A Erdélyi. *Asymptotic expansions*. Dover Publications, Inc., New York, 1956.
- [281] A Erdélyi. Asymptotic expansions. *J. Soc. Industr. Appl. Math.*, 3:17–27, 1955.
- [282] C W J Beenakker and H van Houten. Quantum transport in semiconductor nanostructures. In H Ehrenreich and D Turnbull, editors, *Solid State Physics*, volume 44, pages 1–228. Academic Press, San-Diego, 1991.
- [283] T Chakrabarty and P Pietiläinen, editors. *The Quantum Hall Effect*. Springer-Verlag, Berlin, 1995.
- [284] Y Aharonov and D Bohm. Significance of electronic potentials in quantum theory. *Phys. Rev.*, 115:485–491, 1959.
- [285] S Washburn and R A Webb. Aharonov-Bohm effect in normal metal quantum coherence and transport. *Adv. Phys.*, 35:375–422, 1986.
- [286] D Weiss, K von Klitzing, K Ploog, and G Weimann. *Europhys. Lett.*, 8:179, 1989.
- [287] R R Gerhardts, D Weiss, and K von Klitzing. Novel magnetoresistance oscillations in a periodically modulated two-dimensional electron gas. *Phys. Rev. Lett.*, 62:1173–1176, 1989.

- [288] R W Winkler, J P Kotthaus, and K Ploog. Landau-band conductivity in a two-dimensional electron system modulated by an artificial one-dimensional superlattice potential. *Phys. Rev. Lett.*, 62:1177–1180, 1989.
- [289] F M Peeters. Microscopic magnetic manipulation of electron motion. *Physics World*, October:24–25, 1995.
- [290] H Silberbauer, P Rotter, U Roessler, and M Suhrke. Quantum chaos in magnetic band structures. *Europhys. Lett.*, 31:393–398, 1995.
- [291] H Silberbauer, P Rotter, M Suhrke, and U Roessler. Quantum transport and quantum chaos in antidot superlattices in a magnetic field. *Semicond. Sci. and Technol.*, 9:1906–1911, 1994.
- [292] W Kang, L N Stömer, L N Pfeifer, K W Baldwin, and K W West. *Phys. Rev. Lett.*, 71:3850–3146, 1993.
- [293] R L Willet, R R Ruel, K W West, and L N Pfeifer. Experimental demonstration of a fermi surface at one-half filling of the lowest london level. *Phys. Rev. Lett.*, 71:3846–3849, 1993.
- [294] A Matulis, F M Peeters, and P Vasilopoulos. Wave-vector-dependent tunneling through magnetic barriers. *Phys. Rev. Lett.*, 72:1518–1521, 1994.
- [295] B A Dubrovin and S P Novikov. *Sov. Phys. JETP*, 52:511, 1980.
- [296] Hideo Yoshioka. Effect of magnetic field on the conductance of ballistic quantum wire. *J. Phys. Soc. Japan*, 59:2884–2891, 1990.
- [297] P P Vil’ms and M V Éntin. *Sov. Phys. Semicond.*, 22:1209, 1988.
- [298] F M Peeters and P Vasilopoulos. Quantum transport of a two-dimensional electron gas in a spatially modulated magnetic fields. *Phys. Rev. B*, 47:1466–1473, 1993.
- [299] Xiaoguang Wu and Sergio E Ulloa. Electron states and collective excitations of a two-dimensional electron gas in a unidirectional magnetic field modulation. *Phys. Rev. B*, 47:7182–7186, 1993.

- [300] F M Peeters and A Matulis. Quantum structures created by nonhomogeneous magnetic fields. *Phys. Rev. B*, 48:15 166–15 174, 1993.
- [301] J E Müller. Effect of a nonuniform magnetic field on a two-dimensional electron gas in the ballistic regime. *Phys. Rev. Lett.*, 68:385–388, 1992.
- [302] Miguel Calvo. Exactly soluble two-dimensional electron gas in a magnetic field barrier. *Phys. Rev. B*, 48:2365–2369, 1993.
- [303] Yshai Avishai and Yehuda B Band. Electronic conductance of an orifice in a magnetic field. *Phys. Rev. B*, 40:3429–3432, 1989.
- [304] J Rammer and A L Shel'nikov. Weak localization in inhomogeneous magnetic fields. *Phys. Rev. B*, 36:3135–3146, 1987.
- [305] A V Khaetskii. The hall effect and magnetoresistance of a two-dimensional electron gas upon scattering on microinhomogeneities of a magnetic field. *J. Physics Cond. Mat.*, 3:5115–5124, 1991.
- [306] L Brey and H A Fertig. Hall resistance of a two-dimensional electron gas in the presence of magnetic-flux tubes. *Phys. Rev. B*, 47:15 961– 15 964, 1993.
- [307] E Hofstetter, J M C Taylor, and A MacKinnon. Two-dimensional electron gas in a linearly varying magnetic field: Quantization of the electron and current density. *Phys. Rev. B*, 53:4676–4683, 1996.
- [308] P D Ye, D Weiss, K von Klitzing, K Eberl, and H Nickel. Fabrication and characterization of micromagnet arrays on top of gaas/algaas heterostructures. *Appl. Phys. Lett.*, 67:1441–1443, 1995.
- [309] P D Ye, D Weiss, R R Gerhards, M Seeger, K von Klitzing, K Eberl, and H Nickel. Electrons in a periodic magnetic field induced by a regular array of micromagnets. *Phys. Rev. Lett.*, 74:3013–3016, 1995.
- [310] Shu ichi Izawa, Shingo Katsumoto, Akira Endo, and Yasuhiro Iye. Magnetoresistance oscillation in two-dimensional electron gas under spatially modulated vector potential. *J. Phys. Soc. Japan*, 64:706–710, 1995.

- [311] H A Carmona, A K Geim, A Nogaret, P C Main, T J Foster, M Henini, S P Beaumont, and M G Blamire S A Trugman. Two dimensional electrons in a lateral magnetic superlattice. *Phys. Rev. B*, 74:3009–3012, 1995.
- [312] M A McCord and D D Awschalom. *Appl. Phys. Lett.*, 57:2153, 1990.
- [313] M J Kelly and C Weissbuch, editors. *Les Houches proceedings*, Berlin, Germany, 1986. The physics and fabrications of microstructures and microdevices, Springer-Verlag.
- [314] H Heinrich, G Bauer, and F Kuchar, editors. *Proceedings of the 1988 Mauterndorf Conference, Physics and Technology of Submicron Structures*, Berlin, Germany, 1988. volume 83 of the Springer Series in Solid State Sciences, Springer-Verlag.
- [315] G Ebert, K von Klitzing, and G Weimann. Hall potential distribution in quantum Hall experiments. *J. Physics C*, 18:L257–L260, 1985.
- [316] S Komiyama, T Takamasu, S Hiyamizu, and S Sasa. Electron transport in a spatially non-uniform magnetic field. *Solid State Commun.*, 54:479–482, 1985.
- [317] E K Sichel, H H Sample, and J P Salerno. Equipotential distribution in the quantum Hall effect. *Phys. Rev. B*, 32:6975–6977, 1985.
- [318] D K de Vries and A D Wieck. Potential distribution in the van der pauw technique. *Ann. J. Phys.*, 63:R8629–R8632, 1995.
- [319] A H MacDonald, T M Rice, and W F Brinkmann. Hall voltage and current distribution in an ideal two-dimensional system. *Phys. Rev. B*, 28:3648–3650, 1983.
- [320] R F Wick. Solution of the field problem of the germanium gyrator. *J. Appl. Phys.*, 25:741–756, 1954.
- [321] H J Lippmann und F Kuhrt. Der geometrieeinfluß auf den transversalen magnetischen widerstandseffect bei rchteckförmigen halgleiterplatten. *Zeitschrift für Naturforschung*, 13 a:462–473, 1958.

- [322] H J Lippmann und F Kuhrt. Der geometrieeinfluß auf den transversalen magnetischen widerstandseffect bei rchteckförmigen halgleiterplatten. *Zeitschrift für Naturforschung*, 13 a:474–483, 1958.
- [323] J P Newsome. Determination of the electrical characteristics of hall plates. *Peoceedings I.E.E.*, 110:653–659, 1963.
- [324] S Kawaji. Quantum galvanomagnetic experiments in silicon inversion layers under strong magnetic fields. *Surf. Sci.*, 73:46–69, 1978.
- [325] R W Rendell and S M Girvin. Hall voltage dependence on inversion layer geometry in the quantum Hall effect-regime. *Phys. Rev. B*, 23:6610–6614, 1981.
- [326] B L Altshuler and N N Trunov. *Sov. Phys. JETP*, 42:119, 1985.
- [327] J Heremans. Solid state magnetic field sensors and applications. *J. Phys. D: Appl. Phys.*, 26:1149–1168, 1993.
- [328] Howwen Jou and A M Krivan. Current patterns in magnetically inhomogeneous conductors. *Superlattices and Microstructures*, 19:203–216, 1996.
- [329] B A Fuchs and B V Shabat. *Functions of complex variable*. Nauka, Moscow, 1964.
- [330] M Abramovitz and I A Stegun, editors. *Handbook of Mathematical Functions*. Nauka, Moscow, 1979.

List of publications underlying the dissertation

1. S M Badalyan and A H Melikyan. Threshold anomalies in disintegration of an optic phonon into two acoustic phonons in one dimensional anharmonic crystal. *Sov. Phys. Low Temp.*, **13**:670, 1987.
2. S M Badalyan and Y B Levinson. Bound states of electron and optical phonon in a quantum well. *Sov. Phys. JETP*, **67**:641–645, 1988.
3. S M Badalyan and Y B Levinson. Cyclotron-phonon resonance in a two dimensional electron gas. *Sov. Phys. Semicond.*, **22**:1278–1281, 1988.
4. S M Badalyan and Y B Levinson. Effect of an interface on the scattering of a two dimensional electron gas from acoustic phonons. *Sov. Phys. Solid State*, **30**:1592–1597, 1988.
5. S M Badalian and Y B Levinson. Interface effect on the interaction of a two-dimensional electron gas with acoustic phonons in a quantizing magnetic field. Proceedings of 14th All-Union Conference on Theory of Semiconductors. Donetsk, 1989.
6. S M Badalyan. *Electron-Phonon Interaction in Quasi Two Dimensional Electron Systems*. PhD thesis, Yerevan State University, Yerevan, 1989.
7. S M Badalyan. Scattering of electrons in a two dimensional Fermi gas by acoustic phonons near an interface between elastic half-spaces. *Sov. Phys. Semicond.*, **3**:1087–1091, 1989.
8. S M Badalian and Y B Levinson. Free surface effect on the interaction of a two dimensional electron gas with acoustic phonons in a quantizing magnetic field. *Phys. Lett. A*, **140**:62–66, 1989.
9. S M Badalian and Y B Levinson. Ballistic acoustic phonon emission by a two dimensional electron gas in a quantizing magnetic field with account of the phonon reflection from a GaAs/AlGaAs interface. *Phys. Lett. A*, **155**:200–206, 1991.

10. S M Badalian, Y B Levinson, and D L Maslov. Scattering of electron edge states in a magnetic field by impurities and phonons. *Sov. Phys. JETP LETT.*, 53:595–599, 1991.
11. D L Maslov, Y B Levinson, and S M Badalian. Interedge relaxation in a magnetic field. *Phys. Rev.* **B**, 46:7002–7010, 1992.
12. S M Badalian and Y B Levinson. Suppression of the emission of surface acoustic phonons from a two dimensional electron gas a quantizing magnetic field. *Phys. Lett.* **A**, 170:229–231, 1992.
13. S M Badalian, U Rössler, and M Potemski. Theory of Auger up-conversion in quantum wells. page 1433, Regensburg, Germany, 1993. 13th General Conference of the Condensed Matter Division, European Physical Society.
14. S M Badalian, U Rössler, and M Potemski. Theory of Auger up-conversion in quantum wells in a quantizing magnetic field. *J. Physics Cond. Mat.*, 5:6719–6728, 1993.
15. S M Badalian. Ballistic acoustic phonon emission by quantum edge states. Abstract 1022, Madrid, 1994. 14th General Conference of the Condensed Matter Division, European Physical Society.
16. S M Badalian. Emission of ballistic acoustic phonons by quantum edge states. *J. Physics Cond. Mat.*, 7:3929–3936, 1995.
17. S M Badalian. Electron relaxation in the quantum Hall effect geometry: One- and two-phonon processes. *Phys. Rev.* **B**, 52:14 781–14 788, 1995.
18. S M Badalian, I S Ibrahim, and F M Peeters. Theory of the magneto-transport of electrons in a non-planar two dimensional electron gas. Abstract TuP 75, Würzburg, Germany, 1996. 12th International Conference on the Application of High Magnetic Fields in Semiconductor Physics.
19. S M Badalian, I S Ibrahim, and F M Peeters. Magneto-transport of electrons in a non-homogeneous magnetic field. Abstract TuP–52, Liège, Belgium, 1996. 9th International Conference on the "Superlattices, Microstructures and Microdevices, July 14-19, 1996, (ICSMM-9).

20. I S Ibrahim, S M Badalian, and F M Peeters. Magneto-transport of electrons through a magnetic barrier. Eindhoven, Holland, 1996. Semiconductor days Meeting in Eindhoven.
21. I S Ibrahim, V A Schweigert, S M Badalian, and F M Peeters. Magneto-transport of electrons in a non-homogeneous magnetic field. *Superlattices and Microstructures*, **22**:203-207, 1997.
22. S M Badalian, I S Ibrahim, and F M Peeters. Theory of the magneto-transport of electrons in a non-planar two dimensional electron gas. In G Landwehr and W Ossau, editors, *High Magnetic Fields in the Physics of Semiconductors II*, pages 327–330. World Scientific, Singapore, 1997.

Biographical Sketch

Present employment

From 1995 Leading researcher,
supervisor of a scientific theme, Yerevan State
University, email:badalyan@lx2.yerphi.am

Research in other institutions

1997, 91-93 Institute for Theoretical Physics, University of
Regensburg, Germany

1996 Department of Condensed Matter Theory, Uni-
versity of Antwerp, Belgium

1996, 95 International Center for Theoretical physics,
Italy

1987-1991 Institute of Microelectronics Technology and
High Purity Materials, Chernogolovka, Russia

Doctorate

1989 Candidate of Physics and Mathematics (Ph.D)

Subject of examination: Electron-phonon interaction in 2D-electron
systems

Scientific advisor: Prof. Y. B. Levinson, Institute of Microelectron-
ics, Chernogolovka, Russia

Official opponents: Prof. A. V. Chaplik, Institute of Semiconduc-
tor Physics, Novosibirsk, Russia, Prof. A. A.
Kirakosyan, Yerevan State University, Armenia

Leading organization Institute of Solid State Physics, Chernogolovka,
Russia

Awards

1997 Civilian research and development foundation,
principle co-investigator, grant No. AP1-375.

1994 International science foundation, grant No.
RYU000.

1994 "Young scientists 93" Honour of "Armenia"
foundation for academic research